

# QUALITY ASSESSMENT OF BONDED PRIMARY CFRP STRUCTURES BY MEANS OF LASER PROOF TESTING

Dem Fachbereich Produktionstechnik  
der  
UNIVERSITÄT BREMEN

zur Erlangung des Grades  
Doktor-Ingenieur  
genehmigte

Dissertation

von

M.Sc. Bastien Ehrhart

Gutachter: Prof. Dr. Bernd Mayer (Uni Bremen)  
Prof. Dr. Bernd Valeske (HTW Saar)

Tag der mündlichen Prüfung: 08. Juni 2016



---

## PREAMBLE

I would like to seize the opportunity given by a preamble to thank all the people who made it possible for me to achieve such a work. For this purpose, I want address my thanks personally to everyone in their own language.

Als erstes möchte ich mich hiermit bei allen Teilnehmern meines Prüfungsausschusses bedanken. Beginnen möchte ich mit **Prof. Bernd Mayer**, meinem ersten Gutachter, der das Thema und diese Arbeit von Anfang an unterstützt hat. Bei ihm möchte ich mich besonders für seine Hilfsbereitschaft und seine Tipps für die Arbeit bedanken. Der nächste Dank geht an meinen zweiten Gutachter und früheren Abteilungsleiter, **Prof. Bernd Valeske**, der mir bereits ab 2009 die Chance gegeben hat an diesem Thema zu arbeiten und dann zu promovieren. Ich bedanke mich sehr für das Vertrauen über diese Jahre. Ein besonderer Dank geht auch an **Dr. Clemens Bockenheimer**, meinem Mentor und Freund, mit dem ich alltäglich austauschen konnte. Du hast mich in guten und weniger guten Zeiten motiviert. Manchmal habe ich einfach deinen „Schubs“ gebraucht um weiter zu machen. Vielen Dank auch an **Prof. Alex Herrmann, Barbara Priscila Andreon** und **Eduard Martin** für eure Zeit und eure Interesse an dieser Arbeit. Unerwähnt möchte ich nicht **Dr. Stefan Dieckhoff** lassen, der am Ende nicht in der Prüfungsausschuss sitzen durfte, sich aber stets für Tipps und Korrekturen zur Verfügung gestellt hat.

Ein letzter Dank auch noch an alle Assistentinnen der Professoren, die das Planen für mich stets leicht gemacht haben und mir immer mit Ihrer Hilfe zur Verfügung standen. Diesen Dank geht also an **Giuseppa Iacolino**, mit der ich 4 ½ Jahren im IZFP gearbeitet habe, an **Claudia Röhrs** und **Anja Sander** im IFAM, und an **Corinna Gonzalez** beim FASER Institut. Ohne euch wäre und würde nichts laufen, also vielen Dank !

Außerdem möchte ich mich bei meinen Kollegen von Airbus Bremen bedanken. Zunächst bei **Rudolf Henrich** und allen Mitarbeitern der **Abteilung M&P Zerstörungsfreie Prüfverfahren** für die stetige Unterstützung. Ein besonderer Dank geht da an **Wolfgang Bisle, Heiner Stehmeier, Helge Hicken, Jens Kethler** und vor allem an **Carsten Brandt**. Alle haben reichlich durch Ihre Erfahrung mit Ihren Ideen und Tipps zu dieser Arbeit beigetragen. Auch bei den Kollegen von der **Abteilung M&P Composites** und **M&P Metallografie** und **alle Kollegen in den Laboren** (Geb. 20F, 20B und 10A) möchte ich mich herzlich bedanken.

Eine Gedanke geht auch an die ehemaligen Kollegen vom Fraunhofer Institut IZFP in Saarbrücken, mit denen ich, durch meine Stelle in Bremen, leider doch wenig Kontakt hatte. Ich behalte Gute Erinnerungen von meinen Besuchen im Süden!

Der letzte Dank geht natürlich an meine aktuellen **Kollegen von TESTIA GmbH!** Ihr habt mich in den letzten Zügen dieser Promotion erlebt, beim Zusammenschreiben und bei den Korrekturen neben der Arbeit. Danke für Eure Unterstützung !

In English, I would like to thank the colleagues of **LSP Technologies** for their warm welcome during the measurement campaign in Ohio. Thank you all for the support during the tests.

Je poursuis ses remerciements en français avec tout d'abord, les collègues et maintenant amis qui ont énormément contribué à cette thèse. Merci à **Dr. Romain Ecault** qui travaillait en parallèle avec moi à sa thèse à lui, et qui la achevée depuis quelques années. Nos échanges, notre collaboration dans le projet et tous les bons moments vécus ensemble pendant plus de 3 ans font de toi une pièce essentielle dans la réussite de cette thèse. Je tiens à souligner que

---

c'est grâce à toi et nos discussions sur la thématique du choc laser que j'ai toujours eu la motivation de continuer et d'avancer sur mes travaux. MERCI !

Un grand merci va aussi à **Dr. Michel Boustie** pour ses encouragements et son soutien. Nous avons passés de bons moments avec nos projets communs et j'espère que l'avenir nous donnera de continuer à travailler ensemble. Merci encore pour les conseils et les corrections de la partie théorie des chocs. Ta générosité n'a pas d'égal Michel !

Merci encore à **Dr. Fabienne Touchard** et à **Dr. Laurent Berthe** pour les discussions scientifiques et leur intérêt pour mon travail.

Durant ces quasi cinq ans de travail sur la thèse, j'ai eu l'occasion de travailler aussi avec de nombreux stagiaires, plus ou moins en relation avec mes expériences sur les composites. Je pense particulièrement à deux personnes: **Charles-Edouard Müller**, **Delphine Lopez** et tous les autres que j'oublie de nommer mais qui ont su prendre le temps de me prêter main forte quand j'en ai eu besoin.

Pour conclure, je voudrais finir par remercier les gens qui ont cru en moi et qui ont su me pousser tout au long de l'aventure, surtout dans les phases les plus difficiles.

Tout d'abord mes amis bien sûr, avec les quelques docteurs qui savent ce que c'est (**Pauline**, **Max**), mais aussi tous les autres qui ne croyaient surement plus lire ça un jour...tout arrive **Céline** et **Francois**, oui oui !

Après les amis, je ne peux pas ne pas remercier **ma famille** : c'est mon roc et une motivation de toujours qui me pousse à avancer dans mes projets. Cette thèse en est un parfait exemple. Un énorme merci tout spécial à ma **Maman**, à mon **Papa** et à ma sœur **Manon** qui m'ont toujours encouragé et sans qui je n'en serai littéralement pas là aujourd'hui !

Premier docteur de la famille. Yes !!!

Enfin, un grand merci final à **ma femme**, **Katrin**, qui m'a encouragé et soutenu tout du long. Tu as su faire preuve de beaucoup de patience. Je t'en suis très reconnaissant et je t'aime fort.

## ABSTRACT

The use of adhesive bonding as an assembly technology is still limited because of the absence of NDT method to assess the quality of the adhesion. This work evaluates the state-of-the-art of potential NDT technologies and focuses on laser proof test techniques. The theory of this approach aiming at debonding weak adhesive bond and leaving strong adhesive bond unaffected is introduced. A preparation technique and a characterization strategy for bonded CFRP specimens with defined adhesion levels is presented. Two laser proof test setups are then investigated experimentally. A first test focuses on the determination of threshold energy for debonding of the different adhesive bond states. Further tests (repetition of laser shocks, different laser energy levels, mechanical test after laser shock) are performed to evaluate the effects on the CFRP structures. The main objective is the evaluation of the NDT character of laser proof test. With both laser setups, a debonding intensity threshold was achieved, but not without affecting the CFRP substrates. Ultrasonic inspections and mechanical tests conducted before and after laser shocks are compared to analyze the role of each laser setting in the observations. This study shows the feasibility of the concept with a high potential of improvements for the laser technologies and for approaches towards the industrialization.

Das Kleben als Fügetechnik besitzt ein großes Potenzial für Leichtbaukonstruktionen bei der Luftfahrtindustrie. Leider fehlt zum breiteren Einsatz der Technik eine sichere Prüfmethode, die einen zerstörungsfreien Nachweis der Güte von Klebverbindungen erlaubt. Diese Studie beleuchtet den Stand der Technik bzgl. ZfP-Methoden und befasst sich insbesondere mit den „Laser Proof Test“-Methoden. Diese laserbasierten Methoden induzieren Schockwellen im Bauteil, die sich in lokale Spannungen umwandeln. Damit wird beabsichtigt, schwache Klebverbindungen zu zerstören, während Klebungen mit hoher Festigkeit intakt bleiben. Zur Herstellung geklebter CFK-Proben mit definierten Klebfestigkeiten wurden eine Präparationstechnik und eine angepasste Untersuchungsstrategie entwickelt. Zwei verschiedene Laser-Techniken wurden experimentell untersucht. Hierbei wurde die benötigte Laserintensität zur lokalen Öffnung von Klebverbindungen mit unterschiedlicher Festigkeit ermittelt. Zudem wurde der zerstörungsfreie Charakter der Lasertechniken nach wiederholtem Laserbeschuss an gleicher Stelle und nach unterschiedlichen Laserintensitäten untersucht. Dabei wurden Untersuchungen vor und nach Laserbeschuss mit Standardmethoden wie dem Ultraschallverfahren und mit Hilfe der mechanischen Prüfung durchgeführt, um die Einflüsse des Laserbeschusses zu bestimmen. Diese Untersuchungen führten auch zur Beobachtung von Schädigungen des Laminates. Im Ergebnis belegt die vorgestellte Arbeit die Anwendbarkeit der „Laser Proof Test“-Technik zur Qualitätsbestimmung von geklebten CFK-Strukturen und zeigt Hinweise zur Verbesserung der Technik mit Hinblick auf eine Industrialisierung der Methode auf. Entsprechende Empfehlungen und konkrete Weiterentwicklungsansätze, um einen höheren technologischen Reifegrad zu erzielen, werden abschließend erörtert.



---

# TABLE OF CONTENTS

PREAMBLE .....	iii
ABSTRACT .....	v
ABBREVIATIONS.....	xi
GLOSSARY.....	xiii
INTRODUCTION.....	1
SCIENTIFIC OBJECTIVES .....	3

## CHAPTER A: STATE-OF-THE-ART

1.INTRODUCTION.....	6
2.ADHESIVE BOND STRENGTH & INFLUENCES.....	6
2.1 Bonding today and its limitations .....	6
2.1.1 History of bonding .....	6
2.1.2 Advantages of bonding over other assembling technologies .....	7
2.1.3 Challenges for adhesive bonding .....	7
2.1.4 Limitations in the quality control of adhesive bonded parts .....	8
2.2 Influences on the adhesive bond.....	13
2.2.1 How to describe adhesion – models and descriptions .....	13
2.2.2 Degradation of adhesive bond.....	14
2.3 Quality assessment within bonding process .....	15
2.3.1 Surface preparation.....	16
2.3.2 Methods for the control of the adherent surface .....	17
2.4 Weak Adhesive Bonds .....	19
2.4.1 Definition of a Weak bond and a kissing bond .....	20
2.4.2 How to produce a weak adhesive bond.....	20
2.4.3 Detection of weak bonds .....	22
2.4.4 Conclusion .....	23
3.NON-DESTRUCTIVE TESTING METHOD FOCUSED ON MECHANICAL BOND PERFORMANCES .....	23
3.1 About NDT techniques for mechanical bond performance.....	23
3.2 Ultrasonic (US) methods .....	23
3.2.1 Generalities.....	23
3.2.2 Normal Incidence Narrow-Band Pulsed Spectrometry.....	24
3.2.3 Swept-Frequency (US Spectroscopy) Technique .....	25
3.2.4 Harmonic Imaging (Nonlinear Ultrasonic) Technique .....	25
3.2.5 Oblique Incidence Ultrasonic Technique .....	26
3.2.6 Guided Waves Ultrasonic Technique .....	26
3.2.7 Shear Wave Resonance Ultrasonic Technique .....	27
4.OTHERS PROMISING NDT METHODS .....	27
4.1 Shearography.....	27
4.2 Active Thermography .....	27

---

4.3	Monitoring of Damping and Vibration Frequencies .....	28
5.	LASER METHODS TO ASSESS ADHESIVE BONDING QUALITY .....	28
5.1	Laser Ultrasonic .....	29
5.2	Laser Shock Processing.....	30
5.2.1	Laser Shock Adhesion Test (LASAT) .....	31
5.2.2	Understand the shock waves behavior in CFRP.....	32
5.2.3	Laser Bond Inspection (LBI) .....	34
6.	SUMMARY .....	34
	REFERENCES – CHAPTER A.....	36

## **CHAPTER B: MECHANICS OF SHOCK WAVES AND LASER PROOF TEST PARAMETERS**

1.	INTRODUCTION .....	44
2.	ABOUT SHOCK WAVES.....	44
2.1	Generation of shock wave into the material.....	45
2.1.1	Definition of a shock wave.....	45
2.1.2	Shock induction.....	45
2.1.3	Shock wave sources - interactions with direct/indirect irradiation .....	46
2.2	Mechanics of shock waves propagation – theoretical approach .....	47
2.2.1	Equations of Rankine-Hugoniot.....	47
2.2.2	Characteristic shock curves.....	49
2.2.3	Mechanical models for composite materials .....	50
2.3	Interaction of shock waves in bonded structures .....	52
2.3.1	Propagation and transmission of shocks .....	52
2.3.2	Tension and Spallation.....	55
2.3.3	Other Effects .....	56
3.	TECHNOLOGY PRINCIPLE (STATE OF THE TECHNOLOGIES) .....	58
3.1	The essential laser source parameters.....	58
3.1.1	The laser wavelength .....	58
3.1.2	The pulse duration .....	59
3.1.3	The energy/intensity of the laser beam.....	60
3.2	The plasma generation: confinement and sacrificial layer .....	62
3.3	The integrated diagnosis techniques .....	64
4.	SUMMARY .....	68
	REFERENCES – CHAPTER B.....	69

## **CHAPTER C: PREPARATION AND CHARACTERIZATION OF WEAK ADHESIVE BOND SPECIMENS**

1.	INTRODUCTION .....	72
2.	PROCESSES FOR WEAK ADHESIVE BONDS MANUFACTURING .....	72
2.1	About contamination.....	72
2.1.1	Contaminants.....	72
2.1.2	Contamination processes and effects.....	73
2.2	Selected methodology for contamination.....	75



2.3	Summary on weak bonds production .....	76
3.	EXPERIMENTAL METHODS FOR CONVENTIONAL CHARACTERISATION OF BONDED SPECIMENS .....	77
3.1	Dynamic Scanning Calorimetry (DSC) .....	77
3.2	Ultrasonic and Phased Array Ultrasonic Testing (UT & PAUT).....	78
3.3	X-Ray Photoelectron Spectroscopy (XPS) .....	80
3.4	Wetting behavior with Surface Analyst™ .....	81
3.5	X-ray radiography.....	82
3.6	Optical Microscopy.....	83
3.7	Scanning Electron Microscopy (SEM) .....	84
3.8	Double Cantilever Beam Test ( $G_{1C}$ ).....	85
3.9	Summary on characterization methods .....	87
4.	PREPARATION AND CHARACTERIZATION OF WEAK ADHESIVE BONDED CFRP SPECIMENS .....	88
4.1	Specimens families .....	88
4.2	Specimen nomenclature.....	89
4.3	Monolithic laminates preparation .....	89
4.3.1	Materials choice .....	89
4.3.2	Composite lay-up .....	90
4.3.3	Curing cycle .....	90
4.3.4	Surface pre-treatment .....	91
4.3.5	Contamination of adherent surface and verification .....	93
4.4	Adhesive bonding.....	95
4.4.1	Specimens preparation .....	95
4.4.2	Verification of degree of cure.....	97
4.4.3	Characterization of the adhesive bondline.....	99
4.5	Conditioning of moisture aged composite panels .....	101
4.6	Adhesive bond mechanical performances .....	102
4.6.1	Performances of fully and partially cured bonded specimens .....	103
5.	SUMMARY .....	107
	REFERENCES - CHAPTER C .....	108

## **CHAPTER D: EXPERIMENTAL ASSESSMENT OF LASER PROOF TESTING METHODS**

1.	INTRODUCTION .....	112
2.	LASER PROOF TEST SET-UP .....	112
2.1	Laser source LASAT – CNRS PPRIME.....	113
2.2	Laser source LBI – LSP Technologies .....	114
3.	EXPERIMENTAL APPROACH FOR DETERMINATION OF LASER PROOF TEST EFFECTS ON BONDED STRUCTURES .....	116
3.1	Test A - Determination of intensity threshold for each adhesive bond states .....	116
3.2	Test B - Evaluation of potential damages in materials after repeated shocks .....	118
3.3	Test C - Evaluation of mechanical performances after laser proof test .....	119
3.4	Test D - Use of integrated time-resolved diagnosis from laser proof test methods .....	120
3.5	Characterization methods and type of damages post-shocks.....	121
3.5.1	Evaluation of phased-array ultrasonic scans for damage size determination ..	121

---

3.5.2	Observations of damages with optical microscopy .....	124
4.	RESULTS.....	125
4.1	Evaluation of intensity thresholds .....	125
4.1.1	Intensity thresholds of cured specimens.....	126
4.1.2	Intensity thresholds of partially cured specimens.....	133
4.1.3	Intensity thresholds of moisture contaminated specimens.....	135
4.1.4	Overview for all tests.....	137
4.1.5	Summary of intensity thresholds .....	139
4.2	Evaluation of damage effects due to repeated shots .....	140
4.2.1	Effect of repeated laser shock on reference cured specimens.....	140
4.2.2	Effect of repeated laser shock on the microstructure .....	143
4.2.3	Summary on damage generation after repeated shocks .....	144
4.3	Effect of low intensity laser shots on adhesive bond mechanical performances ....	145
4.3.1	Summary on low intensity shock effect on mechanical performances .....	147
4.4	Integrated time-resolved diagnostic tool for calibration of system.....	148
4.4.1	Investigation of VISAR capabilities with laser 25 ns .....	148
4.4.2	Investigation of EMAT capabilities with laser 200 ns .....	152
5.	SUMMARY .....	154
	REFERENCES – CHAPTER D .....	156

## **CHAPTER E: REVIEW OF ACHIEVEMENTS AND LEADS TO A NON-DESTRUCTIVE ADHESION QUALITY TEST**

1.	INTRODUCTION.....	158
2.	LESSONS LEARNED.....	158
2.1	Manufacturing of weak adhesive bond .....	158
2.2	Intensity threshold for debonding in different bonded composite specimens .....	159
2.3	Effects from repeated occurrences of laser shot at same location .....	160
2.4	Effects of laser shock on the mechanical performances in mode I.....	161
2.5	Evaluation of the associated time-resolved diagnosis techniques capabilities .....	162
3.	POTENTIAL FOR LASER PROOF TEST IMPROVEMENTS .....	163
3.1	Leads to laser sources improvements .....	164
3.1.1	Tunable laser shock parameters .....	164
3.1.2	Repeated laser shock.....	165
3.1.3	Symmetrical laser shock .....	166
3.2	Leads to an advanced diagnosis tool .....	167
4.	REQUIREMENTS AND APPROACH FOR IMPLEMENTATION OF LASER PROOF TESTS .....	170
4.1	Requirements for the laser proof test implementation in production .....	170
4.2	Approach for the use of Laser Proof Test.....	171
5.	SUMMARY .....	174
	REFERENCES – CHAPTER E.....	176

CONCLUSION..... 177

OUTLOOK..... 181

---

## ABBREVIATIONS

### Abbreviations Signification

ABiTAS	Advanced Bonding Technologies for Aircraft Structures
AITM	Airbus Test Method
AP	Atmospheric Plasma
ASTM	American Society for Testing and Materials
AWT	Aerosol Wetting Test
BIAS	Bremen's Institute for Applied Beam Technology
C	Cured (specimens)
CFP	Confocal Fabry Perot
CFRP	Carbon Fiber Reinforced Plastic/polymer
CNRC	Centre National de Recherche du Canada (eng. Canadian National Research Center)
CNRS	Centre National de la Recherche Scientifique (eng. French National Centre for Scientific Research)
CT	Computed Tomography
DCB (T)	Double Cantilever Beam (Tapered)
DMA	Dynamic Mechanical Analysis
DSC	Dynamic Scanning Calorimetry
EDX	Energy dispersive X-ray spectroscopy
ENCOMB	Extended-NDT for Composite Bonds
EOS	Equation Of State
ESCA	Electron Spectroscopy for Chemical Analysis
FTIR	Fourier Transform Infrared Spectroscopy
IP	Intellectual property
IRT	Infrared Thermography Testing
ISO	International Organization for Standardization
LASAT	Laser Shock Adhesion Test
LBI	Laser Bond Inspection
LSP	Laser Shock Peening (name of company also)
MIL	Military
MOC	Moisture contaminated (specimens)
NDE	Non-destructive Evaluation
NDI	Non-destructive Inspection
NDT	Non-destructive Testing
NLUS	Non-linear Ultrasonic
OEM	Original Equipment Manufacturer
PAUT	Phased Array Ultrasonic Testing
PC	Partially Cured (specimens)
PDMS	Polydimethylsiloxan
PTFE	Polytetrafluorethylen (aka Teflon)
RFSV	Rear Free Surface Velocimetry
RT	Resonance Testing
SEM	Scanning Electron Microscope
SHM	Structural Health Monitoring
SRB	Super Release Blue Peel-ply

## Abbreviations

---

TCG	Time-corrected Gain
Tg	Glass transition temperature
TWM	Two-wave mixing
US	Ultrasonic
UT	Ultrasonic Testing
VdW	Van Der Waals
VISAR	Velocimetry Interferometer System for Any Reflectors
VT	Visual Testing
WBT	Water Break Test
XPS	X-Ray Photoelectron Spectroscopy

---

**GLOSSARY**

<b>Term</b>	<b>Definition</b>
<b>Adhesion</b>	Complex mechanism linked to mechanical interlocking, diffusion, electrostatic and thermodynamic adsorption and responsible for the assembly of an adhesive to a substrate.
<b>Adherend</b>	Any body or part which is joined to another by an adhesive.
<b>Adherent surface</b>	Surface brought in contact with the adhesive layer.
<b>Adhesive (or Bond) strength</b>	Measured by load/area, the stress required to separate a layer of material bonded to another material. It can be assimilated to a level of adhesion between bonded surfaces.
<b>Debond</b>	Deliberate separation of the physical, chemical or mechanical forces holding an adhesive bond together by an external force.
<b>Delamination</b>	Failure or defect resulting in the separation of two layer of a laminated material.
<b>Defect</b>	Physical and/or chemical change in the material structure. Typical defects are delaminations, disbonds, cracks, porosity, voids (high volume porosity), incorrect matrix cure.
<b>Disbond</b>	Defect present at the adhesive bond/substrate interface when both are separated. Unplanned event that may occur anytime during the lifetime of the bonding part.
<b>Porosity</b>	Micro-cavities in the material structure, can be resulting from gas being trapped in the material during cure or forming.
<b>Non-destructive Evaluation (NDE) or Inspection (NDI)</b>	Inspection conducted in a non-destructive way whose results are neither normed nor clearly predicable. In opposition to NDT, no criteria for the evaluation is provided.
<b>Non-destructive Testing (NDT)</b>	Inspection conducted in a non-destructive way which can only result in a test passed or not. The notion of criteria for passing the test is implied.
<b>Weak bond</b>	Adhesive bond answering the following criteria: <ul style="list-style-type: none"> <li>A. The strength measured with a lap shear test must be below 20% of the nominal bond strength.</li> <li>B. The mode of failure must be adhesive in type (i.e. purely at the interface between the adherend and the adhesive)</li> <li>C. The weak bond must be undetectable from normal bonds with classical NDT techniques.</li> </ul>



## INTRODUCTION

Carbon fiber reinforced polymers (CFRP) materials are playing a large role in the design of new aircrafts. They enable weight savings, new design and new performances which make them highly attractive for the manufacturers. The use of composite materials is however limited due to the existing and approved assembly processes. The current processes rely on mechanical assemblies with for example riveting concerning the high-loaded primary structures. The mechanical processes are not in line with the composite materials due to corrosion matters and stress concentrations. An alternative process would be adhesive bonding.

Although the aerospace industry already have experience with adhesive bonding on composite technology, a great potential for the development of its use in manufacturing exists. A prerequisite for such an application is that the quality of the adhesive bond can be controlled. Various non-destructive testing (NDT) techniques are adequate for the characterization of defects like pores, delamination or debonding within adhesive bonds. There is however so far no NDT technique able to ensure the detection of a weak bond and, by extension, no method to ensure the quality of an adhesive bond. This lack remains the major issue set against a wider application of the adhesive bonding technology.

This work is dedicated to the investigation of a potential non-destructive technology based on a laser proof test for the assessment of the adhesion quality (see glossary) in composite bonded structures. These laser proof tests generate a shock wave, that disbonds the weak adhesive bonds, making the defect visible for other NDT techniques (thermography, US scan, etc...). This approach is voluntarily identified as potentially non-destructive as this study aims at evaluating if and how the use of laser shock for the inspection of adhesive bonds can harm the bonded structure. The **scientific objectives** of this thesis are therefore derived and the technological points needing to be studied are enumerated directly after the present introduction.

To illustrate the current limitations, the **chapter A** establishes a review of the **state of the art** concerning first the **adhesive bonding** and later **non-destructive testing** technique. The challenge with the detection of weak bond is presented, as well as the innovative approach of conventional NDT techniques being adapted for this purpose. In the end, the approach with laser proof tests methods is presented. The past developments towards a method for adhesion quality assessment are introduced.

Before investigating the **laser proof test method**, **chapter B** presents the **functioning principle and phenomenon** involved. The principle introduced are the generation of shock waves, their propagation in, and, their interaction with the composite substrates. The theoretical model is detailed based on studies which investigated high strain and dynamic ballistic impacts. The key parameters such as the laser properties, the sacrificial layer and the confinement layer are presented. The literature reports the development of the adherence test of coatings and the constant improvements of the technique. This 2<sup>nd</sup> chapter aims at explaining the origins of the effects of laser proof testing on composite materials.

The **chapter C** introduces the **experimental methodology** used to investigate laser proof testing. For this purpose, the first step is the definition of relevant specimens with a range of

different weak adhesive bond. The manufacturing of the weak adhesive composite bonds is mandatory to ensure that proper specimens are available for assessment of laser proof tests capabilities. **Conventional characterization** methods from laboratory techniques, conventional NDT methods and mechanical testing methods are used for the verification of the specimens quality. This chapter presents the different methods and compile the results of the investigations for each family of specimens manufactured according to the detailed test plan.

After the manufacturing and reference characterization of the weak adhesive bonds, the **chapter D** focuses next on the **laser proof test methods** themselves. Two experimental solutions with similar functioning principles are applied on the weak adhesive bond specimens. The differences between both laser solutions are investigated through different tests. As a first key parameter, the threshold energy for each bond state is determined. Further tests (repetition of laser shocks, different laser energy levels, mechanical test after laser shock) are performed to evaluate the effects on the CFRP structures. Finally, the results from the laser parameters are correlated with the results from NDT inspections and mechanical tests conducted before and after laser shocks.

**Chapter E** concludes this work with a review of the laser proof test methods based on the different configuration investigated within this study. This chapter reviews the results obtained in term of damages in the CFRP material in the previous chapter D, in comparison to what is expected for an industrial quality assessment process. A **gap analysis** between the requirements from the manufacturing environment and the current development state is made.

The final conclusion summarizes the achievements of this study. It underlines the scientific gain with the results obtained towards the development of a non-destructive adhesion quality assessment method. An outlook summarizes several leads for improvement of the laser proof test method.



## SCIENTIFIC OBJECTIVES

Weak adhesive bonds are hurdles in the establishment of adhesive bonding as an high potential assembly technology. The quality assessment of adhesive bonded structures may be ensured by NDT techniques, but most of those are still being adapted for this purpose. This will be shown within the state-of-the-art. The principle of functioning of laser proof test methods and recent works towards an adhesion test method speak for this technique as a method for quality assessment of bonded structures. Several parameters of the laser proof test technologies remain unknown for the investigation of bonded composite parts. Similarly, the behavior of composite material toward the shock waves propagation and interaction has not been thoroughly investigated yet. In the context of this work, some essential questions may thus be raised:

- First, is it possible to manufacture a proper weak adhesive bond with a precise adhesion performance? Can some parameters be adjusted to obtain reliably such specimens?
- What are the governing mechanisms of the laser proof tests principle?
- Is it possible to measure the adhesion performance in a non-destructive way or, to what extent does the test method influence the mechanical strength of the structure if the adhesive bond has an optimal quality?
- Considering the high energy and the pressure profile involved, can the laser proof technique damage a sound adhesive bond of optimal quality or even the laminate? What would happen to a laminate of a poor quality i.e. cohesively weaker than the adhesive performance bondline?
- Can a wrong setup/calibration of the laser proof technique damage the composite laminate instead ?
- How is it possible to optimize the laser proof test parameters to match the bondline quality inspection and which parameters offer the best customization potential?
- Would an implementation of the existing techniques in the industrial bonding process chain be possible? Under what conditions?

The objectives of this work will be to verify, evaluate and review in what extent the NDT methods, especially the laser proof tests could fulfil the requirements for a nondestructive evaluation technique. It will be evaluated how this technology can be a future solution for the bond quality assessment. For this purpose, the first step will be to explain in detail how the laser proof test approach work and then, to select a method for the preparation of reliable and relevant specimens. A test program with tests designed to provide answers the previous questions will be conducted. These tests will include different configurations of weak adhesive bonds to obtain a range of adhesion performances. Each laser proof test technology shall be tested and their characteristics compared. Finally, all the tests shall provide results helping to evaluate the capabilities of each technology and form together a basis for discussion of the potential for their implementation in the industry.



# CHAPTER A: STATE-OF-THE-ART

## TABLE OF CONTENTS

1. INTRODUCTION .....	6
2. ADHESIVE BOND STRENGTH & INFLUENCES .....	6
2.1 Bonding today and its limitations .....	6
2.1.1 History of bonding .....	6
2.1.2 Advantages of bonding over other assembling technologies .....	7
2.1.3 Challenges for adhesive bonding .....	7
2.1.4 Limitations in the quality control of adhesive bonded parts .....	8
2.2 Influences on the adhesive bond .....	13
2.2.1 How to describe adhesion – models and descriptions .....	13
2.2.2 Degradation of adhesive bond .....	14
2.3 Quality assessment within bonding process .....	15
2.3.1 Surface preparation .....	16
2.3.2 Methods for the control of the adherent surface .....	17
2.4 Weak Adhesive Bonds .....	19
2.4.1 Definition of a Weak bond and a kissing bond .....	20
2.4.2 How to produce a weak adhesive bond .....	20
2.4.3 Detection of weak bonds .....	22
2.4.4 Conclusion .....	23
3. NON-DESTRUCTIVE TESTING METHOD FOCUSED ON MECHANICAL BOND PERFORMANCES .....	23
3.1 About NDT techniques for mechanical bond performance .....	23
3.2 Ultrasonic (US) methods .....	23
3.2.1 Generalities .....	23
3.2.2 Normal Incidence Narrow-Band Pulsed Spectrometry .....	24
3.2.3 Swept-Frequency (US Spectroscopy) Technique .....	25
3.2.4 Harmonic Imaging (Nonlinear Ultrasonic) Technique .....	25
3.2.5 Oblique Incidence Ultrasonic Technique .....	26
3.2.6 Guided Waves Ultrasonic Technique .....	26
3.2.7 Shear Wave Resonance Ultrasonic Technique .....	27
4. OTHERS PROMISING NDT METHODS .....	27
4.1 Shearography .....	27
4.2 Active Thermography .....	27
4.3 Monitoring of Damping and Vibration Frequencies .....	28
5. LASER METHODS TO ASSESS ADHESIVE BONDING QUALITY .....	28
5.1 Laser Ultrasonic .....	29
5.2 Laser Shock Processing .....	30
5.2.1 Laser Shock Adhesion Test (LASAT) .....	31
5.2.2 Understand the shock waves behavior in CFRP .....	32
5.2.3 Laser Bond Inspection (LBI) .....	34
6. SUMMARY .....	34
REFERENCES – CHAPTER A .....	36

## 1. INTRODUCTION

This first chapter introduces the needs for methods to assess the quality of adhesive bonded structures. Adhesive bonding is a general assembly technique dealing with all materials, but due to the interest for aerospace structures, the focus is here set on carbon fiber reinforced polymers (CFRP) materials as substrate.

The first part of the chapter presents the advantages of bonding over other assembly methods and the current state-of-the-art regarding this assembly technique. The processes in place in the industry, their control parameters as well as the possible defects are explained. The special case of weak adhesive bonds is introduced.

The second part of this chapter focuses on reviewing the capabilities of the non-destructive testing methods in place for the inspection of defects in bonded structure, with a certain interest on the assessment of the adhesion quality (see glossary). A particular attention is given to the methods based on ultrasonic waves, already well implemented for conventional NDT. The technique of laser shock adhesion test is also presented in detail. Finally, few experimental approach for the assessment of the bond quality are introduced to complete the state-of-the-art of the potential inspection methods.

## 2. ADHESIVE BOND STRENGTH & INFLUENCES

### 2.1 Bonding today and its limitations

#### 2.1.1 History of bonding

Adhesive bonding is one of the oldest material joining processes used in the history of the mankind [1], [2]. Already thousands of years ago, people used natural substances such as blood or egg white for manufacturing of decorative objects and where a nice finish was required. However, over time and especially during the past century with the development of industry, the demand for adhesives increased and new adhesive products were developed such as synthetic resins and polymers [2]. The aeronautic industry whose history is closely linked to the World Wars, is one of the most involved industries [3]. Fokker started using adhesive bonding in 1915, showing the way to other manufacturers. In 1940, adhesive bonds were used on wood spars of the DH 98 Mosquito [4]. In the 60s, the whole aerospace industry started using adhesive bonding technology, convinced it was an optimal solution for manufacturing lightweight and robust structures [2].

In constant technological progress, adhesive bonding also reached the civil aviation industry where high performance epoxy based resins are mostly used today. As an example, Airbus started using bonding in 1972 and Airbus now has more than 345 bonding features in their whole aircraft families [5].

The future of adhesive bonding is also promising since the perpetual need for better performance will keep increasing the high demand on the adhesive bonding technology and generate new application fields with new challenges.

### 2.1.2 Advantages of bonding over other assembling technologies

Many reasons can be invoked to justify the development of adhesive bonding. This assembly method has several advantages over others processes [2]–[8]: a structure assembled with adhesive bonding will benefit from an homogeneous stress distribution, thus minimizing any stress concentration that appears with any other types of discontinuous assembly methods (e.g. riveting, screw fastening, point soldering, etc.).

Since additional fastening elements like bolts are not required with adhesive bonding, this method is also a good enabler for light, strong and even complex structures. Stoeven also states that thin metal or composite structures are preferably bonded whereas mechanical fastening is more adequate for thick structures.

Also, the uniform stress distribution enables structures featuring high fatigue resistance and thus longer service lifetime than structures that had to be machined (bored, hardened, etc...) prior to assembly.

Bonding is also a method allowing one to join two materials of different chemical nature. A continuous adhesive joint acts as sealants and so features interesting properties in electrolytic corrosion protection and damping of vibrations and sound. In line with other assembly processes, adhesive bonding benefits from a full automation capability, which is of great interest for its use in the industry on assembly lines.

As a final feature, Kwun et al. stated already in 1989 that adhesive bonding may allow reduction of the manufacturing cost of a structure.

All these advantages present adhesive bonding as the ideal solution for the next generation of joined structures. In opposition to other assembly methods, there are however technical challenges that prevail a larger application field.

### 2.1.3 Challenges for adhesive bonding

Limitations restricting a wider field of application of adhesive bonding are numerous. Although bonding is a wide spread assembly method in industry, the scientific world is still not agreed on a single explanation about how adhesives adhere [3]. A real lack of knowledge exists regarding the mechanisms of adhesion and the corresponding failure mechanisms on the physico-chemical level (molecular models for adhesion and its physical description). For this main reason, the aeronautic industry does not trust this method enough to use it for high loaded, so-called “primary”, structures; instead, adhesive bonding is used for “secondary” structure (e.g. spars, stringers, etc.) where a possible failure would not be directly harmful to the integrity of the aircraft.

Many parameters are important in the quality of the adhesive bond: it all starts with the bonding processes. These processes will be described in detail in a further part of this chapter with focus on aeronautic applications only. However, it has already to be mentioned that the realization of a good bond requires in general a clean adherent surface that has been prepared and that presents a good affinity with the adhesive. In specific cases, the adhesive may be tolerant to contamination but in most cases, contaminations such as dirt, grease, etc. are prohibited and removed prior bonding operations [9], [10]. A good wettability of the adherent surface is also needed for an optimal bonding process. The bonding process including the surface preparation, the materials handling and the adhesive cure require a

demanding control [2], [3], [6]. The process parameters are essential for the quality of the adhesive bond and their control is mandatory in order to avoid defects.

Adhesive bonds as any other material part can contain defects. Within this chapter, defects are here understood as material imperfections like delaminations, disbonds, porosity, voids (high volume porosity), incorrect matrix cure and cracks as represented in Figure A.1 [4], [11]. After the bonding process, quality inspection is performed and must be able to detect any defects in the finally assembled body which cannot be detected by visual inspection, most of the time [6], [12]. For additional definitions of defects, please refer to the Glossary.

It is at this stage that non-destructive testing (NDT) methods are used to carry out the quality control of the produced adhesive bond.

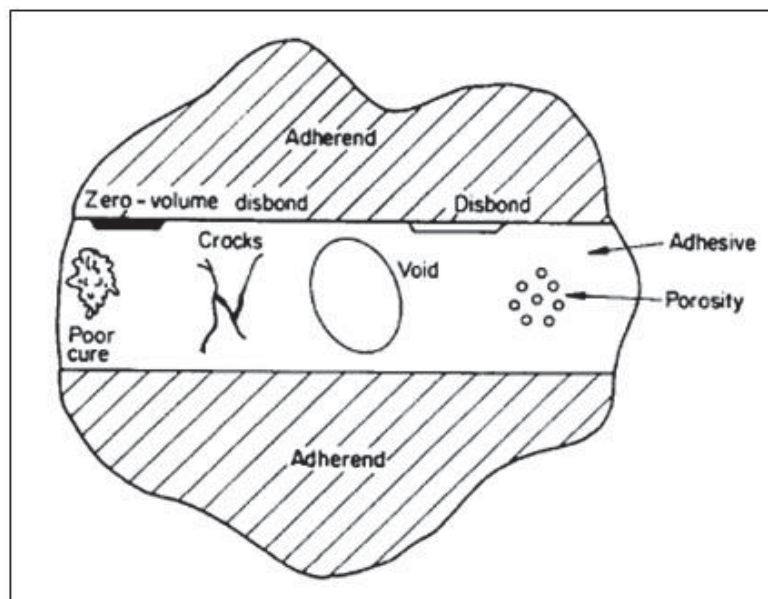


Figure A.1: Typical defects in adhesive bonds [4].

#### 2.1.4 Limitations in the quality control of adhesive bonded parts

Non-destructive Testing (NDT) methods, also known as Non-destructive Evaluation (NDE) or Inspection (NDI) in different industries, are methods implemented in the production process and during the lifetime of a product to enable the control of its structural integrity, and by extension, of its properties. The terms are more or less randomly chosen in the literature since no clear distinction exists. As a common understanding for the use of these terms in this study, it may be referred to the term NDT in the case of a test of a product, performed according to existing and clearly existing inspection standards. In such a case, the term 'Testing' would make sense since the results of the NDT inspection can only be either 'test not passed' or 'test passed' meaning that a defect as specified in the standard has been detected or not. The appellation NDE may be referred to in the case of an inspection leading to a general judgment of the part integrity and lifespan, based on the observations made whether a standard for the process exists or not (see glossary).

In general, NDE represents an important constraint of time and costs for high volume production where a large number of parts need to be treated. It is however often mandatory to ensure the quality of the produced elements. As well as for metal products and metal

bonded structures, NDE is used on adhesive joints for composite materials. The literature reports a large amount of studies about techniques established for the NDE in composites and bonded joints. Out of the five major methods used for metal inspection, only ultrasonic testing [4], [13]–[16] and X-ray radiography [4], [14]–[16] are used for composites up to date, due to the difficulties with an inhomogeneous material. Alternative methods such as low-frequency vibration (Tap test [17], Woodpecker, Fokker bond tester [17], [18]) Acoustic emission, infrared thermography (IRT), shearography [19] were also developed [4], [14]. Those methods are successful in the defect detection as underlined by Baumann et al. [16] in the case of delaminations or in general by Valeske et al.[14] and Nottorf et al.[12]. They are all standardized methods within the aeronautic industries.

Some common techniques are introduced briefly in the next paragraphs [20]:

- Low-frequency vibration tests:

the low-frequency vibration tests include several methods such as the tap test, the automated tap test (with the woodpecker), and the Fokker bond tester. For all those techniques, the surface is tapped with a tool producing a constant frequency and the sound of the intact adhesive bond is recorded as a reference. When a defective bond is tap, the sound generated is changed by a frequency shift.

The Fokker bond tester is based on the damped spring-mass system. The substrate is considered as the mass and the adhesive layer, the weightless spring and damper.

Those test work with a large variety of manual tools (from coins to specific hammers) or electronic hammers with integrated diagnostics. The Woodpecker for instance, is an automated hammer offering selectable tapping intensity and frequencies ranging from 2 Hz to 16 Hz for the inspection. The defect detection is based on a qualitative evaluation of the emitted signal attenuation, by comparison between a safe bonded area (reference) and the part to be measured. Deviations in signal parameters are automatically recorded and displayed.

The Fokker Bond tester uses a piezoelectric oscillator vibrating at a range of frequencies from 20 kHz to 500 kHz. It excites the whole bonded part to evaluate the resonance frequencies and characterize the bonded structures. Two parameters are adjustable: the resonance frequency A and the amplitude B. The evaluation of both parameters delivers information about the adhesive layer nature, the substrate and the adhesive layer thicknesses, the presence of defects and the cohesion in the adhesive layer bondline. The technique however requires a calibration on reference samples and a correlation to results from destructive tests. These information are only relative and qualitative and given in quality classes created with the calibration phase.

Tap tests are easily performed and inexpensive but highly relying on the experience of the inspector. The defects detection with tap test is limited and it is only used for voids, delaminations and disbonds research in all kind of thin structures. The Fokker bond tester has a better sensitivity and is still used for the detection of delamination, voids, porosity, adhesive layer thickness and corrosion. It also allows the characterization of cure degree, ageing (exposure to moisture, heat, fatigue) of the bonded part but fails in the detection of adhesion quality.

- Ultrasonic methods (UT):

Ultrasonic testing (UT) methods are probably the most versatile NDT methods. The common principle of these techniques is the generation of a ultrasonic pulse (1 to 25 MHz) propagating into the material, which would be reflected or attenuated by any obstacle (defects, inhomogeneities, interfaces). The propagation behavior of the ultrasonic waves in the material is directly linked to intermolecular forces and mechanical behavior. Ultrasonic waves are particularly sensitive to the difference of material acoustic impedance  $Z_i = \rho_i \cdot C_i$  where  $\rho_i$  is the density of the material and  $C_i$  the sound velocity in the material. All existing variants of UT techniques involving a contact of a transducer as actuator and/or sensor require the use of a coupling medium (water, oil, gel) to minimize the loss of signal. Once the ultrasonic wave has been reflected or transmitted, a sensor detects it and delivers information such as the intensity (defect size, adhesive properties) and the time of flight of the ultrasonic wave in the inspected part (depth of obstacle).

Two main modes of inspection exist: the pulse-echo mode where the actuator is also the sensor, and the transmission mode where two different actuator and sensor are used. The major hurdle in the use of UT relies in the need of a coupling agent. A large variety exists however: contacts measurements with the sensor on the surface, immersion measurements (usually in water tanks), squirter measurements (flow of water onto the surface to avoid complete immersion), air-coupled ultrasound measurements (without coupling medium but therefore limited in the frequency range), and laser stimulated ultrasound measurements. Finally, a large variety of sensors size, orientation and geometry enable different US waves directions and beam pressure travelling in particular directions in the bonded part. This variety of sensor enable also the generation of longitudinal, transversal and Lamb waves for the detection variable defects orientations and geometries.

Ultrasonic testing offers a wide range of applications for the defect detection starting with the inspection of porosity in bond lines, delaminations and disbonds in bonded parts or even sandwich composite structures, to the determination of the precise position, size and geometry of defects in the complete part.

- X-Ray radiography (RT) and computed tomography (CT):

A X-ray source (up to 75 kV for a standard installation or up to 450 kV for computed tomography) irradiates the bonded part and reveals the presence of various types of defects depending on the absorption of the x-rays. This absorption is linked to the density of an element, and so high atomic number elements tend to absorb more X-rays than lighters such as organic compounds. The transmitted X-rays are measured behind the inspected part, either by a film plate or modern numerical detectors, nowadays directly connected to a computer.

X-ray radiography reveals successfully the inner defects of bonded metallic and composite parts. The computed tomography enables an even finer detection of small defects displaying also three dimensional views of the inspected part. The orientation of the bonded part regarding the irradiation is also a key parameter for an optimal result. In the case of the classical radiography, the X-rays travel through the complete thickness of the bonded part



and are therefore not sensitive to in-plane defects. These techniques are usually selected for the detection of defects in sandwich structures, and mostly for the inspection of defects suspected to involve change of absorbance of X-rays (voids, porosity, water inclusions, presence of metal and composite materials) or reveal a deformation of the structure.

A comparison study of all these methods categorizes the technologies according to their detection capability, cost-efficiency, time-efficiency, mobility, reproducibility, training required, resolution. The results from the comparison in the detection of 15 types of defects in monolithic CFRP panel is given in Table A.1 to illustrate the potential of the visual testing, the ultrasonic testing, the infrared thermography, x-ray digital radiography and computed tomography [21]. These methods are illustrated in Figure A.1. More detailed information can hardly be given for any NDT technique because the effort required is highly dependent on the application targeted.

**Table A.1: NDT Methods comparison based on the detection of 15 artificial defects placed in the mid-thickness in monolithic unidirectional CFRP coupons (6 plies - 0.8 mm thickness) [21].**

	<b>NDT Method</b>				
	<b>legend: - not satisfying, + acceptable, ++ good, +++ optimal, * 3D information</b>				
	<b>VT</b>	<b>UT</b>	<b>IRT</b>	<b>RT</b>	<b>CT</b>
<b>Detection Capability</b> <i>Indicative Range (size)</i>	- <i>Eye resolution at surface only</i>	+++ <i>mm</i>	+++ <i>mm</i>	+ <i>mm</i>	+++ * <i>μm</i>
<b>Cost-efficiency</b>	+++	+	+++	-	-
<b>Time-efficiency</b>	+++	++	+++	++	-
<b>Mobility/Measurement size</b>	+++	++	+++	++	-
<b>Reproducibility</b>	-	+++	+++	+++	+++
<b>Ease of use / Training required</b>	++	++	-	-	-
<b>Maximal resolution</b>	+	+	++	++	+++
<b>Adhesive Strength</b>	-	-	-	-	-

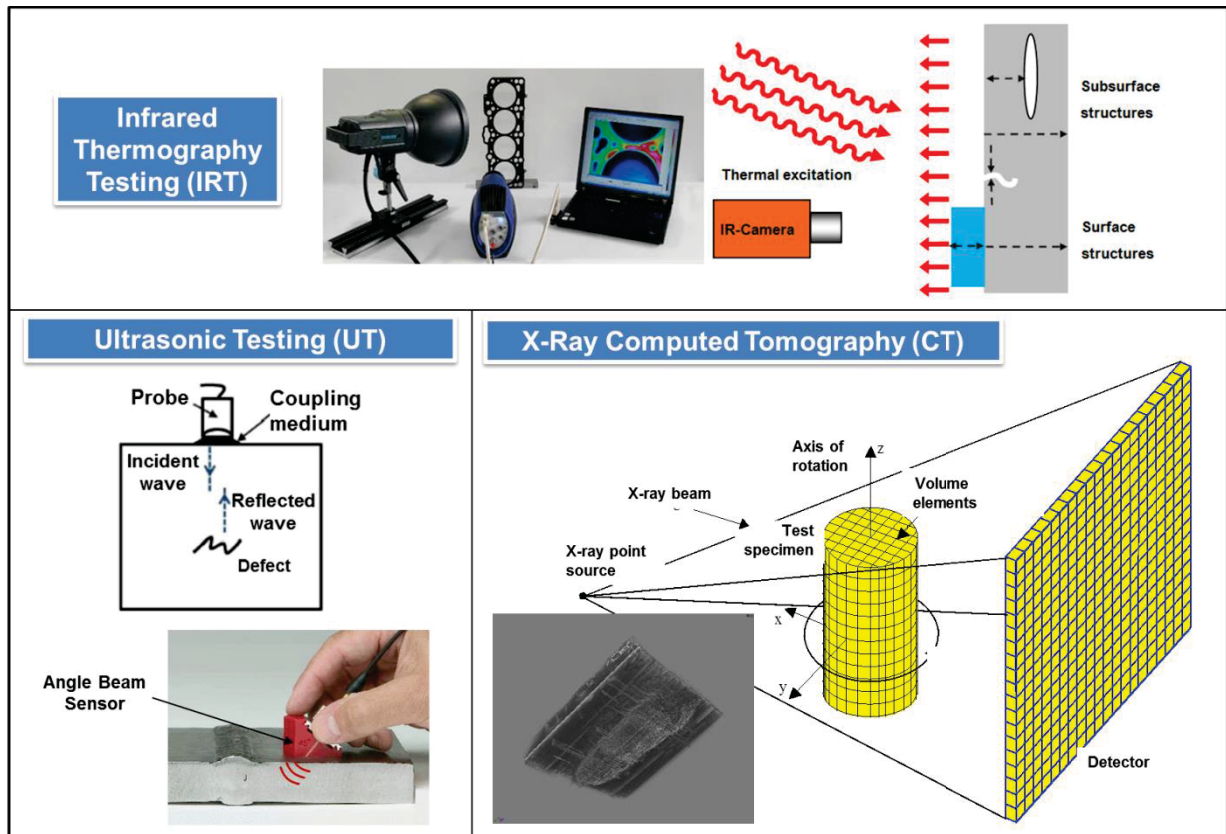


Figure A.1: View of typical experimental setups and principle for the NDT techniques ultrasonic testing (UT), infrared thermography (IRT) and X-Ray Computed Tomography (CT) [14]

It has to be highlighted that none of those techniques, that would be referred to as “conventional” NDT methods, is yet able to assess the **performance of an adhesive bond in term of adhesion quality, its mechanical strength or its properties**. The literature unanimously agrees to this statement [4], [14]–[16], [22].

The determination of such properties directly linked to the bond quality goes beyond the classical ‘defectoscopy’ purpose of the NDT methods and can be referred to as a ‘propertyscopy’ goal. This limitation of the adhesive bonding technology is from utmost importance. It represents one major stake in the further development of this technology.

To summarize, the quality of the adhesive bond can be defined as the absence of defects, durability in the service environment, mechanical performance and the fulfillment of additional optional requirements depending on the final application [6]. The quality is thus a parameter that goes beyond the defect detection currently available thanks to NDT. In opposition to the quality of other assembly technologies, the quality of an adhesive bond requires that the physical and chemical properties of the adhesion and in the interphase with the adherent surfaces could be characterized [22].

## 2.2 Influences on the adhesive bond

To understand the influences that contaminants such as water, or that thermal degradation can have on the physical and chemical properties of an adhesive bonds on CFRP, the mechanisms of adhesion shall be described first.

### 2.2.1 How to describe adhesion – models and descriptions

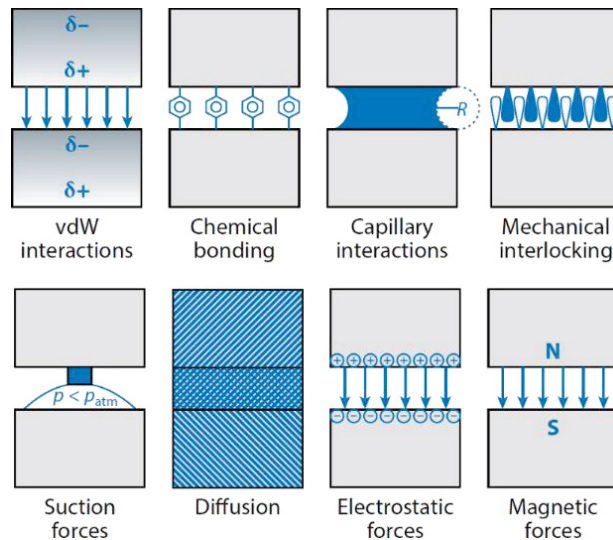
As an introduction to adhesion theory with respect to NDT and NDE, the literature may introduce the adhesion in a simple way, for instance as a well distributed ensemble of many individual contacts with various strength that transmit the forces (the so-called spring mass model) [23], [24]. Scientists however hardly agree on one single detailed mechanism model to explain adhesion. If the literature does not agree on only one mechanism, it is also due to the fact that all mentioned mechanisms are more or less applying at the same time. All those parameters are closely linked and cannot be separated from another. On top of that, the measurement of each of this phenomenon is yet still hardly achievable.

Four main complex theories are proposed to explain the mechanism of adhesion [2], [6], [25]:

- mechanical interlocking, based on friction up to the micro level closely linked to the roughness and the wettability of the adherent surface;
- diffusion, when the penetration of molecules from the adhesive into the substrate is possible depending on the chemistry of both (absorption);
- electrostatic, in some cases with electrostatic forces establishing between the elements from both the adherent surface and the adhesive, and finally;
- thermodynamic adsorption, relying on strong chemical bonds between atoms and molecules from each partner.

Among these mechanisms, the thermodynamic adsorption is however the most accepted one: adhesion comes from the forces that appear between the atoms in the two surfaces when the two surfaces are in intimate molecular contact. To allow this molecular contact, an optimal wettability between the adhesive and the adherent surface is a necessary condition. Common bonds are Van der Waals and Hydrogen (up to 12 kcal/mol), known as secondary bonds, whereas Ionic, Covalent and Metallic bonds are a lot stronger (up to 250 kcal/mol for a ionic bond) and known as primary bonds [6], [26].

The adhesion quality depends on the chemical bonds between atoms of the adhesive and adherent surfaces and the molecular structure and molecular mobility in the interphase region [25]. Boerio et al. stated several factors for an improved adhesion quality: increasing mechanical interlocking through high roughness, maximizing the thermodynamic work of adhesion or, forming specific bonds across the interface [27]. Adherent surface preparation is strongly recommended in order to improve the adhesion performance and exploit the factors mentioned, by increasing the roughness and optimizing the chemistry of the adherent surface for instance. All these mechanisms are roughly synthetized in Figure A.2.



**Figure A.2: Simplified physical and chemical mechanism of adhesion models incl. Van der Waals interactions, chemical bonding, capillary interactions, mechanical interlocking, suction forces, diffusion, electrostatic forces and magnetic [28].**

In opposition to those last approaches for an improved adhesion quality, several other factors have severe influences on the composite matrix and so, the adherent surface and by extension the adhesive bond itself.

### 2.2.2 Degradation of adhesive bond

The literature treats extensively from influences on epoxy materials, including composites [2], [4], [6], [16], [29]–[33]. Although most of the articles refer to bulk epoxy, to epoxy bonded to metal or even glass fiber epoxy composites, the statement is the same: epoxy is subjected to the deterioration of its chemical and physical properties at molecular level due to external influences such as electromagnetic radiation, mechanical loadings, thermo-oxidation, and most of all, chemical contamination (from water to aggressive solvents). Those two last influences being risks present in the manufacturing stage, their effects deserve to be developed.

Thermo-oxidation (exposition to high temperature in presence of air) leads epoxy to experience several chemical and physical changes. At low temperatures, epoxies first have their glass transition temperature ( $T_g$ ) increased: this effect can be attributed to post-curing in the material [34]. However, over time thermal degradation provokes a decrease of  $T_g$ , which characterize chain ruptures in the material and so, a loss of mechanical performances as assessed in the frame of Young modulus (DLTMA) and shear strength (ILSS) measurements [35], [36]. The temperature gradient in the material also generates mechanical loads and stresses, especially in the case of fiber reinforced epoxy where thermal conductivity is different between fibers and matrix. The material can expand and micro-cracks may appear with temperature increase. Over the limit of 250 °C, the damages appearing can be softening, delamination, cracks and charring. Such temperatures lead then to macroscopic defects that are detectable with NDE methods [37].

Chemical contamination can occur due to many different fluids from different chemical nature (acid, alkali, oils, etc.) Among them, the case being most studied might be hydrothermal

degradation. Consequently, the literature reports on moisture ingress in epoxy composite [6], [38]–[42]. Moisture can be absorbed from the humid environment or from direct contact with water up to around 5 wt.% in a thermoset resin [38], [43]. In bulk epoxy, three distinct moisture absorption processes are suggested by Laplante et al.: according to Langmuir two-phase model, the two state of diffusion of water as either rapid absorption of bound water (water molecules having chemical interaction with the epoxy), or diffusion of free water (free water molecule without chemical interaction) and increase of surface concentration [38]. In the case of fiber reinforced composites, it is suggested by Banks et al. that water may diffuse by permeation through the matrix and by percolation along the fibers, accelerating the basic diffusion processes [44].

On both types, water molecules react with the hydrogen bonds and Van der Waals bonds in the epoxy network. Water induces a plasticization and a stress relaxation. The molecular mobility is increased whereas the value of glass transition temperature is decreased. One wt.% of water can be responsible for a loss of 10 °C in Tg according to Banks et al. [44]. The plasticization is reversible but over time, water may cause a swelling and so, an increase of porosity and a debond at the fiber/matrix interface [41], [42], [45].

The consequence of moisture absorption are severe reductions of mechanical properties (up to 25%) [40], loss of tensile resistance [16] and even de-wetting or debonding the adherend interface [44] in the case of epoxy adhesive bonds. In any case, moisture absorption has a global impact on the durability of the material.

The consequences of the degradation or contamination prevent any safe adhesive bonding processes from being performed. The surface state and absence of any degradation must be assessed by a control method to avoid a defective or weak adhesive bond.

### 2.3 Quality assessment within bonding process

The purpose of the following section is to introduce the control methods for the quality assessment implemented in bonding processes in the aeronautic industry as they are defined up to day. Over the past decades, the world of adhesives has been seriously studied by standardization offices and ASTM or even MIL norms currently exists regarding adhesives, bonding processes, environment and many other important parameters to the adhesive bonding in general [8]. Being mostly related to industrial processes, this part will be dedicated to the standards of the aeronautic industry, here represented by Airbus. About that example, it shall be mentioned that though each manufacturer (OEM) in the aeronautic industry has its own standards, no details are disclosed in this chapter as this knowledge is protected as individual knowhow by special intellectual property (IP) contracts and is not allowed to be published.

Structural adhesive bonding is an assembly process used at Airbus for instance in the case of monolithic and sandwich composites, for joining stringers in the role of doublers and/or stiffeners, as well as for load transfer parts. The following three processes are established for composite assemblies [7]:

- Secondary bonding: two solid cured parts are bonded together with an adhesive
- Co-bonding: one uncured part is bonded to a cured solid part with or without any adhesive
- Co-curing: two uncured parts are bonded together with or without any adhesive

These **processes involve several critical steps that require close inspection and control**. Norms and standard internal procedures rule the different steps that are performed in the processes by Airbus. As an example, the steps range from surface preparation, time between pre-treatment process and application of adhesive, work life condition of adhesive and adherend material, shop conditions during the bonding operations, till the preparation for the cure and curing operation.

This introduction shall give the reader an overview of the critical surface preparation protocol as well as the control methods used in the whole process chain of structural adhesive bonding for composite parts.

### 2.3.1 Surface preparation

The **surface preparation** is a decisive step in the realization of an adhesive bond since it sets up the quality of the adherend. This step is closely controlled by procedures written on the basis of qualification and test programs.

As mentioned in the limitations of the adhesive bonding, a decisive parameter of the surface preparation is the demanding control of the environment where the operation of bonding takes place. Norms rule the concentrations of airborne particles, or even specify the temperature and humidity rate for optimal work conditions. The work conditions as specified in the norms are optimal for the handling and the conservation of the chemical and physical properties of raw materials. Any deviations in the process parameters are likely to affect the quality of the final product. The preparation itself shall take place in a clean, dry and isolated area to prevent the surface from any contamination. The surfaces must be clean and free from contaminations such as fatty substances, oils, foreign bodies or any other pollution likely to affect the bonding operation and lead to failures of process, loss of quality and/or defect formation. This cleanliness is usually assessed by means of close control and inspection (detailed in the following paragraph) before and after the numerous critical pre-treatment processes in place in the serial production. They aim at removing the potential contaminants and excess of resin above the reinforcing fibers [11], [46]–[49].

Among those pre-treatments, the use of peel-ply to be removed before the application of post-treatment has become a standard. It ensures a cleanliness and roughness of the adherent surface. The peel-ply removal is still a part of the manufacturing process, allowing at the same time a contamination control and a minimum surface preparation. Further treatments besides the simple cleaning may be applied to even increase the sensitivity of the surface for the next steps (e.g. bonding, etc.). Those treatments may be referred to as activation treatments. Typical activation treatments would involve:

- Mechanical abrasion and grit blasting techniques: dry or wet, those treatments are efficient in removing matrix excess and generating a specific roughness, they are however highly time consuming and operator dependent although they can be automated. Mechanical treatments also require cleaning steps with solvents and/or water to remove the dust generated with the abrasion.
- Chemical surface modification: either by etching or by laser ablation, plasma treatment activation of the surface, those methods enable the modification of the adherent surface chemical composition and contribute to the adhesion mechanisms [50], [51].

Once this preparation is completed, the adherend material has to be processed as fast as possible to avoid re-contamination and potentially, to benefit from a chemical activation of the adherent surface. The relevant and compatible adhesive (formerly qualified through test programs) can be applied on the adherend material and the bonding operation shall start. If however the bonding operation cannot be performed immediately, adherend parts have to be stored and hermetically packed. They may require a new activation in some specific cases.

### 2.3.2 Methods for the control of the adherent surface

A lot of methods other than NDT techniques are established for the critical characterization of bonded composites before, while and after the process of bonding itself. **The methods here introduced are either analytical or mechanical and allow the characterization of the surface and the bonded structures** to obtain information related to the surface state [7]. They are integrated into the bonding operations to guaranty the quality prior to bonding. Unfortunately most of them cannot be integrated into the bonding process itself.

It must be noticed that these methods, which are mostly applied for the surface quality, are additional to NDT techniques for the defect detection (previously mentioned in section 1). They are usually not applied to the real component itself but require additional reference / test specimens manufactured along the component.

**Surface characterization prior to bonding** is thus done by means of:

- Visual inspection: visual inspection of prepared surface shall be performed for each part to check whether the pre-treatment was carried homogeneously on the entire surface. Visual inspection also allows the control of the homogeneity of the visual appearance of treated areas (e.g. spots, shadows). It is performed for the detection of any damage to the component surfaces (e.g. abrasion, scratches), the dimensions of the parts, and of any visible contamination or foreign bodies.
- Water break test: after pre-treatment by abrasion or blasting, a water break test (WBT) is performed on the pre-treated adherent surfaces to be bonded to evaluate if contaminants are present. This method, which relies on the visual inspection of the continuity of a film of water flowing on the surface, is only qualitative and therefore criticized for not being sensitive enough and too subjective [46], [52]. It remain a standardized and used inspection method within most manufacturing processes of CFRP in the aeronautic industries.

Alternative methods for the characterization of the surface are also being developed and are still under development within technology suppliers and research groups:

- The Aerosol Wetting Test (AWT) is an quantitative wetting test to be opposed to the current WBT. The same principle is however applied and the wettability of the surface is checked through the wetting angle of droplets [33], [53]. Droplets of de-ionized water are vaporized on the surface whose energy influence the diameter and repartition of the droplets. The mean size of the droplets is evaluated and correlated to the surface cleanliness state, automatically. Other technologies based on wettability test exists but the statistical evaluation of the droplet size over a surface is a special feature of the AWT, making it a good candidate for a technology applied within the manufacturing process. This alternative technology is still under development (European Project ABiTAS) but a first version is available commercially [48], [54].

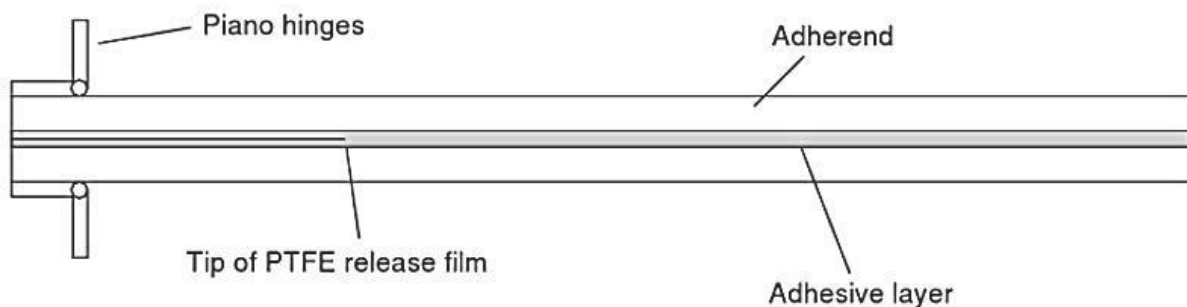
- Spectroscopic methods could also be used to analyze the elemental composition of the adherent surface and even the adherend itself. This purpose has been developed thoroughly in the approach of the European Project ENCOMB (Extended-NDT for Composite Bonds) [55]. The following methods are being adapted in this project but had already been investigated before for detection of contaminants on CFRP parts: EDX and ESCA [33], Laser Induced Breakdown Spectroscopy, FT-IR Spectroscopy [39], [56], Optical Stimulated Electron Emission [52]. They are yet not giving the level of information required to evaluate the presence of a contamination and correlate them to the adhesive bond mechanical performance.

**During the bonding process, it is the process itself that is controlled.** From the autoclaves, curing ovens, presses and related equipment, the parameters like temperature, pressure, vacuum and time are to be recorded and controlled continuously to ensure no derivation from the procedures.

**Mechanical methods for the characterization of the surface** are also used in the industry, mainly **after the bonding process**. These methods are however destructive and therefore applied to representative bonded specimens instead of real structural parts. They deliver information related to the mechanical performance of the adhesive bond and the failure behavior reveals help revealing what is responsible for this performance.

In the literature, mechanical testing is recognized for being the most adequate way to characterize the adhesive bond mechanical performances [56] if not the only one [6], [11], [57]. Those mechanical tests are quasi-static and their diversity allow the determination of either the energy necessary to debond an adhesive bond, or the energy necessary to generate and propagate a crack along the adhesive interface, both continuously or as a whole. They are standardized internationally, by ISO and/or ASTM norms and sometimes even by intern manufacturers norms derived from international ones [58].

Among the test methods applied to bonded specimens, one of the most famous is the determination of the double cantilever beam test (DCB) and its tapered variant. This test aims at determining the interlaminar fracture toughness energy in mode I (perpendicular to the adhesive bondline) " $G_{1C}$ " since its result as the mechanical solicitation of the interface adhesive bondline – substrate can be related to the surface substrate state prior to bonding [58]–[60].

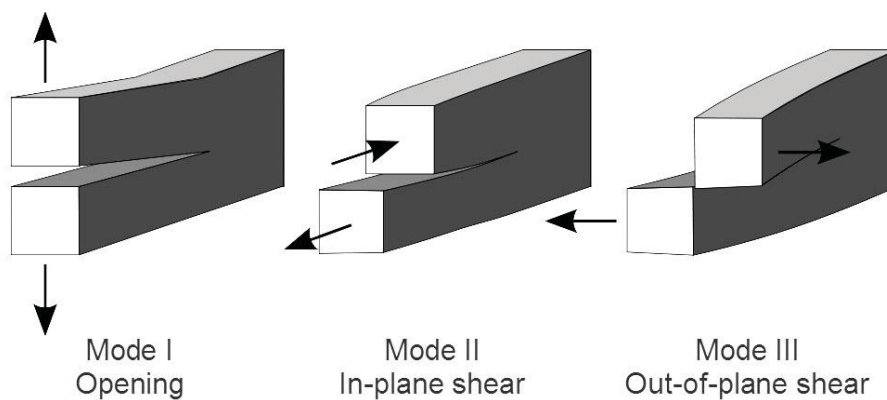


**Figure A.3: Double Cantilever Beam specimen with piano hinges and release film for crack initiation [58].**



This cleavage test is performed with use of a pre-cracked double cantilever beam specimen and consists in opening it by applying a stress on both sides of the pre-cracked extremity (Figure A.3). To be representative, the specimens are manufactured with the same material and under identical conditions including surface treatment as the original part. The absolute requirement is that the failure behavior in the crack propagation must never be adhesive i.e. the rupture must not take place at the interface between the adhesive and the adherent surface.

Other characteristic measures are the Single Lap Shear Strength and the Interlaminar Shear Strength [53]. In those cases, the specimens are not pre-cracked and the specimens are tested in shear (Figure A.4). The interlaminar shear strength is a measurement of the resistance of the composite to delamination under shear forces parallel to the layers of the laminate. It is defined as the maximum shear stress calculated at half thickness of the specimen at the moment of first failure [61].



**Figure A.4: Mechanical Failure modes I, II and III (en.wikipedia.org)**

Finally, to evaluate a successful curing operation, the measure of the Glass Transition Temperature with Dynamic Mechanical Analysis (DMA) and of the Degree of Cure with Dynamic Scanning Calorimetry (DSC) can be performed respectively on the cured laminate and adhesive.

All methods introduced herein are standardized. The performance of several controls, for instance DSC and DMA is mandatory to check the compliance of the adhesive bonding process with the requirements. Mechanical tests are performed to assess that the adhesion is of high mechanical performance and that no contamination or other surface pollution has weakened the bond. It is however not mandatory for all manufactured parts to perform them along the manufacturing.

## 2.4 Weak Adhesive Bonds

The previous sections stated that adhesive bonding is well implemented in the industry. Quality is ensured thanks to care in the surface preparation, rigorous monitoring of bonding processes, standard control methods that are proven to be efficient for the detection of defects. An important lack in adhesive bonding is still the ability to assess the adhesive bond mechanical strength.

The notion of weak adhesive bond need to be detailed in this section, therefore.

### 2.4.1 Definition of a Weak bond and a kissing bond

A term to refer to weak adhesive bonding well spread in the literature is the appellation 'kissing bond' [15], [16], [62]. The use of the expression „kissing bond“ is strongly depending on the scientific focus of the corresponding researcher, coming either from the „NDE community“ or being part of the „adhesion society“. It is usual to read kissing bond for weak bond in the literature, and some authors use this name as a generic for all types of weakened bonds (slip bond, smooth bonds, partial bonds, zero-volume disbonds and imperfect interfaces) [63]; In this study, the name kissing bond shall be kept for the particular case where the adherent surface and the adhesive are in intimate contact i.e. “kisses” each other but without chemical bonding to the substrate surface. This would mean that no adhesion exists between the two interfaces. The case of a zero-volume disbond is identical.

With regard to inaccurate use of the term kissing bond, the more general term 'weak bond' shall be privileged in this study. The present definition is present in the glossary. According to the literature, a “weak bond” shall also be understood as a defective adhesive bond presenting the following characteristics [64]–[66]:

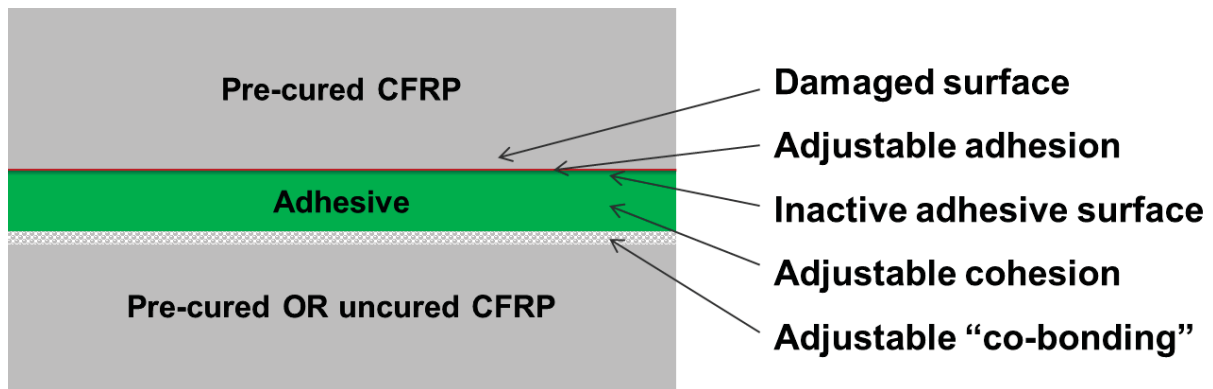
- A. The strength measured with a lap shear test must be below 20% of the nominal bond strength.
- B. The mode of failure must be adhesive in type (i.e. purely at the interface between the adherend and the adhesive)
- C. The weak bond must be undetectable from normal bonds with classical NDT techniques.

**In this study, the term “weak bond” will be employed.** It will refer to all possible adhesive bonds whose manufacturing process has undergone any deviation from the standards, leading to a significant decrease of the adhesive bond mechanical performances to mitigate the 20% below the nominal bond strength, either by lap shear test or another test, but shall also show an adhesive failure profile and shall not be detectable by any NDT method.

The adhesive failure is the worst case scenario where the load propagation provokes a failure at the interface instead of within the material. This failure mechanism must be avoided whereas cohesive failure is the ideal case.

### 2.4.2 How to produce a weak adhesive bond

If the presence of weak bonds has been clearly recognized as a problematic for an expansion of the application fields, proper methods to produce such weak bonds and, to study them are still to be defined. This concept of weak bond includes several factors: adjustable adhesion, adjustable cohesion, adjustable co-bonding process, damaged surface and inactive surface as represented in Figure A.5.



**Figure A.5: Possible influence factors for the generation of a weak adhesive bond in CFRP structures (depending on adhesive bonding process)**

The previous studies found the literature agree on the fact that a combination of several key parameters [63]–[67] is necessary for the production of weak bonds matching the criteria required. It shall be possible to affect the material chemistry (composition of the epoxy adhesive, cure grade, ageing prior to bonding operations, etc.) but those effects have not proven reliably in the literature that they could be tuned to focus on the adhesion quality and so, lead to an adhesive failure. Indeed, the cohesion within the adhesive layer is concerned in those cases. Regarding the adhesion studies, the most cited key parameters are surface roughness (mechanical interlocking) and contamination (chemical modifications).

Among contaminations, fuel, hydraulic and de-icing fluids are frequent sources possible bond weakeners in the aeronautic industry. Still, studies on weak bonds production nevertheless used other contaminants:

One proposed solution is to use PTFE, either as spray [68] or in the form of Teflon tape and sheets [69], [70] at the interface of the bond and the adherent surface. One other well spread technique at this time consists in applying a thin layer of a silicone-based or siloxane-based mold release agent (Frekote, Marbocote, etc.) between the adherend and the adhesive. The use of a silicon based agents can also be either in the form of a dry layer [64], or as a fluid [33], [49], [53], [71], [72].

Those two solutions are relatively simple and do not request complex chemical substances. The release agents tend to transfer automatically to the composite products, more or less homogeneously depending on the mold used as highlighted by Peter and Waghorne [46]. Engholm insists on the importance that the contaminant must not diffuse into the material but stay at the interface. It shall neither be thicker than 10% of the bond line whole thickness to avoid any mechanical interaction in the performance of the adhesive joint [71]. Rieck and Wetzal et al. observed that even until a volume concentration of 1%, the effects of release agents on the adhesive layer were still visible [33], [53].

An alternative solution is to influence the chemical reaction of the adhesive cure, by modifying the stoichiometric ratio of a two components epoxy paste adhesive. In such a case it is however decisive to make sure that all the polyfunctional hardener and polyepoxides have reacted. In the other case, unreacted groups may react with other chemical elements from the environment over the lifespan of the material. The reaction kinetic is however very low in such a case. The addition of amine hardeners not participating in the adhesive layer was studied only on metal substrates by Barroeta et al. but has shown weak mechanical bond performance [72]. Another method having an effect on the adhesive is the exposition to

hot/wet environment to generate a skin effect particularly efficient on two components paste adhesive. This skin effect due to water and CO<sub>2</sub> inactivates the adhesive surface which cannot wet the substrate any more. This method is however only useful with paste adhesives.

It is also possible to proceed to proper bonding operations and contaminate the adhesive joint by immersing it in different aggressive contaminants as suggested by Jastrzebski [73]: the use of water, either pure or salted (NaCl) with increased temperature to boost the diffusion is an example [73], [74]. This solution uses the effect of hydrothermal damage on epoxy as described in the previous section.

A last possible solution found in the literature is the use of an electrically debonding epoxy [64]. However, this solution was not ideal since the bond was completely debonded. It could not match the criteria of a so-called weak bond through precise control of electrical parameters.

### 2.4.3 Detection of weak bonds

The detection and first assessment of the presence of a weak bond was naturally studied in the same sources. Following their definitions, weak bonds are hardly (if not) detectable by means of NDT methods. This statement is confirmed by the literature. Most studies of weak bonds are related to metal bonding with epoxy adhesive; research work of Zaeh et al. relates to the capability to detect weak bonds thanks to thermography on glass bonded to metal frames, only if appropriate algorithms are designed [68].

Marty et al. employed the Fokker Bond-Tester and the Sonic Bond-Master which were both unable to detect any differences between a good and a weak bond. Shearography was also investigated and showed encouraging results but still too far from a mature technology that could be implemented in the manufacturing process [64].

Chance implemented many established NDT techniques such as oblique incidence ultrasonics and high frequency ultrasonics and concluded that the small difference detectable between a good and a weak bond was not relevant enough in addition to very costly regarding both time and calculations [75].

Brotherhood et al. studied the impact of compressive loading on weak bonds generated by liquid contaminants and dry contact weak bonds. The study demonstrated that even if the liquid contaminants were detectable with conventional ultrasonics, the use of compressive pressure could simulate a perfect intimate contact in the adhesive bond and so, making the detection a lot more complex. In case of a dry weak bond, the role of the surface roughness is pointed out: the smoother the surface is, the harder it is to detect an adhesive joint [63].

In case of our interest, the complex composite bonded to composite case, the literature is rare. Chance and Engholm et al. refer to ultrasonic methods and technologies in adaptation phase that are promising but no significant detection could be performed yet and the reproducibility of any attempts seemed to be an issue [71], [75].

#### 2.4.4 Conclusion

To conclude this part, the NDT technologies are not sensitive enough according to the literature. Several conventional methods are being optimized and developed for a better detection capability but up to today, no method can detect weak adhesive bond reliably and with a good reproducibility, either on metal or composite substrate. The following part will now introduce the most promising methods being under development for the detection of weak adhesive bonds.

### **3. NON-DESTRUCTIVE TESTING METHOD FOCUSED ON MECHANICAL BOND PERFORMANCES**

#### 3.1 About NDT techniques for mechanical bond performance

In the previous parts of this chapter, it has been stated that conventional NDT methods are not able to measure the adhesive bond mechanical strength. A review of the alternative solutions, that may also derive from further development of conventional NDT methods (such as ultrasonics) are presented in this chapter. Their adaptation towards inspection of the adhesive bond performance goes in the direction of NDE, and even an extension of the those appellations since the target will be different from physical defects.

All presented methods have in common that they rely on mechanical waves for the evaluation of the bond strength, which is itself seen as a mechanical parameter [24], [76]. This mechanical parameter is not affected in the same way depending on its history and damages it undergoes. Hence different parameters such as frequency, signal form, amplitude, etc. of the response signal coming back from the adhesive joint are key criteria for the understanding of the quality of the adhesive joint [23].

Most of the methods presented here are developed so that their detection capability (measuring probe, sensitivity, etc.) has been optimized for the characterization of adhesive bonds.

#### 3.2 Ultrasonic (US) methods

##### 3.2.1 Generalities

Ultrasonic inspection is besides using mechanical waves one of the most commonly used NDT techniques. Conventional ultrasonic methods such as pulse-echo and through transmission are widely applied for the detection of defects of all kind in all material types. Despite the enthusiasm in the use of ultrasonics, this NDT technology is known for not being able to detect changes in the adhesive bond strength [77].

The ultrasonic waves can nevertheless yield information regarding the morphological and elastic features at the interface of adhesive bonds by their behavior in the material inspected, and so be used as an NDE technique [78].

Their propagation behavior in the material is directly linked to intermolecular forces and mechanical behavior: depending on the mechanical properties (decreased modulus, nonlinear stress-strain behavior) the most adequate method of ultrasonic inspection may be

selected [76]. Hence, as an example, depending on the strain applied the material may have a nonlinear strain-stress curve and transmit the ultrasound nonlinearly, providing higher harmonics and so, information about the bond strength [24], [79].

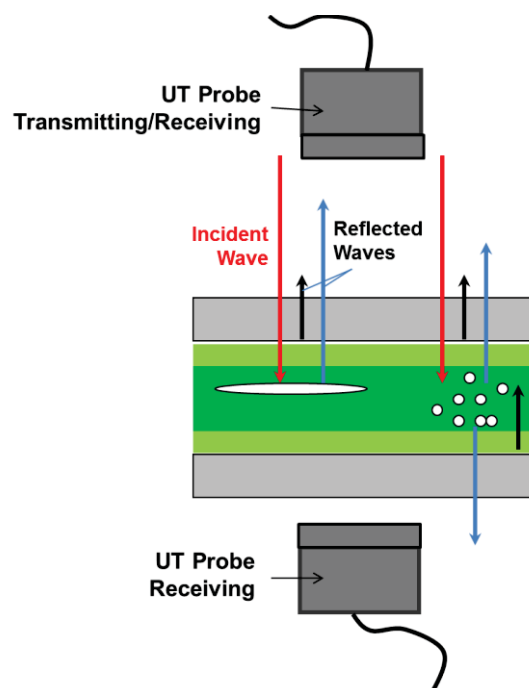
Smith et al. performed a large experimental campaign regarding several different ultrasonic methods [76]. Among all ultrasonic inspection techniques, Smith et al. assume that such methods might be sorted in two categories whether the technique focuses on measurements of out-of-plane (with compression waves) or in-plane (with shear waves) stress-strain properties regarding the bond interface. It is also suggested that the use of shear waves may be wiser since an adhesive bond is designed to support shear stress more than compressive stress.

A description of each ultrasonic technique found in the literature is provided here for an overview on this technology to characterize adhesive bond strength. The first introduced techniques are using compression-wave ultrasonics for out-of-plane stress-strain measurements.

### 3.2.2 Normal Incidence Narrow-Band Pulsed Spectrometry

The first technique is in the principle like the basic one, used also for conventional ultrasonic inspection (see Figure A.6). It corresponds to the emission of ultrasonic waves with a defined frequency. Two modes can be highlighted: ultrasonic can be performed whether in the pitch-catch (through transmission) mode, by using one transducer to emit the sound wave and one other for receiving it, or in the pulse-echo mode, by using the same transducer for the emission and detection of the sound wave.

Each of these modes have their advantages and are applied in most of the other existing ultrasonic variants.



**Figure A.6: Ultrasonic Testing in normal incidence with pitch-catch (one single transmitting and receiving transducer) or through transmission (two different transducers).**

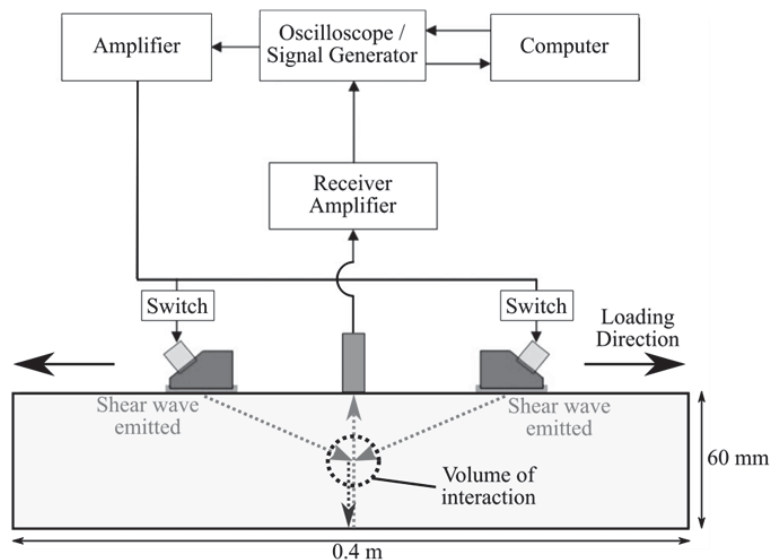
### 3.2.3 Swept-Frequency (US Spectroscopy) Technique

The swept-frequency method, also known as US spectroscopy involves the capture of multiple superimposed reflections through the structure and determining the amplitude and frequency of each reflection in the material, as they are characteristic to each interfaces and layer present in the bonded composites.

Smith et al. tested this method on an adhesive bond immersed in water at 50 °C over a period of 17 weeks. They observed that peaks can be selected in the whole frequency spectrum to monitor the properties of adhesive joints; measures showed that the amplitude and frequency between the peaks are indeed dependent on the properties of the adhesive layer (thickness, interaction with ultrasonic, etc.) [62], [76].

### 3.2.4 Harmonic Imaging (Nonlinear Ultrasonic) Technique

The method of nonlinear harmonics, also called harmonic imaging, relies on the principle that binding forces have a nonlinear mechanical behavior and as a consequence, generate a nonlinear modulation of the transmitted or reflected sound wave. The amplitude of the ultrasonic wave needs to be high enough to cause a local mechanical deformation in the adhesive bond to generate non-harmonic components. These components are hence expected to yield information regarding the adhesive bond strength [1], [77], [80]. An illustration of the ultrasonic waves with interacting shear waves emission is given in Figure A.7 [81].



**Figure A.7: Experimental setup for the generation of ultrasonic shear waves for the non-collinear investigations according to [81].**

Bockenheimer et al. studied the case of acoustic resonance in a four weeks hydrothermal aged multi-layered bonded metallic system [1]. They used a typical standard nonlinear pulse receiver ultrasonic system at the frequency of 2.12 MHz for a power around 6 kW. They stated that the amplitude of the fundamental wave (A1) and second wave (A2) were increased and did depend on the thicknesses of the layers. No difference in the amplitude

between the second harmonic and the first one could be observed in the scatter of the measurements. In similar experiments, Baumann et al. concluded that no correlation could be done with regard to the second harmonic A2 due to consequent interferences [16]. Smith et al. managed to detect a small difference in the third harmonic (A3) of 3 dB with the second harmonic, but by comparing bonded and disbonded joints, only [76]. Brotherhood et al. and more recently Yan et al. focused their work on the investigation of the effect of loading a nonlinear parameter such as respective  $A2/A1$  or  $A2/A1^2$  ratios [63], [80]. Their studies are based on varying the compression of Al rods with one layer of adhesive in between and so enhancing the 'perfect' intimate contact as in a kissing bond, until no nonlinearity could be detected anymore. Above a value of 4.0 MPa, the nonlinearity with load decreases much slower than below which was attributed to the major effect of a clapping mechanism below and the acoustic contact adhesive material nonlinearity above. Also, a nonlinearity effect was to be seen due to the presence of the PUR adhesive between the rods, which was absent between the simple Al-Al rods contact. This effect may not be present in the case of an epoxy adhesive bond layer in CFRP material, where all substrates and adhesive would have a similar nonlinear behavior.

All research work on this technique agrees on the fact that the technique is not mature enough for an application on adhesive bonds, especially in the case of weak bonds in epoxy composite materials. Even if it is considered a promising technique, nonlinear ultrasonic still suffers lots of errors originating from all possible sources (bonded material, measuring devices, probes and coupling system, etc.) that need to be solved [16], [77], [80].

Next development steps for this technique involve further investigations with a better control of the disturbance parameters and theoretical calculations and models. They shall help developing a quantitative measurement of the adhesion strength. Also, a combination of this technique with other ultrasonic techniques such as the oblique spectroscopy ultrasonic method is considered to be a possibility for better results [78].

The next techniques are based on shear-wave ultrasonics for in-plane stress-strain measurements. The physical idea behind this approach is that the use of shear waves may yield more information since in-plane stresses are applying along the bondline and its interface with the substrate.

### 3.2.5 Oblique Incidence Ultrasonic Technique

The oblique incidence technique has been the first method involving shear waves. Shear waves are generated due to the angle of incidence in the material (generally optimal with an angle of  $14^\circ$  for the shortest ultrasonic path in a composite bonded structure) and allow a potentially more sensitive examination of interfacial properties. In Smith et al.'s study, the detection of 'kissing bonds' could however not be achieved even though the method was proven sensitive to degradation through water contamination.

### 3.2.6 Guided Waves Ultrasonic Technique

Guided waves are a variant of the oblique incidence technique, easily performed by moving apart the transducer in charge of the emission and reception. The signal is reflected in the material several times before reaching the detection probe and so, has different modes yielding information about various properties. Smith et al. relate that good results are claimed



for the detection of weak bonds, yet only in materials with highly different acoustic impedance. As a consequence, one may doubt any detection capability in the case of an epoxy composite bonded with epoxy adhesive.

### 3.2.7 Shear Wave Resonance Ultrasonic Technique

Shear wave resonance is a method experimented on metallic adhesive joints. Based on the condition that the longitudinal velocity of the metallic material being twice the shear velocity, a series of thickness-shear resonance with particle motions, relatively parallel to the surface and so the adhesive bond interface can be observed.

In such cases, an adhesive bond causes a damping and a modulation of the shear wave resonance. The importance of the damping and shift in frequency is believed to be determinant for the characterization of the adhesive bond modulus. Considered promising in metallic bonded structures, no results of experiments with this technique for adhesive bonds in composites have been found in the literature, yet.

## 4. OTHERS PROMISING NDT METHODS

Besides the ultrasonic techniques introduced in part 3, other NDT techniques are being adapted for the inspection of adhesive bonds quality. 'Exotic' solutions are also being developed to be either used for an inspection or to be integrated within the bonded structure. This last approach deals with integrated monitoring concept also known as Structural Health Monitoring (SHM) solutions which are introduced in the end of the present part.

### 4.1 Shearography

Digital shearography consists of the measurement of in-plane and out-of-the-plane deformations thanks to acquisition from coherent electromagnetic waves (light) between an object and the detector on the inspected surface in first, a standard state, and secondly, in a stressed state (due to e.g. thermal, vacuum, vibration excitation). The difference of the light registered between the two states delivers a shearogram which reveals down to nanometers deformations at the surface thanks to a change in the stiffness in the material [15]. Thin metal or composite panels and sandwich skins are good candidates for this technique in the frame of NDT inspections.

For NDE of mechanical bond strength, first tests conducted showed detectability of stiffness changes under certain conditions: heat applied at the surface of the bond caused a larger displacement in the case of a good bond [64]. Other tests showed that weak bonds detectable were in fact delaminations in the epoxy [82].

The detection of delaminations was assessed as feasible using shearography applied to epoxy composite exposed to piezo electrically and laser generated lamb waves [83].

### 4.2 Active Thermography

Active thermography is a well-established NDT technique already widely developed. It corresponds to the simulation of a thermal flow in the specimen to be examined and the

detection of the resulting temperature on the surface part with a sensitivity of mK. As an NDT technique, the active thermography was established unable to assess the presence of weak bond in composite specimens due to anisotropy of the composite material and the low response in the heat diffusion [16], [84]. It can however be suggested that with better resolution and improved tools, adhesive bond quality could be distinguished with active thermography. Activities focusing on this topic have been handled in the European project ENCOMB [85] and are not the focus of this work.

### 4.3 Monitoring of Damping and Vibration Frequencies

Vibrational techniques are quite known in the NDT domain with conventional time domain ultrasonics, ultrasonic spectroscopy, vibro-thermography or even sonic tests like tap tests, as seen in section 2.1.4. Each one of these methods is able to achieve good characterization of materials and locate small defects within. The approach of Yang et al [67] is based on the same principle but focus on a parameter which is not targeted by the previously cited methods: the monitoring of damping and vibration frequencies to provide a fast screening of the adhesively bonded structure. Damping is indeed a property considered very sensitive to micro-structural properties of the material, and so assumed to be an adequate technique for the monitoring of bondline quality. In their study, Yang et al. investigated the combination of the half power band method to evaluate the damping loss factor and the impulse-frequency response technique to measure vibration factors. In the case of weak adhesive bond in CFRP structure produced by the absence of surface pre-treatment by sanding, the observations were that nonlinear behavior predominates. The modal parameters were shown consistent with the theory observed with NLUS, that the nonlinear vibration behavior is amplitude dependent. Those conclusions enhanced the difficulty of characterizing the adhesive bond performances with such techniques and encouraged their use in the frame of physical defects instead [67].

## 5. LASER METHODS TO ASSESS ADHESIVE BONDING QUALITY

As another alternative, a major approach in the characterization of the adhesive bond strength is the use of high power lasers for the generation of ultrasonic waves or even shock waves in the bonded material. In the case of sonic waves, the principle is similar to the one of classical UT. In the case of shock waves, the principle is different: above a certain level of intensity, the shock wave generates over few nanoseconds a pressure high enough (up to megabars) to generate a dynamic damage in the material. This phenomenon is known under the name of spallation.

Originally developed for others purposes than adhesive bonding inspection, the use of laser beams has been significantly developed over the past decades. With this development, new fields of application including strength characterization for adhesive bonding appeared recently.

Several research groups dedicated to laser technologies are to be found in the literature and deserve attention for their respective activities. The following sections summarize these approaches.

## 5.1 Laser Ultrasonic

The research groups from the Centre National de Recherche du Canada (CNRC), Airbus Innovations France and Bremen's Institute for Applied Beam Technology (BIAS) have been working on the development of the laser ultrasonic.

The principle of the laser ultrasonic inspection method is defined as follow: a pulse laser sends single or multiple pulses of controlled magnitude which are absorbed by the material surface and generate a local heating. A thermos-elastic excitation is caused and induces an ultrasonic surface- and bulk- wave propagation in the material. It is the detection and capture of this thermos-elastic response that deliver information regarding to the state of the specimen [86]–[88].

An alternative approach is the laser tapping, which consists in focusing the thermal stresses produced by the laser in order to cause a lifting and bending effect, and so induce vibration of a potential debonded layer [89]. Both techniques can be used concurrently for more information on the inspected specimen. The principle of laser tapping is similar to the mechanical tap test where a hammer is used to knock on the structure and frequency shift induced by a shallow delamination is recorded. Kopylow et al. also pointed out that ultrasound wave can be distinguished between two regimes: non-destructive thermo elastic and ablative due to the power level of the laser [87].

Depending on which application is addressed for the laser tapping/laser ultrasonic system, the emission of the shock wave is done in the case of inspection of sandwich epoxy composite structures with use of a CO<sub>2</sub> TEA laser, which delivers pulse duration of 120 ns at around 10 μm wavelength for laser tapping. The excitation used is harmless for the material surface and purely elastic. For the laser ultrasonic use, a higher frequency range is used with an infrared wavelength 1,064 μm and pulses of tenths of ns width. The laser power is kept low to benefit from a high resolution in the power control adjustment and relatively low but have fine resolutions [86].

The detection of the ultrasound is performed with use of another laser: a Nd:YAG laser which delivers stable pulses of few dozen of μs duration at full width half maximum with the infrared 1,064 μm wavelength [87], [89]. Again here depending on the application, the scattered light emitted by the second laser is recorded by a different interferometer: Blouin et al. used a TWM photorefractive interferometer using an InP:Fe photorefractive crystal with response time of the interferometer (also called grating build-up time) of 10 ms fast enough to detect changes in the speckle pattern for the inspection of delamination in sandwich composite parts for frequency detection between 10 kHz and 1 MHz [90]. On the other hand, Campagne et al. and Kopylow et al. used a Confocal Fabry Perot (CFP) interferometer for laser ultrasonic and also a interferometer based on two-wave mixing (TWM) in a photorefractive GaAs crystal for laser tapping purposes with operating range between 10 kHz and 15 MHz [91].

The analysis of the received signal is processed as conventional ultrasonics so that A- B- and C-scans are made and analyzed for the defect recognition [87], [90], [91].

The results obtained with this method up to today are positive. The inspection of detached skin area in honeycomb sandwich structures which can be excited and brought to vibration like membranes due to short excitation pulses was successful [90], as well as the detection of all types of defects in composite materials [86]–[88].

The use of laser ultrasonic as a non-destructive technique have the advantage that they are contactless, in opposition to conventional ultrasonic inspection, which make them ideal tools for the inspection of complex parts [88], [90], [91]. Compared to the PAUT, the laser UT however only have one single probe due to the measuring laser spot and so, are much slower for the complete inspection of large structural parts.

Assessment of the quality of the adhesive bonds with Laser ultrasonic is considered to be relevant. Unfortunately, no literature is yet available on this particular topic.

## 5.2 Laser Shock Processing

In other regimes than ultrasonic waves generation, laser can be used for shock waves generation. In the late seventies, Vossen was one of the first to investigate the use of adhesion test with laser shock [92]. In the early eighties, Fairand et al. and Clauer et al. performed experiments with high power Q-switched neodymium laser for the hardening treatment of metallic parts through stress waves emitted by plasma. High energy pulses for the generation of surface pressures through plasma were studied.

Further investigations on this topic were conducted in the following decade. The workgroup of Gupta focused on testing of thin specimens and thin adhesive film [93], [93]–[95]. Successful, Gupta finally patented as first this technique in 1994 [96].

Over the years, laser techniques evolved to become a lot more efficient and allowed their use as new inspection tools. The techniques presented here are called LASer Adhesion Test (LASAT), developed by the CNRS, and Laser Bond Inspection (LBI), developed by LSP Technologies and Boeing. Their backgrounds are different but they both have the same principle. They use a shock wave generated by a plasma originating from a high power laser with short pulse on the front surface. In contrast to the ultra-/sound wave effects seen in the previous sections, a shock wave involves a compressing wave front propagating faster than sound and generating a violent discontinuity in the characteristic values of a medium state (thermodynamical and physical).

Figure A.8 represents the functioning principle of those techniques: a shock wave arises from an increasing high pressure. This shock wave propagates through the inspected structure in compression waves which are reflected when they reach the back surface. The crossing of the end of the incident compression wave and the release wave coming back from the rear surface generates the tensile forces at a precise depth in the material. It is then the tensile force, normal to plies or bondline that can induce a delamination or respectively, a debond [97]–[101].

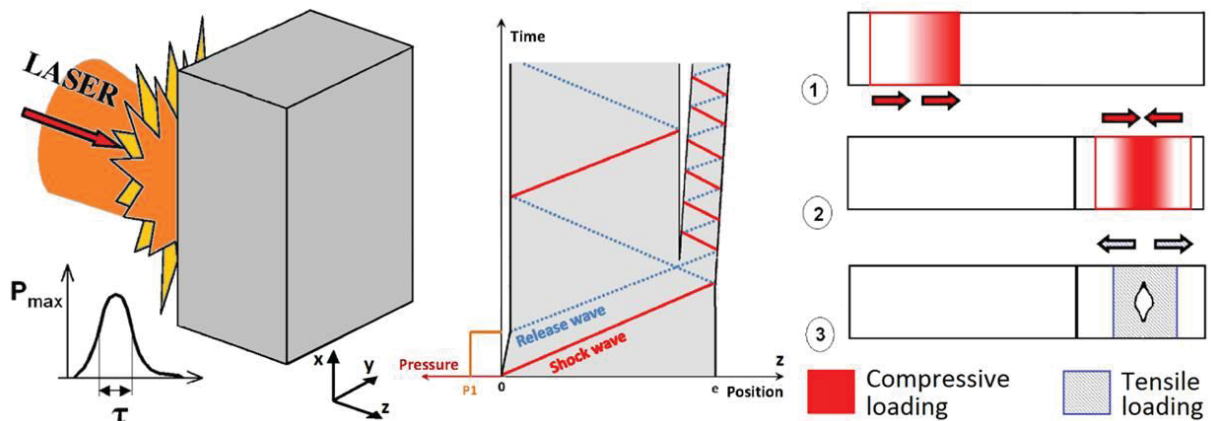


Figure A.8: Laser proof test functioning principle (case of defect generation) [102].

For the purpose of the adhesive bonding inspection, the concept of application for those techniques relies on the fact that a weak adhesive bond would be damaged by the tensile stress generated in the at the bondline-substrate interface whereas a sound adhesive bond would resist to above a precise level of stress induced by the shock wave [12], [103]–[105].

### 5.2.1 Laser Shock Adhesion Test (LASAT)

Tests with LASAT were performed for several applications: several PhD students working together on the LASAT system investigated the adhesion of coated systems and thin films, principally on thin metallic substrates [106], [107] and also in the frame of cold spray coatings [108]. They also started developing numerical modeling approaches for the shock wave phenomenon. These applications were successful with the very short pulse laser existing at that time. The short laser pulse generates a tensile stress close to the free surface of the substrate and so was adapted for the control of coatings.

Later on, Arrigoni et al. published also a comparative study of conventional adhesion test such as bulge and blister test with the LASAT [109]. The results obtained were consistent and indicated already a high potential for the laser adhesion test as a standalone technique with the characteristic of being a local and dynamic test. After a long time with focus on thin metallic substrates and metallic or ceramic coatings [110], the LASAT technique was extended to the domain of adhesive bonded structures, especially alu-epoxy-alu bonded assemblies studied by Laporte, also in the frame of his PhD Thesis [111]. Experiments on aluminum films bonded with epoxy involved a Nd:Glass laser delivering 25 J in nanosecond regime was used to attain the power density of range 1-300 GW/cm<sup>2</sup> [112]. This power could generate pressure in GPa range on the surface target. Jagdeesh et al. found a threshold value of 0,36 GPa for the delamination appearance in the case of epoxy bonded aluminum thin sheets, what value should not be considered as general for these kind of assemblies. This value was validated by simulation in their attempt to determine the threshold tensile stress [112]. The use of LASAT required power density in ns duration in the range of 1-500 GW/cm<sup>2</sup> [113].

In his experimentations with Alu-epoxy-alu, Arrigoni et al. managed to observe systematic delamination in the velocity signal peaks for power density higher than 4.7 GW/cm<sup>2</sup> [101]. It

was also stated thanks to the changes in the peaks visible with the FFT, that even for lower power density (around 3,7 GW/cm<sup>2</sup>) the adhesive bond was affected at the interface.

Introducing a new challenge due to the composite anisotropy, experiments were also performed on bulk epoxy composite materials to observe the behavior of the laminates with an exposure to different intensities ranging from 0,1 to 1340 GW/cm<sup>2</sup> with pulses each 3 or 10 ns [104], [114]–[116]. It was found that with much lower power density (1,03 GW/cm<sup>2</sup> in Gay's case), a delamination was already detectable in the laminate.

Below this value of about 1 GW/cm<sup>2</sup>, the compressive waves are not generating damages obviously and, it could be concluded that the stress wave propagates in the elastic regime without damaging the laminates. This result is encouraging since propagation of the compressive wave can be harmless to the CFRP laminate itself. Perton et al. emphasize that the “elastic limit for the carbon fiber is well above the rupture threshold of the epoxy” and the epoxy rupture is itself brittle at high strain rate, without any prior plastic deformation. The LASAT would hence be indeed a non-invasive and receivable NDT technique if a laser proof test is conducted at lower energy than the epoxy threshold and so do not generate any delamination or debond in the material [105]. Dynamic loads applied for the proof test are however to oppose to quasi-static conditions where the load can be around 10 times lower [101]. This remark was also done by Bossi et al. regarding the LBI [100].

The understanding of the shock wave propagation in the CFRP assemblies however was however not sufficient with these studies.

### 5.2.2 Understand the shock waves behavior in CFRP

For the application on CFRP assemblies, the understanding of shock phenomenon in composite materials was missing. This lack was the motivation for a thorough study focusing on the understanding of the dynamic behavior of composite materials. A parallel PhD thesis led by R. Ecault dealing with the Laser Shock adhesion Test (LASAT) technique ended in December 2013. This work is complementary to this study in the way that its scientific objectives included modeling the phenomenon in order to further adapt the technology to the composite applications.

To perform this study on composite materials, few laser sources of very high intensities and pulse length in the ns and ps range were tested. On top of these laser sources, pressured air lancers were used to allow longer shock waves generation. To monitor the shock wave propagation, a large range of time-resolved techniques such as the Velocimetry Interferometer for any reflectors (VISAR), similar velocimeters and shadowscopy were used. Other diagnosis tools for observations of damages post-shocks were including optical microscopy, confocal microscopy, x-ray radiography, DSC and DMA. Specimens were also inspected by means of ultrasounds in cooperation with a partner.

The first experimental approach consisted in testing the components of the CFRP separately: the epoxy resin without fibers and the composite substrates, in different plies orientation. In the first step, shear stresses could be detected during the shock wave propagations. For very low pulse length (fs range), neither residual stress nor microstructural changes could be observed [117]. For short pulse length (ns range), only residual stress in MPa range were detected [117]. The analyze of crossed plies composite substrates finally evidenced the

anisotropy of the spall depending on the ply orientations. The elliptic deformation was investigated by confocal microscopy applied on the CFRP back face. This ellipse study led to the creation of models for a possible characterization of the damage type based on the back face observation. The VISAR was tested and the reproducibility of its measurements could be demonstrated on all types of CFRP configurations. Also to be noticed, the VISAR evidenced increasing damages in the case of unidirectional laminates after repeated shocks [117].

In earlier studies, numerical modeling of the rear free surface velocity has also been performed, especially in the case of LASAT development, thanks to shock waves simulation codes such as SHYLAC, a 1D hydrodynamic Lagrangian Simulation Code and HUGO [112], [113], [118]. Based on the preliminary investigations, a consequent work was performed on numerical modeling in order to determine the stress, the rear free surface velocity and the shock waves nature in composite. Due to a lack of existing literature on dynamic mechanic on CFRP, a simple mechanical model, namely an elastic/orthotropic was chosen for the CFRP ply modeling. The Chang-Chang criteria chosen for damage modeling is also basic and shall describe well at least the damage initiation [117]. The parameters for the models were derived for experimental data from pure resin, unidirectional laminates and quasi-static material parameters. Anisotropy could be observed in stress propagation, but the essential transversal compressive/tensile stress, responsible for the spallation, was shown to be isotropic [117]. The selected models were based on restrictive hypothesis but seemed to fit the experimental results and were therefore used for the whole work.

Bonded composite assemblies were tested in symmetrical (two identical laminates bonded) and non-symmetrical (two different laminates bonded) configurations. The confocal microscopy was used to identify the damage present in the composite substrate while the Ultrasonic testing was used to identify the intensity thresholds to open the bondline. The observation of micro-cuts after impact was also performed to observe the cracks depending on the contamination states of the bonded samples. The shot parameters of the laser available revealed that the laser was inadapted to the geometry of both configuration of samples. Most of the samples tested feature damages in the composite laminate instead of the bondline. All tests could however be well correlated to the numerical model and so, validated it [117]. Additionally, ten repeated laser shocks at the same location with an intensity of ~30% of the debonding threshold did not reveal any structural changes or influence on the debonding threshold from the sample [117].

The whole study concludes with a final proposal towards improvements for a better adapted laser solution. It must be underlined that this proposal is mainly based on simulation from numerical modeling. The actual setup available could debond successfully an adhesive bond with an cohesive strength of 40% from the composite intralaminar cohesion [117]. To improve this performance, the optimal laser beam spot size was determined to be above 4 mm for the best tensile stress generation in the thickness [117]. The laser pulse duration can also be increased to hundreds of ns to localize the stress area near the bonded interface and rise the discrimination range from 40% to 100% [117]. The highest stress levels are however also located in other depth region in the laminates [117]. To prevent these inaccuracies, alternative setups are proposed and discussed [117]. It was however not possible to evaluate the propositions experimentally.

### 5.2.3 Laser Bond Inspection (LBI)

A similar other approach, called Laser Bond Inspection (LBI), has been patented by LSP Technologies and developed for Boeing in cooperation of US research programs [119]. A direct analogy to the LASAT laser parameters can be observed, however, the LBI was developed for the particular case of the bond inspection instead of coating inspection. Therefore, the laser settings such as the pulse duration and energy have been tailored to suit the requirements of bonded thick structures inspection. A Nd:Glass Laser manufactured by LSP Technologies itself has been used [120]. It produces a wavelength of 1054 nm (infrared) and a Gaussian like pulse ranging from 3 to 50 J with a duration ranging from 70 ns to 300 ns [98], [119].

In the case of the LBI, which focused more on inspection of adhesive bond than other applications, Bossi et al. established through numerous experimentations that the laminate failure prior to bond line failure was not to fear. Limitations regarding thickness of the adhesive bond due to attenuation of the stress were however suspected even if this issue may be irrelevant for weak bond inspection [98]. The same issue was again later on addressed with a maximal thickness of 23 mm for the whole samples and the satisfaction that no edge effects were influencing the measurement [99]. In comparison to the LASAT results, it is to be noted that the pulse duration enable the analysis of thicker laminates.

A “fatigue” effect was observed in the results where bond line delamination occurs at lower input/velocity if repeated pulse were applied at the same location, but no precise information about the conditions of tests were provided [98]. As a conclusion of the LBI results, it can be underlined that no mechanical performance reduction was measured (lap shear, DCB tests) on the specimens which were attested as damaged by ultrasonic scans. Finally, only very few information is available regarding modeling work from LSP and Boeing side [98].

These original techniques appear as the most promising for the inspection of adhesive bonds and the optimization of the integrated bonded design. A more detailed presentation of the characteristics of both techniques will be the object of the next chapter.

## 6. SUMMARY

The numerous literature sources evaluated in this paper clearly demonstrate that the adhesive bond quality is a critical parameter that cannot be assessed by any NDT techniques, yet. Several conventional methods are being optimized and developed for a better detection capability but up to today, no method can reliably and with a good reproducibility detect weak adhesive bonds, either on metals or on composite substrates.

Ultrasonic alternative methods (US spectroscopy; Nonlinear US; Guided Waves ; Oblique Incidence; Shear Wave Resonance; Laser Tapping/Ultrasonic, etc.) as well as laser proof tests (LASAT; LBI) and are reported as methods with high potential for the measurements of adhesive bond strength. Those methods have already been applied to the characterization of delamination, defects, or coating strength measurement in complex structures. Materials including bonded aluminum, epoxy composites laminates bulk or bonded, and even honeycomb sandwich panels have been tested based on those techniques. Further



development of all those methods needs however to be realized in the different research groups to reach significant achievements in the characterization of adhesive bond strength. The evolution in term of detection capability, resolution, etc. shall demonstrate the true potential for their use as an enabler for adhesive bonding as a major assembly technique.

The advanced studies already performed on adhesive bonded structures, either in composite or metal assemblies, however give a particular advantage to the techniques of laser proof test methods, the LASAT and LBI approaches. The efforts made for the characterization of laminates and composite bonded structures deserve a large interest from the aerospace companies. The state of the technic and its potential for improvement shall be investigated with relevant materials and 'reliable' weak adhesive bonds, generated by realistic causes in the aerospace fields such as contamination.

To develop the scientific approach, the following chapter will introduce the mechanic of shock wave propagation and transmission in a medium. The interaction shock wave-medium will be presented in order to ease the understanding of the technique. The chapter B will also present a review of the most important parameters for the application of laser proof test on an adhesive bonded structure.

**REFERENCES – CHAPTER A**

- [1] C. Bockenheimer, D. Fata, W. Possart, M. Rothenfusser, U. Netzelmann, und H. Schaefer, „The method of non-linear ultrasound as a tool for the non-destructive inspection of structural epoxy-metal bonds--a résumé“, *Int. J. Adhes. Adhes.*, Bd. 22, Nr. 3, S. 227–233, 2002.
- [2] H. Simon, „Assemblage par collage - Joining by adhesive bonding“, *Techniques de l'ingénieur*. S. 16, 1994.
- [3] P. Cognard, „Collage des matériaux: Mécanismes & Classification des colles - Adhesive joining: mechanisms & adhesive classification“, *Techniques de l'ingénieur*, Bd. 4. 2002.
- [4] R. D. Adams und P. Cawley, „A review of defect types and nondestructive testing techniques for composites and bonded joints“, *NDT Int.*, Bd. Vol. 21, Nr. 4, S. 208–222, Aug. 1988.
- [5] T. Stöven, „Rivetless Aircraft Assembly - a dream or feasible concept“, gehalten auf der Eucomas 2010, Berlin, Mai-2010.
- [6] G. M. Light und H. Kwun, „Nondestructive Evaluation of Adhesive Bond Quality: State of the Art Review“, NONDESTRUCTIVE TESTING INFORMATION ANALYSIS CENTER SAN ANTONIO TX, San Antonio, Texas, State of the art review SwRI Project 17-7958-838, 1989.
- [7] T. Stöven, „CFRP-Bonding - Seminar Composites und Kleben“, gehalten auf der Seminar Composites und Kleben, IFAM Bremen, 21-Nov-2006.
- [8] P. Cognard, „Collage des composites, Secteur aéronautique“, *Techniques de l'ingénieur*. Editions T.I., S. 12, 2010.
- [9] G. D. Davis, „Contamination of surfaces: Origin, detection and effect on adhesion“, *Surf. Interface Anal.*, Bd. 20, Nr. 5, S. 368–372, 1993.
- [10] S. Markus, R. Wilken, und S. Dieckhoff, „Fehlervermeidung durch Inline-Monitoring des Oberflächenzustandes“, *Adhäsion Kleb. Dicht.*, Bd. 50, Nr. 4, S. 20–22, 2006.
- [11] R. D. Adams und B. W. Drinkwater, „Nondestructive testing of adhesively-bonded joints“, *NDT E Int.*, Bd. 30, Nr. 2, S. 93–98, Apr. 1997.
- [12] E. Nottorf, S. Engelstad, und M. Renieri, „Certification Aspects of Large Integrated Bonded Structure“, gehalten auf der ASIP Conference, San Antonio, Texas, 30-Sep-2006.
- [13] C. Scarponi und G. Briotti, „Ultrasonic technique for the evaluation of delaminations on CFRP, GFRP, KFRP composite materials“, *Compos. Part B Eng.*, Bd. 31, Nr. 3, S. 237–243, Apr. 2000.
- [14] C. Bockenheimer und B. Valeske, „Non-destructive tests for bonded joints - European Adhesive Engineer - EAE“, gehalten auf der Bonding in Bremen, Certified training at the Center for Bonding Technology, Bremen, 2006.
- [15] T. Wilhelm, M. Hinnen, W. Schmidt, J. Montnacher, und A. Verl, „Produktionstaugliche Methode zur Quantifizierung der Adhäsionseigenschaften“, *Adhäsion Kleben&Dichten*, Bd. JG 54, Nr. June 2010, S. 14–21, Juni-2010.
- [16] J. Baumann und U. Netzelmann, „Zerstörungsfreie Prüftechniken für Materialverbunde“, *Zerstörungsfreie Prüftechniken für Materialverbunde* ISSN 0948-1427, Jan. 2003.
- [17] C. C. H. Guyott, „The Non-destructive Testing of Adhesively Bonded Structure“, Doctor Thesis, Imperial College London, London SW7, 1986.
- [18] A. Higgins, „Adhesive bonding of aircraft structures“, *Int. J. Adhes. Adhes.*, Bd. 20, Nr. 5, S. 367–376, 2000.
- [19] C. Garnier, M.-L. Pastor, F. Eyma, und B. Lorrain, „The detection of aeronautical defects in situ on composite structures using Non Destructive Testing“, *Compos. Struct.*, Bd. 93, Nr. 5, S. 1328–1336, Apr. 2011.

- [20] V. M. Karbhari, *Non-destructive evaluation (NDE) of polymer matrix composites: techniques and applications*. Cambridge, UK; Philadelphia, PA: Woodhead Publishing, 2013.
- [21] B. Plank, F. Ellert, J. Gruber, C. Gusenbauer, und J. Kastner, „Detektion von Fehlern in kohlenstofffaserverstärkten Kunststoffen mittels Sichtprüfung, Ultraschallprüfung, Radioskopie, aktiver Thermografie und Röntgen Computertomografie“, in *ZfP in Forschung, Entwicklung und Anwendung. DGZfP-Jahrestagung 2013. CD-ROM*, 2013, S. 9.
- [22] B. Valeske, C. Bockenheimer, und R. Henrich, „New NDT Approach for Adhesive Composite Bonds“, *NDT APPLICATIONS 1*, S. 203–209, 05-Dez-2008.
- [23] W. Arnold, „Nondestructive Determination of the Strength of Adhesive Joints“, 1996.
- [24] W. Arnold und N. Meyendorf, „Nondestructive Testing of Adhesive Joints“, 1998.
- [25] C. Bischof und W. Possart, *Adhesion: Theoretische und experimentelle Grundlagen*. Akademie-Verlag, 1983.
- [26] C. Bretton und G. Villoutreix, „Familles d'adhésifs et caractérisation d'un collage structural“, *Techniques de l'ingénieur*. S. 16, 2005.
- [27] F. J. Boerio, B. Roby, R. G. Dillingham, und R. H. Bossi, „Effect of surface engineering processes on the surface properties and adhesive bonding of graphite/epoxy composites“, in *International SAMPE Technical Conference*, Cincinnati, OH, 2007.
- [28] S. N. Gorb und K. Koch, „From sticky to slippery: Biological and biologically-inspired adhesion and friction“, *Beilstein J. Nanotechnol.*, Bd. 5, S. 1450–1451, 2014.
- [29] J. D. Minford und A. J. Kinloch, „Adhesives - Durability of structural adhesives“, in *Durability of structural adhesives*, Applied Science Publishers LTD., Springer, 1983, S. 135–215.
- [30] R. D. Adams, J. Comyn, und W. C. Wake, *Structural Adhesive Joints in Engineering*, 2nd Aufl. Springer, 1997.
- [31] K. L. DeVries, „Environmental Effects“, in *Engineered Materials Handbook: Adhesive and Sealants*, ASM international., Bd. 3, USA: Dostal C.A., 1999, S. 613–681.
- [32] C. Bockenheimer, „Epoxid und Aluminium im Klebverbund nach mechanischer Vorbehandlung und nach Alterung“, Universität des Saarlandes, Saarbrücken, 2003.
- [33] T. Rieck, „Einfluss unterschiedlicher Kontaminationen auf den Klebeprozess“, Master-Thesis, Hochschule Aalen - Studiengang: Produktentwicklung und Fertigung, Erding, 2011.
- [34] D. Lévéque, A. Schieffer, A. Mavel, und J.-F. Maire, „Analysis of how thermal aging affects the long-term mechanical behavior and strength of polymer-matrix composites“, *Compos. Sci. Technol.*, Bd. 65, Nr. 3–4, S. 395–401, März 2005.
- [35] N. Chobaut, „Heat damage detection and assessment in CFRP by means of Extended-NDT“, Airbus Operations GmbH, Universität des Saarlandes, Fraunhofer IZFP, Bremen, „Diplomarbeit“ report, Sep. 2010.
- [36] S. Eibl und J. Wolfrum, „Prospects to separately estimate temperature and duration of a thermal pre-load on a polymer matrix composite“, *J. Compos. Mater.*, S. 0021998312460714, Okt. 2012.
- [37] N. Chobaut, „Heat damage detection and assessment in CFRP by means of Extended-NDT - Basic understanding and development of test procedure“, Airbus Operations GmbH, Universität des Saarlandes, Fraunhofer IZFP, Bremen, „Studienarbeit“ report, Juni 2010.
- [38] G. A. LaPlante, A. V. B. Ouriadov, P. C. Lee-Sullivan, und B. J. . Balcom, „Anomalous moisture diffusion in an epoxy adhesive detected by magnetic resonance imaging“, *J. Appl. Polym. Sci.*, Bd. 109, Nr. 2, S. 1350–1359, 2008.
- [39] W. T. K. Stevenson, I. Alcalen, und S. Lamia, „Quantifying methods for the evaluation of carbon-based composite surfaces for subsequent adhesive bonding“, *Airframer - J. Aircr.*, S. 3, Sep. 2006.

- [40] R. Vodicka, B. Nelson, J. van der Berg, und R. Chester, „Long-Term Environmental Durability of F/A-18 Composite Material“, DSTO Aeronautical and Maritime Research laboratory, Melbourne Victoria 3001 Australia, DSTO-TR-0826, 1998.
- [41] S. Kajorncheappunngam, „The Effects of Environmental Aging on the Durability of Glass/Epoxy Composites“, West Virginia University, Morgantown, West Virginia, 1999.
- [42] M. Sarambe, „Detection and assessment of moisture content in CFRP by means of Extended-NDT - Basic understanding and development of test procedure“, Airbus Operations GmbH, Universität des Saarlandes, Fraunhofer IZFP, Bremen, Studienarbeit „Report“, Juni 2010.
- [43] M. C. Lee und N. A. Peppas, „Water transport in graphite/epoxy composites“, *J. Appl. Polym. Sci.*, Bd. 47, Nr. 8, S. 1349–1359, 1993.
- [44] W. M. Banks, F. Dumolin, S. T. Halliday, D. Hayward, Z.-C. Li, und R. A. Pethrick, „Dielectric and mechanical assessment of water ingress into carbon fibre composite materials“, *Comput. Struct.*, Bd. 76, Nr. 1–3, S. 43–55, Juni 2000.
- [45] J. S. R. Giguère, „Damage Mechanisms and Nondestructive Testing in the Case of Water Ingress in CF-18 Flight Control Surfaces“, Defence R&D Canada, Canada, Technical Memorandum DCIEM TM 2000-098, Aug. 2000.
- [46] B. M. Parker und R. M. Waghorne, „Surface pretreatment of carbon fibre-reinforced composites for adhesive bonding“, *Jt. Fibre-Reinf. Plast.*, Bd. Vol. 13, Nr. 3, S. 280–288, Juli 1982.
- [47] J. Bishopp, „A Review of Current Trends in Surface Pretreatment prior to Structural Adhesive Bonding“, gehalten auf der MMS 7, MMS 8 and MMS 11 IAG Meeting, Teddington, Middlesex, Nov-2003.
- [48] G. Wachinger, C. Thum, L. Llopart, A. Maier, H. Wehlan, und T. Stöven, „New Trends in CFRP Treatment and Surface Monitoring for Automated Structural Adhesive Bonding“, gehalten auf der International Conference on Composite Materials ICCM17, Edinburgh, 2009.
- [49] C. Mueller-Reich, R. Wilken, und S. Kaprolat, „Bonding of plastics: Well-bonded despite residual release agents“, *Adhes. SEALANTS*, Bd. 3/2011, S. 36 – 41, 2011.
- [50] J. K. Kim und D. G. Lee, „Adhesion characteristics of plasma-surface-treated carbon fiber-epoxy composite with respect to release films used during demolding“, *J. Adhes. Sci. Technol.*, Bd. 18, Nr. 4, S. 473–494, 2004.
- [51] J. C. Osborne, „Improving the Bond Strength of a Composite Repair with an Atmospheric Plasma Treatment“, Graduate Faculty of North Carolina State University, Raleigh, North Carolina, Master Thesis, 2011.
- [52] B. M. Parker und R. M. Waghorne, „Testing epoxy composite surfaces for bondability“, *Surf. Interface Anal.*, Bd. Vol. 17, Nr. 7, S. 471–476, Juni 1991.
- [53] M. Wetzel, T. Rieck, und J. Holtmannspötter, „Contamination in adhesive bonding for aviation applications: Detection and effect of adhesion-limiting contaminations“, *Adhes. Adhes.*, Nr. 2011–03, S. 29 – 33, 2011.
- [54] ABITAS, *ABiTAS Advanced Bonding Technologies for Aircraft Structures - Annex I - Description of Work*. 2006.
- [55] S. Markus, C. Tornow, S. Dieckhoff, M. Boustie, R. Ecault, L. Berthe, und C. Bockenheimer, „Extended Non-Destructive Testing of Composite Bonds“, SAE International, Warrendale, PA, 11 ATC-0492 2011-01-2514, Okt. 2011.
- [56] L. H. Pearson, „Diffuse reflectance IR spectroscopy for bonding surface contamination characterization“, *Rev. Prog. Quant. Nondestruct. Eval. Proc. 17th Annu. Rev.*, Bd. 10A, S. 581–588, Juli 1990.
- [57] ASTM international, „ASTM D\_897-08 Standard test method for tensile properties of Adhesive bonds“. 2008.
- [58] L. F. M. da Silva, D. A. Dillard, B. Blackman, und R. D. Adams, *Testing Adhesive Joints: Best Practices*. John Wiley & Sons, 2013.

- [59] ISO Standard, „ISO 25217:2009 Adhesives -- Determination of the mode 1 adhesive fracture energy of structural adhesive joints using double cantilever beam and tapered double cantilever beam specimens“. ISO International, 23-Apr-2009.
- [60] ISO Standard, „ISO 15024:2001 Fibre-reinforced plastic composites -- Determination of mode I interlaminar fracture toughness, GIC, for unidirectionally reinforced materials“. ISO International, 12-Jan-2001.
- [61] ISO Standard, „ISO 14130:1997 Fibre-reinforced plastic composites -- Determination of apparent interlaminar shear strength by short-beam method“. ISO International, 15-Dez-1997.
- [62] V. Weise, C. Scruby, E. Birt, und L. Jones, „Report on "Kissing Bond and Environmental Degradation Detection using Nonlinear Ultrasonics“, QinetiQ Ltd, QinetiQ, Farnborough, Report from METEOR Project QINETIQ/FST/CR023457, Mai 2002.
- [63] C. J. Brotherhood, B. W. Drinkwater, und F. J. Guild, „The Effect of Compressive Loading on the Ultrasonic Detectability of Kissing Bonds in Adhesive Joints“, *Journal of Nondestructive Evaluation*, S. 95–104, 01-Sep-2002.
- [64] P. Marty, N. Desai, und J. Andersson, „NDT of kissing bond in aeronautical structures“, gehalten auf der 16th World Conference of NDT Proceedings, Linköping, Sweden, 2004, S. 8.
- [65] N. Decourcelle und E. J. C. Kellar, „Development of a methodology to produce samples and ultrasonic techniques for kissing bonds in adhesive joints“, *Research Reports for Industrial Members of TWI*, Granta Park, Cambridge, UK, S. 1–12, Sep-2009.
- [66] C. Jeenjitkaew, Z. Luklinska, und F. Guild, „Morphology and surface chemistry of kissing bonds in adhesive joints produced by surface contamination“, *Int. J. Adhes. Adhes.*, Bd. Vol. 30, Nr. 7, S. 643 – 653, Okt. 2010.
- [67] S. Yang, L. Gu, und R. F. Gibson, „Nondestructive detection of weak joints in adhesively bonded composite structures“, *Compos. Struct.*, Bd. 51, Nr. 1, S. 63–71, 2001.
- [68] M. F. Zaeh, C. Thiemann, S. Boehm, C. Srajbr, C. Lammel, und J. Noak, „Cost-effective defect detection in bonded glass element modules - NDT for Adhesives Bond“, *Adhäsion Kleben&Dichten*, Nr. October 2009, S. 30–34, Okt-2009.
- [69] V. M. Karbhari, H. Kaiser, R. Navada, K. Ghosh, und L. Lee, „Methods for Detecting Defects in Composite Rehabilitated Concrete Structures“, Oregon Department of Transportation, Research Unit, 200 Hawthorne SE, Suite B-240, Salem, Oregon 97301-5192, University of California, San Diego, Final Report FHWA-OR-RD-05-09, Apr. 2005.
- [70] E. Wall, R. Sullivan, und J. Carpenter, „Progress Report for Automotive Lightweighting Materials Volume II“, U.S Department of Energy, Washington, DC 20585-0121, Progress report FY 2006 Progress Report, Okt. 2007.
- [71] M. Engholm, „A Narrowband Ultrasonic Spectroscopy Technique for the Inspection of Layered Structures“, Licence, Uppsala Universitet, Sweden, 2006.
- [72] J. Barroeta-Robles, R. Cole, und J. M. Sands, „Development of Controlled Adhesive Bond Strength for Assessment by Advanced Non-Destructive Inspection Techniques“, gehalten auf der SAMPE 2010, Seattle, WA, 2010, S. 15.
- [73] M. Jastrzebski, A. Sinclair, und J. Spelt, „Mechanical and Industrial Engineering, Development of Adhesive Bonds with Reduced Strength as Ultrasonic NDE Benchmarks“, gehalten auf der Canadian Aeronautics and Space Institute 18th Aerospace Structures and Materials Symposium, Toronto, Canada, 2005, Bd. E.
- [74] M. Hinchliffe, „Characterisation of Bond Line Porosity“. 2008.
- [75] R. Chance, „Nondestructive Inspection (NDI) of Reduced Strength Bonds“, Grumman Corporation, Bethpage, New York, New York, Final report DOT/FAA/CT-93/42, 1994.
- [76] R. . Smith, V. . Weise, und R. . Dalton, „The Potential for Advanced Ultrasonic Detection of Weak Adhesion“. NDE Group - QinetiQ Ltd, 2003.

- [77] S. Hirsekorn, A. Koka, A. Wegner, und W. Arnold, „Quality Assessment of Bond Interfaces by Nonlinear Ultrasonics Transmission“, *Review of progress in Quantitative Nondestructive Evaluation*, S. 1367 – 1374, 2000.
- [78] S. I. Rokhlin, N. Wang, O. Lobkis, und J. H. Cantrell, „Development of linear and nonlinear ultrasonic methodology for quantitative assessment of environmental degradation of adhesive bonds“, The Ohio State University, 2010.
- [79] S. U. Fassbender, M. Kröning, und W. Arnold, „Measurement of adhesion strength using nonlinear acoustics“, gehalten auf der Materials Science Forum, 1996, Bd. 210–213, S. 783 – 790.
- [80] D. Yan, B. W. Drinkwater, und S. A. Neild, „Measurement of the ultrasonic nonlinearity of kissing bonds in adhesive joints“, *NDT E Int.*, Bd. 42, Nr. 5, S. 459–466, Juli 2009.
- [81] A. J. Croxford, P. D. Wilcox, B. W. Drinkwater, und P. B. Nagy, „The use of non-collinear mixing for nonlinear ultrasonic detection of plasticity and fatigue“, *J. Acoust. Soc. Am.*, Bd. 126, Nr. 5, S. EL117–EL122, Nov. 2009.
- [82] P. Pandurangan und G. D. Buckner, „Defect identification in GRID-LOCK® joints“, *NDT E Int.*, Bd. 40, Nr. 5, S. 347–356, Juli 2007.
- [83] A. Hildebrand, O. Focke, und C. v Kopylow, „Full Field Measurement of Transient Lamb Wave Propagation in Carbon Fibre Reinforced Plastics Using Digital Sherography“, gehalten auf der The Sixteenth International Congress on Sound and Vibration, Krakow, Poland, 2009.
- [84] T. Zweschper, A. Dillenz, und G. Busse, „NDE of adhesive joints and riveted structures with lock-in thermography methods“, in *Proceedings of SPIE Thermosense XXIII*, 2001, Bd. 4360, S. 567–573.
- [85] B. Ehrhart, U. Netzelmann, G. Walle, und B. Valeske, „Quality assessment of CFRP bonded structures with active thermography techniques“, gehalten auf der 5th International Symposium on NDT in Aerospace, Singapore, 2013.
- [86] B. K. Siu, „System and method for laser ultrasonic bond integrity evaluation“, US 20020043109 A1, 18-Apr-2002.
- [87] C. von Kopylow, O. Focke, und M. Kalms, „Laser ultrasound: a flexible tool for the inspection of complex CFK components and welded seams“, 2007, Bd. 6616, S. 66163J.
- [88] B. Campagne, „Laser NDT for Bonding“, EADS Innovation Works, Suresnes, Airbus Report for EADS Innovation Works 2011-31807/1-IW/SP, Feb. 2011.
- [89] A. Blouin, B. Campagne, C. Néron, und J. P. Monchalain, „Detection of skin disbond in honeycombs and coating detachment by a laser acoustic technique“, *Quantitative Nondestructive Evaluation*, Bd. 26, 2007.
- [90] A. Blouin, C. Néron, B. Campagne, und J.-P. Monchalain, „Applications of laser tapping and laser ultrasonics to aerospace composite structures“, *Insight Non-Destr. Test. Cond. Monit.*, Bd. 52, Nr. 3, S. 130–133, 2010.
- [91] B. Campagne und H. Voillaume, „Development of Laser Ultrasonics: Application to Complex Shape Aeronautical Parts“, gehalten auf der 1st International Symposium on Laser Ultrasonics: Science, Technology and Applications, Montreal, Canada, 2008.
- [92] J. L. Vossen, „Adhesion measurement of thin films, thick films and bulk coatings“, *ASTM Spec. Tech. Publ*, S. 122–131, 1978.
- [93] V. Gupta und J. Yuan, „Measurement of interface strength by the modified laser spallation technique. I. Experiment and simulation of the spallation process“, *J. Appl. Phys.*, Bd. 74, Nr. 4, S. 2388–2396, Aug. 1993.
- [94] V. Gupta und J. Yuan, „Measurement of interface strength by the modified laser spallation technique. II. Applications to metal/ceramic interfaces“, *J. Appl. Phys.*, Bd. 74, Nr. 4, S. 2397–2404, Aug. 1993.
- [95] V. Gupta, J. Yuan, und A. Pronin, „Measurement of interface strength by the modified laser spallation technique. III. Experimental optimization of the stress pulse“, *J. Appl. Phys.*, Bd. 74, Nr. 4, S. 2405–2410, Aug. 1993.

- [96] V. Gupta, „A system and method for measuring the interface tensile strength of planar interfaces“, WO1994020829 A1, 15-Sep-1994.
- [97] R. Bossi, K. Housen, W. Shepherd, und M. Voss, „Bond Strength Measurement System Using Shock Loads“, US 2003/0079552 A1, 01-Mai-2003.
- [98] R. Bossi, K. Housen, und W. Shepherd, „Application of Stress Waves to Bond Inspection“, *SAMPE Proc. Long Beach CA*, S. 1–14, 2004.
- [99] R. Bossi, K. Housen, und C. Walters, „Laser Bond Inspection Device for Composites: Has the Holy Grail Been Found?“, *NTIAC Nondestruct. Test. Inf. Anal. Cent. - Newsl.*, Bd. 30, Nr. 2, 2005.
- [100] R. Bossi, „Assessing the Quality of Bonded Joints“, gehalten auf der ASIP, Xan Anotnio, TX, 28-Nov-2006.
- [101] M. Arrigoni, S. E. Kruger, A. Blouin, D. Lévesque, B. Arsenault, J. P. Monchalin, M. Boustier, und L. Berthe, „Adhesive Bond Testing by Laser Induced Shock Waves“. National Research Council Canada, Industrial Materials Institute, 25-Okt-2008.
- [102] R. Ecault, M. Boustie, F. Touchard, F. Pons, L. Berthe, L. Chocinski-Arnault, B. Ehrhart, und C. Bockenheimer, „A study of composite material damage induced by laser shock waves“, *Compos. Part Appl. Sci. Manuf.*, Bd. 53, S. 54–64, Oktober 2013.
- [103] R. Bossi, „Nondestructive Testing for the Adhesion Strength“. AdhesionSociety, 2010.
- [104] R. Ecault, M. Boustie, F. Touchard, L. Berthe, L. Chocinski, B. Ehrhart, und C. Bockenheimer, „Damage of composite materials by use of laser driven shock waves“, gehalten auf der Proceedings of the American Society for Composites 26th Annual Technical Conference/2nd Joint US-Canada Conference on Composites, Montreal, Quebec, Canada, 2011, S. 14.
- [105] M. Pertou, A. Blouin, und J.-P. Monchalin, „Adhesive bond strength evaluation in composite materials by laser-generated high amplitude ultrasound“, *J. Phys. Conf. Ser.*, Bd. 278, Nr. 012044, Jan. 2011.
- [106] M. Arrigoni, „Étude de l'influence des rugosités d'interface, de porosités et de l'épaisseur d'échantillon sur la propagation des chocs laser dans des systèmes revêtus. application au procédé LASAT (laser adhérence test)“, E.N.S.M.A. et Faculté des sciences fondamentales et appliqués, Poitiers, PhD, Dez. 2004.
- [107] C. Bolis, „Etude numérique et expérimentale de la séparation par chocs brefs d'interface de revêtements multi-couches. Application au test d'adhérence par chocs laser.“, E.N.S.M.A. et Faculté des sciences fondamentales et appliqués, Poitiers, PhD, Dez. 2004.
- [108] M. Jeandin, D. Christoulis, F. Borit, M. H. Berger, S. Guetta, G. Rolland, V. Guipont, E. Irissou, J. G. Legoux, C. Moreau, M. Nivard, L. Berthe, M. Boustie, W. Arnold, K. Sakaguchi, Y. Ichikawa, K. Ogawa, und S. Costil, „Lasers and Thermal Spray“. 2009.
- [109] M. Arrigoni, S. Barradas, M. Braccini, M. Dupeux, M. Jeandin, M. Boustie, C. Bolis, und L. Berthe, „A comparative study of three adhesion tests (EN 582, similar to ASTM C633, LASAT (LASer Adhesion Test), and bulge and blister test) performed on plasma sprayed copper deposited on aluminium 2017 substrates“, *J. Adhes. Sci. Technol.*, Bd. 20, Nr. 5, S. 471–487, 2006.
- [110] L. Berthe, M. Arrigoni, M. Boustie, J. P. Cuq-Lelandais, C. Broussillou, G. Fabre, M. Jeandin, V. Guipont, und M. Nivard, „State-of-the-art laser adhesion test (LASAT)“, *Nondestruct. Test. Eval.*, Bd. 26, Nr. 3–4, S. 303–317, 2011.
- [111] D. Laporte, „Analyse de la réponse d'assemblages collés sous des sollicitations en dynamique rapide. Essais et modélisations“, E.N.S.M.A. et Faculté des sciences fondamentales et appliqués, Poitiers, PhD, Okt. 2011.
- [112] R. Jagdheesh, M. Boustie, L. Berthe, M. Arrigoni, und M. Jouiad, „Interfacial Strength Measurement of Bonded Aluminum Foils by Laser-Driven Shock Waves“, *Surface Modification Technologies XXII*, S. 3–10, 2009.
- [113] C. Bolis, L. Berthe, M. Boustier, M. Arrigoni, S. Barradas, und M. Jeandin, „Physical approach to adhesion testing using laser-driven shock waves“, *J. Appl. Phys.*, Bd. 40, S. 3155 – 3163, 2007.

- [114] M. Boustie, E. Gay, L. Berthe, M. Arrigoni, J. Radhakrishnan, T. De Résséguier, A. Blouin, J.-P. Monchalin, S. Kruger, M. Perton, A. Johnston, R. Cole, und E. Buzaud, „LAsEr Shock Adhesion Test (LASAT) of composite materials for aerospace“, gehalten auf der 23rd Int. Conf. on Surface Modification Technologies (SMT23), Madras, India, 2009.
- [115] E. Gay, L. Berthe, M. Boustie, M. Arrigoni, J. P. Monchalin, M. Perton, A. Blouin, A. Johnston, R. Cole, J. Barroeta-Robles, und E. Buzaud, „Experimental Investigation of a Composite Behaviour under short Laser-Shock Loading“, 2010.
- [116] E. Gay, „Experimental and Numerical Investigation of Composite Behaviour at High Strain Rate“, 2010.
- [117] R. Ecault, „Experimental and numerical investigations on the dynamic behaviour of aeronautic composites under laser shock - Optimization of a shock wave adhesion test for bonded composites“, E.N.S.M.A. - Sciences et Ingénierie en Matériaux, Mécanique, Energétique et Aéronautique, Poitiers, PhD, 2013.
- [118] E. Gay, „Experimental and Numerical Investigation of Composite Behaviour at High Strain Rate“, 2010.
- [119] D. W. Sokol, C. T. Walters, J. L. Dulaney, und S. M. Toller, „Laser System and Method for Non-destructive Bond Detection and Evaluation“, US 2005/0120803 A1, 09-Juni-2005.
- [120] D. W. Sokol, C. T. Walters, H. M. Epstein, A. H. Clauer, J. L. Dulaney, und M. O’Loughlin, „Quality Control Plasma Monitor for Laser Shock Processing“, US 2001/0045416 A1, 29-Juni-2001.



# CHAPTER B: MECHANICS OF SHOCK WAVES AND LASER PROOF TEST PARAMETERS

## TABLE OF CONTENTS

1. INTRODUCTION .....	44
2. ABOUT SHOCK WAVES.....	44
2.1 Generation of shock wave into the material.....	45
2.1.1 Definition of a shock wave.....	45
2.1.2 Shock induction.....	45
2.1.3 Shock wave sources - interactions with direct/indirect irradiation .....	46
2.2 Mechanics of shock waves propagation – theoretical approach .....	47
2.2.1 Equations of Rankine-Hugoniot.....	47
2.2.2 Characteristic shock curves.....	49
2.2.3 Mechanical models for composite materials .....	50
2.3 Interaction of shock waves in bonded structures .....	52
2.3.1 Propagation and transmission of shocks .....	52
2.3.2 Tension and Spallation.....	55
2.3.3 Other Effects .....	56
3. TECHNOLOGY PRINCIPLE (STATE OF THE TECHNOLOGIES) .....	58
3.1 The essential laser source parameters.....	58
3.1.1 The laser wavelength .....	58
3.1.2 The pulse duration .....	59
3.1.3 The energy/intensity of the laser beam.....	60
3.2 The plasma generation: confinement and sacrificial layer .....	62
3.3 The integrated diagnosis techniques .....	64
4. SUMMARY .....	68
REFERENCES – CHAPTER B.....	69

## 1. INTRODUCTION

This chapter presents the principle and phenomenon involved in the methods of laser proof tests, either the LASAT-CNRS or LBI-LSP whose principles are the same. The principle introduced here is the generation of a shock waves and their propagation in the substrate. The following content is based on information based on existing literature to explain how this technique should be applied on CFRP structures for bondline proof tests and to understand the corresponding physical principle.

In the first part, the physic behind shock waves is introduced. This involves:

- i. the mechanisms of shock wave generation in the material,
- ii. the propagation of the wave in the material and the response with the defects, back wall and induced response wave,
- iii. the interaction of the waves in the composite material, effect of propagation in Epoxy (observations in monolithic laminate), mechanical effects (compression & tension).

In the second part, the constituting elements of the laser proof test approaches and their principle of functioning is described:

- iv. the parameters of the laser source,
- v. the plasma generation and its confinement with an overlay, and the sacrificial layer which protects the surface and ensures the integrity of a surface state for the shot,
- vi. the existing diagnosis implemented along with each technology (VISAR, EMAT)

Finally, the approach for the use of Laser Proof Test as well as the challenges have been presented in this chapter and allow the reader to understand in which directions the next chapters are going i.e. the generation of weak bonds for having reliable samples, the setup of a test program to evaluate the challenges of the technique.

## 2. ABOUT SHOCK WAVES

The study of shock waves is as the study of adhesive bonding, closely linked to technical progress entailed by wars, and especially here, the evolution of bombs. From early ages and first experiments with saltpeter to the atomic bomb, all bombs are based on the generation of a shock wave to shock and so destroy. The arise of the electricity and laser technologies allowed later the capacity to focus photons enough to provoke a local but intense pressure increase, showing the way to several applications from laser peening (local hardening) to laser adhesion tests where the shock wave is the mean used for testing the adhesion quality.

This part will therefore present how shock waves are generated and how it is possible to describe them and their interaction with the medium.

## 2.1 Generation of shock wave into the material

### 2.1.1 Definition of a shock wave

A shock wave is the propagation of a “discontinuity” in the thermodynamic characteristic values of a medium.

An analogy to the mechanical sound wave can be made: sound waves travelling in material have a speed depending on the pressure discontinuity amplitude. A shock wave is a mechanical wave generated when the pressure applying over the time is very high and increasing over a very short time, almost instantaneously. When these conditions are fulfilled, the pressure ramp of the sound wave is so straight that a shock wave is generated. This is the discontinuity of the thermodynamic characteristics. Once generated, the shock wave travels into the medium rapidly and applies serious mechanical constraints to the medium.

### 2.1.2 Shock induction

Shock waves can be induced via several approaches: from the simple mechanical impact gun (low strain rate) through the air pressured canon systems (high strain rate) to laser (ultra high strain rate), a wide range of shock regimes can be produced.

When a high intensity pulsed power laser beam ( $\lambda$  typically around 1064 nm) interacts with a material surface, a significant energy is being absorbed by the material. The laser wavelength is a key characteristic for the absorption and is detailed later in this chapter. The energy deposition increases the temperature locally at the upper  $\mu\text{m}$ . If the energy is high enough (above  $10^9 \text{ W/cm}^2$ ), a plasma is generated.

The expansion of this plasma generates a pressure at the surface which itself leads to the shock wave. It may be noticed that the energy used for the shock has a direct influence on the pressure generated at the surface, and so, on the shock wave intensity.

The energy intensity is an important parameter that will be used in the next chapters to compare the performance of each laser method. This intensity  $\Phi$  ( $\text{GW/cm}^2$ ) is defined by the energy  $E$  (J) delivered to the medium surface  $S$  ( $\text{cm}^2$ ) in the pulse length  $\tau$  (ns) as in equation Eq. 1 :

$$\Phi = \frac{E}{\tau \cdot S} \quad \text{Eq. 1}$$

The areas where the shock wave is being produced by the laser beam and its resulting plasma are illustrated in the following Figure B.1 [1]. Different areas are to be considered in Figure 1: at the point of impact, the energy brought by the laser beam is absorbed by the surface and generates the **plasma**. Due to the ablation occurring for the generation of plasma, it is recommended to use a coating or **sacrificial layer** to protect the surface material. The plasma is generated instantly due to the high level of energy. The electrons present in the plasma have a specific density that allows a certain transmission rate of photons incoming. The rate of absorbed photon is depending on the conditions of irradiations (laser parameters and experimental setup) [2]. These parameters will be introduced in detail in part 3.

The incoming energy from the laser beam is being transferred by the plasma expansion and ablation occurring due to thermal conductivity during the pulse. The electron density at the ablated level is maximal. The results of the thermal shock and plasma expansion is an intense

pressure, with a steep rise time turning into a **shock wave** that propagates in the medium. The shock induction can be done in several interaction regimes that are presented in the next section.

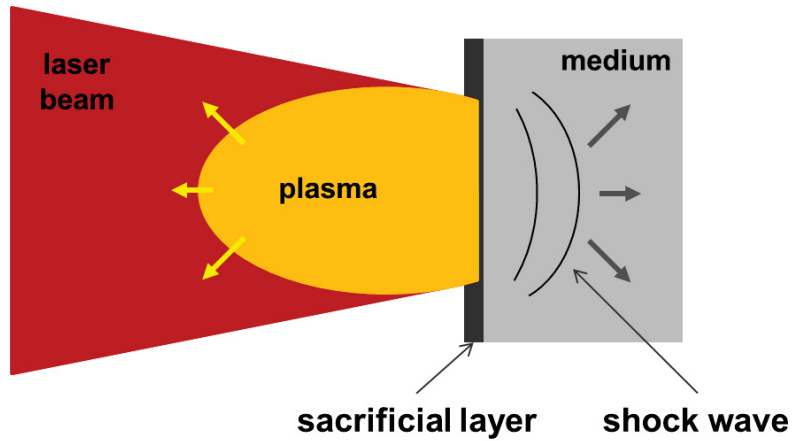


Figure B.1: Description of laser-matter interaction in the case of laser shock wave generation

### 2.1.3 Shock wave sources - interactions with direct/indirect irradiation

The generation of a shock wave with a pulsed laser beam requires that the photons from the laser reach the surface of the material. The laser beam pulse has usually to go through air or vacuum, or any other transparent medium to reach this surface. When the medium is not vacuum, it may be ionized by a high power density of the laser beam. This phenomenon of ionization of the medium and resulting opacification to the photon hinders a proper plasma generation and hence, induces a loss in the power and pressure of the shock wave. This phenomenon is called “optical breakdown”. The threshold for an optical breakdown is depending on the medium where the laser beam travels between the source and the surface. The breakdown power density threshold is about a few  $\text{GW}/\text{cm}^2$  in the air. The order of magnitude of  $\text{GW}/\text{cm}^2$  may be noticed [3].

In laser shock experiments, two different modes of irradiation are generally used in order to modify the shock loading parameters with a single laser source [4]: direct (represented in Figure B.1- without confinement) or indirect (Figure B.2b - with confinement).

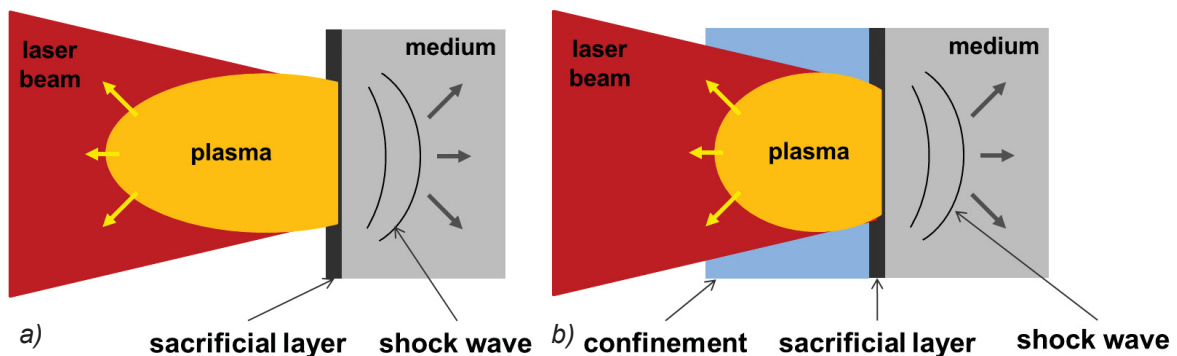


Figure B.2: Illustrations of the laser shock in a) direct irradiation and in b) indirect irradiation/with confinement layer

The followings observations are hence derived from several studies on the confinement and parameter dependencies for an optimal shock wave generation.

- Direct irradiation:

the direct irradiation is obviously limited in power density by the ionization of the medium (air). Therefore it is often chosen to work with vacuum to be able to apply higher power densities. Bolis references shots with power densities ranging from 1 GW/cm<sup>2</sup> to 3 TW/cm<sup>2</sup> in vacuum, leading to pressure between 0.1 GPa to 100 GPa at the surface of the impacted material [5]. A vacuum between the laser source and the object surface is however a major challenge to setup, and does not represent a realistic approach for the use of a laser proof test as a serial control method of adhesion quality in an industrial environment. This point will be developed later in this chapter with the introduction to the sacrificial layer.

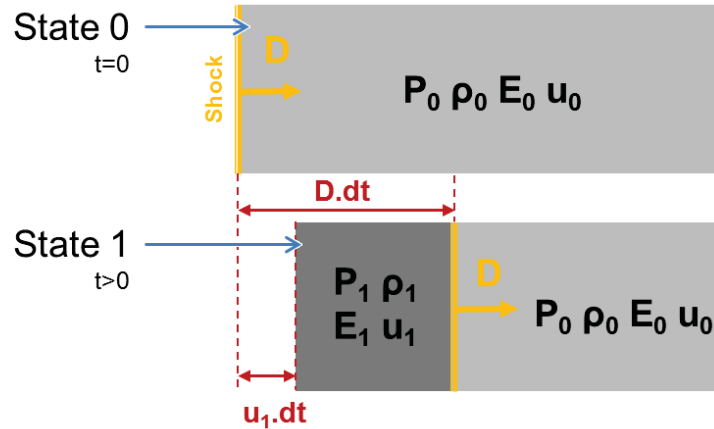
- Indirect irradiation/ shock with confinement:

in the case of an indirect irradiation, a transparent layer to the laser wavelength is chosen. Water or glass can be used as transparent layer. The plasma is confined and both the pressure level and duration can be increased this way. The phenomenon of optical breakdown however also appears in the transparent confinement layer, as it appears in air. For a given laser intensity, glass confinement yields to a higher level of pressure than water due to its higher density. It is however hard to establish an intimate contact between the glass layer and the medium surface. For this reason, water is preferred to glass in our case also as introduced in part 2. Berthe stated in the study of the dependencies of laser parameters regarding breakdown thresholds, that higher laser wavelengths as well as shorter pulse durations lead to higher breakdown threshold, and so increase the pressure level [6], [7]. Wider pulse durations imply that a lower pressure level is requested for breakdown threshold. Sollier determined that the threshold for a laser shock generated with water confinement with a gaussian laser pulse of 25 ns duration and 20 J max. was about 8 GW/cm<sup>2</sup> [8].

## 2.2 Mechanics of shock waves propagation – theoretical approach

### 2.2.1 Equations of Rankine-Hugoniot

The propagation of a shock wave is considered at first in an isotropic homogeneous medium in a one dimensional plane. It is also considered that the shock wave generated is stable, its pressure ramp is straight and that all external thermal exchanges are negligible. The referential for the description of the shock and medium states is absolute. Figure B.3 illustrates the propagation of the shock wave in a medium, with  $D$  the shock wave velocity,  $P_i$  the pressure,  $\rho_i$  the density,  $E_i$  the energy and  $u_i$  the material velocity for each state  $i$ . The difference  $u_i - u_0$  can also be noted  $u$ . The state 0 (before shock) and 1 (after shock) are represented.



**Figure B.3: Propagation of a shock wave in a medium**

Even if the shock wave is a “discontinuity” (see section 2.1.1), the conservation of the mass (Eq. 2), the momentum (Eq. 3) and the energy (Eq. 4) gives the following equations:

$$\text{Conservation of mass} \quad \rho_0(D - u_0) = \rho_1(D - u_1) \quad \text{Eq. 2}$$

$$\text{Conservation of momentum} \quad P_1 - P_0 = \rho_0(D - u_0)(u_1 - u_0) \quad \text{Eq. 3}$$

$$\text{Conservation of energy} \quad E_1 - E_0 = \frac{1}{2}(P_1 + P_0) \left( \frac{1}{\rho_0} - \frac{1}{\rho_1} \right) \quad \text{Eq. 4}$$

Those conservation equations are named the equations of Rankine-Hugoniot, who derived them [9]. They yield information regarding the partial state of the shocked material, but are not sufficient to describe the thermodynamic state, which is in this case defined by the thermodynamic parameters (the pressure  $P$ , the energy  $E$ , the specific volume  $V=1/\rho$ ) and the velocity parameters (shock velocity  $D$ , material velocity  $u$ ).

An additional empirical equation defines the shock velocity. Marsh et al. have investigated this velocity for thousands of materials and it has been shown experimentally in most cases that the shock velocity  $D$  is defined by Eq. 5, provided the fact that the initial state is unloaded ( $P_0 = 0$ ) [10]:

$$D = C_0 + s \cdot u \quad \text{Eq. 5}$$

with  $C_0$  being the sound velocity in the material and  $s$  a material constant without dimension but representing the slope in the linear shock velocity-particle velocity relation. Both are characteristic values of the medium that can be measured experimentally. It must be noted that the parameter  $C_0$  can be determined by the relation  $C_0 = \sqrt{C_L^2 - \frac{4}{3}C_T^2}$  with the sound velocity in longitudinal  $C_L$  (in tensile - mode I with regard to the adhesive bond) and transverse  $C_T$  direction in the medium (in shear – mode II with regard to the adhesive bond).

To complete the equation system in order to describe the thermodynamic state, an equation of state (EOS) is still required. In the case of high energy shocks with low pulse durations

inducing pressures up to the Mbar, the EOS of Mie-Grüneisen (Eq. 6) [10] can be used to describe the behavior of the shock wave in the material. This EOS links the parameters  $P$ ,  $E$ ,  $V$  as follows:

$$P(V) - P_{ref}(V) = \frac{\Gamma(V)}{V} (E + E_{ref}(V)) \quad \text{Eq. 6}$$

with  $P_{ref}$  and  $E_{ref}$  the pressure and the energy in the medium at the reference state,  $\Gamma(V)$  the coefficient of Grüneisen being a characteristic from the medium varying linearly with  $V$  for pressures until the Mbar (100 GPa). It can hence be assumed that the ratio  $\frac{\Gamma(V)}{V} = \frac{\Gamma_0}{V_0}$  is almost constant.

### 2.2.2 Characteristic shock curves

The system of equations from Eq. 2 to Eq. 6 can be used to represent the states generated by the shock wave in the medium [11]. By combination of those equations, it can be written:

$$P_1 - P_0 = \frac{C_0^2 (1 - \frac{V_1}{V_0})}{V_0 \left[ 1 - s \left( 1 - \frac{V_1}{V_0} \right) \right]^2} \quad \text{Eq. 7}$$

The Eq. 7 gives the end states achieved in the medium in the plane  $(P, V)$ . The curve obtained by the Eq.7 is named the Hugoniot curve, or also Hugoniot (standalone) or shock adiabat [9]. This curve allows one to determine the locus of any state starting from the reference state 0, based only on the pressure  $P_i$ , the specific volume  $V_i$  and three materials constants  $V_0$ ,  $s$  and  $C_0$  (ref. to Eq.5). Figure B.4 shows the Hugoniot curve and the shock polar, which is also named Hugoniot in English.

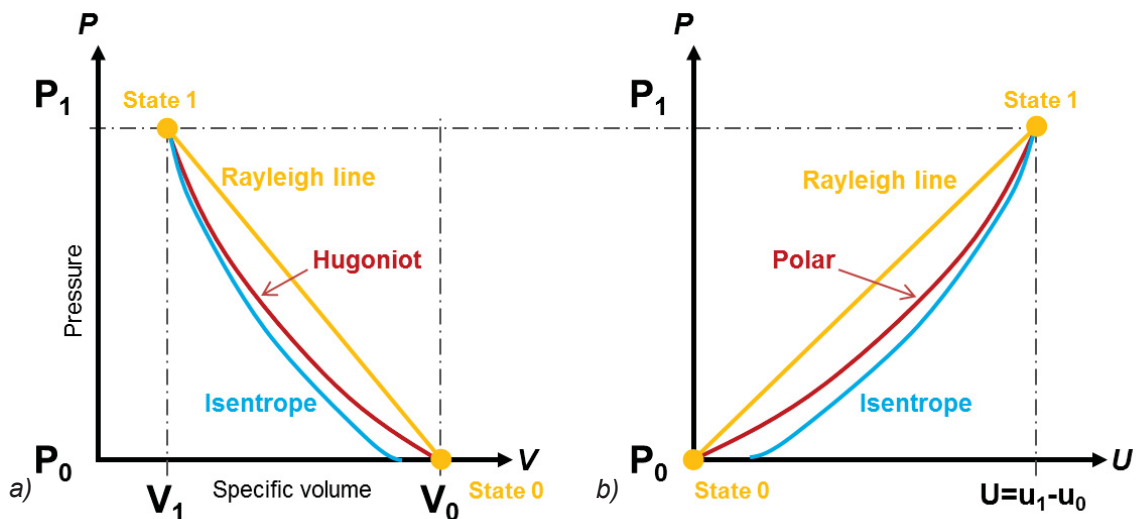


Figure B.4: a) Hugoniot curve  $(P, V)$  and b) shock polar  $(P, u)$  [12]

Finally, it is also possible to represent a curve of all states under shock in the plane (P, u): the shock polar. This curve is based on the conservation of momentum (Eq. 3) where D is replaced by its formulation of Eq. 5.

$$P_1 - P_0 = \rho_0 \cdot C_0 \cdot u + \rho_0 \cdot s \cdot u^2 \quad \text{Eq. 8}$$

The shock polar is a characteristic of one material since the properties linked by the relation are intrinsic to the medium itself. The Eq. 8 links the pressure applied P to the medium velocity u. The line between state 0 and state 1 represents also the Rayleigh line, whose slope is given by the shock impedance  $Z = \rho_0 \cdot D$ .

In the case of low pressure (<10 GPa), the medium velocity u is also very low in comparison to the shock velocity D. In such cases the shock impedance is also the standard acoustic impedance and the polar tends to straighten to be similar to the Rayleigh line. Hence it is assumed that  $D = C_0$ .

In general, for moderate pressures (<100 GPa), it may be assumed that only one Hugoniot exists, no matter if it starts from the state 1 or state 0. As well, it can be assumed that the shock polar and isentrope are similar since the changes of entropy are negligible in a solid medium where the pressures decreases with the sound velocity [3], [12]. This last assumption allows one to avoid using a state equation like Mie-Grüneisen and ease the description of the phenomenon.

It must be reminded that the behavior presented is only applicable to an hydrodynamic medium or a fluid, whose behavior is slightly different from the composite materials. The presented state equations are relevant for the description of the wave regardless of the elastic behavior of the medium and regardless of the damaging process. Those relations are hence valid in the elastic deformation domain and above, until the dynamic limit load.

The behavior of the material under shock in elastic deformation mode may be described better by a mechanical model [3].

### 2.2.3 Mechanical models for composite materials

The description of the shock wave propagation in an hydrodynamic medium needs to be completed with mechanical law when the medium is a solid. In the presence of low pressures, the elasto-plastic or visco-elastic behavior of the medium is not negligible and must be taken into account. For the description of the interaction between shock waves and induced pressures with the material elastic and plastic properties, constitutive models have been developed. Complex models including the effects of various parameters playing a role in high-strain deformation have been developed. In many cases, the models however focus on metallic materials, what has the advantage that properties are mostly isotropic and the material homogenous.

The homogeneity of CFRP may be discussed since the whole thickness is built up with stacking of plies with fibers in varying direction embedded in a polymer resin matrix. CFRP are per definition orthotropic and only particular stacking sequences can approach a quasi-isotropic behavior. In the present study, the models for metallic materials are not relevant due to the anisotropy of the composite assemblies. The choice of a right model developed for composite materials is conditioned by the velocity of the impact. In cases of impacts above 1



km/s to 3 km/s, typically corresponding to plate impacts, 3D anisotropic viscoplastic models were developed for GFRP materials [13]. Cohesive laws were used for interface modeling. In the study from Espinosa, the conclusion showed that there were shear stresses but no influences on the velocity signal but on the tension leading to delamination of the structure.

More complex models as the anisotropic viscoplastic were created for the description of the damage initiation and propagation [14]–[17]. The model proposed by Chang and Chang in a study of high strain damage modeling in composite structures is a simple approach [18]: the focus is set on the damage initiation since the purpose is the proof test of adhesive bonded structures. The damage propagation after its initiation is not as relevant if the bond was not able to withstand the high strain applied. Therefore, the criteria of Chang-Chang implies that each one of the criterion, namely i. tensile failure in fiber direction, ii. compressive failure in fiber direction, iii. tensile failure in matrix direction, and iv. compressive failure in matrix direction is set to zero when the stress applying leads to failure. In the other case, each criterion gives relation between all oriented mechanical properties of the CFRP material, as long as the strain remains in the elastic domain. This criteria is well indicated for damage initiation but is limited with the propagation. Other models consider more parameters for the damage propagation such as the RADIOSS model [14] or approach the damage with progressive opening thanks to softening of material properties, proven only in cases of ballistic impacts studies [15], [16]. These models give good results where the interest is set on damage extent, residual strength, and other residual material properties. Modeling laser shock is however different than ballistic impacts since the duration of the impact is contained in  $\mu\text{s}$  domain and the shock wave propagation is the phenomenon of interest instead of the material properties after impact.

To address the modeling of shock wave propagation, the material models have to implement the equation of state. This is reported in few studies investigating the high strain rate effects on mechanical properties [19]–[22]. The equation of Mie-Grüneisen (Eq.6) is often implemented to add the hydrodynamic components between pressure and density in elastic models. The use of elastic models is justified by considering the brittle character of CFRP materials. Vignjevic et al. thus developed a thermo-elastic damage model for CFRP with the EOS of Mie-Grüneisen applied on a stress tensor [20]. Wicklein et al. developed a similar approach for the CFRP model, based on linear relations between stresses and strains and by using elastic constants [22]. This approach however implies that material constants must be known or experimentally determined to feed the model. One can consider that the determination of materials parameters experimentally is also complex and linked with errors

To summarize, the choice of the model must account the properties of the composite material. The anisotropic character is essential in the case of CFRP. As highlighted by Ecault, the use of commercial elastic and hydrodynamic model is possible but these last ones are still under developments [23]. An additional challenge for these models are the material parameters and properties required to feed to model. They are hard to obtain for each variant of composite materials existing because of the numerous experimental tests required for their determination. The use of elastic models is well adapted considering the low pressure applied by the plasma from the laser shock (<1 GPa). This choice could be validated in the frame of his investigations. The fitting between model and experimentation was verified thanks to the

measurements of shock waves propagation realized by rear free surface velocimetry (RFSV) [23].

To better understand the difficulties of modelling the shock wave propagation, the next section introduces how the shock waves interacts with the matter and the interfaces as in bonded composites.

## 2.3 Interaction of shock waves in bonded structures

### 2.3.1 Propagation and transmission of shocks

In a material composed by several medium, the shock wave is being transmitted and reflected depending on the shock impedance  $Z$  of each medium. In composite structures, this implies also a reflection at each different layer since each layer is itself a relatively inhomogeneous polymer matrix with carbon fibers embedded. The case of bondline inspection implies also that an adhesive bond is present. This one can also be from a different nature than the polymer present in the laminate. In general, the type of wave propagating depends on material impedance variations between layers, and transmission and reflection properties.

In the 1D plan, the transmission and reflection phenomena can be introduced according to the material respective acoustic impedance ratio and the shock polar diagram enable a visualization of the pressures in the targets (section 2.2.2) [3], [23]. Figure B.5 and Figure B.6 represents targets made of two mediums perfectly bonded together and unloaded (state (0)) at time  $t_0$ . An incident shock on the front face (left) is applied at time  $t_0$  and starts propagating in the target from medium A to medium B. The continuity of pressure and material velocity from one interface A-B must be considered. The incident shock wave induces a compressive pressure in medium A and loads the medium in state (1). This shock wave is reflected in either a release wave or a shock wave at the interface A-B, depending on the impedances ratio  $Z_A/Z_B$ . The impedance ratio is also responsible for the pressure  $P_2$  in state (2) which applies in medium B, initially unloaded (state (0)).

- In Figure B.5:  $Z_B < Z_A$  corresponds to the case where the medium A has an higher acoustic impedance than the medium B. The shock polar shows the Hugoniot (Fig. 5b) displaying the increases of the pressure in medium A to the value  $P_1$  higher than  $P_2$ . The shock wave transmitted in the medium B leads to the pressure state (2) lower than the pressure state (1). Meanwhile, the reflected wave in medium A is a release wave. A rear free surface or zero impedance frontier would have the same effect on the reflected wave.
- In Figure B.6:  $Z_B > Z_A$  corresponds to the case where the medium B has an higher acoustic impedance than the medium A. This time, the shock polar shows the Hugoniot (Fig. 6b) displaying the increases of the pressure in medium A to the value  $P_1$  lower than  $P_2$ . The shock wave transmitted in the medium B leads to the pressure state (2) higher than the pressure state (1). Meanwhile, the reflected wave in medium A is a shock wave. The use of material with such a ratio of impedances can hence be helpful to enhance the level of pressure in the second layer, as highlighted by Ecault [23].

To summarize, it can be noticed that the transmitted wave is always from the same nature than the incident one. If  $Z_B < Z_A$ , the reflected wave will be from the opposite type, and when  $Z_B > Z_A$ , the reflected wave is from the same type. Whenever there is a mismatch in the acoustical impedances  $Z_B$  compared to  $Z_A$  after interaction at the surfaces / interfaces, multiple types of waves are propagating and are interacting / interfering with each other thereby producing positive or negative superposition of shock waves (i.e. states of increased or decreased pressure depending on the interference situation).

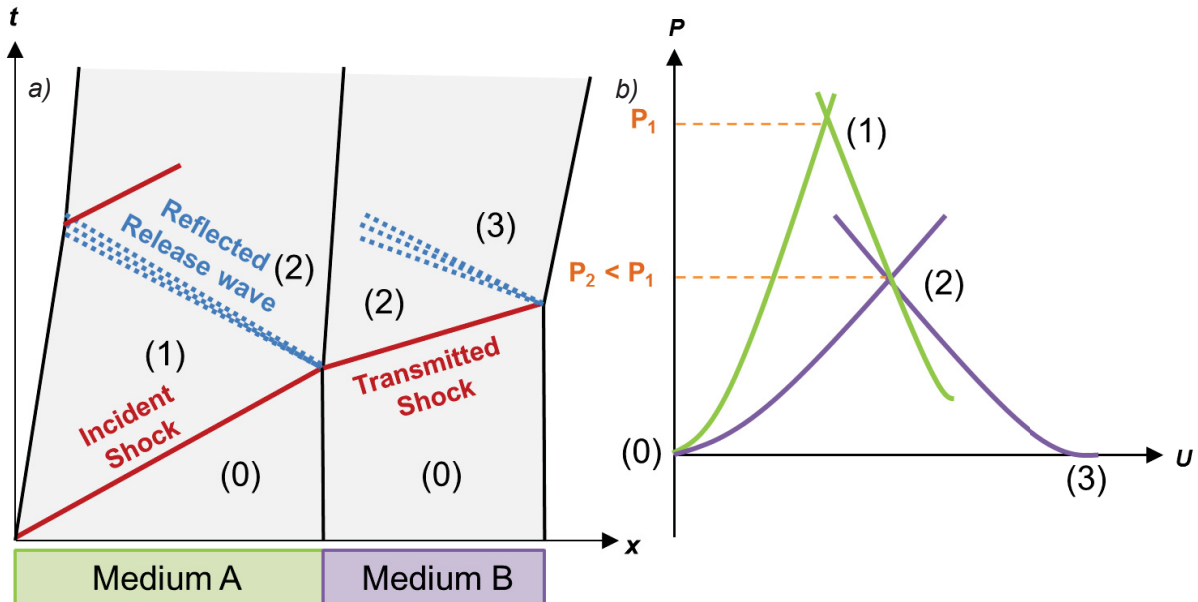


Figure B.5: a) Time-position diagram ( $x, t$ ) representing the shock wave propagation in a two-layers targets with acoustic impedance  $Z_B < Z_A$  and the according b) shock polar diagram with the pressure increase  $P_2 < P_1$  ( $P, u$ ) [23]

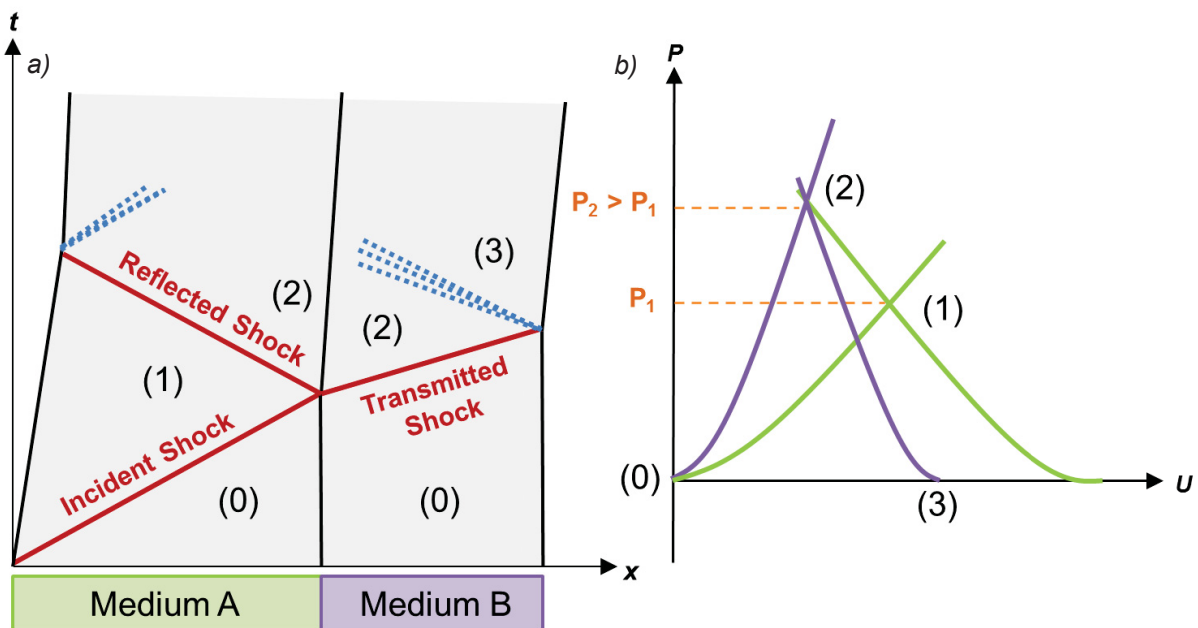


Figure B.6: a) Time-position diagram ( $x, t$ ) representing the shock wave propagation in a two-layers targets with acoustic impedance  $Z_B > Z_A$  and the according b) shock polar diagram with the pressure increase  $P_2 > P_1$  ( $P, u$ ) [23]



This example does not involve a possible failure of the medium under the tensile stress. In such a case, the waves would keep propagating through the medium thickness until complete attenuation. The case of failure is detailed in the next section.

### 2.3.2 Tension and Spallation

The transmission and reflection of waves principles as exposed in part 2.3.1 can be used to generate a local tensile stress on purpose at a precise depth in the medium i.e. one uses the interference pattern to reach the desired pressure. This is the phenomenon desired to test and assess the quality of the adhesion with laser proof test.

A similar example to the one presented in Figure B.7 may be used to illustrate the spallation principle. This illustration is given in Figure B.8a and the according pressure and velocity states are presented in the shock polar in Figure B.8b: an unloaded single layer target is submitted to a laser shock inducing loading to the pressure state (1)  $P_1$ . The shock wave travels through the layer until it reaches the back free surface where it is reflected backwards as a release wave setting the medium in state (3). In the same time, after the peak pressure, a release wave starts propagating through the thickness and relaxes the medium from state (1) to state (2). When both release waves intersect, the pressure is tending to  $-P_1$  as illustrated by the Rayleigh lines in Figure B.8b. In this case, the tensile stress exceeds the dynamic failure limit  $\sigma_{fail}$  and leads to a crack initiation and/or failure, depending on the mechanical behavior of the medium. This phenomenon is called **spallation**.

In the case of spallation, the shock wave transmission and reflection is affected. The crack has generated a new zero impedance surface within the layer and the waves cannot propagate through it. They are reflected back and forth in both the spall and the rest of the layer at the front face. Accordingly, the pressure states are affected and reduced. This effect can be measured by certain diagnosis methods such as rear free surface velocimetry as introduced in part 3 section 3.

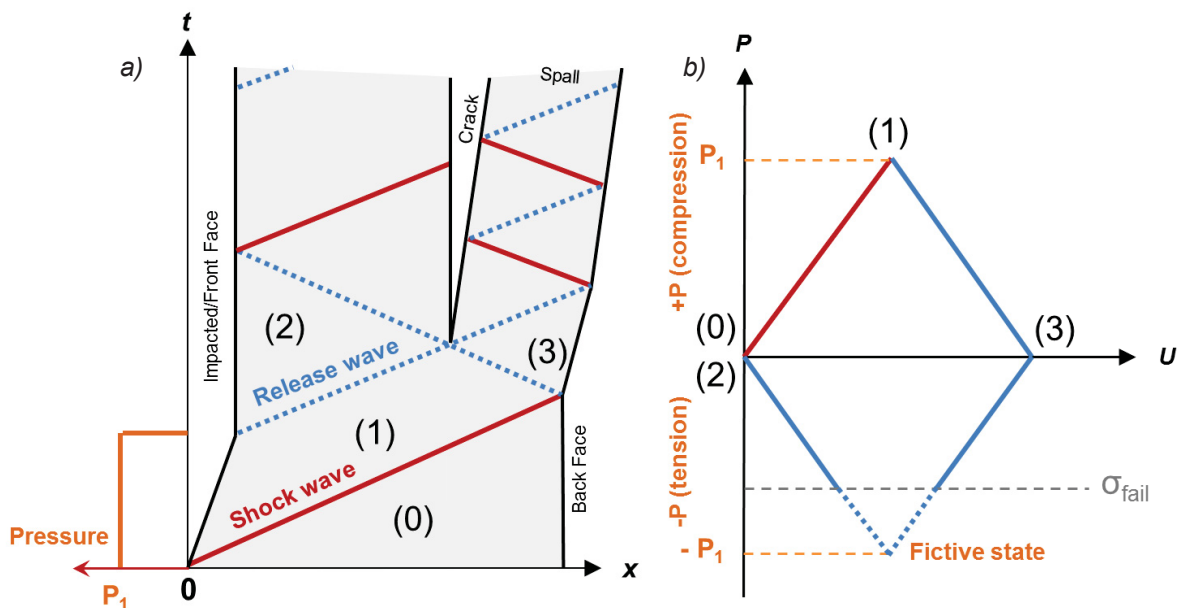


Figure B.8: a) Time-position diagram ( $x,t$ ) representing the principle of spallation in case of dynamic tensile loading and the simplified b) shock polar diagram ( $P,u$ ) without attenuation consideration [23]

### 2.3.3 Other Effects

The shock wave propagation in a medium has other important effects which have not been discussed yet. These effects have been neglected in the previous parts for an easier description of the generation and transmission phenomenon. They are however essential regarding the aim of this study, namely the bond quality assessment. They are introduced in the present section.

- Hydrodynamic and elasto-plastic attenuation:

based on section 2.2.1, the shock wave is due to a pressure pulse released in the medium travelling at the velocity  $D$ . The propagation of this shock waves set the medium initially at  $P_0$  with a velocity  $u_0$  in the state  $P_1$  and induces the velocity medium  $u_1 > u_0$ . For this reason the shock wave front is straightening while the propagation goes on as displayed in Figure B.9. For the same reason but inversely, after the pressure pulse, the pressure is decreasing and the release wave follows, bringing the pressure  $P_1$  to  $P_0$ . The start of the release wave travels at the wave velocity  $C_1$  in the medium at velocity  $u_1$ , while the bottom reaches  $P_0$  and  $u_0$ . This difference of velocities make the release wave spread over the propagation. Based on this hydrodynamic considerations seen in section 2.2.1, it can be summarized that the velocities of the shock wave front is  $D$  while the upper part of the release wave is  $C_1 + u_1$ . This implies that the release wave front eventually reaches the shock wave front and start attenuating it. This phenomenon is called the hydrodynamic attenuation [5], [8].

The hydrodynamic attenuation can also be combined with the elasto-plastic attenuation, valid of course in the case of materials with an elasto-plastic behavior .

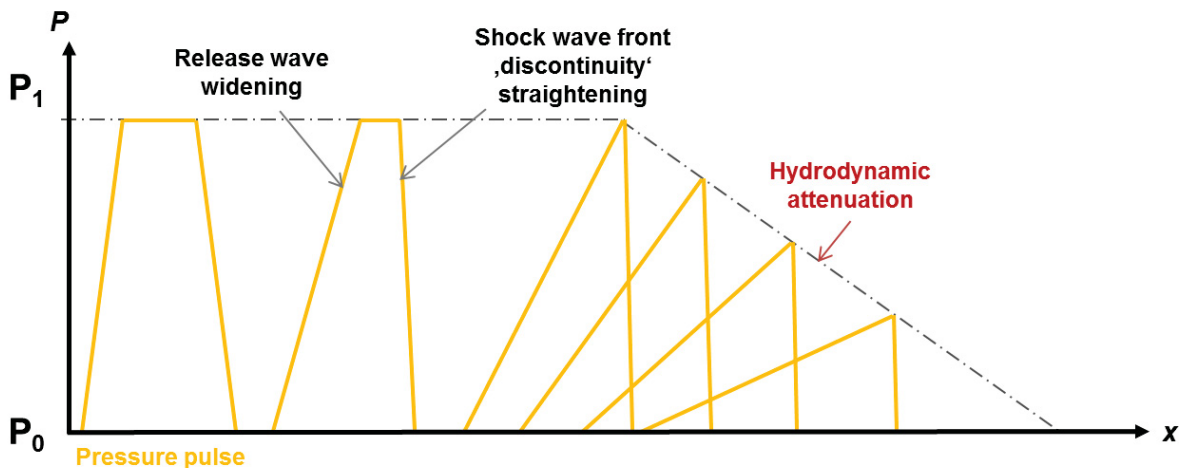


Figure B.9: Influence of elasto-plastic attenuation on pressure pulse profile over thickness

In the case of the elasto-plastic mechanical regime, the high pressure applied by the laser shock is likely to generate a strain exceeding the Hugoniot elastic limit  $\sigma_H$ . In this case the Hugoniot curve is a straight line (Rayleigh line) in the elastic regime, and a typical Hugoniot curve as represented in Figure B.4 in the plastic domain. It is impossible to draw a single Rayleigh line from the pressure  $P_1$  to  $P_0$ . The shock waves is thus divided in two parts as represented in Figure B.10: one involves the shock wave travelling in the elastic regime

(between  $P_0$  and  $\sigma_H$ ) and another one travelling in the plastic one (between  $\sigma_H$  and  $P_1$ ). The first elastic part is called the elastic precursor. It travels at the sound velocity  $C_L$  which is greater than the shock velocity  $D$  based on Eq.5. This behavior enables the elastic precursor to propagate faster in the medium. Its effects shall also be detectable on rear free surface velocity measurements [5], [24], [25].

This is also applying to the upper part of the release wave directly below  $P_1$ . Since the release wave travels faster than the shock wave, it reaches eventually the peak pressure and attenuates it. This phenomenon is named the elasto-plastic attenuation. It may apply in solid with an elasto-plastic behavior and in the range of low pressure (<10 GPa).

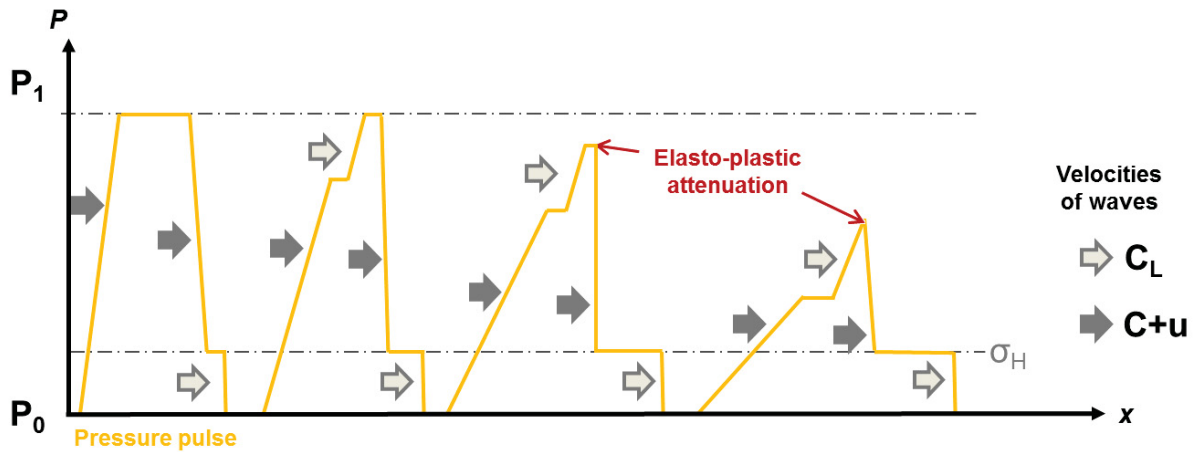


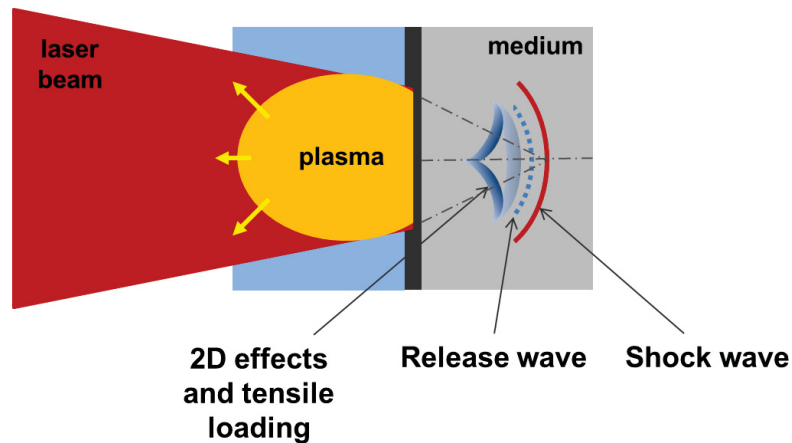
Figure B.10: Influence of elasto-plastic attenuation on pressure pulse profile over thickness

In general, the attenuation phenomena illustrates that the pressure and so the strain generated at the surface is not exactly the one reaching the place where the tension due to release wave crossing should happen. The strain cannot exceed the amplitude of the incident shock wave measured at the rear free surface [3].

- Lateral release waves « 2D effects »:

an edge effect interfering with the shock wave propagation may appear depending on geometrical considerations. Directly after the emission of the shock wave in the medium, the shock wave is followed by release waves generated at the interface loaded-unloaded (edges of the laser beam spot) area by the laser. These release waves do not propagate properly in the same direction as the shock waves but also perpendicular to it (see Figure B.11). As the laser spot is spherical, the field of generation of those 2D effects is as well spherical and the propagation is cone-shaped. Their crossing generates additional local concentrations of tensile stresses in the medium over this cone shape [12], [23], [26].

To avoid these edge effects, an empirical observation advises to load the structure with a focal spot diameter at least two times larger than the thickness of the material [3].



**Figure B.11: Illustration of 2D effects following the shock and release wave and responsible for tensile stress in the medium**

### 3. TECHNOLOGY PRINCIPLE (STATE OF THE TECHNOLOGIES)

The chapter A already reported the principles of the both similar techniques LASAT and LBI techniques. After many theoretical notions dealing with shock waves generation, propagation and transmission in part 2, This 3<sup>rd</sup> part focuses now on the key parameters for the experimental success and will introduce how each parameter is linked to a particular effect for the proper realization of an adhesive bond quality assessment.

#### 3.1 The essential laser source parameters

The first essential parameters correspond to the ones from the laser source itself. Only few information from literature can be found in the case of the LBI because of the private research funded by Boeing. The studies for the development and optimization of the LASAT is in the contrary abundantly documented due to public funding and several PhD Thesis run on this topic.

The principal laser source parameters comprise the type of laser (eg. Nd:YAG, Nd:Glass, etc.) with the associated wavelength (also responsible for the color and density of the laser), the energy/intensity of the laser beam and the laser pulse duration. Other secondary parameters that may be mentioned are the repetition rate of laser shots and the focal spot size, which may also appear important in case of repeated shot but is only a secondary parameter in the frame of this study. The repetition rate is indicated later in Table 1.B but is voluntarily not discussed in details in this study. It may however represent the time limit for the repeatability between two measurements in a future industrial adhesive quality assessment process.

##### 3.1.1 The laser wavelength

Different type of laser offer also different types of wavelengths. In general, laser shock is performed with solid state lasers (Nd:YAG or Nd:Glass in most of the literature) These laser have generally a wavelength of about 1  $\mu\text{m}$ , much more intense than CO<sub>2</sub> lasers for instance. The wavelength choice is essential for a proper plasma generation because of the



photoionization mechanism. Berthe et al. investigated the effect of the wavelength choice on plasma generation at the substrate surface [7]. The study, a comparison of IR (1064 nm), Green (532 nm) and UV (355 nm), highlighted the importance of the stable plasma generation at the surface for an efficient and long enough pressure pulse induction. The plasma breakdown in the confined regime was favored by shorter wavelengths even though they could lead to higher pressure levels. In the end, the 1064 nm wavelength offers one of the best compromise for stability of plasma for the shock generation, but not as much power as a shorter wavelength could offer.

This wavelength (about 1050-1060 nm) is therefore the one used the most often for laser proof tests techniques.

### 3.1.2 The pulse duration

The pulse duration from the laser pulse is often a property of the laser defined at the design stage. Several lasers with different pulse durations are available and can be found by laser manufacturers. In case of particular requirements, laser can of course also be ordered with precise laser pulse duration on demand.

The shock propagation and initiation mechanisms presented in part 2, underlines the decisive role of the laser pulse length. Figure B.12 illustrates the consequences of the crossing of release waves with an energy corresponding to the threshold value of the interface A-B (considered as the weakest position in the target). The effect would be as follow in case of:

- a) Short pulse duration (typically 1 – 50 ns): the crossing of release waves is likely to happen close to the back free surface of the medium impacted. A short pulse duration implies also a thin loading curve, which would be affected by the attenuation phenomenon described in section 2.3.4. The stress generated may not be significant enough to debond any bonded/coated interface.
- b) Large pulse duration (50 – 300 ns): due to the longer loading, the crossing of the release waves takes place later than directly after reflection on the back free surface. It is possible to generate a tensile stress closer to the center of the target. Furthermore, attenuation is minimized by the long pulse, and hence the pressure intensity is conserved longer over the propagation in the thickness.

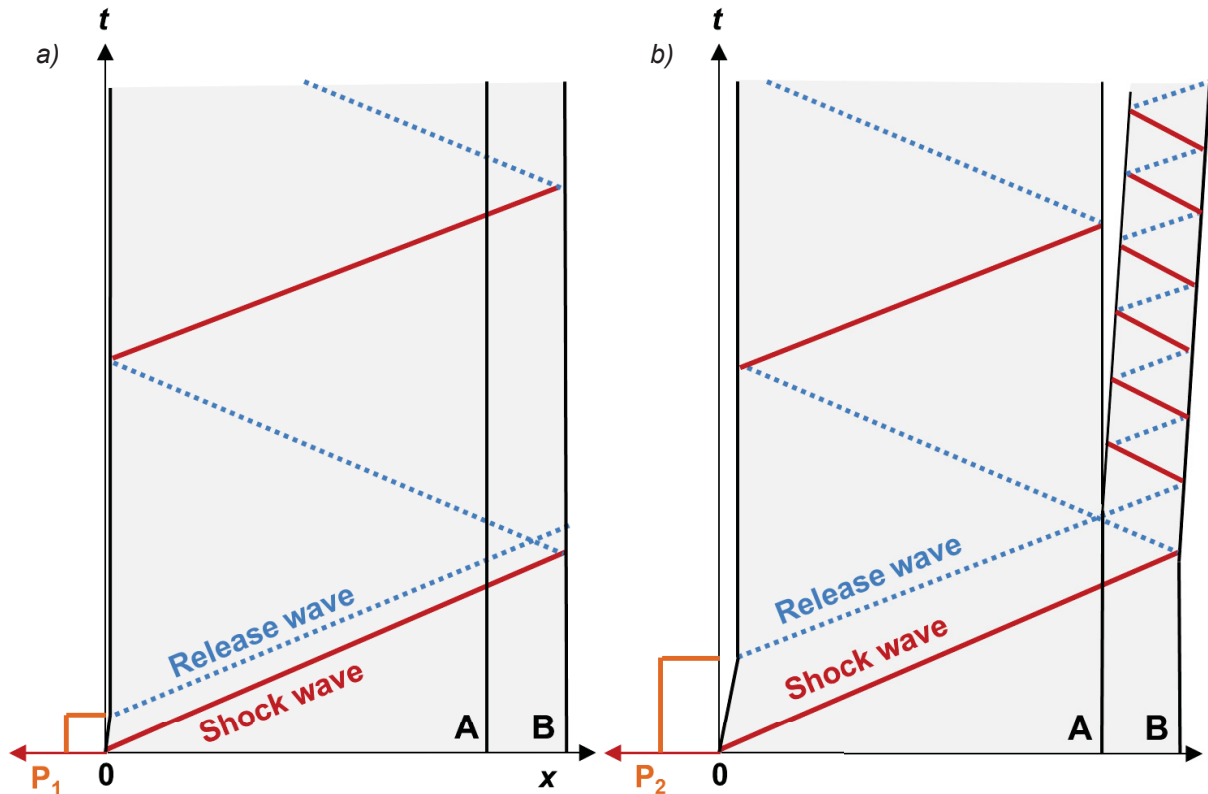


Figure B.12: Time-position diagrams (x,t) representing a) inadapted intersection of waves (in the layer) and b) adapted intersection of waves for the interface A-B strength test

Most of the LASAT applications presented in Chapter A refer to relatively short pulse length. This is normal since the original LASAT technology development was driven towards testing of coating adhesion on thin metal substrates. It could however be an issue in the case of adhesive bond testing in composite structures, where substrates are thicker than thin films. The use of a broader pulse duration is relevant to this particular application in opposition to the inspection of coatings strength [27], [28]. On the other hand, the LBI was developed especially for this adhesive bond inspection. The laser used has an interesting particularity which is its tunable pulse duration ranging from 100 to 300 ns. Such a long pulse was seen as mandatory by Sokol et al. to avoid damaging the composite materials and bond [29].

### 3.1.3 The energy/intensity of the laser beam

It has been explained how the laser pulse length could be affected by the attenuation. The energy of the laser shock is of course also critical in this context. In most of the literature sources about laser proof tests, the energy of the laser beam is the variable used for the experiments. Authors use their laser configuration as it is, and try to reach the desired effect (debond, delamination, spallation) by increasing the energy until the threshold value for which the effect is reached. Similarly to Figure B.12, Figure B.13 illustrates how a laser shock with inadequate wave crossing and too high energy can provoke a damage (here spallation) in the target layers instead of the interface.

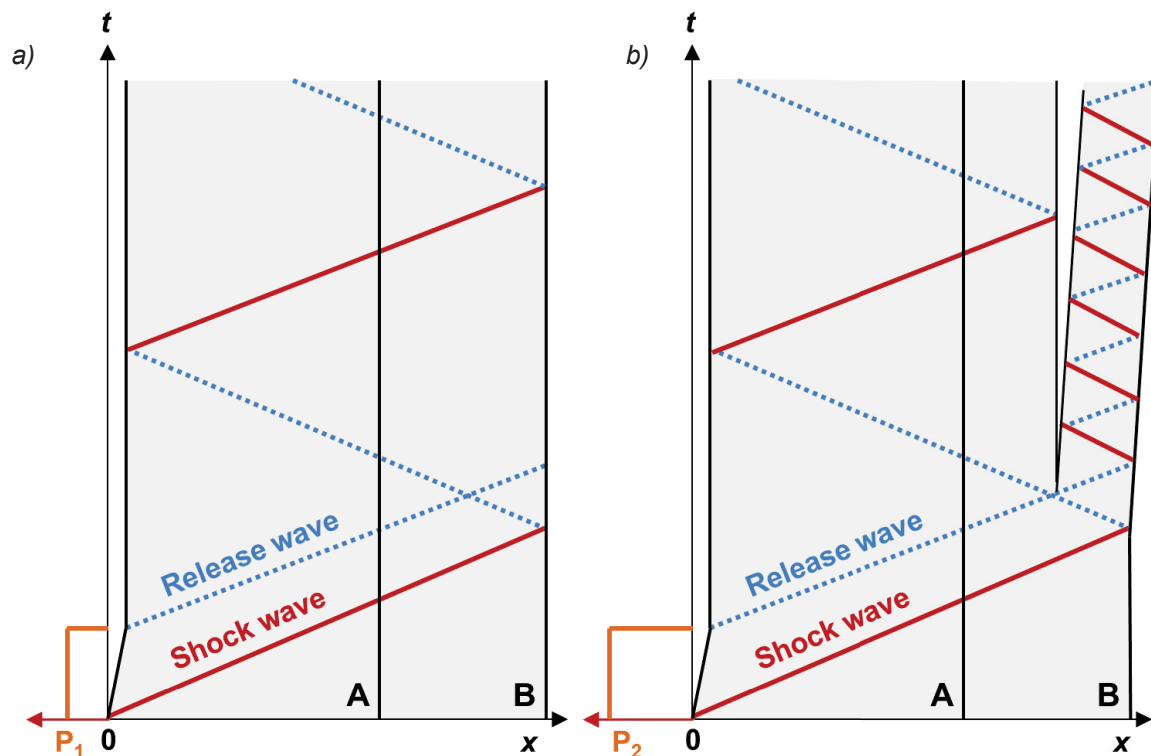


Figure B.13: Time-position diagrams ( $x,t$ ) representing inadapted intersection of waves (in the layer) a) below critical energy for target or b) over critical energy causing spallation

The laser energy is however most of time limited by its amplification system and each laser is purchased with a maximum energy. The energy setting available for each laser shock can be either tuned by adjusting the amplification power (most robust solution), or also by optical means with filters and optical densities to reduce the intensity of the focal beam. The repetition rate of the laser is linked to the laser and especially the amplifying technology, since it represents the time necessary for the system to cool down before a new laser shot.

The focalization of the laser beam is often performed to increase even more the energy locally. Most of the time, optical lenses are used. The beam spot size reaching the surface should however not be too small in order to reduce the edge effects with the lateral release waves (see section 2.3.4). In the case of the LASAT recent investigations on composite assemblies, the spot size diameter was 4 mm for max 4 mm thickness of CFRP specimens while the literature refer to 10 mm diameter for the LBI also for 4 mm thicknesses.

Finally, the effects of the energy alone can hardly be expressed without the parameter of pulse duration and the beam spot size after focalization. Eq. 1 allows one to calculate the flux of energy, its power, reaching the surface. This value is a combination of all parameter and facilitates the comparison of each laser system performances. The wavelength is not directly a critical parameter because it principally affects the pressure duration at the surface and the maximal pressure level before any optical breakdown (see §2.1.3) [7].

To summarize, the main characteristics of the laser proof test approaches, LASAT and LBI techniques, are presented in Table 1.B.

**Table B.1: Summary of laser shock sources appearing in literature for CNRS [23] and LSP**

Laboratory	Laser source	Characteristics			
		Wavelengths (nm)	Pulse duration (ns)	Energy (J)	Repetition rate
CNRS LULI	LULI 200	1053 nm	1 – 5 ns	1000 J	1 shot/ 60min
CNRS ELFIE	ELFIE	1053 nm	300 fs	0 – 10 J	1 shot/
CNRS PIMM	LASAT Nd:Glass	532 nm	3 – 10 ns	0 – 1.5J	10 shots/ s
CNRS PIMM	Hephaistos	532 nm	10 ns	2 x 7J	2 shots/ s
CNRS-PPRIME	LASAT Nd:Glass	1053 nm	25 – 30 ns	0 – 20 J	1 shot/ 5min
LSP	LBI Nd:Glass	1053 nm	70 – 300 ns	0 – 50 J	1 shot/ 8s

### 3.2 The plasma generation: confinement and sacrificial layer

The laser parameters are a first essential key characteristic when it comes to laser proof testing. As seen in section 2.1.3, the interaction mode at the impacted surface can also affect significantly the properties of the shock wave generated in the medium.

At the beginning of the technology development, experiments tailoring stress waves were conducted with metallic overlays like zinc and lead, black paint or plastic tapes [30], transparent overlay like water or fused quartz [31]–[33]. They all proved that the shot shape of the thermal expansion provoked by the confined plasma could enhance the peak pressures required for the generation of the plastic deformation. Two main parameters were identified and can be pointed out: the decisive role of confinement of the plasma blow-off for the control of the stress wave amplitude and, the protection of the material surface due to its exposition to the laser generated and ablative plasma. The use of confinement regime and sacrificial layers was hence widely studied in the following years [6], [31], [34].

Regarding the confinement regime, the ‘purest’ solution to avoid plasma breakdown is to use vacuum chamber for the atmosphere of the shock. Due to the effort required and the limiting size of vacuum chambers, other solutions for a practical use were investigated. Fabbro stated that the use of solids like glass was advantageous for the level of pressure generated. The intimate contact with the material below was however the main difficulty in this process, so that in the end, water was offering the best compromise as a transparent overlay. The plasma expansion is confined in this layer and hence the pressure and shock duration may be multiplied by up to a factor 2 to 3 in comparison to direct irradiation without confinement regime [31], [6]. Meanwhile, water has been used in most of the following studies and is now well established.

Additionally to the essential water confinement layer, the use of a sacrificial layer is important for the surface protection as the plasma is slightly burning the upper layer of the impacted surface. This phenomenon is even more relevant for polymer composite materials. The sacrificial layer plays also a role in the stress generation, as a constant type of interaction layer. In the literature, the use of an absorbing metalized paint layer or a black adhesive tape have been applied for a better control of the shock pressure and its duration, and simultaneously, to avoid surface damages via burning [28], [35]. Two solutions are mainly established: the use of a polyvinyl adhesive black tape [35]–[37] or the use of an aluminum painting spray [28].

Several authors underline the importance of the sacrificial layer for the stress calibration in the material [23], [31], [37]. Fabbro et al. and Arrigoni et al. already identified in the nineties that the pressure  $P$  induced in aluminum target was a function of the laser beam intensity  $I$  shown in Eq. 11 [31], [38], [39].

$$P \propto \sqrt{I} \quad \text{Eq. 11}$$

LSP Technologies performed measurements of rear free surface velocity to evaluate which confinement and sacrificial layer was giving the best result in term of ratio energy input vs. stress generated [37]. The laser shots were performed on pyrex with different overlays as represented in Figure B.14. The stress peak (pressure) is plotted in function of the laser fluence. The material chosen for the shock (pyrex) is however hardly representative from the composite substrate that will be investigated in this study.

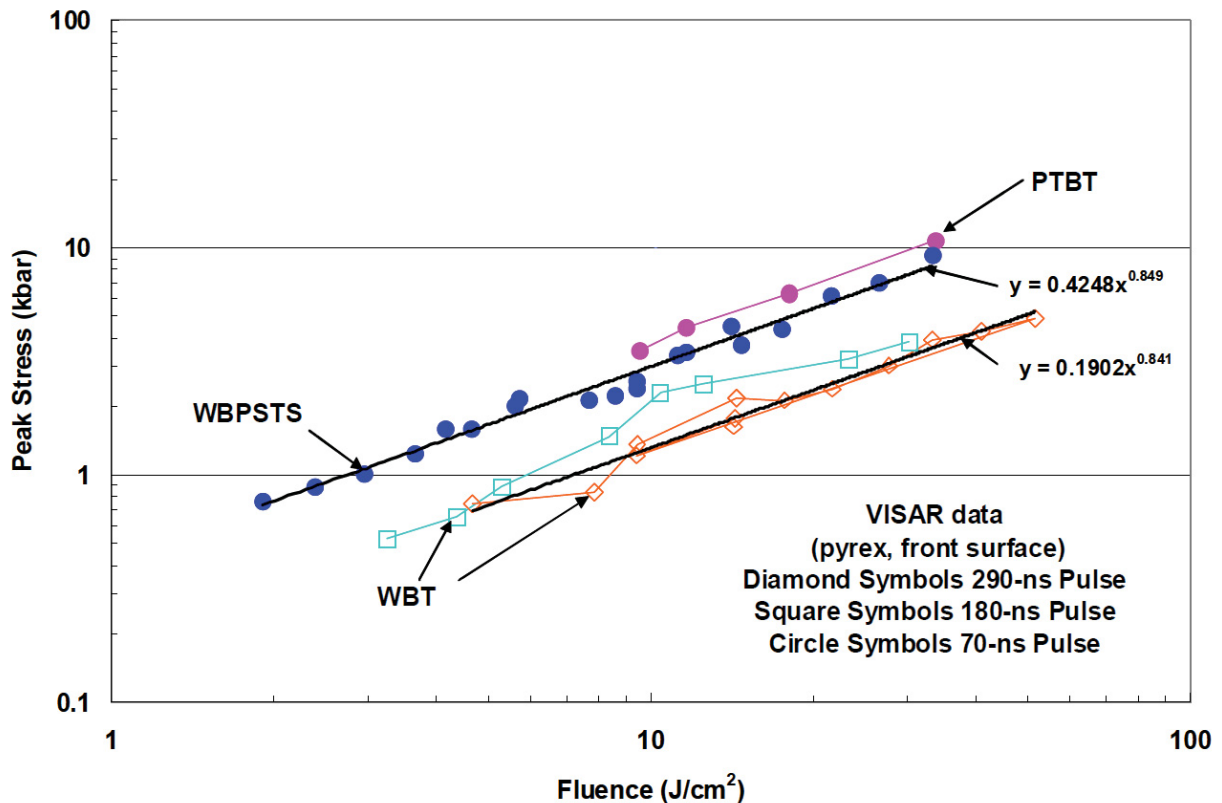
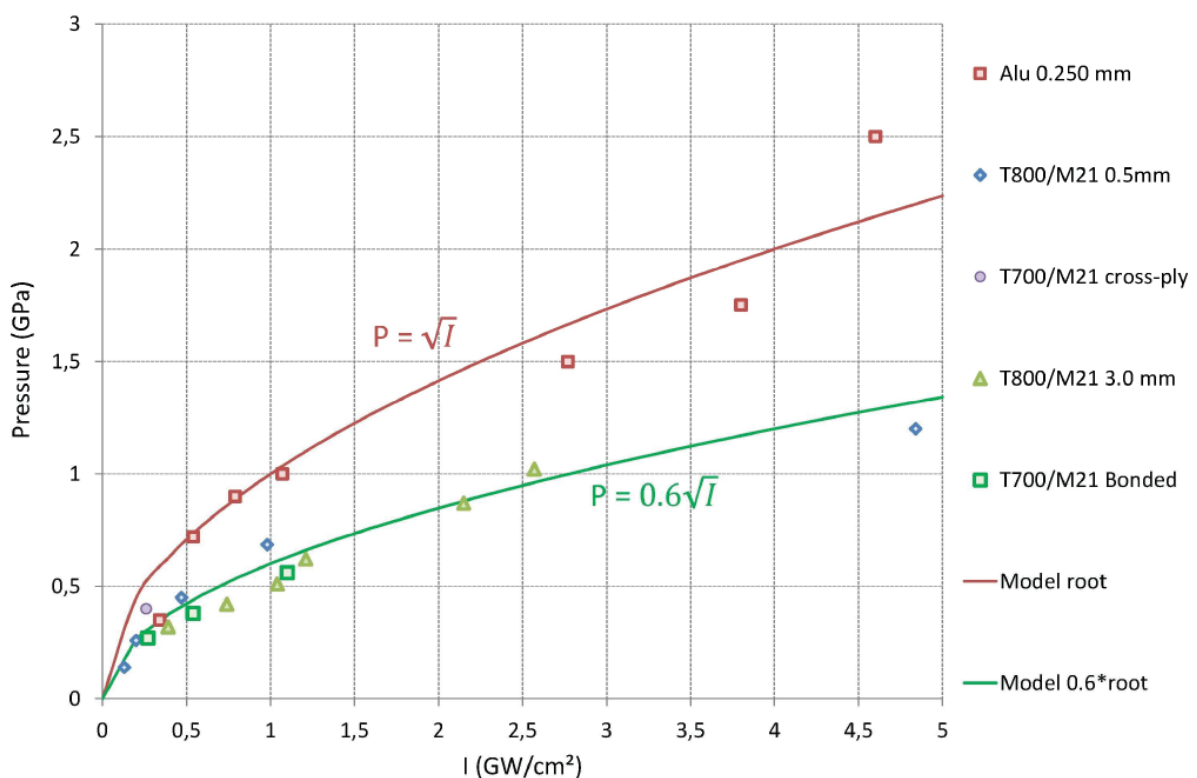


Figure B.14: Calibration curve in case of the LBI varying pulse duration laser (1054 nm wavelength) for different confinement and sacrificial layer couples for pyrex targets [37]: PTBT: packing tape, black tape; WBPSTS: water, black paint, stainless steel; WBT: water, black tape

Ecault underlines however in his thesis that the calibration has to be done for each shot configuration (target type with confinement and sacrificial layer) and review the use black adhesive tape as unsure due to the fact that the tape represent an new bonded layer on top of the target [23]. In his case, the sacrificial layer applied to the composite targets bond was aluminum spray painting to approach the well-known aluminum interaction modes. The calibration curves are displayed in Figure B.15. The pressure is assumed lower than in aluminum due to the lower density of composite targets compared to pure aluminum, but this parameter was not verified. However, the relation in Eq.11 could be verified and adjusted to the case of epoxy composite with M21 resin into  $P = 0.6\sqrt{I}$ . It must finally be kept in mind that this relation is only valid in the particular configuration of laser source and water confinement overlay.



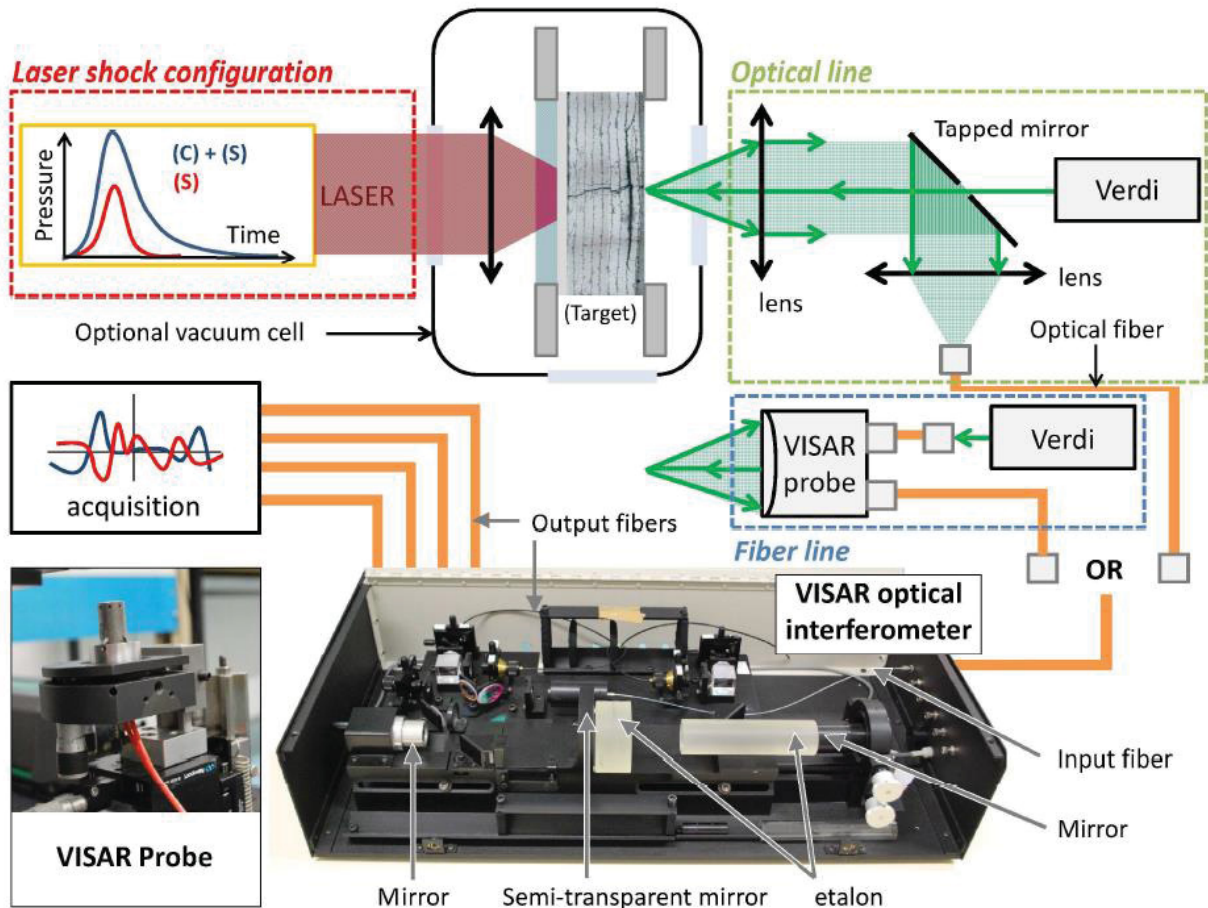
**Figure B.15: Calibration curve in case of the Pprime 25 ns laser shock in water confinement configuration for aluminum samples and all the composite targets with aluminum painting added sacrificial layer [23].**

### 3.3 The integrated diagnosis techniques

In the different previous sections, the measurement of the critical characteristic being the rear free surface velocity (RFSV) is indicated as a solution to evaluate the stress generated by the shock wave and even, a solution for failure analysis [27]. In both techniques presented, LASAT and LBI, an integrated diagnosis in the form of a time resolved method may be used for the detection of shock waves coming through the structure. This last section finally introduces how this is realized and the techniques for the detection of shock waves effects present in the literature.

First studies reporting on laser spallation in the nineties mentioned the use of Doppler velocity interferometer for the measurements of the free surface velocity [40]. In the LASAT studies, the detection is performed based on this Doppler principle on the rear side of the sample with help of a second single frequency laser, a ND:YAG Laser with 0,532  $\mu\text{m}$  wavelength. It delivers 400  $\mu\text{s}$  duration pulses with quite low peak power. The spot diameter is up to 400  $\mu\text{m}$  and the light scattered is recorded either by a Fabry-Perot etalon interferometer which gives a signal proportional to the back surface velocity [41]. It is alternatively also realized with a continuous 5W Verdi laser with 0,532  $\mu\text{m}$  wavelength and a Velocimetry Interferometer System for Any Reflectors (VISAR) [23], [35], [42], [43]. The VISAR is a Michelson type interferometer with measuring capabilities from 1 to several km/s with nanosecond resolution. Its complete functioning principle is represented in Figure B.16. A condition for an optimal use of the VISAR is that the surface reflectivity is high. In the case of composite, Ecault noticed the strong absorbance of the laser wavelength in composite and burning traces due to the Verdi energy. These issues can be partly solved by polishing the rear surface of samples and applying a little aluminum paint also to improve the reflectivity [23]. On the whole, the VISAR implementation for composite materials is very demanding for those last reasons.

Other diagnosis tools are mentioned as potential techniques for future evaluations such as transverse visualization with shadowgraphy technique for a real time visualization of potential delamination occurring [44]. Ecault has shown how these methods could be implemented with a simple setup for the visualization of plate impacts. He also used a more complex configuration of shadowgraphy for the live visualization of stressed areas, based on light deflection changes induced by density variations in impacted targets [23].



**Figure B.16: Sketch of the two VISAR practical setups (the optical line and the fiber line) and picture of the VALYN VISAR interferometer and the barker probe used to irradiate the target and collect the reflected light [23]**

In the case of the LBI, the VISAR was also investigated for RFSV measurements on both the opposite and front side (with the front side being the impacted surface). However, principally due to the complexity in setup and cost of a VISAR, another method has been privileged: a simple electromagnetic acoustic transducer gauge (EMAT), represented in Figure B.17. While the laser generates a shock putting the target in motion, an electrical current is induced in a metallic sticker bonded to the target impacted face. As the panel is put in vibrations, one EMAT coil generates a magnetic field and another picks up the affected electrical field from the inspection sticker. This solution is customizable for each application [29], scanning a larger area and allowing use on either the front or the back surface but implying physical contact with the sample [27]. The velocity signals obtained are visible under the form of peaks coming from the reverberations of the shock wave in the material. The signal is recorded by the EMAT (or other sensors) and is analyzed by Fast Fourier Transformation to improve the bond state diagnostic.



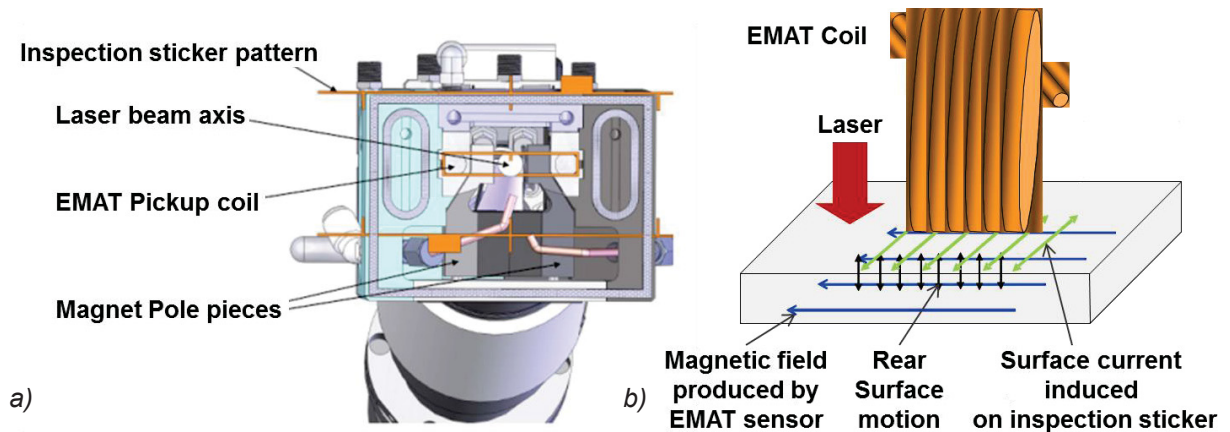


Figure B.17: Sketch of the a) LBI EMAT probe head (applicable only on front face) and b) the EMAT functioning principle [45]

Finally, it can be observed that in the case of adhesive bonding inspection and especially for failures, the use of conventional NDT testing additionally or alternatively to the velocity measurements is advised. The literature reports several conventional ultrasonic scans made after the proof test for the characterization of the bond line [23], [35], [36], [41]. Ultrasonic testing methods are among the most reliable methods to assess non-destructively that the shock wave generated a delamination or debond in the target. These methods are however not time-resolved and imply that the inspection is realized after the laser proof test. This would mean an additional inspection step in the frame of an industrial implementation of laser proof test in the industry.

## 4. SUMMARY

Laser Proof Test methods are based on the shock wave theory. This theory is highly complex and different from classical elastic wave propagation theory (applicable for ultrasound waves). The presentation of the shock wave theory was done according to the hydrodynamic hypothesis, which is hardly applicable in the case of a composite target. To account the material response to a shock wave, complex state equations should be applied such as Mie-Grüneisen, when the pressure is considered high. In the low range of pressure investigated (<10 GPa), the behavior can be approached by the classical sound wave propagation.

The mechanical behavior of the material needs to be described as the elasticity, plasticity and failure are essential parameters to evaluate the pressure levels and response to the tensile stress generated. The case of composite material is again relatively complex, as the material is brittle and do not present an elasto-plastic behavior like metals. The difficulty is even higher since the shock wave phenomena are high strain rate dependent. Few literature sources give model of composite for proper modeling approach but an elastic orthotropic model could be implemented to verify the shock wave effects in the case of Ecault's PhD.

The approach of Laser proof test is based on the generation of high pressure loading that travels through and back a target. Depending on numerous properties of this target, including i.e. the acoustic impedance, the waves are reflected and transmitted. The crossing of release waves following the incident shock wave and the reflection of this shock wave on the rear free surface produces the tensile stress in the target thickness. This tensile stress can lead to the phenomenon of spallation i.e. delamination or debonding in the case of adhesive bond performance.

The shock wave propagation is however affected by attenuation and other edge effects that respectively lower the pressure and disturb the shock waves. To counter these effects, several properties of the laser such as wavelength, pulse duration and naturally energy can be adjusted. They are mostly all linked together and several previous investigations of their optimal setup were realized. The plasma induced by the laser shock, responsible for the stress/pressure generation in the target, can also be controlled. Its efficiency can be enhanced by the use of confinement and sacrificial overlays. The two methods, LASAT and LBI, both use water confinement and respectively aluminum paint or black polyvinyl tape for the sacrificial layer.

Finally, for the development of both the LASAT and the LBI methods, time-resolved diagnosis tools have been implemented: the Doppler velocimetry, the Velocity interferometer for any reflectometer (VISAR) or the Electromagnetic Transducer (EMAT) all allow one to measure the target vibrations under shock and so, the effect of spallation when it occurs. Other techniques non time-resolved such as ultrasonic inspection after shock waves are also well adapted for detection of spallation effects.

This chapter has underlined the state of the technology and reviewed the critical parameters that will have to be investigated for the assessment of adhesive bond quality.

## REFERENCES – CHAPTER B

- [1] R. Fabbro, J. Fournier, P. Ballard, D. Devaux, und J. Virmont, „Physical study of laser-produced plasma in confined geometry“, *Journal of Applied Physics*, Bd. 68, Nr. 2, S. 775, Juli 1990.
- [2] P. Mulser und D. Bauer, *High Power Laser-Matter Interaction*. Springer Science & Business Media, 2010.
- [3] M. Arrigoni, „Étude de l'influence des rugosités d'interface, de porosités et de l'épaisseur d'échantillon sur la propagation des chocs laser dans des systèmes revêtus. application au procédé LASAT (laser adhérence test)“, E.N.S.M.A. et Faculté des sciences fondamentales et appliqués, Poitiers, PhD, Dez. 2004.
- [4] P. Darquey, Ondes de choc et accélération de feuilles minces par impulsion laser en interaction confinée : tests d'application à la compaction dynamique de poudres métalliques. Poitiers, 1989.
- [5] C. Bolis, „Etude numérique et expérimentale de la séparation par chocs brefs d'interface de revêtements multi-couches. Application au test d'adhérence par chocs laser.“, E.N.S.M.A. et Faculté des sciences fondamentales et appliqués, Poitiers, PhD, Dez. 2004.
- [6] L. Berthe, „Processus de claquage de milieux transparents sous irradiation laser. Application au choc laser en régime de confinement par eau.“, Université de Paris XI, PhD N°5256, 1998.
- [7] L. Berthe, R. Fabbro, P. Peyre, und E. Bartnicki, „Wavelength dependent of laser shock-wave generation in the water-confinement regime“, *Journal of Applied Physics*, Bd. 85, Nr. 11, S. 7552, Juni 1999.
- [8] A. Sollier, „Etude des plasmas générés par interaction laser-matière en régime confiné. Application au traitement des matériaux par choc laser.“, Université de Versailles St-Quentin, PhD, Sep. 2002.
- [9] T. Antoun, L. Seaman, D. R. Curran, G. I. Kanel, A. V. Razorenov, und A. V. Utkin, *Spall Fracture*. Springer, 2003.
- [10] S. P. Marsh, *LASL Shock Hugoniot Data*. University of California Press, 1980.
- [11] Y. B. Zel'dovich, *Physics of Shock Waves and High-Temperature Hydrodynamic Phenomena*. Courier Corporation, 2002.
- [12] J. P. Cuq-Lelandais, „Etude du comportement dynamique de matériaux sous choc laser subpicoseconde“, E.N.S.M.A. et Faculté des sciences fondamentales et appliqués, Poitiers, PhD, Okt. 2010.
- [13] H. D. Espinosa, S. Dwivedi, und H.-C. Lu, „Modeling impact induced delamination of woven fiber reinforced composites with contact/cohesive laws“, *Computer Methods in Applied Mechanics and Engineering*, Bd. 183, Nr. 3–4, S. 259–290, März 2000.
- [14] O. Allix, M. Dommangeat, M. Gratton, und P.-L. Hérel, „A multi-scale approach for the response of a 3D carbon/carbon composite under shock loading“, *Composites Science and Technology*, Bd. 61, Nr. 3, S. 409–415, Feb. 2001.
- [15] C.-F. Yen, „Ballistic impact modeling of composite materials“, in *Proceedings of the 7th international LS-DYNA users conference*, 2002, Bd. 6, S. 15–23.
- [16] L. J. Deka und U. K. Vaidya, „LS-DYNA® Impact Simulation of Composite Sandwich Structures with Balsa Wood Core“, in *10th international LS-DYNA users conference*, 2008.
- [17] M. Loikkanen, G. Praveen, und D. Powell, „Simulation of ballistic impact on composite panels“, in *10th International LS-DYNA users conference*, 2008, S. 1–12.
- [18] F.-K. Chang und K.-Y. Chang, „A Progressive Damage Model for Laminated Composites Containing Stress Concentrations“, *Journal of Composite Materials*, Bd. 21, Nr. 9, S. 834–855, Sep. 1987.
- [19] A. A. Lukyanov, „An equation of state for anisotropic solids under shock loading“, *Eur. Phys. J. B*, Bd. 64, Nr. 2, S. 159–164, Aug. 2008.
- [20] R. Vignjevic, N. Djordjevic, und T. De Vuyst, „Progressive Damage in Woven CFRP in Presence of Shock Waves“, in *ECCM*, Venice, 2012, S. 8.
- [21] M. Wicklein, S. Ryan, D. M. White, und R. A. Clegg, „Hypervelocity impact on CFRP: Testing, material modelling, and numerical simulation“, *International Journal of Impact Engineering*, Bd. 35, Nr. 12, S. 1861–1869, Dez. 2008.
- [22] S. Ryan, M. Wicklein, A. Mouritz, W. Riedel, F. Schäfer, und K. Thoma, „Theoretical prediction of dynamic composite material properties for hypervelocity impact simulations“, *International Journal of Impact Engineering*, Bd. 36, Nr. 7, S. 899–912, Juli 2009.
- [23] R. Ecault, „Experimental and numerical investigations on the dynamic behaviour of aeronautic composites under laser shock - Optimization of a shock wave adhesion test for bonded

- composites“, E.N.S.M.A. - Sciences et Ingénierie en Matériaux, Mécanique, Energétique et Aéronautique, Poitiers, PhD, 2013.
- [24] P. Ballard, „Contraintes résiduelles induites par impact rapide. Application au choc-laser.“, phdthesis, Ecole Polytechnique X, 1991.
- [25] P. Peyre, *Traitement mécanique superficiel d’alliages d’aluminium par ondes de choc-laser. Caractérisation des effets induits et application à l’amélioration de la tenue en fatigue*. Compiègne, 1993.
- [26] M. Boustie, J. P. Cuq-Lelandais, C. Bolis, L. Berthe, S. Barradas, M. Arrigoni, T. de Resseguier, und M. Jeandin, „Study of damage phenomena induced by edge effects into materials under laser driven shocks“, *Journal of Physics D: Applied Physics*, Bd. 40, Nr. 22, S. 7103–7108, Nov. 2007.
- [27] R. Bossi, K. Housen, und W. Shepherd, „Application of Stress Waves to Bond Inspection“, *SAMPE Proceedings, Long Beach, CA*, S. 1–14, 2004.
- [28] R. Ecault, M. Boustie, F. Touchard, L. Berthe, L. Chocinski, B. Ehrhart, und C. Bockenheimer, „Damage of composite materials by use of laser driven shock waves“, gehalten auf der Proceedings of the American Society for Composites 26th Annual Technical Conference/2nd Joint US-Canada Conference on Composites, Montreal, Quebec, Canada, 2011, S. 14.
- [29] D. W. Sokol, C. T. Walters, J. L. Dulaney, und S. M. Toller, „Laser System and Method for Non-destructive Bond Detection and Evaluation“, US 2005/0120803 A1, 09-Juni-2005.
- [30] B. P. Fairand und A. H. Clauer, „Laser generation of high-amplitude stress waves in materials“, *Journal of Applied Physics*, S. 1497–1502, 1979.
- [31] R. Fabbro, J. Fournier, P. Ballard, D. Devaux, und J. Virmont, „Physical study of laser-produced plasma in confined geometry“, *Journal of Applied Physics*, Bd. 68, Nr. 2, S. 775, Juli 1990.
- [32] B. P. Fairand und A. H. Clauer, „Laser generated stress waves: their characteristics and their effects to materials“, in *Laser-Solid Interactions and Laser Processing*, 1979, Bd. 50, S. 27–42.
- [33] B. P. Fairand und A. H. Clauer, „Applications of Laser-Induced Stress Waves“, gehalten auf der Lasers in Modern Industry Seminar, Cambridge, Massachusetts, 1978.
- [34] A. Clauer, J. Dulaney, R. Rice, und J. Koucky, „Laser Shock Processing for Treating Fastener Holes in Aging Aircraft“, gehalten auf der Durability of metal aircraft structures: proceedings of the International Workshop on Structural Integrity of Aging Airplanes, March 31-April 2, Atlanta, 1992, S. 350.
- [35] M. Perton, A. Blouin, und J.-P. Monchalain, „Adhesive bond strength evaluation in composite materials by laser-generated high amplitude ultrasound“, *Journal of Physics: Conference Series*, Bd. 278, Nr. 012044, Jan. 2011.
- [36] R. Bossi, K. Housen, C. Walters, und D. Sokol, „Laser bond testing“, *Materials Evaluation*, Bd. Vol. 67, Nr. 7, S. 819–827, 2009.
- [37] LSP Technologies Inc., „Laser Bond Inspection.“ LSP Technologies, Inc., 2011.
- [38] L. Berthe, R. Fabbro, P. Peyre, L. Tollier, und E. Bartnicki, „Shock waves from a water-confined laser-generated plasma“, *Journal of Applied Physics*, Bd. 82, Nr. 6, S. 2826, Sep. 1997.
- [39] R. Fabbro, P. Peyre, L. Berthe, A. Sollier, und E. Bartnicki, „Physics and applications of laser shock processing of materials“, 2000, Bd. 3888, S. 155–164.
- [40] V. Gupta und J. Yuan, „Measurement of interface strength by the modified laser spallation technique. I. Experiment and simulation of the spallation process“, *Journal of Applied Physics*, Bd. 74, Nr. 4, S. 2388–2396, Aug. 1993.
- [41] M. Arrigoni, S. E. Kruger, A. Blouin, D. Lévesque, B. Arsenault, J. P. Monchalain, M. Boustier, und L. Berthe, „Adhesive Bond Testing by Laser Induced Shock Waves.“ National Research Council Canada, Industrial Materials Institute, 25-Okt-2008.
- [42] C. Bolis, L. Berthe, M. Boustier, M. Arrigoni, S. Barradas, und M. Jeandin, „Physical approach to adhesion testing using laser-driven shock waves“, *Journal of Applied Physics*, Bd. 40, S. 3155 – 3163, 2007.
- [43] R. Jagdheesh, M. Boustie, L. Berthe, M. Arrigoni, und M. Jouiad, „Interfacial Strength Measurement of Bonded Aluminum Foils by Laser-Driven Shock Waves“, *Surface Modification Technologies XXII*, S. 3 –10, 2009.
- [44] E. Gay, L. Berthe, M. Boustie, M. Arrigoni, J. P. Monchalain, M. Perton, A. Blouin, A. Johnston, R. Cole, J. Barroeta-Robles, und E. Buzaud, „Experimental Investigation of a Composite Behaviour under short Laser-Shock Loading“, 2010.
- [45] LSP Technologies Inc., „Laser Bond Inspection“, Dublin, OH, Dez-2010.

# CHAPTER C: PREPARATION AND CHARACTERIZATION OF WEAK ADHESIVE BOND SPECIMENS

## TABLE OF CONTENTS

1. INTRODUCTION .....	72
2. PROCESSES FOR WEAK ADHESIVE BONDS MANUFACTURING .....	72
2.1 About contamination.....	72
2.1.1 Contaminants.....	72
2.1.2 Contamination processes and effects.....	73
2.2 Selected methodology for contamination.....	75
2.3 Summary on weak bonds production .....	76
3. EXPERIMENTAL METHODS FOR CONVENTIONAL CHARACTERISATION OF BONDED SPECIMENS .....	77
3.1 Dynamic Scanning Calorimetry (DSC) .....	77
3.2 Ultrasonic and Phased Array Ultrasonic Testing (UT & PAUT).....	78
3.3 X-Ray Photoelectron Spectroscopy (XPS) .....	80
3.4 Wetting behavior with Surface Analyst™ .....	81
3.5 X-ray radiography.....	82
3.6 Optical Microscopy.....	83
3.7 Scanning Electron Microscopy (SEM) .....	84
3.8 Double Cantilever Beam Test ( $G_{1C}$ ).....	85
3.9 Summary on characterization methods .....	87
4. PREPARATION AND CHARACTERIZATION OF WEAK ADHESIVE BONDED CFRP SPECIMENS .....	88
4.1 Specimens families .....	88
4.2 Specimen nomenclature.....	89
4.3 Monolithic laminates preparation .....	89
4.3.1 Materials choice .....	89
4.3.2 Composite lay-up .....	90
4.3.3 Curing cycle .....	90
4.3.4 Surface pre-treatment .....	91
4.3.5 Contamination of adherent surface and verification .....	93
4.4 Adhesive bonding.....	95
4.4.1 Specimens preparation .....	95
4.4.2 Verification of degree of cure.....	97
4.4.3 Characterization of the adhesive bondline.....	99
4.5 Conditioning of moisture aged composite panels .....	101
4.6 Adhesive bond mechanical performances .....	102
4.6.1 Performances of fully and partially cured bonded specimens .....	103
5. SUMMARY .....	107
REFERENCES - CHAPTER C .....	108

## 1. INTRODUCTION

This 3<sup>rd</sup> chapter introduces a methodology used to investigate the technology of laser proof test presented in the previous chapter B. First, the scientific objectives of this thesis are presented and technological points needing to be studied are enumerated. Afterwards, the state of the art regarding the first key criteria, namely the controlled generation of weak adhesive bonds already introduced in chapter A is detailed. The selection of one relevant method for the generation weak adhesive composite bonds is important to ensure that proper specimens are available for the assessment laser proof tests capabilities.

The following part 4 refers to all the methods of conventional characterization previously mentioned in the manufacturing and tests procedure. Each measuring principle from laboratory characterization method (DSC, XPS) to conventional NDT method (UT & PAUT, X-Ray) and mechanical testing method (DCB) is explained.

Finally, this chapter is concluded with the presentation of the manufacturing process and the results from the all conventional characterization for each family of specimens manufactured according to the detailed test plan.

## 2. PROCESSES FOR WEAK ADHESIVE BONDS MANUFACTURING

The preparation of reliable weak adhesive bond is the first essential step when it comes to the development of a method for assessing weak adhesion. In Chapter A, part 2.4 introduced the studies present in the literature, which attempt to investigate weak adhesive bonds though several methods. If those methods varies depending on the aim of each author, it is in general however agreed that the key parameters for adhesion properties are surface roughness (mechanical interlocking) and contamination (chemical modifications). The contamination parameter has been selected in many studies that may be shortly summarized here again. Its application is depending on the nature of the adhesive, the substrate but also the processes in place. In this study focusing on the aeronautic industry and lightweight materials, the substrate of interest is carbon fiber reinforced and typical adhesives are epoxy adhesive films systems.

### 2.1 About contamination

#### 2.1.1 Contaminants

Several investigations presented in chapter A involved **contaminations of adhesive bonds after bonding** (ageing) with the example of immersion in pure or salted water at high temperature [1]–[3] to damage a good adhesive bond and weaken it. This approach does not represent the safest method for weak bond generation since it assumes that the bonding process itself has been carried out perfectly and that the adhesive bonds are of high adhesion performance before starting the damaging process, itself not easy to master.

The contamination of the surface substrate is more likely to have a direct influence on the adhesion quality by influencing the chemistry of the adherent surface. In this connection, a wide variety of exotic substances have already been tested: artificial human sweat, mineral and vegetal oils, detergents, etc. are mentioned in the literature. The interest is however

focused in this study on aeronautic relevant contamination sources. In this context, fuel, hydraulic fluids and de-icing fluids are relevant contaminants for the aeronautic industry but rather in the case of repair purposes. Other manufacturing relevant contaminants are typically based on mold release agents.

**Mold release agent**, also **release agent**, are of various nature and are used for composite manufacturing on order to have a smooth unloading process with tooling roughness aspect. The nature of release agents can be either PTFE, as spray [4] or polymer film [5], [6] placed at the interface of the bond and substrate, or a silicon-based or siloxane-based mold release agent diluted in dibutylether (Frekote, Marbocote, etc.) or water-based (Departure). Like PTFE, the use of silicon-based release agents can also be either in solid [7] or in the fluid form [8]–[10] and is well documented in the literature. Alternative contaminants, fluor or silicon-based may also be applied in diverse forms. The contaminant itself is only partly responsible for the bond performance. The method for application of the contaminant, as well as the bonding process parameters play indeed decisive roles on the adhesion strength since they condition the thickness, and so amount, of contaminant at the adherent surface.

### 2.1.2 Contamination processes and effects

The literature reports different application of the contaminants: the first method involves the application of Frekote by means of a **fine and tightly spun cotton bud**. In the work of Jeenjitkaew et al., two coats were applied with a dwell time of 20-30 minutes between both applications. A SEM observation with WDX showed the presence of a 1  $\mu\text{m}$  interlayer at the aluminum-epoxy interlayer. The SEM observation indicated that the Frekote layer was observed to be on the atomic scale. Also the presence of C, O and Si at the substrate surface and within a few micrometers away from the surface was determined. This confirmed the content of PDMS (polydimethylsiloxane) in Frekote. As a result, the measurement of the total free surface energy showed a decrease of 67% in comparison to the non-contaminated control specimen. Frekote provided a full release with the experiments showing a reduction of 27% in joint strength with only 25% of contaminated joint area [10]. Others could not achieve a good differentiation between “normal” and weak bond even though they applied three times the contaminant to form a thicker layer [11]. These experiments highlight the important role of type of application without giving any clear indication on the concentration of release agent applied. Rieck and Wetzel et al. observed that even until a volume concentration of 1%, the effect of release agents on the adhesive layer were still detectable [12], [13]. Furthermore, the manual application with a cotton bud or even a soaked cloth implies a human factor and so, a lower repeatability compared to an automated process. Two possible alternative may be considered.

The second variant is **only applicable in the case of composite** manufacturing. In this case, a **contaminated peel-ply** (either voluntarily with liquid contaminant or due to a bonding incompatible coating e.g. Super Release Blue SRB) can be used during the manufacturing process of the raw composite. The contaminant remains at the composite surface after the peel-ply removal. The surface substrate is then irremediably textured by the peel-ply, which has an impact on the surface roughness. The homogeneity of the coating on the peel-ply is however an important parameter that cannot be completely ensured in such a method. Also, the manufacturing of composite panels with this technique implies that the whole substrate

surface has the same contamination. Different contamination grades can hence only be obtained by post-treatment of this surface, for example with sandpapering or with atmospheric plasma treatment (see Figure C.1).

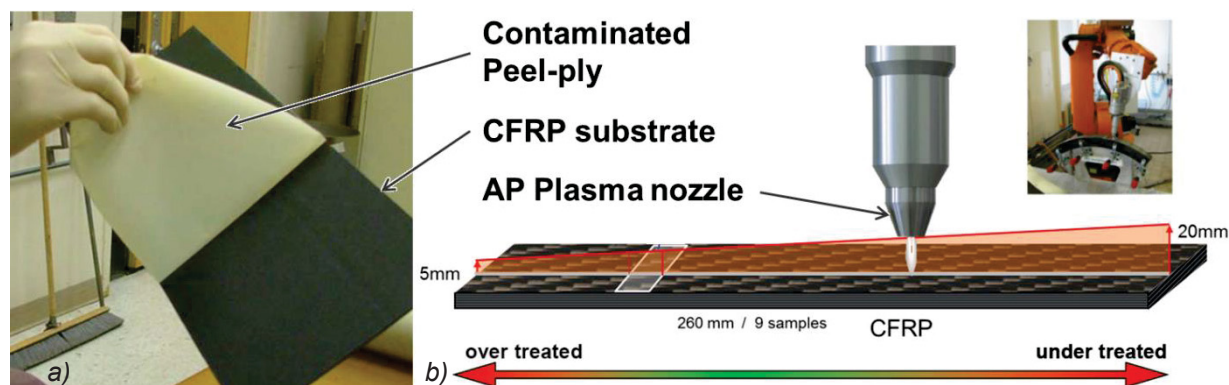


Figure C.1: a) Illustration of contaminated peel-ply removal and b) scheme of atmospheric pressure plasma cleaning process with effects of nozzle distance inspired from [14]

The most common methods are sandpapering, grit-blasting or grinding. These methods are however badly reproducible due to the difficulty to describe the mode of operation and to define how to produce different levels of contamination. At last, the plasma treatment could be an optimal solution which has known a rapid development. The current state of the art technologies allow an exact regulation of power, distance and speed of the plasma while being fully user-independent.

Finally, the third variant is the most adaptable solution: the contamination with mold release agent carried out by **dip-coating**. Dip-coating enables the homogenous application of contaminant on the adherent surface based on the immersion at a precise rate in a contaminated solution. The system used is represented by Figure C.2.

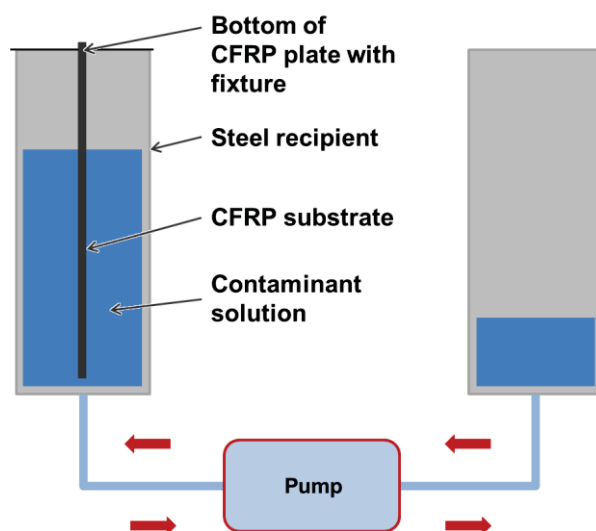


Figure C.2: Scheme from contamination with dip-coating process

Two steel recipients are connected by pipes and a continuous pump enabling an immersion at constant speed rate and so, the application of an homogenous thickness of contaminant at the surface. The solution used is generally made of Frekote diluted into hexane/heptane to adjust



the concentration of the contaminant and hence the thickness of the layer applied on the surface. Dip-coating has the advantage to have only few machine parameters and to be user-independent. It enables a uniform thin release agent films (few nm) with a high reproducibility. Markus performed CFRP surfaces preparation based on dip-coating process successfully, showing that layers of 8 nm with a standard deviation of 12% between 3 different manipulations could be obtained [15]. Naturally, an optimal dip-coating process demands an homogenous contamination solution (diluted or not), and the outcomes are affected by the solution viscosity and the substrate surface free energy. This third method allows the application of different concentrations and an easy repetition capability (to increase the layer thickness) in comparison to the use of a contaminated peel-ply during production. The substrate surface can be pre-treated or post-treated whereas it can only be post-treated in the case of the peel-ply technique.

These three methods all have pros and cons. In general, to obtain a weak adhesive bond with an adhesive failure, the contaminant must not diffuse into the materials but stay at the substrate interface. Therefore, all the approaches presented include a dry-out of the contamination layer to ensure its cross-linking. Engholm showed also that the contaminant layer shall not exceed 10% of the bond line whole thickness to avoid any mechanical interaction in the mechanical performance of the adhesive joint [16].

## 2.2 Selected methodology for contamination

The experiences of close work groups from Airbus as well as the literature have influenced the choice for the material and the preparation method for weak adhesive bond. For an optimal comparison with the results generated by parallel working groups, the approach for this study was selected similarly.

The material selected is the epoxy composite tape material from Hexcel M21 with carbon fibers T800S. The lay-up is made of 6 layers  $(0_2, 90)_S$  for a standard monolithic plate of thickness of 1.5 mm. The monolithic plates are however manufactured with a release film instead of a peel-ply on both surfaces (bag side and tool side) due to one sandpapered side before contamination and the other in order to provide smooth and shiny surfaces for the tests with time-resolved measurements (VISAR and EMAT) and also ease the UT inspections by contact methods.

The contamination of the adherent surface takes place after the adherent surface sanding and cleaning steps, also including a water break test. It is performed with help of the dip-coating process with however lower concentrations of release agent. The dip-coating is followed by a dry-out for 30 min at room temperature and for 60 min at 80 °C in an oven with air-circulation. The contaminated surfaces are characterized to quantify the amount of silicon remaining at the top surface: in this case also XPS was chosen to indicate the residual concentration of Silicon in at.% from at least two distinct vertical positions on the substrate surface. This approach for the contamination has been privileged over contamination due to peel-ply due to the impossibility to ensure the homogenous peel-ply contamination and the dependency on the cleaning process with AP Plasma necessary afterwards.

After contamination, the panels in this work were not bonded with secondary bonding but with the co-bonding process (uncured + adhesive film on cured). Co-bonding offers two main advantages over secondary bonding: i) the process is the actual bonding process in Airbus manufacturing and ii) it spares the preparation of the surface from the adherend composite. Jeenjitkaew also evidences that the diffusion of Silicon into the adhesive or even the uncured composite panel is very limited if the contamination has been dried out before. Only few microns in depth in the adhesive or in the surface interphases displayed traces from Frekote after an hour at 175 °C [10]. The 180 °C epoxy adhesive film FM300 K.05 was used for the co-bonding process.

Three parameters can be highlighted in the selected approach for the present work:

- the **CFRP surfaces** were *sandpapered* and had their cleanliness assessed by water-break test,
- the **contamination** by *dip-coating with different Frekote concentrations* enabled different grades of adhesion strength thanks to the contamination process itself,
- the **bonding process** involved *co-bonding with a 180 °C* adhesive system.

### 2.3 Summary on weak bonds production

The choice of specimen preparation has been based on results from the literature. The most important change compared to the literature consists in the co-bonding process, which matches currently used bonding production processes. Table C.1 summarizes the approach of the present work. The names of the products used are not mentioned anymore in the next sections.

**Table C.1: selected approach for the preparation of weak adhesive bonds**

	<b>Selected approach</b>
<b>Material</b>	Epoxy Tape UD M21/T800S
<b>Monolithic Composite Lay-up</b>	(0 <sub>2</sub> , 90) <sub>S</sub> – 1.6 mm thick
<b>Adherent Surface preparation</b>	Sandpapered & water break test
<b>Contaminant / Release agent</b>	Frekote 700 NC (PDMS)
<b>Contamination process</b>	Dip-coating
<b>Adhesive</b>	Cytec FM 300 K.05 180 °C
<b>Adhesive bonding process</b>	Co-bonding with clean laminate

The next part will introduce in detail the different characterization methods used in this work for the investigation of the specimens during the specimens preparation, prior and after laser tests.

### 3. EXPERIMENTAL METHODS FOR CONVENTIONAL CHARACTERISATION OF BONDED SPECIMENS

The present part introduces the experimental methods used for the conventional characterization of the composite laminates, the contamination, as well as the adhesive bond quality. Each method and its functioning principle is presented. These methods for conventional characterization are more or less laboratory methods with a broad variety of technologies and measurement principles (destructive and non-destructive), which require specific specimens and which are therefore at least partially destructive testing methods in most cases. Several methods are also only applied to the base materials. Also, conventional NDT techniques like UT or X-Ray Radiography or computed tomography are applied. They also are restricted to small samples and parts with simple geometry.

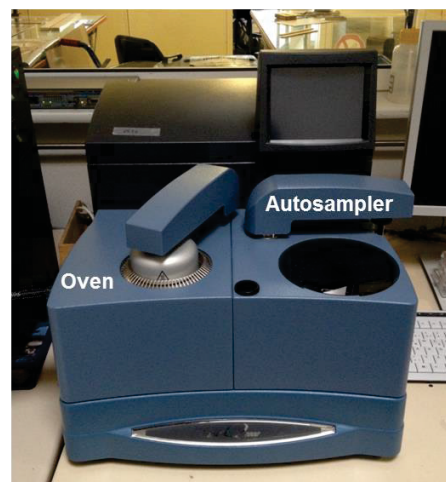
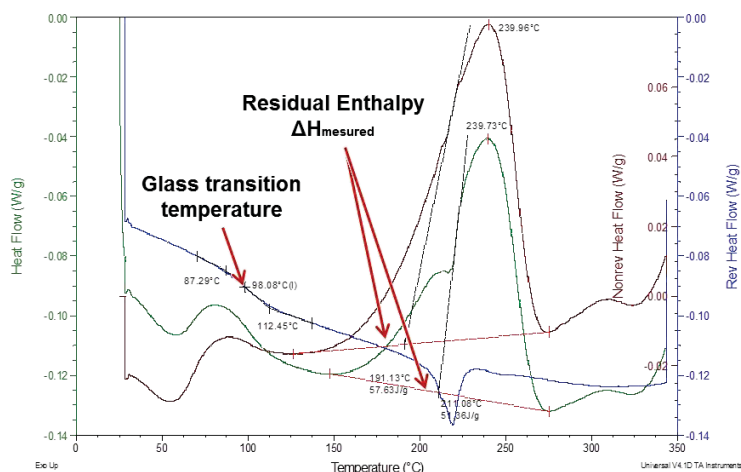
#### 3.1 Dynamic Scanning Calorimetry (DSC)

Dynamic Scanning calorimetry (DSC) is a thermal analysis technique which monitors heat effects associated with phase transitions (fusion, crystallization, glass transitions, etc.) and chemical reactions as a function of temperature. The difference in heat flow  $dH/dt$  between the investigated sample and a reference in the same oven is recorded as a function of a temperature cycle. This difference of heat flow is either positive or negative depending on the endo- or exothermic process. In general, the reference is an inert material such as alumina or an empty aluminum pan. In classical DSC, the temperature of both samples and reference is increased at a constant and linear rate. The latest evolution called modulated DSC involves a modulation in the linear temperature. The modulation allows the simultaneous measurement of both heat flow and heat capacity and separates the reversible processes from the irreversible ones. The periodic mix of low heat rate and high heat rate combines the advantages of high resolution and high sensitivity, allowing a more precise detection of fine changes in the analysis [17], [18].

In this work, the variation of enthalpy  $\Delta H_{\text{measured}}$  is calculated to evaluate the cure degree  $\alpha$  of the adhesive film and the composite substrates. This evaluation is conducted based on Eq.1.

$$\alpha = 1 - \frac{\Delta H_{\text{measured}}}{\Delta H_{\text{reference}}} \quad \text{Eq.1}$$

To evaluate the reaction enthalpy for a fully cured part  $\Delta H_{\text{reference}}$ , samples from the adhesive film and the composite pre-preg batch are taken as reference. The glass transition temperature is also measured to allow a comparison with literature data on the used materials.

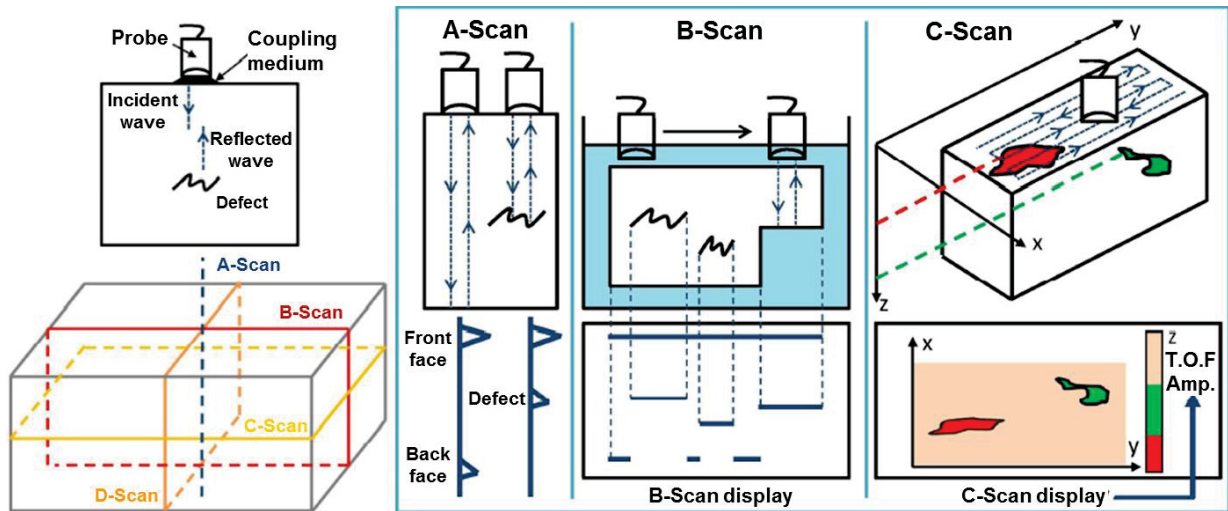


**Figure C.3: DSC plots of partially cured M21/T800 as example and illustration of the used experimental DSC Calorimeter TA Q2000**

The modulated DSC analysis is performed with a Q2000 calorimeter from the company TA Instruments (see Figure C.3). The preparation of the samples is conducted by grinding of corners and edges of the cured composite plates and the analysis of  $11 \pm 2$  mg of grinded dust or uncured material. The material are weighted, placed carefully in the pans and with the lid previously pinched to enable the escape of gas during the test. The pans are installed in the DSC sampler and the test parameters are programmed. In this work, the DSC samples are stabilized 2 minutes at 25 °C and then heat up to 350 °C with a linear heating ramp of 5 °C/min. A modulation of the heating rate of  $\pm 0.5$  °C every 40 seconds is used. The analysis of the results is then realized with the software TA Universal Analysis 2000 from TA Instruments.

### 3.2 Ultrasonic and Phased Array Ultrasonic Testing (UT & PAUT)

Ultrasonic testing (UT) and its phased array variant are methods based on the sound wave propagation and reflection phenomenon in materials. UT can be used to detect defects generating new interfaces like pores, crack, delaminations, disbonds, etc. and were identified as best solution for visualizing indications of potential defects in CFRP before and after laser proof tests. A piezoelectric transducer vibrating at a Mhz frequency generates an ultrasonic wave which propagates in the inspected material. The sound waves are affected by changes of acoustic impedance  $Z_i$ . The signal is reflected or attenuated before being detected either from a single emitter-receiver (pulse-echo mode) or on the opposite side with a separated receiver (through transmission mode). This reflection and attenuation gives an indication of depth and size of the defect thanks to the Time Of Flight (TOF) and Amplitude (Amp) that allow a quantitative evaluation. The result of the sound beam of one single transducer in 1D is represented by a so-called A-scan. Other representation in 2D are available: the B-scan is a cut view of the specimen in the direction of the sound beam; the C-scan is a view from the top surface plane, orthogonal to the sound wave. All these representations are illustrated in Figure C.4.



**Figure C.4: Illustration of pulse-echo technique with representations of A-, B-, C- and D-scan in space with their corresponding signals [19]**

The first UT inspection was performed for the quality control of the monolithic composite structure with UT techniques in immersion according to the test method AITM 6-0045. The pulse-echo mode (Figure C.4) was used with a focused probe Olympus V309F operating at 5 MHz and with a beam width of 12.7 mm. The step size was of 2 mm and no time corrected gate (TCG) was applied. Data were acquired and the evaluation was made manually with NDT Kit® (also named Ultis).

The second and third inspections were conducted on the adhesive bonded panels ( $250 \times 200 \times 3 \text{ mm}^3$ ), respectively prior and after the application of laser proof tests. A R/D Tech Omniscan MX, with phased array module and an Olympus probe head 5L-I3 5 MHz with 128 elements and a 2 cm Plexiglas delay line were used. The data were acquired with a TCG of 15 dB at 4 mm depth. The signals were later visualized and analyzed with help of the Olympus TomoView software or NDT Kit v2.5.1. Both setups including the typical scans pattern are represented in Figure C.5. The view of UT signals in A-, B- and C-scans is also represented, especially in the case of the PAUT mobile inspection.

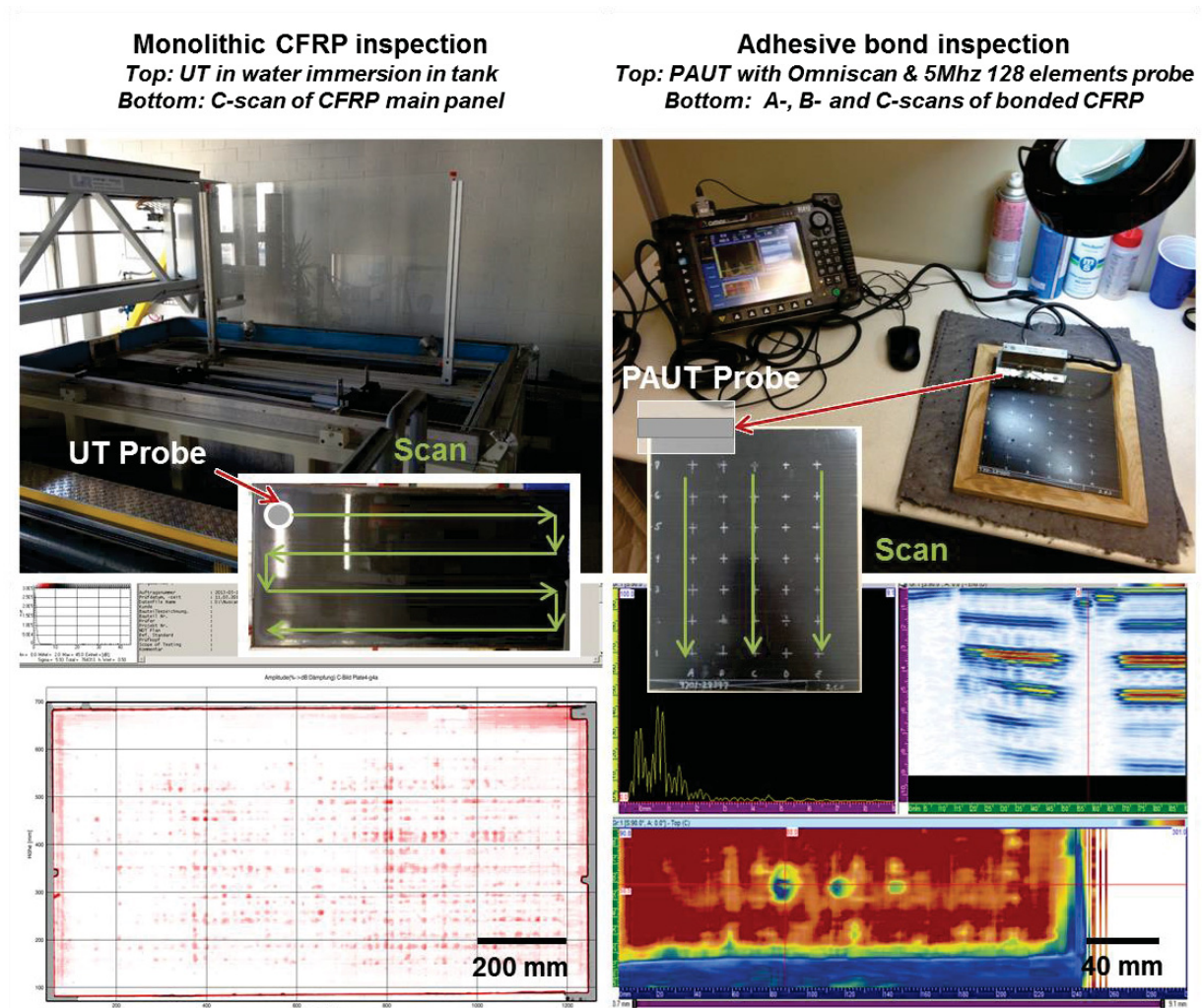
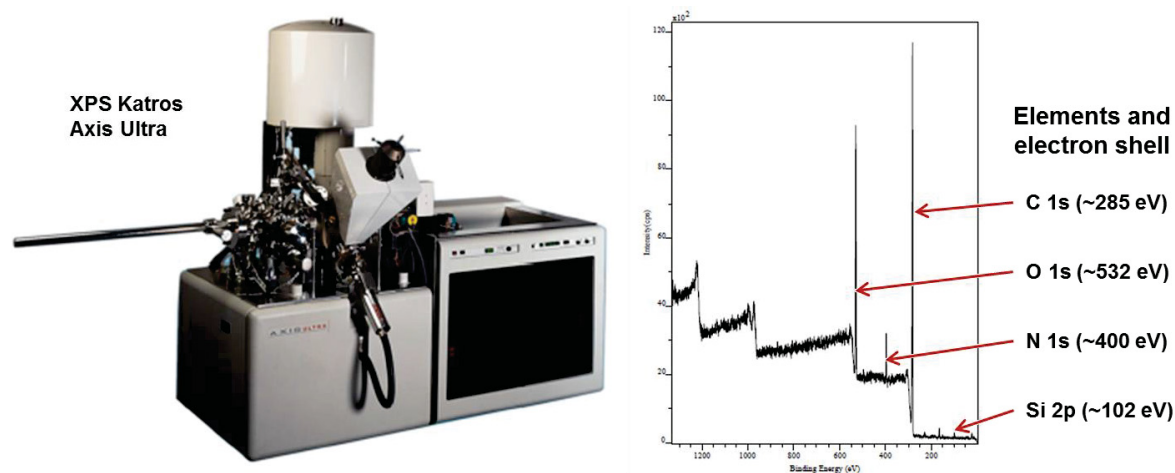


Figure C.5: ultrasonic inspection setups in UT immersion or mobile PAUT with according scans performed and results visualization

### 3.3 X-Ray Photoelectron Spectroscopy (XPS)

The X-Ray Photoelectron Spectroscopy (XPS) measures the photoelectrons emitted by an object exposed to x-rays radiation based on the photoelectric effect. The kinetic energy of these electrons can be analyzed using the relation  $E_{hv} = E_{kin} + E_B$ , where  $E_{hv}$  is the total energy,  $E_{kin}$  is the kinetic energy and  $E_B$  is the binding energy of the electrons. The calculated binding energy is characteristic for each element and its chemical binding state which enable the determination of the atomic composition of examined surface. XPS is only surface sensitive since it can only detect electron emitted in a depth of about 10 nm.



**Figure C.6: XPS Kratos Ultra system and obtained spectra (intensity in A.U. in function of electron binding energy in eV)**

XPS requires small specimens (few  $\text{mm}^2$ ) due to the small measurement chamber where an ultra-high vacuum needs to be done. Process control specimens were hence manufactured to be contaminated and cut in order to be measured by XPS. Measurements were conducted using Kratos Ultra (Figure C.6) applying the following acquisition parameters: base pressure:  $4 \cdot 10^{-10}$  mbar, sample neutralization applying 3.3 eV electrons, hybrid mode (electrostatic and magnetic lenses are used), take off angle of electrons  $0^\circ$ , pass energy 20 eV in high resolution spectra and 160 eV in survey spectra, excitation of photoelectrons by monochromatic  $\text{Al}_k$  radiation. The analysis area is elliptically shaped with main axes of  $300 \mu\text{m} \times 700 \mu\text{m}$ . All spectra (see ) taken are quantified using the “relative sensitivity method” which is based on the assumption of a homogeneous distribution of the considered elements within the information depth (up to 10 nm). XPS spectra are documented without charge correction. The energy scale can be corrected by referring the C1s component of C-C and C-H species to 285.0 eV binding energy [20].

### 3.4 Wetting behavior with Surface Analyst™

The Wetting behavior evaluation of a substrate surface characterizes the surface energy and its wettability for the adhesive. The Surface Analyst (SA)™ is not an established reference characterization tool but is based on the same principle as most of the wetting aerosol devices: the surface energy is calculated from the contact angle of a drop of probe liquid on the surface to be evaluated. The particularity of the Surface Analyst is the ballistic deposition of the probe fluid drop on the surface. Indeed, the drop is spread on the surface from a pulsed stream of microdrops, providing the on-growing drop with kinetic energy which helps the drop to reach its equilibrium shape. Heterogeneities from composite structure (roughness or chemistry effects of the surface) are avoided and the results are more accurate than with classical methods. The volume  $V$  of the final drop is known and controlled by the device and stays below  $2 \mu\text{L}$ . The use of little volumes guarantees that the drop will be spherical. The Surface analyst can then optically detect its total perimeter and calculate the average diameter  $d$  of the drop. Knowing the volume and the diameter of the drop, the average contact angle  $\theta$  is obtained using Eq. 2. The entire drop perimeter is evaluated what reduced errors.

$$\frac{d^3}{V} = \frac{24 * \sin(3\theta)}{(\pi(2 - 3 * \cos(\theta) + \cos(3\theta)))} \quad \text{Eq. 2}$$

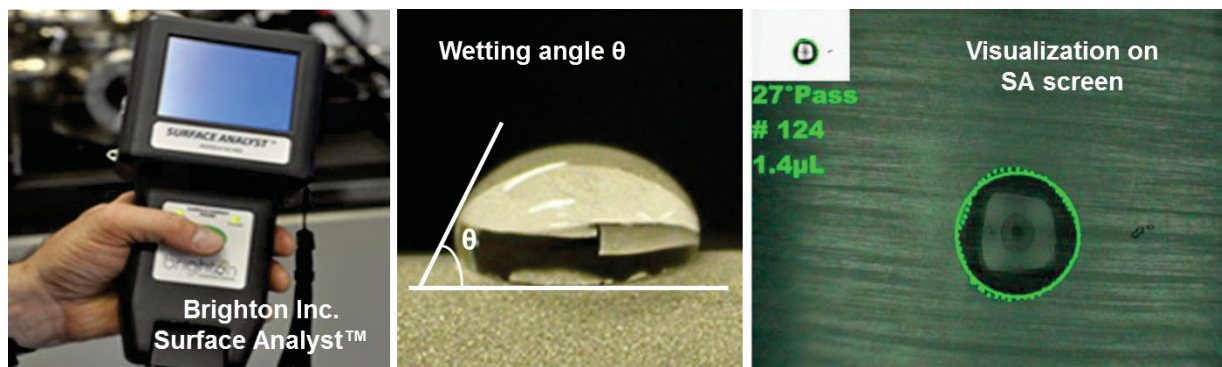


Figure C.7: Brighton Inc. Surface Analysis™, wetting angle and view from a measurement as visible on SA screen

Measurements are taken randomly on the surface of the reference and the conditioned CFRP panels. The determined angles are averaged and correlated to XPS data in at.% Si measured at the surface.

### 3.5 X-ray radiography

X-Ray Radiography uses the principle of differential absorption of x-ray penetrating radiation. Each specimen under evaluation has differences in density, thickness, shape, size, in absorption characteristics which results in the different amounts of radiation absorbed and transmitted (Figure C.8a). The unabsorbed radiation that passes through the part is recorded on a photographic film, fluorescent screens or other radiation monitors. Indications of internal and external conditions appear as variants of grey on exposed film, or variants of color on fluorescent screens. This technique is suitable for the detection of voids and porosity, or also for the detection of foreign bodies incorporated in a part.

In this work, the bonded panels (250\*200 mm<sup>2</sup>) were placed at 5 cm distance before the electronic detector to be inspected in one shot. The X-Ray installation MCN 165 from the company Yxlon GmbH was used in direct exposition mode (Figure C.8b,c,d,e). Measurements were taken with 25 kV and 80 mA for the global radiography. Specific zooms in suspicious areas were done with microfocus using 50 kV and 3 mA in order to enable detection of defects ranging from 50 to 100 μm, especially post laser shocks.



### X-Ray Radiography

- a) Radiography of CFRP specimen
- b) Separated command room
- c) X-Ray source and emitter
- d) CFRP specimen on support
- e) Electronic detector

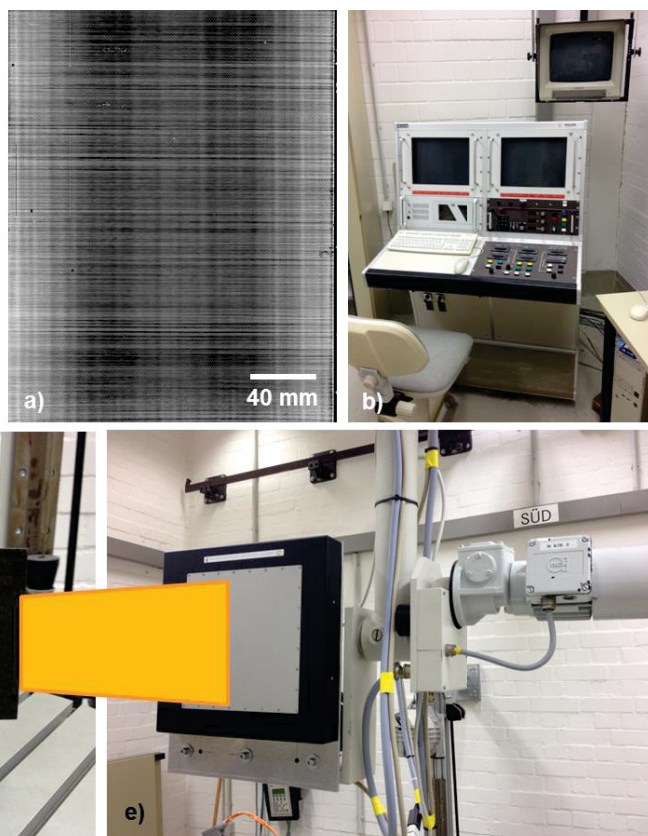
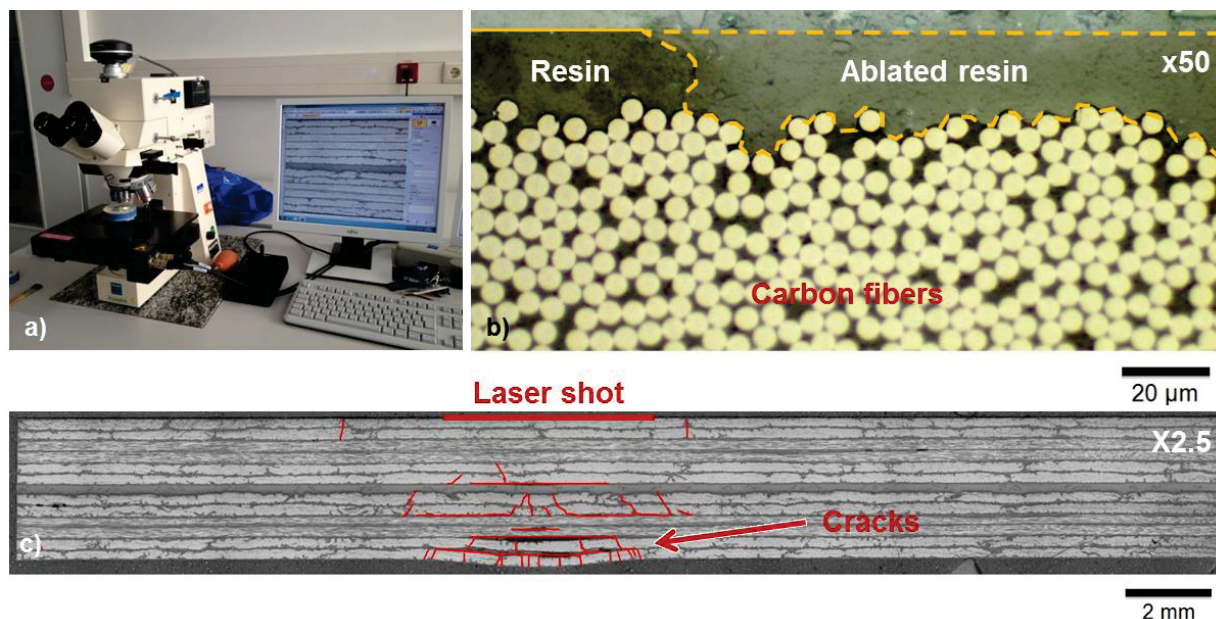


Figure C.8: X-Ray Radiography with a) radiography of one bonded CFRP specimen with revealed fibers orientation and b,c,d,e) general X-Ray installation MCN 165 from Yxlon GmbH and experimental setup

### 3.6 Optical Microscopy

For detailed observations of the laser effects on the CFRP bonded structures, micro-cuts of selected locations for cross-section micrographies have been prepared. This characterization is based on the visual inspection of cross-section with help of different microscopes (Figure C.9a). The range of magnification is depending on the microscope used and rises up to 50x for fine details observation in this work (Figure C.9b). Optical microscopy is a simple but very important final diagnostic because it allows one to observe directly how the structure was impacted by the laser proof test at microscopic level (Figure C.9c). It is the reference way to compare the results obtained with Ultrasonic testing. It is thus applied for the verification of NDT diagnosis, for the determination of crack, delamination real size and for the optimal correlation between NDT data and real defect in presence.



**Figure C.9: Representation of (a) a microscope used with automated table and computer observations, (b) a micrograph of the laser impacted surface (x50) and (c) the cracks observation under microscope in the complete thickness**

The preparation of micro cuts is done by first cutting the composite panels in stripes in the horizontal direction (parallel to the outside  $0^\circ$  layer). Later, the finest cuts are performed directly with a thin ( $<1$  mm) diamond disc mounted on a circular saw perpendicularly to the  $0^\circ$  fibers. This cut is done at the precise location which will be observed. The direction of observation is chosen perpendicular to the  $0^\circ$  fibers (also in majority in the composite) in order to have a better visualization of the cracks. Unfortunately, it is not possible to visualize other crack in the other planes. The specimens were cut in cross section of about 30 mm width, including a location of a laser shot in the middle.

### 3.7 Scanning Electron Microscopy (SEM)

In precise cases where the adhesive interface has to be investigated, detailed images of the adherent surface aspect after  $G_{1C}$  testing have been captured with help of a Scanning Electron Microscope (SEM). The SEM was only applied in particular cases of rupture to evaluate the nature of the rupture and any possible influence from the laser shocks on the adhesive-substrate interface, in comparison to a non-affected interface. A Zeiss SEM model LEO1530 in secondary electron imaging mode (Figure C.10a), with 5 kV voltage and an working distance of 14.5 mm were used. Images were captured with a magnification up to 1000x in resolution 1024\*768 and 112 nm/pixel in 8 bits grey levels. The images from the SEM reveal the failure profiles of the adhesive bond at microscopic level. Carbon fibers or rest of adhesive can be identified precisely (Figure C.10b) and provide an additional level of information regarding the effects of laser shock on the failure mechanism.

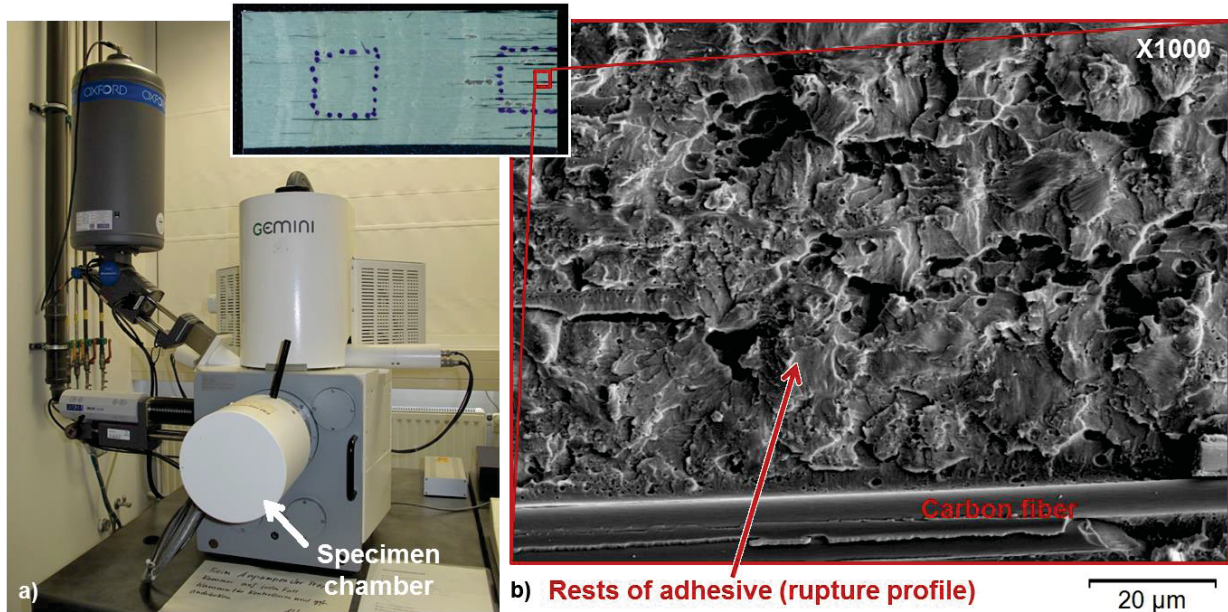


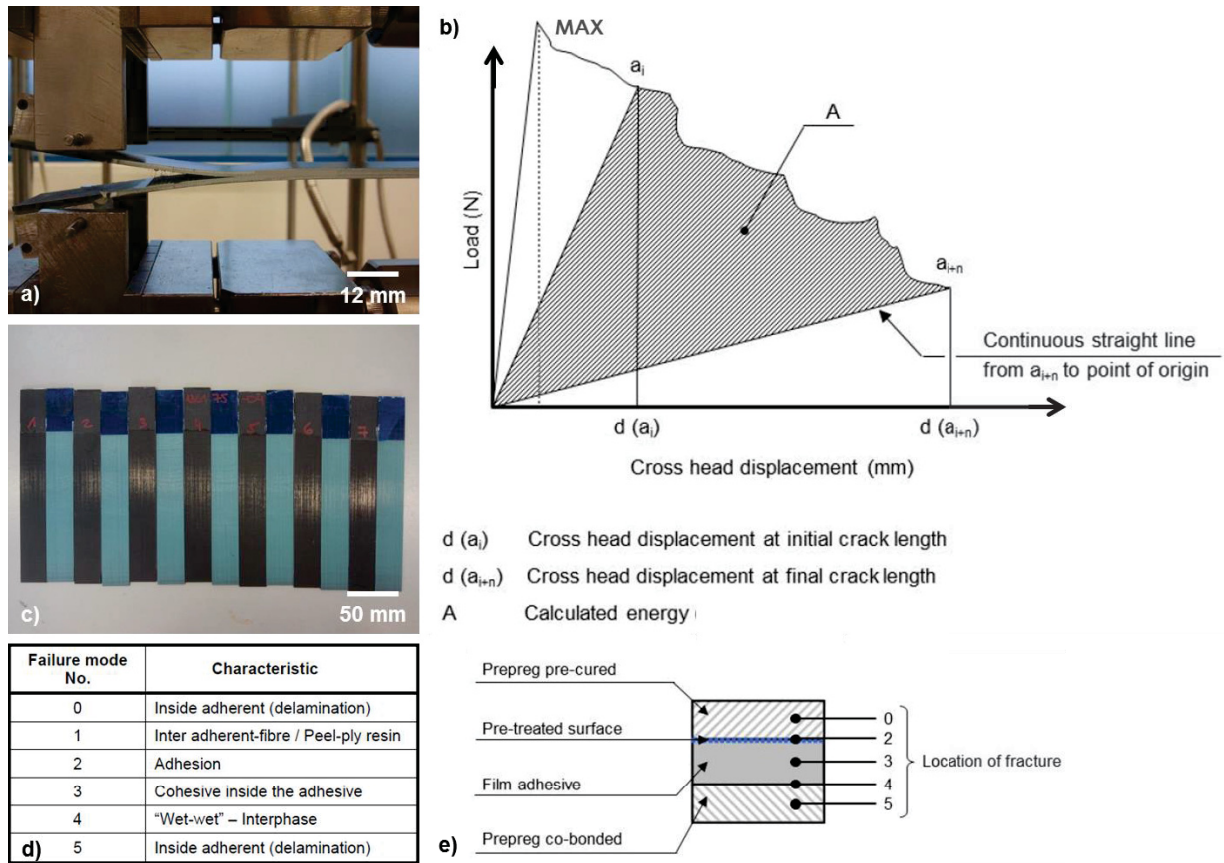
Figure C.10: Representation of (a) the Zeiss LEO 1530 Scanning Electron Microscope used and (b) a micrography of a the adherent surface (x1000) after  $G_{1C}$  test

### 3.8 Double Cantilever Beam Test ( $G_{1C}$ )

The double cantilever beam (DCB) test  $G_{1C}$  is the mechanical test used in this work for the correlation with the laser and contamination data. The  $G_{1C}$  test, already presented in Chapter A, consists in loading the adhesive bondline in pure tension. A pre-crack is first generated by the use of a release film insert in the first 40 mm of the specimens. Its length is of 10 mm further and it correspond to the initiation crack for the measurement. After pre-cracking, the tensile strength is applied in the mode I, perpendicular to the crack plane which hence loads the bond line (Figure C.11a). The crack propagation and the according load are recorded until a crack length of around 110 mm from the initial crack is reached. The fracture toughness  $G_{1C}$  is later calculated based on the AITM Eq. 3 where  $A$  is the energy to achieve the total propagated crack length in J (integration under the curve - Figure C.11b),  $a$  is the propagated crack length after crack initiation in mm and  $w$  is the width of the specimen in mm. The formula is hence an integral from the pre-crack until the final crack. This feature of the AITM formula allows a simpler test than with the ISO norm where the position of crack during propagation has to be marked and later measured.

$$G_{1C} = \frac{A}{a * w} * 10^6 \text{ (J/m}^2\text{)} \quad \text{Eq. 3}$$

The final evaluation of results is correlated to the observation of the specimens failure type, represented here for a co-bonded composite with sanding pre-treatment in Figure C.11c, d and e. The failure modes can be *adhesive* (failure targeted through contamination and weak bond criteria - Figure C.11c here), *cohesive* if the adhesive remaining are on both substrates, *delamination* in case of rupture inside the composite substrate, “*wet-wet*” at the interphase co-bonded/adhesive.



**Figure C.11: Double Cantilever Beam Test  $G_{1C}$  with a) specimen under test, b) the typical load-cross displacement diagram (extract from AITM 1-0053 [21]), c) the failure profile (here adhesion) and d) the existing failure modes with e) the locations in the bonded specimen cross-section**

The tests were performed according to the test method 'AITM' 1-0053 [21]. The specimens were dimensioned shorter than recommended by the AITM norm without any consequence, with only 180 mm instead of 250 mm length. This was done to maximize the amount the number of specimens manufactured out of the CFRP main plates. Seven specimens ( $180 \times 25 \times 3 \text{ mm}^3$ ) were cut out of each bonded panel using water abrasive jet cutting. This process was chosen in order to avoid detrimental vibration effects from conventional diamond saws on the adhesive bond mechanical performance observed in ENCOMB pre-tests. Aluminum load blocks MP005310 in compliance with the AITM norm were used. Each  $G_{1C}$  test was performed in ambient temperature and moisture conditions on a Zwick test machine Z10 1445. A load cell of 10 kN, a crosshead extensometer and a test speed of 10 mm/min were used.

### 3.9 Summary on characterization methods

All characterization techniques used in this work are summarized in Table C.2. For each technique, the information delivered and the application are described.

**Table C.2: Summary of characterization techniques and information expected in this work.**

<b>Characterization Technique</b>	<b>Information targeted</b>	<b>Use in the present work</b>
<b>Dynamic Scanning Calorimetry (DSC)</b>	Remaining reaction enthalpy ( $\Delta H_{\text{measured}}$ ), glass transition temperature (Tg)	Control of degree of cure (adhesive & co-bonded composite)
<b>Ultrasonic and Phased Array Ultrasonic Testing (UT &amp; PAUT)</b>	Size and position of potential defects (delamination, disbonds, pores, etc.)	Control of defects after manufacturing (monolithic plates & bonded panels). Inspection after laser tests for debonds detection
<b>X-Ray Photoelectron Spectroscopy (XPS)</b>	Atomic concentration of contaminant (Si at.%)	Verification of contaminant presence on pre-cured composite surface
<b>Surface Analyst™</b>	Surface energy through wetting angle	Verification of contaminant presence on pre-cured composite surface (experimental)
<b>X-Ray Radiography</b>	Detection of defects (porosity, foreign bodies)	Control of bonded panels after manufacturing
<b>Micrographies</b>	Delaminations and disbonds profile in material microstructure	Evaluation of cracks and debonds after laser proof tests
<b>Double Cantilever Beam Test <math>G_{1c}</math></b>	Fracture toughness energy (mechanical parameter) of bonded specimens	Evaluation of mechanical performance of adhesive bond in pure tension, for correlation with Laser Proof tests results

The next part will introduce in detail the different steps and care taken for the production of the specimens. The composite material, the contamination, the adhesive bonding operations and the intermediate characterization results of the specimens are presented. They introduce the test specimens families used for the laser test designed to provide answers to the scientific objectives.

## 4. PREPARATION AND CHARACTERIZATION OF WEAK ADHESIVE BONDED CFRP SPECIMENS

In this part, the specimens preparation for all specimen families is being introduced. Based on the scientific approach and the questions raised, three different conditioning treatments are performed on top of the adherent surface contamination. All conditioning treatments are introduced hereafter.

### 4.1 Specimens families

With regard to the problem statement and the scientific objectives three families of specimens are being produced in the frame of this work. In each family, five adhesive bond states i.e. one reference and four contamination levels are prepared. In each family, the composite used is the CFRP M21 with T800S fibers. The difference and reason for the families can be introduced as follow:

- Specimen family standard - fully cured - **type 'C'**

The standard type **'C'** of specimen is based on **fully cured** CFRP panels. They define the standard type of materials where no defect should be present. No deviations from norms, apart for the contamination process, is applied. The sole variations in the specimens type **'C'** is the contamination by release agent with different concentrations.

The **'C'** type is designed to be representative for real industrial bonded composite material. The laser proof tests are performed on the specimens as they would be after manufacturing, in a manufacturing environment. The tests conducted on standard specimens focus on the bondline adhesive performance assessment.

- Specimen family - partially cured - **type 'PC'**

In opposition to the standard family **'C'**, the type **'PC'** stands for **Partially Cured**. This deviation of the norms recommendations is being realized during the co-bonding process where a lower temperature as the 180 °C recommended is selected to avoid the full cross-linking of the epoxy molecules in the uncured composite layer. This family also involves a full range of contaminated specimens as well as reference ones (not treated).

This family has been designed to evaluate the effects of laser proof tests on the composite laminate itself instead of the adhesive bondline, when the composite substrate is weaker than the adhesive bondline. This hypothesis is often neglected by the consideration of a stronger cohesion in the laminate as adhesion at the bondline/substrate interface.

- Specimen family - moisture saturated - **type 'MOC'**

The **type 'MOC'** stands for **MOisture Contaminated**. It involves standard specimens (type C) which have been first dried out from ambient humidity and then saturated in a climatic chamber at 80 °C /85% r.H. until saturation. All conditioned adhesive bonds, are saturated

with moisture and then tested with laser proof test. The mechanical performances are also investigated through DCB mechanical testing.

The aim of the MOC family is to evaluate the effect of laser proof test on aged specimens to simulate a control of bondline after entry in service, or even a possible repair environment. Indeed, after manufacturing of an adhesive bonded structure, the adhesive joint and the whole structure may be exposed to moisture ingress, which itself may affect the performances of the adhesive bond through plasticization and so, even decrease the properties of a weak(er) adhesive bond.

## 4.2 Specimen nomenclature

The specimens are marked with engravings to avoid loss of names during all specimen conditioning and pre-treatment (cleaning with organic solvent) steps. The code specified in Table C.3 includes information related to the origin of the specimen (main plate, 1200\*600\*1.5 mm<sup>3</sup>), the specimen cut out (10 out of each main plate, 250\*200\*1.5 mm<sup>3</sup>), the contamination state (5 levels from reference to 10% release agent) and in case of additional tests, the specimens family (see section 4.1) and the initial position (from bottom to top resp. 1 to 7) of the specimen in the test panels with help of a dedicated numbering.

**Table C.3: Specimens nomenclature and codes for markings and engravings**

<b>#.##.# ( _type_#)</b>					
<b>Main plate</b>	<b>Specimen</b>	<b>Contamination state (Release Agent concentration)</b>		<b>Additional numbering for special tests incl. cut-outs (i.e. G<sub>1c</sub>)</b>	
<b>1 to 4</b>	<b>1 to 10</b>	<b>0</b>	<i>reference</i>	<b>_C_1 to 7</b>	<i>cured</i>
		<b>1</b>	<i>1% Release agent</i>	<b>_PC_1 to 7</b>	<i>partially cured</i>
		<b>2</b>	<i>2% Release agent</i>	<b>_MOC_1 to 7</b>	<i>moisture aged</i>
		<b>3</b>	<i>5% Release agent</i>	<b>(_LAS_1 to 7)</b>	<i>laser tested</i>
		<b>4</b>	<i>10% Release agent</i>		

Example:

Specimen 2.8.3 originates from main plate N°2, specimen N°8 and is contaminated with release agent diluted to 5%.

## 4.3 Monolithic laminates preparation

### 4.3.1 Materials choice

Already mentioned in section 2.1.2, the carbon prepreg selected for specimen manufacturing in this work is referenced HexPly UD/M21/ 35%/268/T800S). It is a unidirectional tape (UD), intermediate modulus carbon fiber reinforced epoxy prepreg with a fiber areal weight of 268

g/m<sup>2</sup> and a prepreg resin content of 35% nominal. The same batch is used for the manufacturing of the monolithic main plates.

The epoxy adhesive film with carrier mesh from Cytec Engineered Materials FM300 K.05 is selected. The 'K.05' in its reference indicates that the carrier is knitted and the areal weight is 0.05 pounds per square foot, or in metric system, 244 g/m<sup>2</sup>.

### 4.3.2 Composite lay-up

The first steps involved the manufacturing of four main monolithic composite plates numbered from one to four (1200\*600\*1.5 mm<sup>3</sup>). The stacking sequence of six plies (0<sub>2</sub>, 90<sub>2</sub>)<sub>S</sub> for a total thickness of approximately 1.56 mm is displayed in Figure C.12.

The surface are covered by a release film Richmond type ET 6335-OR from 3.8 μm thickness in order to guarantee a smooth surface aspect.

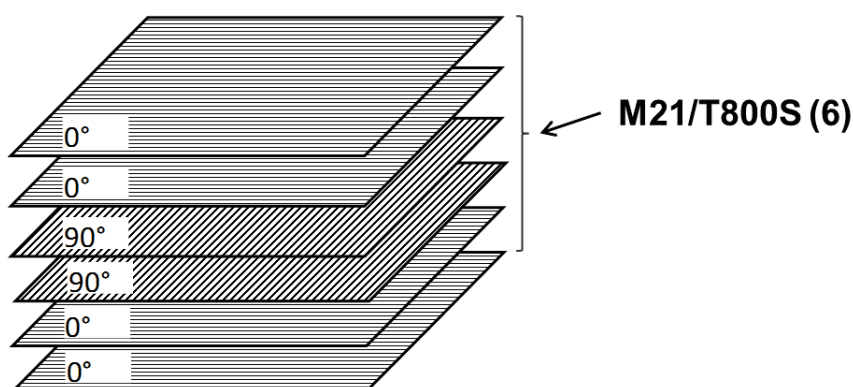


Figure C.12: Lay-up (0<sub>2</sub>, 90<sub>2</sub>)<sub>S</sub> from first monolithic composite plates

This lay-up of 1.56 mm thickness is also used for the uncured part, later co-bonded to this pre-cured and treated monolithic layer. The symmetrical specimens derived are fulfilling the geometrical criteria of the selected mechanical test G<sub>1C</sub> as in the AITM 1-0053 [21]: they are symmetrical, of the same material, approximately 3 mm thick and the external layers are in the 0° direction.

### 4.3.3 Curing cycle

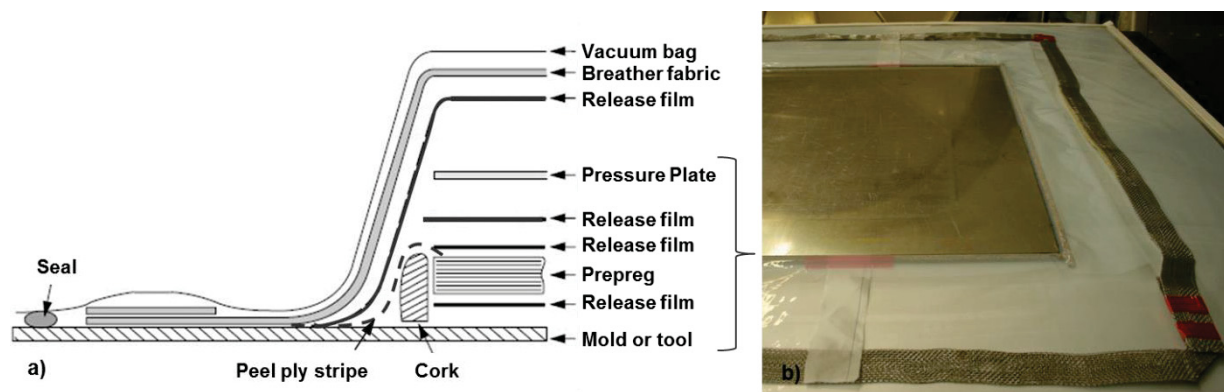
Once laminated, the plates have been prepared for curing in the autoclave. The cure cycle parameters are standard for the used material. It is given in Table C.4 and the autoclave setup is represented by Figure C.13. It must be noted that in classical cases the layers in contact with the prepreg are peel-ply films instead of the here used release film Richmond type ET 6335-OR. The use of a caul plate (aluminum, 1.5 mm thick) allows a better repartition of the pressure on the complete surface of the laminate.

Table C.4: Autoclave cure cycle for M21/T800S

Temperature increase	2 °C/min (+0.5/-0.5 °C)
Pressure increase rate	0.2 bars/min
Plateau at 180 ± 5 °C	120 min +15/-0 minutes



<b>Temperature decrease rate</b>	2 °C/min (+0/-1 °C)
<b>Pressure</b>	7 ± 0.5 bars
<b>Vacuum</b>	0.8 ± 0.1 bars



**Figure C.13: a) Scheme and b) illustration of autoclave preparation for CFRP curing (with release films on tool and bag side)**

After curing, the main plates were successfully inspected by conventional UT inspection. A probe head of 5 MHz in through transmission mode in immersion into a water tank was used. Very little heterogeneities with attenuation ranging from 2 to 5/6 dB could be revealed within the plates without having an importance on the laminates health. These attenuations are assumed to be due to porosity.

The main plates were then surface treated to enhance the surface wettability for first the contamination step and later, the co-bonding process.

#### 4.3.4 Surface pre-treatment

After the monolithic plates cure, all plates had one surface pre-treated to provide a cleaned and bonding ready surface for the later steps.

At first, a dry paper sanding treatment was performed with an rotating sanding machine Festool and a new paper with grit size 150 for each plate (Figure C.14a). The resin abraded and carbon dust were collected by suction during the sanding operation. The surface was finally rinsed with de-ionized water (Figure C.14b) and cleaned to remove the dust rests with a white lint free cloth. After the rinsing, the panels were put in almost vertical position for the water-break test. For this purpose, de-ionized water was flown over the surface and the continuity of the water film was observed over the abraded surface during about 1 min. No contamination or improperly sanded area could be identified by the water-break test for any of the four main plates (Figure C.14c).

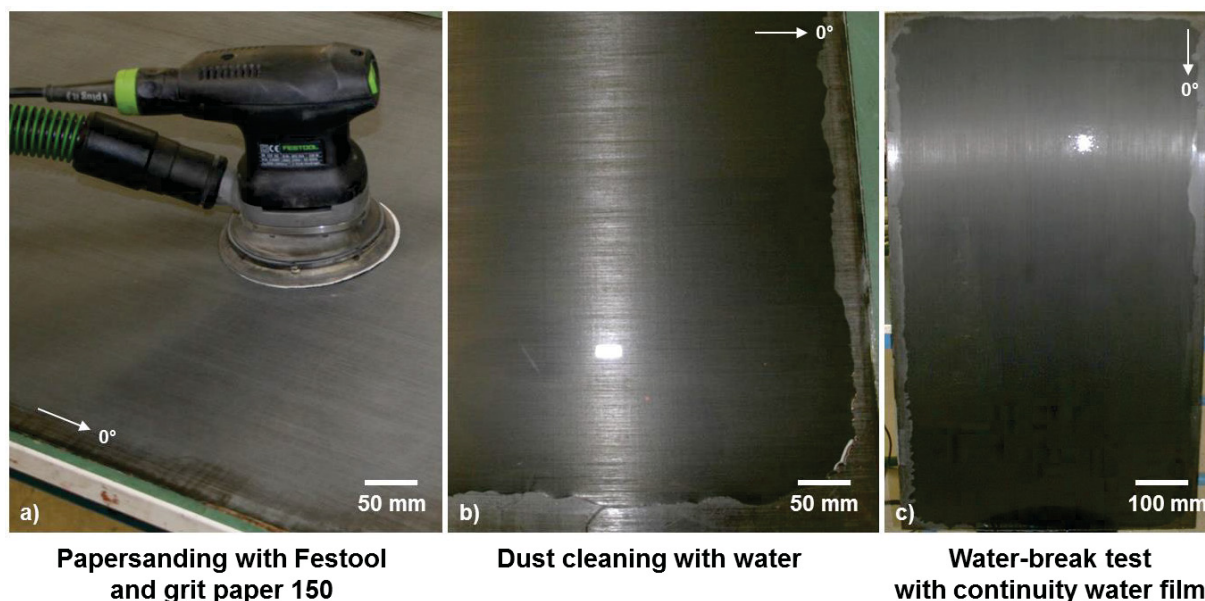


Figure C.14: a) Surface pre-treatment per paper sanding, b) cleaning with de-ionized water and c) water break test on a M21/T800S main plate (1200\*600\*1.5 mm<sup>3</sup>)

The plates were trimmed and cut into the final panel size of 250\*200\*1.5 mm<sup>3</sup> with use of a dry diamond disc saw (see Figure C.15). The panels were also engraved with the nomenclature for the referencing of all specimens.

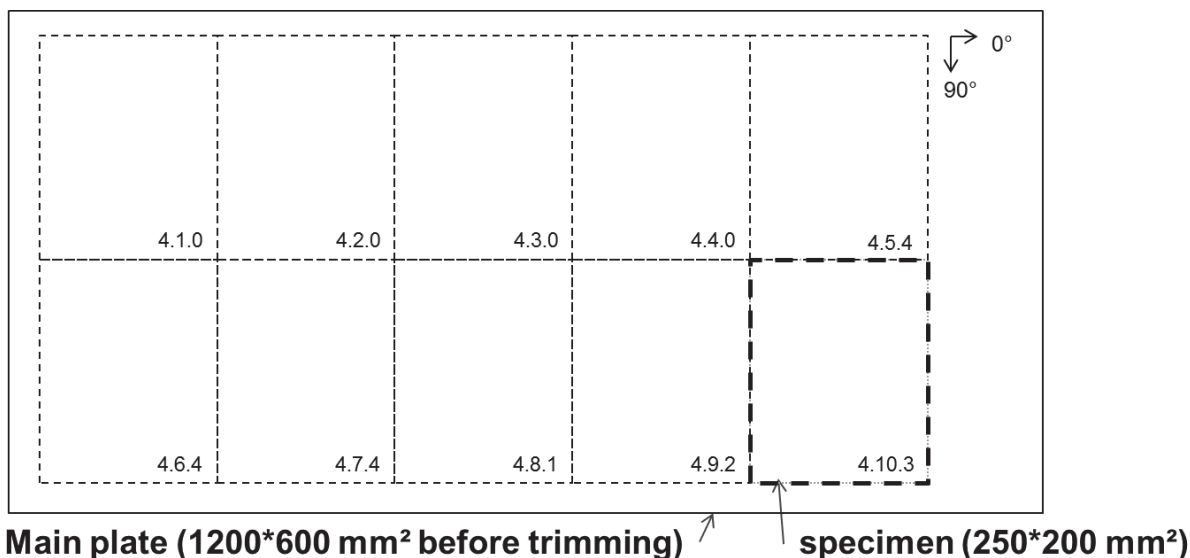


Figure C.15: Main composite plate (Number 4 here - 1200\*600 mm<sup>2</sup>) with schematic view of final size CFRP panels (250\*200 mm<sup>2</sup>) and trimming zones

Finally, the cutting operations were conducted on a dry diamond circular saw, and finally followed by a last cleaning to remove the carbon dust produced by the cutting. Specimens were cleaned with isopropanol on lint-free cloth until no black dust could be observed anymore. They remained 30 minutes at room temperature for drying and were then sealed into polyethylene films before the next step: the contamination.

### 4.3.5 Contamination of adherent surface and verification

After the adherent surface pre-treatment, the pre-cured panels were contaminated. The silicon based release agent is diluted in heptane solvent at the concentration of 1%, 2%, 5% and 10%. It must be noted that to avoid recurrent bias from surface pre-treatment and manufacturing of the main composite plates, each contamination is not systematically performed on a similar located panel out of the main plates, but originates from different locations e.g. the panel out of bottom left from the main plate is not always the panel contaminated to level 1.

The contamination is applied by dip-coating (see section 2.1.2). Two steel recipients (50\*250\*300 mm<sup>3</sup>) connected by pipes and a continuous pump are used. The solution is first brought into the recipient where the panel is held, and after stabilization of the solution surface, is pumped back in the second recipient. The speed of the immersion is set at 4000 mL/min. The surfaces are then dried out of 30 min at room temperature and subsequently heated for 60 min at 80 °C in an air circulating oven to ensure the cure of the PDMS at the surface.

The **XPS analysis** are performed at three or two different positions depending on the contamination level: 1-top, 2-bottom, or 3-middle (see Figure C.16). The silicon amount is given in at.% at the surface in Table C.5. This amount is an indicator for the degree of surface contamination by release agent (PDMS) and so, an indicator from the surface energy and wettability. The results reveal a satisfying contamination for each level, with a noticeable results for the unexposed reference panel as the Si at.% is not zero. This result can be explained by an insufficient paper sanding which would have let fine traces of the release film coating.

**Table C.5: Si concentration based on XPS results after dipcoating contamination on CFRP panels**

Contamination		Position of XPS measurement	O (at.%)	N (at.%)	C (at.%)	S (at.%)	Si (at.%)	Average Si (at.%)	Std Dev
Level	Concentration of Release agent in solution								
0	- (Reference)	Pos. 1	17.6	5.3	76.3	0.6	0.1	0.43	0.29
		Pos. 2	17.4	3.7	77.7	0.6	0.6		
		Pos. 3	16.5	3.7	78.5	0.7	0.6		
1	1%	Pos. 1	19.0	2.5	77.1	0.7	0.8	0.7	0.14
		Pos. 2	17.2	4.3	77.1	0.8	0.6		
2	2%	Pos. 1	18.2	5.0	74.3	0.9	1.6	1.30	0.42
		Pos. 2	17.5	4.6	76.0	1.0	1.0		
3	5%	Pos. 1	21.4	3.5	70.8	0.7	3.6	3.50	0.14
		Pos. 2	20.7	3.1	72.0	0.8	3.4		
4	10%	Pos. 1	24.0	2.5	68.1	0.7	4.7	6.37	1.70
		Pos. 2	25.1	3.1	63.3	0.4	8.1		
		Pos. 3	24.5	2.6	65.7	0.9	6.3		

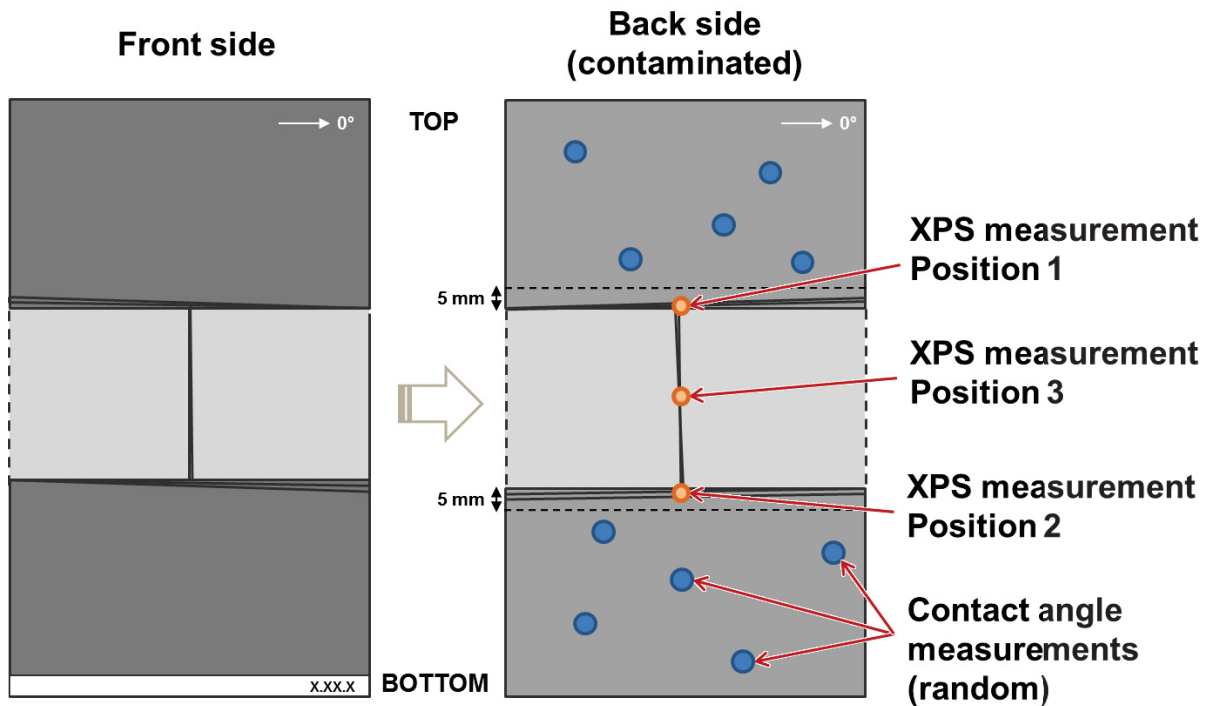
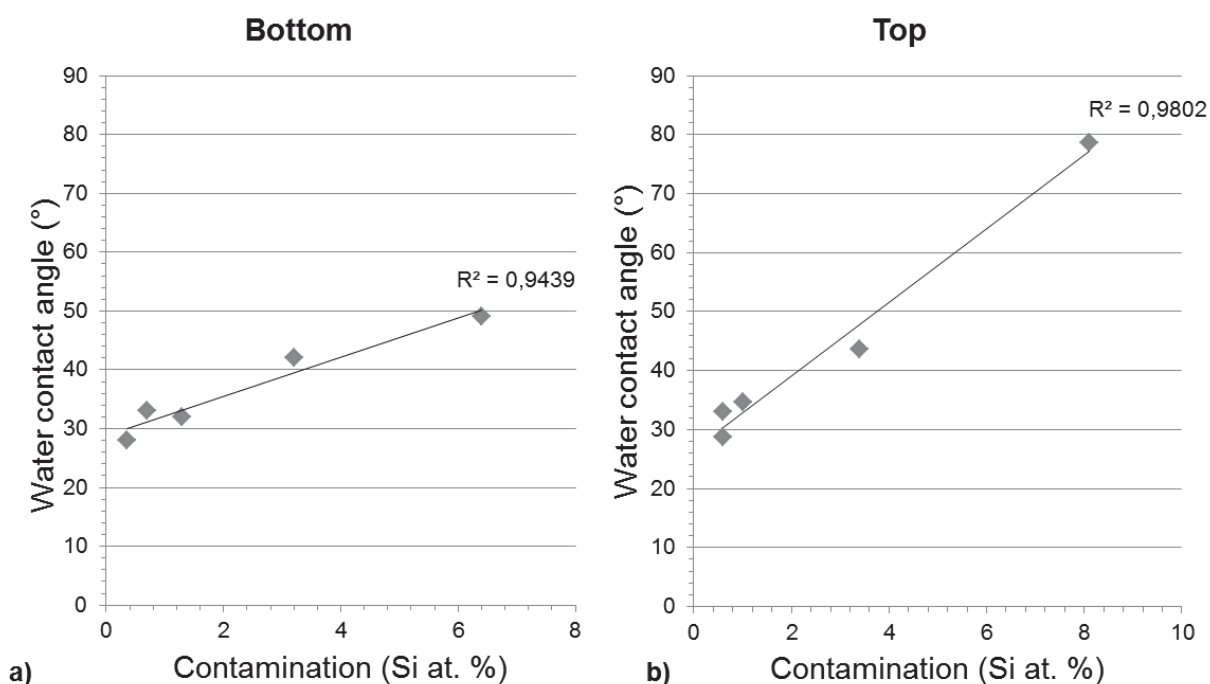


Figure C.16: Scheme of the XPS and Contact angle measurements on CFRP monolithic panel (250\*200\*1.5 mm<sup>3</sup>)

The wetting behavior was then evaluated with help of the Surface Analyst™ from Brighton technologies. This approach was experimental and shall be considered as a potential technique for wettability testing on CFRP. The results of up to five random measurements on the bottom and top part (see Figure C.16) of the pre-cured and conditioned M21/T800S substrates is introduced in Table C.6. The correlations with the XPS data provided in Table C.5 and corresponding to each local region (top or bottom) is done separately. The correlations of the bottom and top parts are presented respectively in Figure C.17.

Table C.6: Contact angles determined by Surface Analyst™ random measurements on up to five locations on top and bottom of conditioned composite substrates

Bottom	Contact angle (°)					Average Angle (°)	Std Dev	Top	Contact angle (°)			Average Angle (°)	Std Dev
-	28	28	27	-	-	27.7	0.6	-	31	29	26	28.7	2.5
1%	34	31	34	33	-	33	1.4	1%	33	32	34	33	1
2%	30	30	35	-	-	31.7	2.9	2%	31	34	39	34.7	4
5%	43	41	33	-	-	42.3	1.2	5%	46	42	43	43.7	2.1
10%	44	46	50	49	49	47.3	2.5	10%	81	78	77	78.7	2.1



**Figure C.17: Correlation between XPS data (contamination in Si at.%) and water contact angle measured by Surface Analyst™ on a) bottom and b) top parts of conditioned M21/T800 panel**

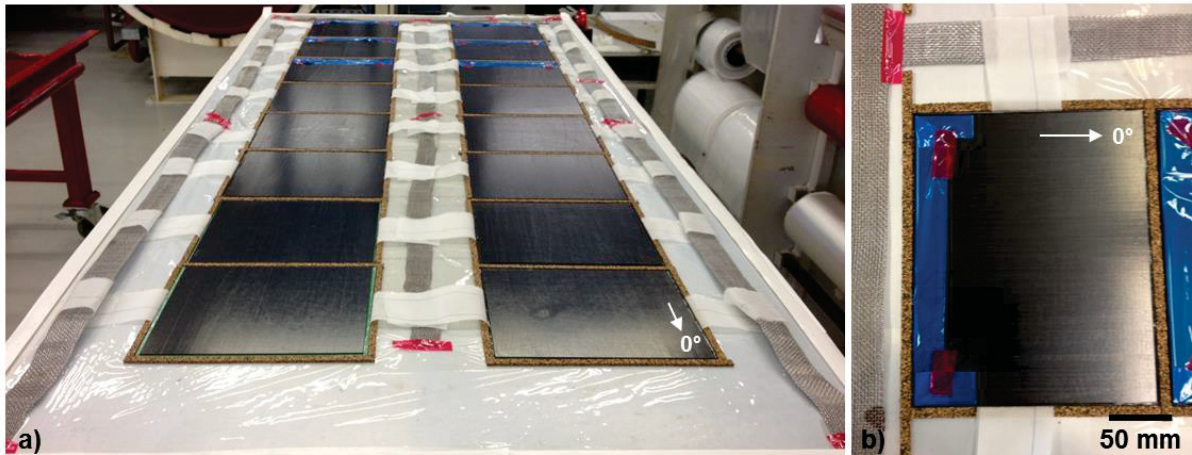
A linear regression was plotted to enhance the correlation between the Si at.% and the averaged contact angles. For the bottom and top parts,  $R^2$  are resp. equal to 94.4% and 98.0%. Despite this precision, the standard deviation is around 5% and the sensitivity to concentration  $< 1.6$  Si at.% is relatively low: all three lowest values are in the same range when the standard deviation is considered. In general, a consistent relation between the Si concentration and the contact angles measured by the SA™ is however observed and the surface analyst has shown potential for detection of higher concentration Si at.%.

## 4.4 Adhesive bonding

### 4.4.1 Specimens preparation

The CFRP panels are bonded by co-bonding process. This involves the cure of the adhesive film and prepreg simultaneously on the cured and pre-treated panel. Co-bonding process is selected to approach manufacturing applications i.e. composite stringer on skin or skin on stringer, and so show the feasibility of weak adhesive bond specimen preparation with the actual industrial process.

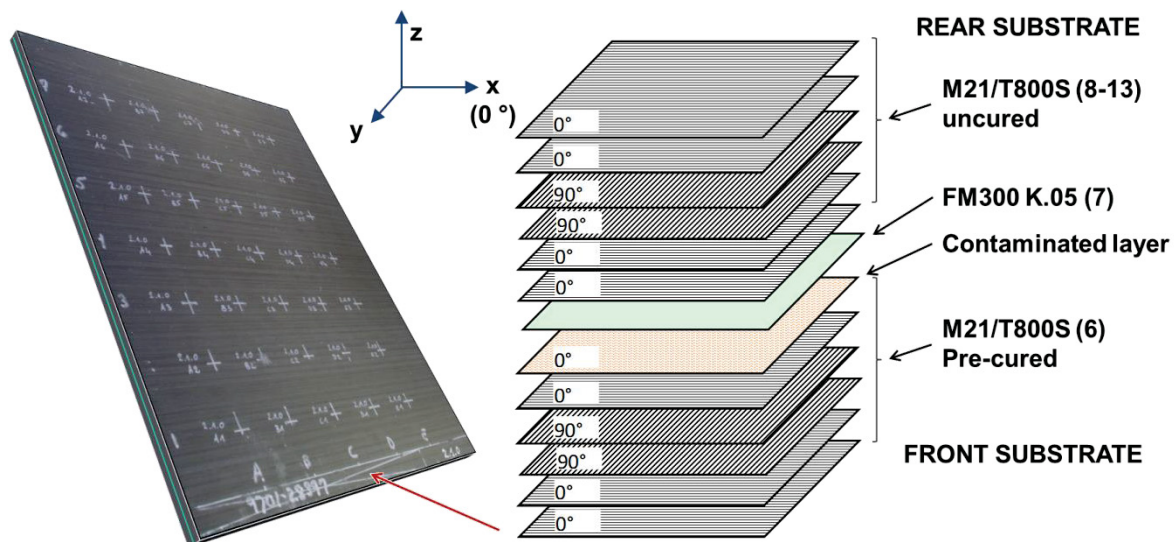
The autoclave is prepared for standard co-bonding operations according to the specification of the adhesive film FM300 and similarly to the setup illustrated by Figure C.13. The autoclave table is arranged with the CFRP panels pre-cured and contaminated used as caul plate and placed on top of the uncured prepreg to optimize the pressure (see Figure C.18).



**Figure C.18: a) autoclave preparation for CFRP co-bonding with use of pre-cured CFRP as caul plates and b) example of panel setup for bonding with release film insert (in blue) for mechanical test specimens**

The lay-up for the co-bonded layer is the same as for the monolithic panels  $(0_2, 90)_S$  in order to produce fully symmetric specimens of about 3 mm thickness, fitting the mechanical testing requirements. The lay-up, including the representation of the adhesive film and contaminated face is represented in Figure C.19. The same figure introduces also the axis system that is used during the complete work: the x-axis is the  $0^\circ$  fiber direction and the z-axis is chosen as the thickness direction, without fibers). The uncured panels were manufactured and cut wider than  $250 \times 200 \text{ mm}^2$  in order to avoid shrinkage during curing. These edges were trimmed with the same dry diamond circular saw as for the cutting of the main plates.

The cure cycle is by default the same as for the manufacturing of the main M21/T800S basic plates (section 4.3.3 – Table C.4) Only in the case of the type PC –partially cured–specimens, the curing temperature is reduced to  $120^\circ \text{C}$  instead of  $180^\circ \text{C}$ . The degree of cure is evaluated by the determination of the rest enthalpies by DSC for both the adhesive bond and the co-bonded CFRP panel.



**Figure C.19: Complete lay-up of adhesive co-bonded panels including contamination on pre-cured and pre-treated panel and view of the bonded panel from the front substrate [22]**

#### 4.4.2 Verification of degree of cure

The degree of cure could be estimated based on Eq.1 and the data given in the product specifications. Regarding M21/T800S, the released enthalpy  $\Delta H_{100}$  corresponding to the full cure (100%) shall be comprised between 310 and 500 J/g. This value is referring to pure resin and must therefore be pondered with the resin content of the used material. With the actual 35% of resin involved, the  $\Delta H_{\text{reference}}$  is hence around 108 to 175 J/g. The adhesive FM300 K.05 has a released enthalpy of 270-320 J/g according to material specification.

The two composite substrates co-bonded at curing states NC and C, as well as the adhesive FM300.K05 are controlled by DSC to evaluate the degree of cure in the material. For each state, at least 3 measurements on separated specimens have been performed. The features of resulting DSC curves can be observed on Figure C.20.

Specimen	DSC Results	Observations
CFRP ,PC' Partially Cured		<ul style="list-style-type: none"> <li>- Low glass transition temperature <math>T_g</math> due to <b>unachieved cure of epoxy (55%)</b></li> <li>- Large exothermic peak of rest enthalpy <math>\Delta H</math> due to unreacted epoxy (measured in Non reversible Heat Flow)</li> </ul>
CFRP ,C' Cured		<ul style="list-style-type: none"> <li>- No large exothermic peak due to <b>full cure of epoxy (99%)</b>.</li> <li>Rest enthalpy <math>\Delta H</math> (measured in Non reversible Heat Flow)</li> </ul>
Adhesive ,PC' & ,C'		<ul style="list-style-type: none"> <li>- Glass transition temperature <math>T_g</math> indicating <b>full cure (95%)</b></li> <li>- Strong exothermic peak due to degradation of adhesive (starting <math>T = 253\text{ }^\circ\text{C}</math>)</li> </ul>

Figure C.20: DSC results and general observations for each specimen type: composite substrate M21/T800S in state C (cured), PC (partially cured) and the epoxy adhesive FM 300 K.05 (both C and PC)

- Specimens type 'PC': the lower temperature for the cure cycle has led to a **cure degree of about 55%** ( $\pm 8\%$ ), based on the reference value from pre-preg  $\Delta H_{ref} = 133.5\text{ J/g}$ . The glass transition temperature of the PC state co-bonded laminate reaches  $T_g = 102\text{ }^\circ\text{C}$  ( $\pm 4\text{ }^\circ\text{C}$ ) whereas a standard value for M21/T800S should be ranging around  $T_g = 180\text{ }^\circ\text{C}$ .



- Specimens type 'C': the DSC curves do not allow any Tg determination. Only the little rest enthalpy could be determined. The cure degree of 'C' specimens is of **99.5%** ( $\pm 0.2\%$ ), again with consideration of the pre-prep reference value of 133.5 J/g.
- The adhesive layer from the 'PC' type specimens was investigated. The results show an advanced cure grade with an average **Tg = 162 °C** corresponding to a cure degree of **93.7%** ( $\pm 4.7\%$ ) according to Sprute [18]. On the basis of this high cure degree and the previous results for PC and C specimens, the adhesive layer is implicitly assumed fully cured for type C specimens. The cure degree can be explained by the very low thickness of the adhesive film and its direct contact to the pre-cured and pre-treated CFRP substrate, which diffuses heat faster than the uncured substrate. Also, the two material being different, the reaction kinetic may be in favor of the adhesive layer.

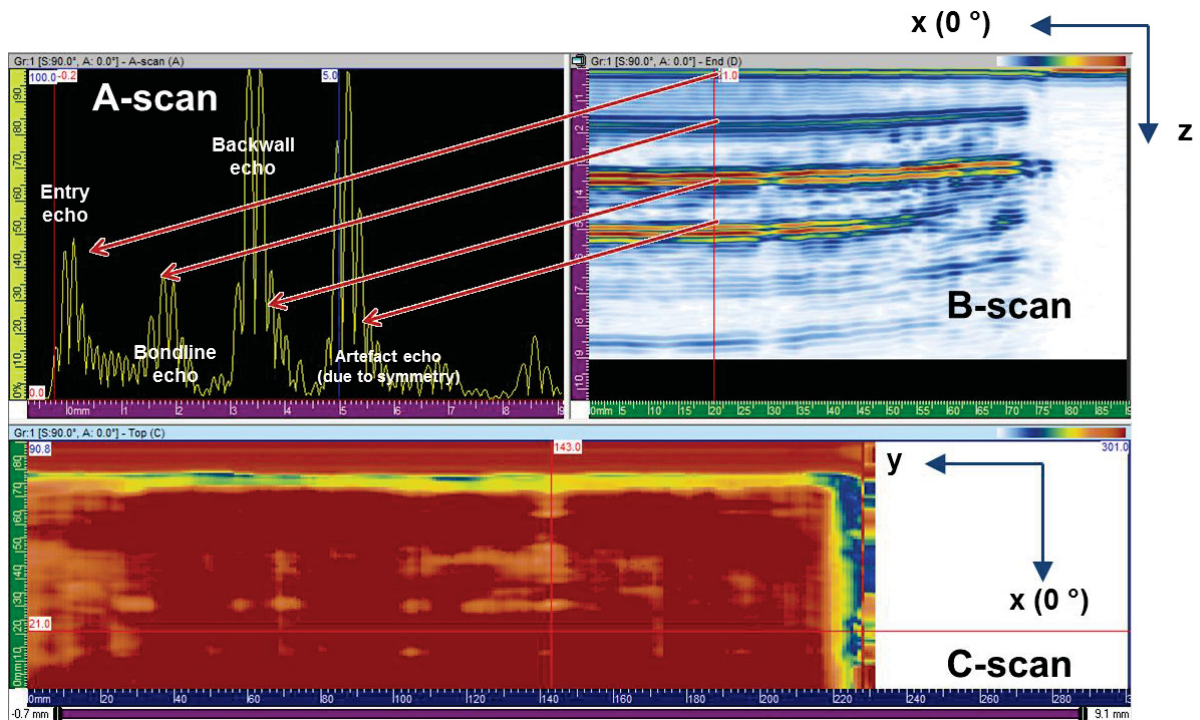
The cure degree evaluated with rest enthalpies are in line with the expectations. The adhesive layer is fully cured in each configuration. The standard deviation on the cure degree can be mitigated by the numerous influencing parameters, both in DSC and evaluation of DSC curves for the determination of the Tg and rest enthalpies.

#### 4.4.3 Characterization of the adhesive bondline

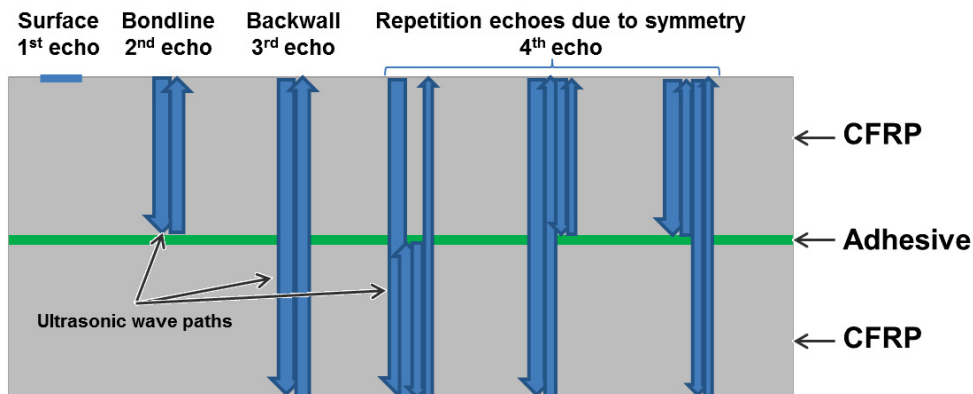
Independently from the contamination state, a weak adhesive bond should not present any defect in the bondline. This condition was one of the three main criteria defined in Chapter A. To verify the absence of defects in the CFRP bonded panels, each of the adhesive bond panel is therefore inspected by Phased Array ultrasonic PAUT and X-Ray radiography.

The PAUT inspection is performed after bonding operations on each of the small bonded panels. Signals are acquired from the rear surface in the form of three stripes vertical stripes as represented earlier in Figure C.5 or with focus on the A-, B- and C-scans in Figure C.21. The data are recorded and stored for 'before and after' laser proof test comparisons presented in the chapter D. In general, no major defects were detected in the adhesive bonded layer before laser tests. Inhomogeneities in the adherent composites layers can be detected but are not of a representative size, or large enough to prevent the use of the affected panel.

A particularity due to the symmetry of the panel (1.5 mm CFRP substrate on each side of the adhesive layer) is the 4<sup>th</sup> echo. It is indeed an artefact caused by the constructive reflections on each frontier, the adhesive bondline and the backwall/rear free surface. A representation of this phenomenon due to the geometry of the sample is given in Figure C.22. This 4<sup>th</sup> echo has no physical meaning and will not be further considered.



**Figure C.21: A-, B- and C- scans from one bonded panel (250\*200\*3 mm<sup>3</sup>) for the phased array ultrasonic inspection after bonding operations showing a standard indication-free structure and the according UT echoes**



**Figure C.22: Representation of ultrasonic wave paths in the symmetrical bonded composite materials. The different echoes visible in the B-scan are conditioned by the length of the path.**

The X-Ray radiography with microfocus mode has enabled a visualization the fibers orientation in the laminates as well as veins (brighter colors left in Figure C.23a) in the adhesive at the border of the composite panels. No indications could however be found with UT in such areas. The visualization of the release film inserted in the bonded panel as crack initiator for DCB coupons is possible. Also light micro porosity can be observed in few areas of bonded panels. The orientation of pores indicates their presence in the bondline near the adhesive polyester knit, which can be observed in Figure C.23b.

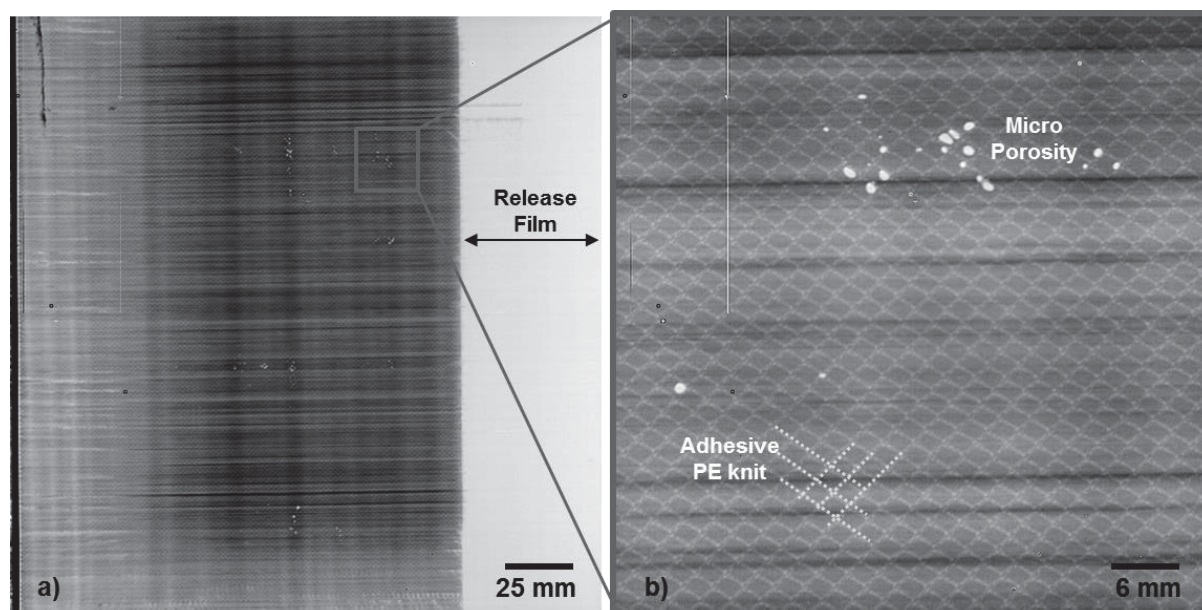


Figure C.23: X-Ray through transmission visualization of the composite bonded panels showing a) a complete panel with  $G_{1C}$  release film insert b) focus on the micro porosity visible and the adhesive layer knit

#### 4.5 Conditioning of moisture aged composite panels

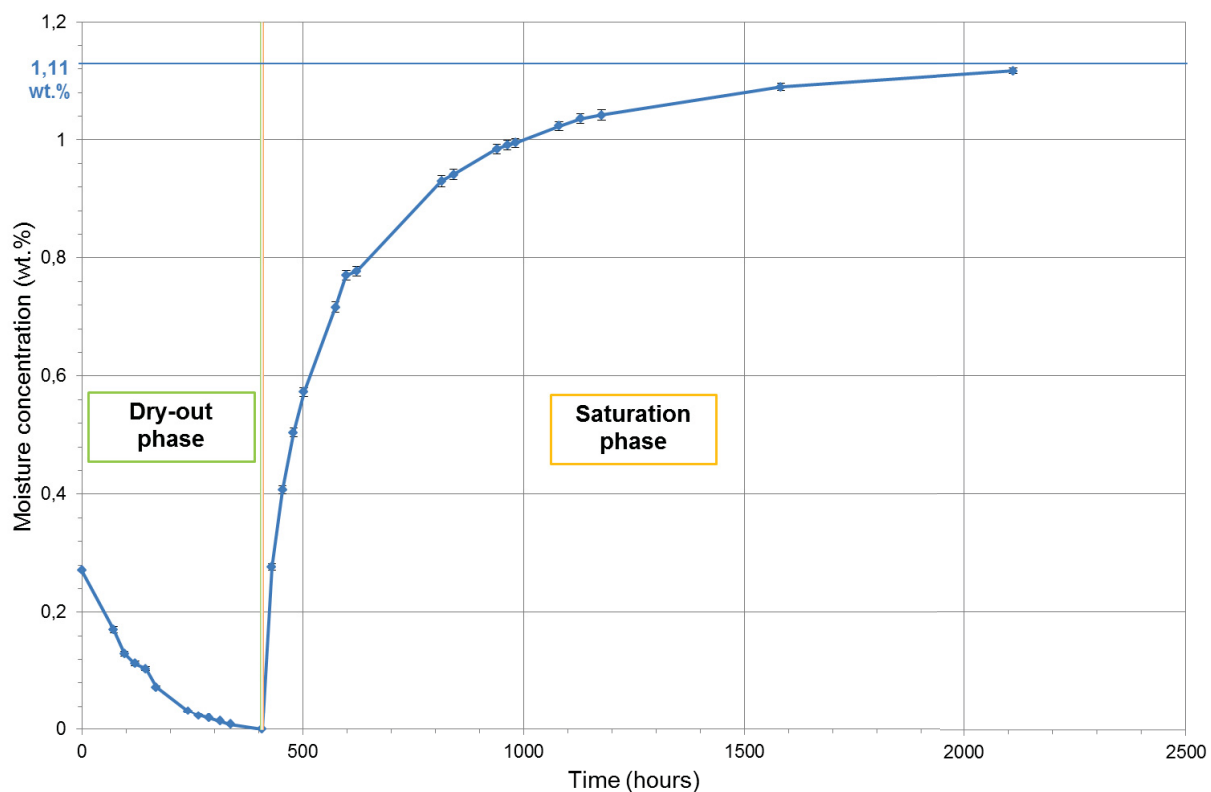
The adhesive bonded specimens MOC were conditioned with moisture exposure to investigate moisture ageing effects on laser proof tests performances. Specimens from each adhesive bond state have been pre-cut in DCB specimens size to prepare the finite test coupons for DCB tests and simultaneously allow a precise weight of each small coupon in the first dry-out phase and in the saturation phase.

Before saturation, all MOC coupons are dried out to remove standard ambient moisture and bring them at the same moisture level. The dry out is performed in an oven with air circulation with the temperatures and times defined in Table C.7 according to the AECMA standard EN 3615 for exposure to humid atmosphere and moisture absorption [23]. The saturation cycle is as well performed according to the same standard and in compliance with the parameters from Table C.7.

Table C.7: Cycle and criteria for moisture dry-out and saturation operations for composite materials according to AECMA standard EN 3615 [23]

according to AECMA EN 3615 [23]	Dry-out	Saturation
<b>Cycle</b>	- 72 (+20/-0) hours at 50 ( $\pm 5$ ) °C - 72 (+20/-0) hours at 70 ( $\pm 5$ ) °C - x hours at 90 ( $\pm 5$ ) °C until a constant mass is reached	- x hours at 80 °C/85 r.H. until a constant mass is reached
<b>End Criteria</b>	Constant mass is defined as three successive weighing of coupons carried out at <b>72 h</b> intervals and	Constant mass is defined as three successive weightings of coupons carried out at <b>168 h</b> intervals and

	matching the following equation: $\frac{ P_{j-2}-P_j }{P_j} \leq 5 \cdot 10^4$ With $P_j$ , the mean weights of the specimen at $t_j$	matching the following equation: $\frac{ M_{j-2}-M_j }{M_j} \leq 5 \cdot 10^4$ With $M_j$ , the mean weights of the specimen at $t_j$
--	--	--



**Figure C.24: Average moisture concentration (in wt.%) versus time (in hours) in bonded M21/T800S coupons MOC during dry-out and moisture saturation phase**

Figure C.24 gives the average weight with a precision scale of 0.1 mg from seven coupons. Weighing operations are conducted on coupons 10 minutes after removal from oven or climatic chamber to let the weight and diffusion behavior stabilize. The result of the weighing control is presented on one single graph for better clarity. The dry-out cycle on the left shows an average loss of 0.27 wt.% of moisture in 408 hours (17 days). The saturation phase leads to a moisture ingress of 1.11 wt.% in 1702 hours (71 days).

Once the saturation is completed, the MOC coupons are let in the climatic chamber further until the test period. The coupon are then taken out, wrapped individually in a lint free cloth soaked with de-ionized water, wrapped in aluminum foil and packed in plastic bags, later sealed to avoid any re-drying of the coupons before laser or mechanical testing.

## 4.6 Adhesive bond mechanical performances

After all preparation steps and first characterization with NDT methods, the adhesive bonded specimens are tested mechanically to determine their fracture strength in mode I. This step is essential to determine the adhesive strength of each designed type of specimen prior to testing laser proof test methods on them.

The double Cantilever Beam test is the chosen test because it corresponds to pure tension on the adhesive layer. It is assumed to be therefore the most representative for the local tension generated by laser proof tests within the bonded structure.

#### 4.6.1 Performances of fully and partially cured bonded specimens

Seven  $G_{1C}$  coupons from bonded laminates with pre-treatment ranging from reference state to level 4 contamination state were prepared and tested.

Results are discussed by type of specimens, cured C; partially cured PC and moisture contaminated MOC considering the failure profile presented by Figure C.25.

- **Cured C specimens:** it can be observed that the  $G_{1C}$  values from the cured specimens are stable for  $< 0.70$  Si at.% around  $700 \text{ J/cm}^2$  and strongly decrease of more than 60% with increasing Si at.% concentrations.

In case of level 0 (ref), 1 and 2, the crack initiation energy of up to three coupons per family did not match the expected values. The observation of failure mechanisms revealed an adhesive failure for these particular coupons, whereas the rest of the specimens had shown mix failure modes of cohesive and delaminations from the substrates, with a tendency to adhesive in some rear parts of the specimens. A comparison in between the coupons with other failure patterns does not make sense since the failure modes are not similar. For this reason, the presented  $G_{1C}$  values for levels 0, 1 and 2 do not include the specimens whose failure pattern are adhesive. The average is made with the coupons whose crack initiation energy and failure patterns are featuring mix failure patterns.

In the case of level 3 and 4, the concentration of Si at.% is high enough to provoke a clean adhesive failure, as expected in case of significant release agent contamination. The standard deviation is at its maximum (23.7%) for the reference value. This standard deviation is relatively high and can be explained by the delamination visible where mixed failures are present. The delaminations are indeed directly impacting the scatter because the force account the tension applied on the carbon fibers in this case. The  $G_{1C}$  scatter is on the whole acceptable knowing that standard deviations of 20% are often applying for DCB tests. This value decreases down to 17% with increasing contamination levels and adhesive rupture behavior.

- **Partially Cured PC specimens:** the incomplete cure of the co-bonded layer is responsible for a parasitic effect for the level 0, 1 and 2. The partial cure does not enable the optimal cohesive strength of the composite substrate. During the DCB test, intralaminar failure occur (see view in level 0 and 1 in Figure C.25) and the data recorded did not focus on the adhesive bond but on both cracks propagating. This phenomenon invalids the test results which cannot be attributed to any of these crack especially because of the mix of both cracks propagations. No data are hence available for level 0, 1 and 2.

Level 3 and level 4 could however be tested. The CFRP intralaminar cohesion is assumed stronger than adhesive bondline contaminated with high Si at.% concentration. This is emphasized by the clean adhesive failure. The  $G_{1C}$  performances are approx. twice lower but along the cured specimens performances of

levels 3 and 4. The standard deviation is anecdotic for so low fracture toughness results.

- **Moisture aged MOC specimens:** due to a lower amount of samples due to material restrictions, only four specimens were for the moisture ageing  $G_{1C}$  performance. The moisture ageing of samples fully cured shows a direct effect on the adhesive failure mechanisms of all contaminated states. Only in the case of reference state, a slight mix of adhesive failure pattern and cohesive can be distinguished on small areas. The failure patterns for specimens of level 1, 2, 3 and 4 is adhesive, and similar to the one of the cured specimens in level 3 and 4. The standard deviation is kept below 20% for level 0, 1 and 2 but drastically increase for levels 3 and 4 (up to 75% on low values).

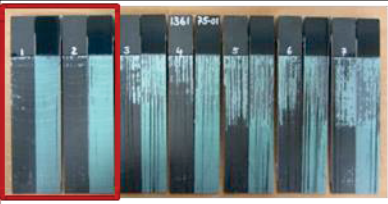


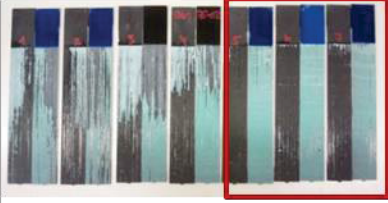
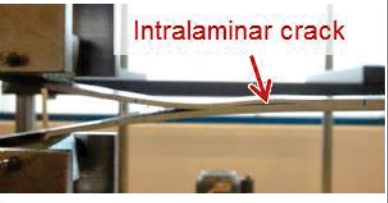
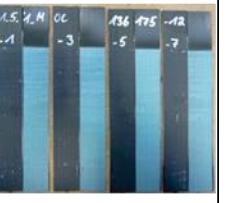
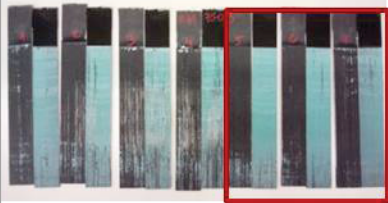
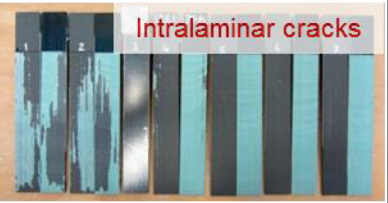
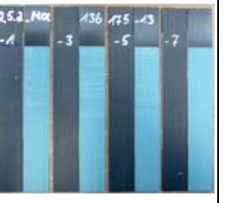
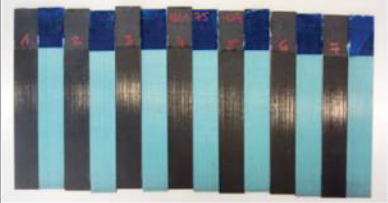

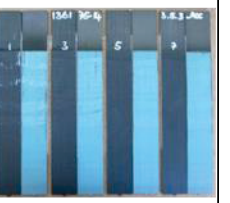
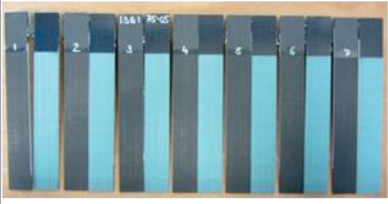
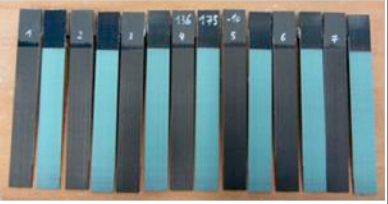
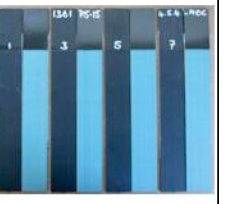
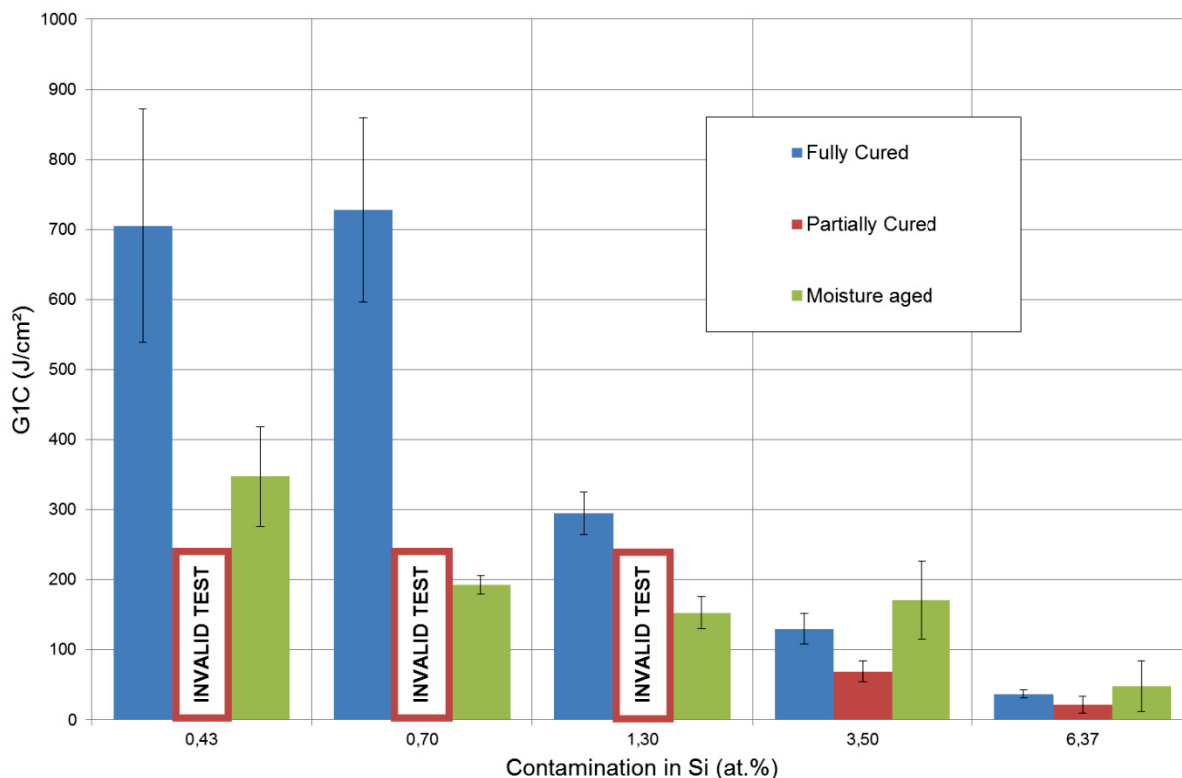
Specimen		Failure profiles / Results		
Level	Si (at%)	Cured CFRP 'C'	Partially Cured 'PC'	Moisture aged 'MOC'
0 (ref)	0.43 ± 0.29	 Adhesion      Mixed	 INVALID TESTS	 Mixed
1	0.70 ± 0.14	 Mixed      Adhesion	 INVALID TESTS	 Adhesion
2	1.30 ± 0.42	 Mixed      Adhesion	 INVALID TESTS	 Adhesion
3	3.50 ± 0.14	 Adhesion	 Adhesion	 Adhesion
4	6.37 ± 1.70	 Adhesion	 Adhesion	 Adhesion

Figure C.25: Failure profiles and remarkable results for all tested  $G_{1C}$  coupons from coupon families cured C, partially cured PC and aged with moisture MOC

In conclusion, Figure C.26 introduces the results for the cured composite C, partially cured PC and moisture aged MOC composite. The adhesive bond performances determined by DCB tests are matching the expectations. The influence of the substrate contamination is clearly evidenced by a loss of more than 60% of fracture toughness  $G_{1C}$  with concentration of Si

superior to 0.70 at.%. The criterion defined in chapter A, a loss of 20% of the nominal mechanical value, is validated for levels 2, 3 and 4.



**Figure C.26:  $G_{1C}$  results of Cured C, partially cured PC and moisture aged MOC specimens showing decrease of fracture toughness energies with increasing contaminations of adherent surface**

The adhesive failures for level 0 coupons is in line with the XPS data scatter seen in part 4.3.4, and reveal that local higher concentrations of Si or bad sanding may be responsible for these adhesive failures. This observation is however not prejudicial. The mix of failure patterns indicates regions with delaminations appearing surprisingly in parallel. These delaminations encourages the effect of fiber bridging during the test which is responsible for higher  $G_{1C}$  values that are however not representative of the adhesive itself but more of the adhesive bond assembly as a whole. Later results from DCB tests in Chapter D will be discussed on the base of the failure profiles.

In case of partially cured PC composite, the intralaminar cracks have revealed that the adhesive bond is stronger than the laminate cohesion itself in case of a cure of 55%. This is valid until a concentration of 1.3 Si at.% where few laminates could be opened but have shown an adhesive failure, due to the Si contamination. In this range of contamination, both phenomena of adhesive rupture and intralaminar delamination are equally competing. When the contamination is higher, its effects dominate and provoke an adhesive failure. The objective of preparation of weak composite substrate with substrate cohesion less efficient than the adhesive bondline is hence validated with the PC specimens.

The specimens aged with moisture MOC have revealed a significant drop of fracture toughness  $G_{1C}$  performance for level 0, 1 and 2 with respectively drops to 49%, 26% and 52% from the sound cured C specimens  $G_{1C}$  values at similar levels. For the highest levels of contaminations (3, 4), the  $G_{1C}$  values is increased of respectively 31% and 29%, with however



a large standard deviation inhibiting any conclusion about an improvement of performances. The adhesive failure pattern present on all levels leads to the assumption that moisture ingress (after bonding) is responsible for a degradation of the adhesive-substrate interphase. Moisture, due to the plasticization and the induced swelling, could be responsible for a de-wetting at this interphase and so, would lead to adhesive failures. This effect is in line with the observations of Banks et al. in his study on water ingress in CFRP [24].

## 5. SUMMARY

The scientific approach has highlighted the challenges of the use of laser proof testing and the questions to be answered in priority. Questions regarding the assessment of the NDT aspect of laser proof test are raised. Before starting assessing laser proof test methods, the first decisive step is the preparation of weak adhesive bonds in a controlled way. Approaches for manufacturing weak adhesive bond have been presented based on relevant literature.

The characterization methods involved in this work and their principle have been presented: laboratory characterization method (DSC, XPS, contact angle measurements), conventional NDT method (UT & PAUT, X-Ray) and mechanical testing method (DCB) are used complementarily to ensure the proper manufacturing of weak adhesive bonds.

Monolithic plates are produced, are pre-treated by sanding, cleaned and further contaminated with diluted release agent prior to co-bonding operations. Different level of contaminations, level of cure and one ageing with moisture configuration offer a large spectra of specimens for further laser proof tests. The characterization methods did not reveal at all stages of the manufacturing any major defects such as void, delaminations or disbonds. The mechanical testing with DCB test has shown the expected tendency of decreasing  $G_{1C}$  bonded performances with increasing adherent surface contamination. Criteria for weak adhesive bonds (absence of defect detected via NDT, 20% or more reduction of nominal mechanical performances, adhesive failure) could be verified for the three highest levels of contamination.

The next chapter will present the test campaign with the laser proof test techniques. It will focus on providing answers to the question raised regarding the non-destructive character of laser proof test techniques.

## REFERENCES - CHAPTER C

- [1] M. Jastrzebski, A. Sinclair, und J. Spelt, „Mechanical and Industrial Engineering, Development of Adhesive Bonds with Reduced Strength as Ultrasonic NDE Benchmarks“, gehalten auf der Canadian Aeronautics and Space Institute 18th Aerospace Structures and Materials Symposium, Toronto, Canada, 2005, Bd. E.
- [2] M. Hinchliffe, „Characterisation of Bond Line Porosity“. 2008.
- [3] J. Barroeta-Robles, R. Cole, und J. M. Sands, „Development of Controlled Adhesive Bond Strength for Assessment by Advanced Non-Destructive Inspection Techniques“, gehalten auf der SAMPE 2010, Seattle, WA, 2010, S. 15.
- [4] M. F. Zaeh, C. Thiemann, S. Boehm, C. Srajbr, C. Lammel, und J. Noak, „Cost-effective defect detection in bonded glass element modules - NDT for Adhesives Bond“, *Adhäsion Kleben&Dichten*, Nr. October 2009, S. 30–34, Okt-2009.
- [5] V. M. Karbhari, H. Kaiser, R. Navada, K. Ghosh, und L. Lee, „Methods for Detecting Defects in Composite Rehabilitated Concrete Structures“, Oregon Department of Transportation, Research Unit, 200 Hawthorne SE, Suite B-240, Salem, Oregon 97301-5192, University of California, San Diego, Final Report FHWA-OR-RD-05-09, Apr. 2005.
- [6] E. Wall, R. Sullivan, und J. Carpenter, „Progress Report for Automotive Lightweighting Materials Volume II“, U.S Department of Energy, Washington, DC 20585-0121, Progress report FY 2006 Progress Report, Okt. 2007.
- [7] P. Marty, N. Desai, und J. Andersson, „NDT of kissing bond in aeronautical structures“, gehalten auf der 16th World Conference of NDT Proceedings, Linköping, Sweden, 2004, S. 8.
- [8] C. Mueller-Reich, R. Wilken, und S. Kaprolat, „Bonding of plastics: Well-bonded despite residual release agents“, *Adhesion ADHESIVES & SEALANTS*, Bd. 3/2011, S. 36 – 41, 2011.
- [9] B. M. Parker und R. M. Waghorne, „Surface pretreatment of carbon fibre-reinforced composites for adhesive bonding“, *Composites*, Bd. Vol. 13, Nr. 3, S. 280–288, Juli 1982.
- [10] C. Jeenjitkaew, Z. Luklinska, und F. Guild, „Morphology and surface chemistry of kissing bonds in adhesive joints produced by surface contamination“, *International Journal of Adhesion and Adhesives*, Bd. Vol. 30, Nr. 7, S. 643 – 653, Okt. 2010.
- [11] N. Decourcelle und E. J. C. Kellar, „Development of a methodology to produce samples and ultrasonic techniques for kissing bonds in adhesive joints“, *Research Reports for Industrial Members of TWI*, Granta Park, Cambridge, UK, S. 1–12, Sep-2009.
- [12] T. Rieck, „Einfluss unterschiedlicher Kontaminationen auf den Klebeprozess“, Master-Thesis, Hochschule Aalen - Studiengang: Produktentwicklung und Fertigung, Erding, 2011.
- [13] M. Wetzel, T. Rieck, und J. Holtmannspötter, „Contamination in adhesive bonding for aviation applications: Detection and effect of adhesion-limiting contaminations“, *Adhesion ADHESIVES&SEALANTS*, Nr. 2011–03, S. 29 – 33, 2011.
- [14] T. Meer, „Pre-treatment of CFRP surfaces for secondary adhesive bonding“, gehalten auf der EADS Composite and Metallic Days, Nantes, 22-Okt-2013.
- [15] S. Markus, „Die Laser Induced Breakdown Spectroscopy (LIBS) als Inline-Verfahren zur Detektion von Oberflächenkontaminationen im Bereich der Klebtechnik“, Universität Bremen, Bremen, Germany, PhD, Nov. 2007.
- [16] M. Engholm, „A Narrowband Ultrasonic Spectroscopy Technique for the Inspection of Layered Structures“, Licence, Uppsala Universitet, Sweden, 2006.
- [17] G. Habenicht, *Kleben: Grundlagen, Technologien, Anwendungen*. Springer, 2008.
- [18] T. Sprute, „Untersuchung und Modellierung der Aushärtung von Epoxidharzen aus der Flugzeugindustrie unter chemo-rheologischen Gesichtspunkten“, Universität Paderborn, Airbus Bremen, Diplomarbeit, Oktober 2010.
- [19] R. Ecault, „Experimental and numerical investigations on the dynamic behaviour of aeronautic composites under laser shock - Optimization of a shock wave adhesion test

- for bonded composites“, E.N.S.M.A. - Sciences et Ingénierie en Matériaux, Mécanique, Energétique et Aéronautique, Poitiers, PhD, 2013.
- [20] B. M. Parker und R. M. Waghorne, „Testing epoxy composite surfaces for bondability“, *Surface and Interface Analysis*, Bd. Vol. 17, Nr. 7, S. 471–476, Juni 1991.
- [21] Airbus, „Determination of mode I fracture toughness energy of bonded joints (G1C Test), Carbon Fibre Reinforced Plastics, AITM 1-0053 Airbus test Method“. Feb-2013.
- [22] T. Stöven, „CFRP-Bonding - Seminar Composites und Kleben“, gehalten auf der Seminar Composites und Kleben, IFAM Bremen, 21-Nov-2006.
- [23] European Association of Aerospace Industries (AECMA), „PR EN 3615 - Determination of the conditions of exposure to humid atmosphere and of moisture absorption“. Nov-1998.
- [24] W. M. Banks, F. Dumolin, S. T. Halliday, D. Hayward, Z.-C. Li, und R. A. Pethrick, „Dielectric and mechanical assessment of water ingress into carbon fibre composite materials“, *Computers & Structures*, Bd. 76, Nr. 1–3, S. 43–55, Juin 2000.



# CHAPTER D: EXPERIMENTAL ASSESSMENT OF LASER PROOF TESTING METHODS

## TABLE OF CONTENTS

1. INTRODUCTION .....	112
2. LASER PROOF TEST SET-UP .....	112
2.1 Laser source LASAT – CNRS PPRIME .....	113
2.2 Laser source LBI – LSP Technologies .....	114
3. EXPERIMENTAL APPROACH FOR DETERMINATION OF LASER PROOF TEST EFFECTS ON BONDED STRUCTURES .....	116
3.1 Test A - Determination of intensity threshold for each adhesive bond states .....	116
3.2 Test B - Evaluation of potential damages in materials after repeated shocks .....	118
3.3 Test C - Evaluation of mechanical performances after laser proof test .....	119
3.4 Test D - Use of integrated time-resolved diagnosis from laser proof test methods	120
3.5 Characterization methods and type of damages post-shocks .....	121
3.5.1 Evaluation of phased-array ultrasonic scans for damage size determination ..	121
3.5.2 Observations of damages with optical microscopy .....	124
4. RESULTS .....	125
4.1 Evaluation of intensity thresholds .....	125
4.1.1 Intensity thresholds of cured specimens .....	126
4.1.2 Intensity thresholds of partially cured specimens .....	133
4.1.3 Intensity thresholds of moisture contaminated specimens .....	135
4.1.4 Overview for all tests .....	137
4.1.5 Summary of intensity thresholds .....	139
4.2 Evaluation of damage effects due to repeated shots .....	140
4.2.1 Effect of repeated laser shock on reference cured specimens .....	140
4.2.2 Effect of repeated laser shock on the microstructure .....	143
4.2.3 Summary on damage generation after repeated shocks .....	144
4.3 Effect of low intensity laser shots on adhesive bond mechanical performances ....	145
4.3.1 Summary on low intensity shock effect on mechanical performances .....	147
4.4 Integrated time-resolved diagnostic tool for calibration of system .....	148
4.4.1 Investigation of VISAR capabilities with laser 25 ns .....	148
4.4.2 Investigation of EMAT capabilities with laser 200 ns .....	152
5. SUMMARY .....	154
REFERENCES – CHAPTER D .....	156

## 1. INTRODUCTION

This chapter D introduces the results of the scientific approach for the evaluation of the laser proof test technologies.

In a first step, both investigated laser proof tests set-up, the LASAT from CNRS and the LBI from LSP Technologies, are shortly presented. The chapter introduces then the specific laser tests designed to assess laser proof tests methods and evaluate their effects on adhesive bonded composite structures. Four different tests have been designed to review laser proof tests techniques. These tests whose results will be presented in the chapter concern:

- the determination of the damage intensity threshold for debonding for all samples,
- the evaluation of damages size and numbers evolution in case of repeated shocks at a same location,
- the evaluation of laser shots below debonding threshold on the mechanical DCB performance of a bonded structure, and finally,
- the demonstration of the capabilities of each time-resolved measuring technique, the Electro Magnetic Acoustic Transducer (EMAT) and the Velocity Interferometer System for Any Reflector (VISAR), both introduced in detail in chapter B.

These tests allow one to compare the laser proof test techniques performances with regard to conventional characterization, with NDT methods and with mechanical destructive testing results (DCB test). In particular, ultrasonic testing (UT) for the determination of the damage size are correlated to the type of damage observed and number of damages measured via optical microscopy.

The results are finally discussed with regard to the analysis of the laser parameters and their effects on the damage observed.

## 2. LASER PROOF TEST SET-UP

Two experimental setups were investigated in the frame of this study. The principle for testing is the same in both case and only the laser properties and experimental setup are different. With this approach, both results can be opposed and the most adequate parameters can be identified. Both laser setups are summarized in Table D.1 and are described hereafter.

**Table D.1: Summary of laser shock sources investigated in the present study**

Laboratory	Laser source	Characteristics			
		Wavelengths	Pulse duration	Energy	Repetition rate
CNRS-PPRIME	LASAT Nd:Glass	1053 nm	25 - 30 ns	0 – 20 J	1 shot/ 5min
LSP	LBI Nd:Glass	1053 nm	70 – 300 ns	0 – 50 J	1 shot/ 8s

## 2.1 Laser source LASAT – CNRS PPRIME

The LASAT source from the French CNRS laboratory PPrime has been used for the laser shock investigations. The experimental setup for this laser is presented in Figure D.1. This Nd:Glass laser can deliver an energy up to 20 J at a 1053 nm wavelength. The pulse duration is about 25 ns in a Gaussian pulse at full width and medium height. The laser spot diameter available goes up to 25 mm but is kept to 4.5 mm to enable intensities of about 5 GW/cm<sup>2</sup>, which is in the range of the confinement layer breakdown energy. As a reminder, the breakdown must be avoided since it is responsible for a release of the plasma into the environment instead of the specimen.

The experimental lab is made of three separated rooms. A first command room (Figure D.1a) is used for adjusting the laser amplification and oscilloscopes. The laser itself is placed in the second room on an optical table (Figure D.1b). Finally the laser beam coming from the second room enters the experimental room where it goes through optical densities in order to reduce the energy and so, the intensities hitting the specimens. A mirror system enables a measure of the energy shot via an electronic sensor. The beam is then focalized by convergent lenses to reach its 4.5 mm diameter and driven to the target.

Figure D.2a shows the setup with the last mirror and lens. The laser beam arrives to the surface of the CFRP sample after a final glass protection to prevent water spatters from the confinement layer to reach the last lens (Figure D.2b). At the impact location, a sacrificial layer made of aluminum paint spray is used to ensure a similar laser/matter interaction at all locations on the samples. A water confinement made of 10 drops of de-ionized water is placed on top in a plastic seal ring in order to increase the pulse pressure level (see chapter B section 3.2). The time-resolved diagnostic used for specific test with the LASAT setup is the VISAR, previously introduced in chapter B section 3.3. The scheme of the specimen derived from Figure D.2b illustrates the cut view of the specimen at the impact and the VISAR laser arriving at the rear free surface of the sample.

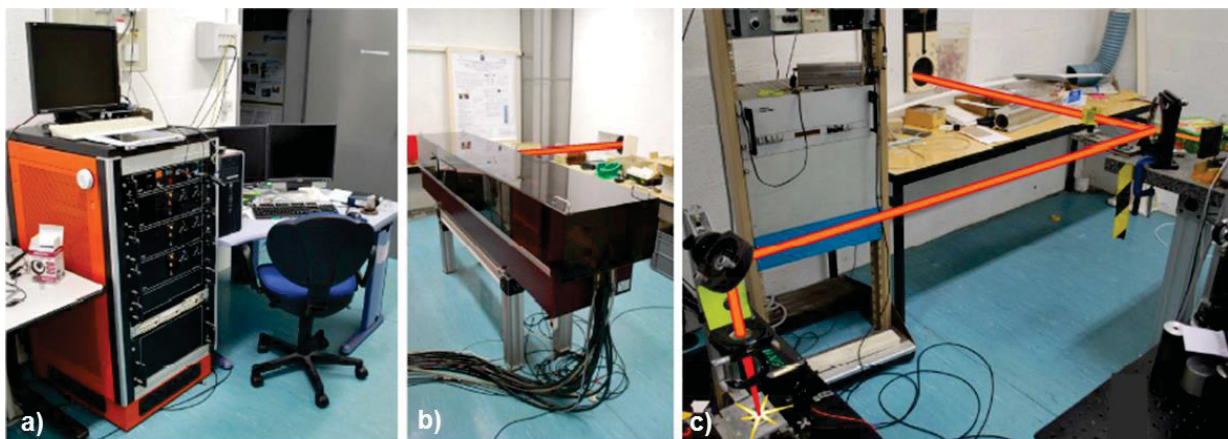


Figure D.1: Experimental setup of laser CNRS PPRIME 25 ns with (a) the command room, (b) the laser source and (c) the experimental room with the target [1]

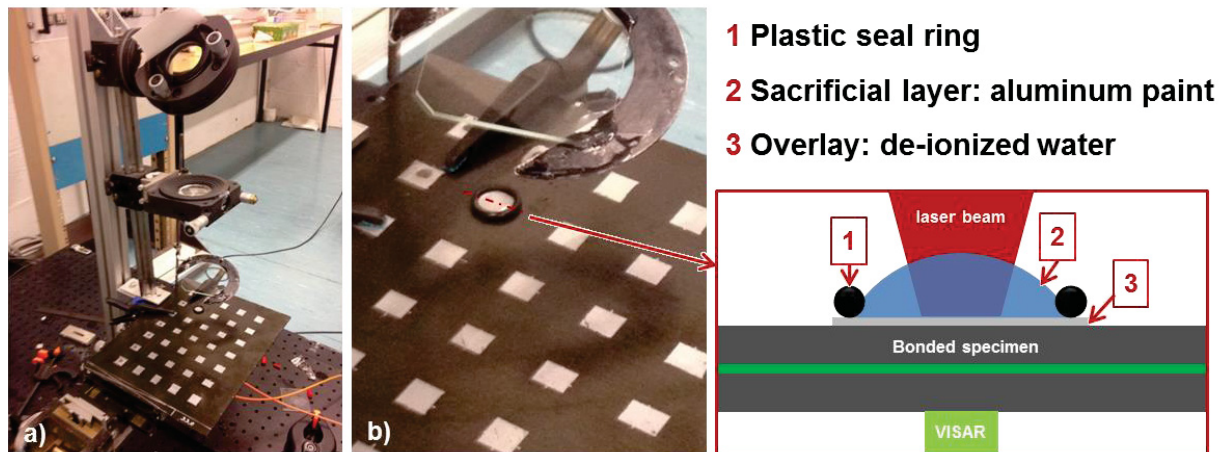


Figure D.2: Representation of (a) the composite target and (b) magnification with scheme of preparation for laser shot

## 2.2 Laser source LBI – LSP Technologies

The LBI source from the American company LSP Technologies has also been used for laser shock experimentations. The experimental setup for laser tests is shown in Figure D.3. Compared to the LASAT source, the laser properties are slightly different with a maximum delivered energy of 50J at a 1053 nm wavelength. The pulse duration is also adjustable in a large range from 70 to 300 ns. This feature is a proprietary development, which makes the LBI laser particular compared to the commercial laser sources available [2], [3]. In the experimental setup, the laser source on its optical table (Figure D.3a) with power amplification and measuring devices are placed in the command room. The laser beam is sent to the adjacent experimental room, conducted via mirrors and lenses that focus the beam to 10 mm diameter. An industrial robot holds the clamped CFRP sample in a vertical position before the laser shock (Figure D.3b). The laser shots take place in this experimental room. In the case of the LBI, the sacrificial layer is an adhesive vinyl tape which can be removed directly after laser shock. The vertical position of the sample also demands a continuous flow of water at the surface of the CFRP sample, in order to ensure a proper plasma confinement layer. This flow of water before a laser shot is so limited in time that no diffusion of water in the CFRP matrix is considered.

The time-resolved EMAT diagnosis tool was tested to demonstrate its potential. The tests were however realized with another similar laser, designed as a transportable laser proof test commercial prototype. The laser and all electronic and optical systems are assembled as shown in Figure D.4a. The mobile arm shown in Figure D.4b illustrates how the probe head includes the laser beam delivery and the EMAT sensor. The water confinement application and removal is also included in the probe head.



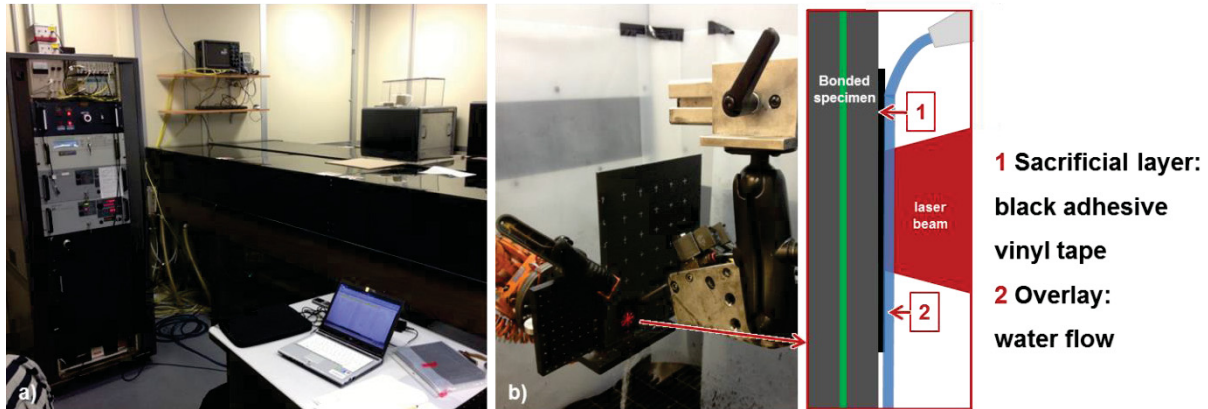


Figure D.3: Experimental setup of laser LSP Tech 200 ns with (a) the command room and (b) the experimental room with the target

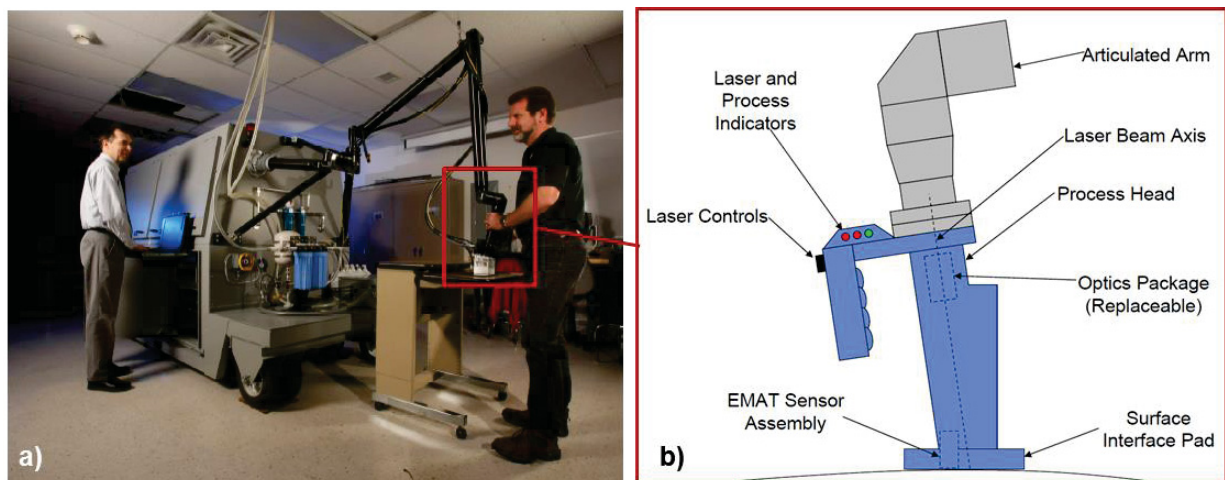


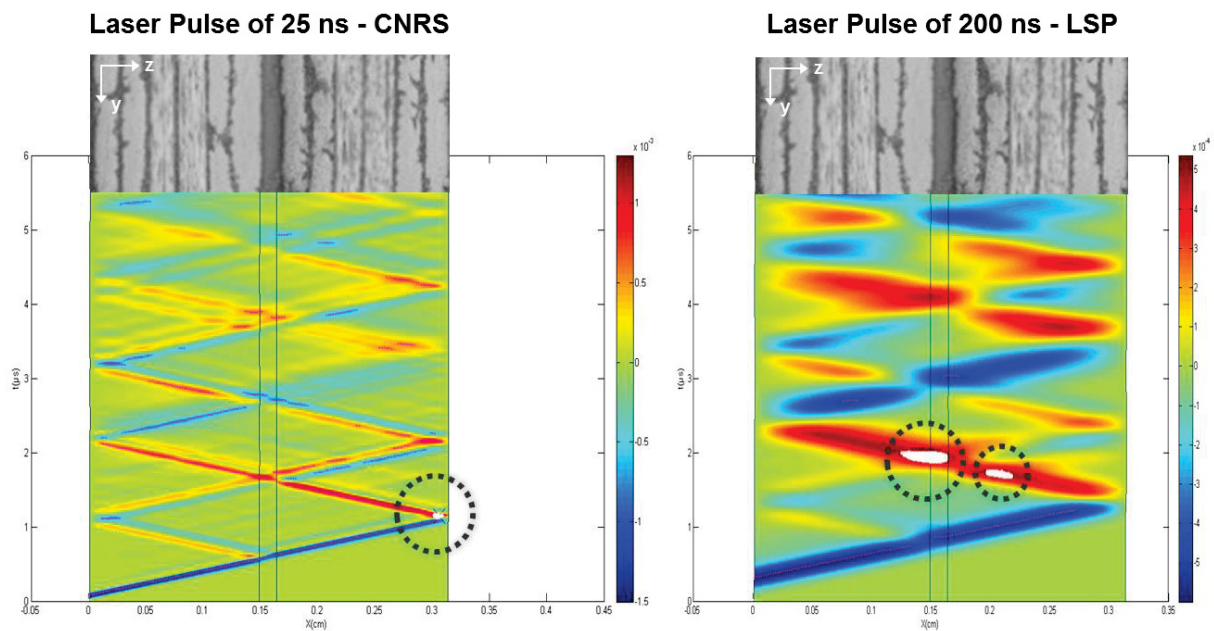
Figure D.4: Experimental setup of the (a) mobile laser prototype from LSP Tech and (b) the detail scheme of the probe head including the EMAT diagnosis tool [4]

Both laser setups are tested in this study. The parameters of shots for the laser tests are selected in the way that a comparison between the two sources is made possible: the only parameter adjusted is the energy of the laser beam. The laser beam spot size, the laser pulse duration, the approaches for confinement and sacrificial layer stay specific to each source and will be discussed. The pulse duration was identified in chapter B as being responsible for the depth of generation of the tensile stress. It is set at 25 ns for the LASAT source tested, corresponding to the short pulse duration. In opposition, the pulse duration is set at 200 ns for the LBI source, the large pulse duration. In the rest of this study, the lasers will be referred to as “laser 25 ns” for the LASAT setup and “laser 200 ns” for the LBI setup.

Based on the theoretical consideration exposed in chapter B, a numerical model for shock waves has been developed [1]. The particular case of the composite system with resin M21 and T800S fibers in a symmetrical 6 plies laminate with adhesive bond has been simulated and are provided by R. Ecault based on personal communication. This is possible thanks to the validation of the MATLAB model on the similar composite material, carbon fibers and epoxy adhesive. The two time/position diagrams in Figure D.5 represent the results of the MATLAB simulation in tensile stress loading in the z-direction (through the thickness). The shock wave propagation is evidenced and the stress levels range from compression stress (blue) to tension (in red). For both laser setups, the position where spallation may occur in the

laminate is also marked by the dashed circle. This region corresponds to the highest 5% of tension in the thickness (also in white).

Cross-sections of the actual CFRP laminate are represented to illustrate the lay-up and thickness organization used for the model. One can observe that for the laser 25 ns, the tensile stress concentrates close to the back free surface of the laminate. In comparison, the larger pulse duration with the laser 200 ns concentrates the tensile stress first in the rear laminate and second in the adhesive/substrate interface. This last area corresponds to the targeted depth with the adhesive bond strength to be tested. The NDT- and micro-observations of the shocked locations will be compared to these simulations to determine where the spallation really occurred.



**Figure D.5: Numerical time/position diagrams showing the 5% max. tensile stress loadings in z-direction (white areas) in a 3.2 mm thick symmetrical adhesive bonded CFRP laminate for laser 25 ns (left) and laser 200 ns (right)**

### 3. EXPERIMENTAL APPROACH FOR DETERMINATION OF LASER PROOF TEST EFFECTS ON BONDED STRUCTURES

Several tests with laser sources have been designed to understand the effects from laser shots on composite bonded structures. Four tests are presented hereafter. They aim at assessing the non-destructive character of the laser proof test approach for the inspection of adhesive bonded composite structures.

#### 3.1 Test A - Determination of intensity threshold for each adhesive bond states

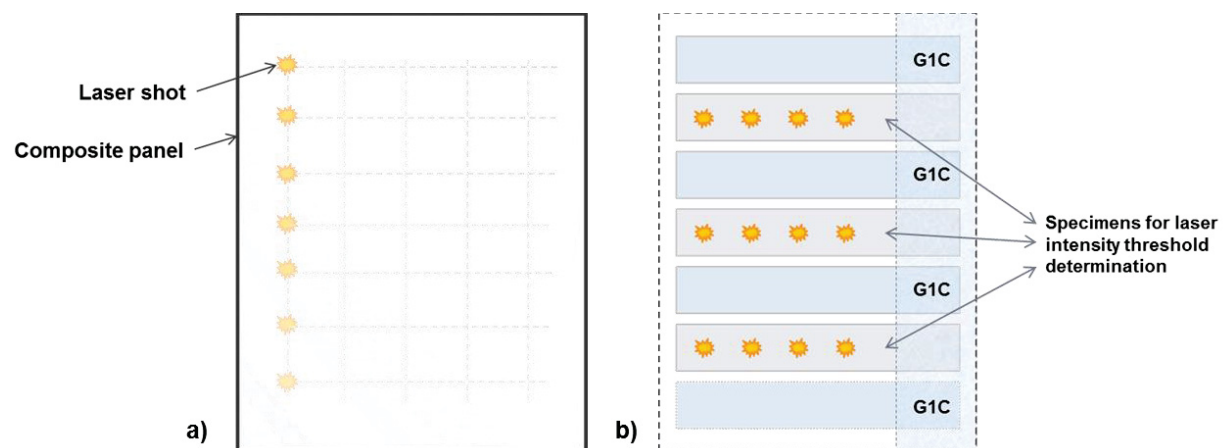
The first test, to be referred as Test A, is the first important step in the evaluation of the laser proof test capacities in discriminating adhesive bond quality. Test A must be conducted at first in order to determine for which intensity a spallation at the bondline/substrate, i.e. a debonding, is created in the adhesive bond tested.

The intensity requested for a debonding is considered to be the maximal intensity that an adhesive bond can withstand. It is here defined as the threshold intensity. It is hence also considered that if the intensity does not reach the threshold, no debonding shall occur. This maximal and threshold intensity will later be referred to as 100% intensity and inferior intensity levels will be considered in percentage of this maximal level.

The threshold intensity is specific for each material configuration, adhesive performance and geometrical properties. Each laser configuration is thus provided with CFRP specimens from the C, PC and MOC families and with the four states of contamination i.e. weak adhesive bond state, in addition to the reference state.

The laser shot is applied on the front face of the specimen at a precise location marked by a grid to ensure a regular distance between all shot locations. Figure D.6a introduces the setup for specimens for the cured C and partially cured PC families while Figure D.6b introduced the setup for moisture contaminated MOC specimens including four  $G_{1C}$  coupons due to reduce the amount of samples manufactured. In comparison, laser shocks are applied on whole specimen for the C and PC tests whereas they are only applied on  $G_{1C}$  cut-outs for the MOC specimens family.

The target is the determination of the threshold intensity, which will only be precisely defined by NDT inspection and observations of micro-sections of laser impacts. The characterization of the specimens is ensured prior and after laser proof test by means of the phased-array ultrasonic (PAUT) inspection. The results after laser shock have also been verified by microscopic observation of the impacted locations. While higher intensities than threshold lead consequently to a debonding, a lower intensity may not be damageable. This characteristic of the laser proof test setup is investigated in test B.

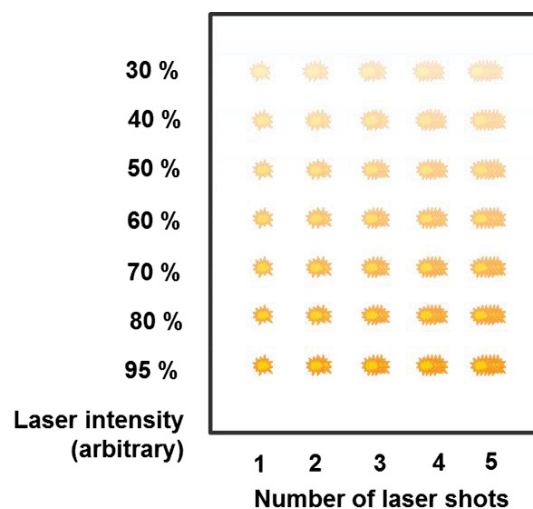


**Figure D.6: Setup of laser test A for the determination of threshold intensities for debonding of (a) each adhesive bond state specimen ( $250 \times 200 \times 3.2 \text{ mm}^3$ ) and (b) particular setup for moisture contaminated specimens including  $G_{1C}$  coupons for fracture toughness evaluation**

### 3.2 Test B - Evaluation of potential damages in materials after repeated shocks

The second test focuses on the effect of assessment of adhesive bond quality performed with a lower intensity than the intensity threshold value. It is based on the assumption that a bonded composite structure will have a long lifetime and undergo multiple inspections. Therefore, the test B aims at evaluating the effects of repeated laser shots on the adhesive bond and the complete composite structure. The purpose is to investigate a possible weakening or destructive effect over the structure if a precise location is impacted several times at a certain laser beam intensity. This test can be performed based on the information obtained from test A, which provides the threshold intensity for a reference state (without contamination) specimen from the cured C state. The characterization of the specimens post-shock is ensured by NDT phased-array ultrasonic inspection and cut views observed with optical microscopy.

Different lower intensities below threshold are chosen and laser shots are repeated up to 5 times at a precise marked position indicated by the grid pattern on the specimen as described in Figure D.7. The laser shots are repeated with intervals of several minutes because of the time needed to mount/unmount the specimen and reapply a sacrificial layer (adhesive tape or aluminum paint) to protect the specimen surface from the plasma. The intensities applied and number of impacts are registered in order to map the eventual damages that will be correlated with a standardized ultrasonic NDT inspection and cracks observations.



**Figure D.7: Setup of laser test B for the evaluation of effects of repeated shocks below threshold limit at same locations on a bonded CFRP specimen (250\*200\*3.2 mm<sup>3</sup>)**

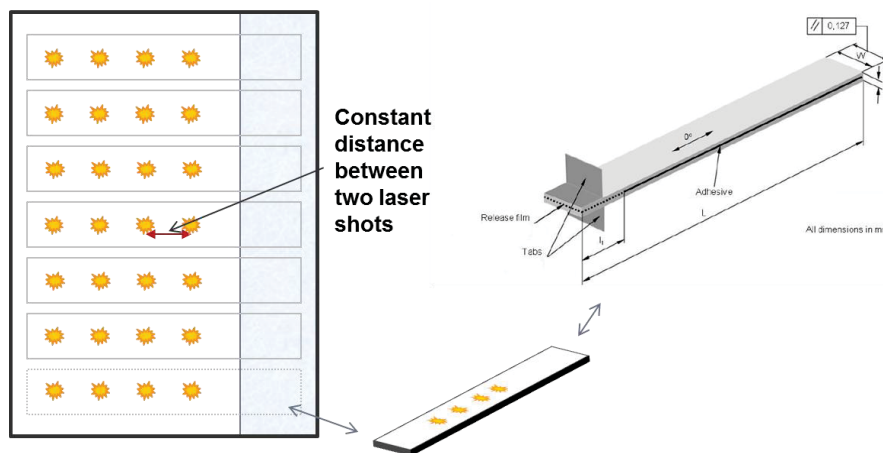
The nature of shock waves described in Chapter 2 may lead to the assumption that damages can occur even with lower intensities than threshold. The possible effects of laser shot at lower intensity, if no damage is observable, is investigated in the next test C.

### 3.3 Test C - Evaluation of mechanical performances after laser proof test

In the frame of Test C, an investigation of the possible effects of laser proof test on the mechanical  $G_{1C}$  performances of a reference state adhesive bond is conducted.

Laser shots are performed at a relatively high level of intensity (around 70% of the threshold intensity), each one separated by a distance of about 30 mm along a line, corresponding to what could be later for example, an inspection of a stringer foot adhesively bonded to a CFRP skin. Figure D.8 introduces the design of the CFRP plate specimen where four laser shots on seven  $G_{1C}$  coupons are foreseen. The shots are performed at first over the complete CFRP plate.

The characterization of the specimens post-shock is ensured by NDT phased-array ultrasonic inspection to make sure that no damage has been generated consequently to any laser shocks. The reference specimen tested is then cut in  $G_{1C}$  coupons by means of water jet. The  $G_{1C}$  coupons are tested mechanically and the results are then compared to the reference  $G_{1C}$  results, without any laser shocks.



**Figure D.8: Setup of laser test C for the determination of mechanical  $G_{1C}$  performances after a simulated inspection with laser proof test on a reference adhesive bond state specimen ( $250 \times 200 \times 3.2 \text{ mm}^3$ )**

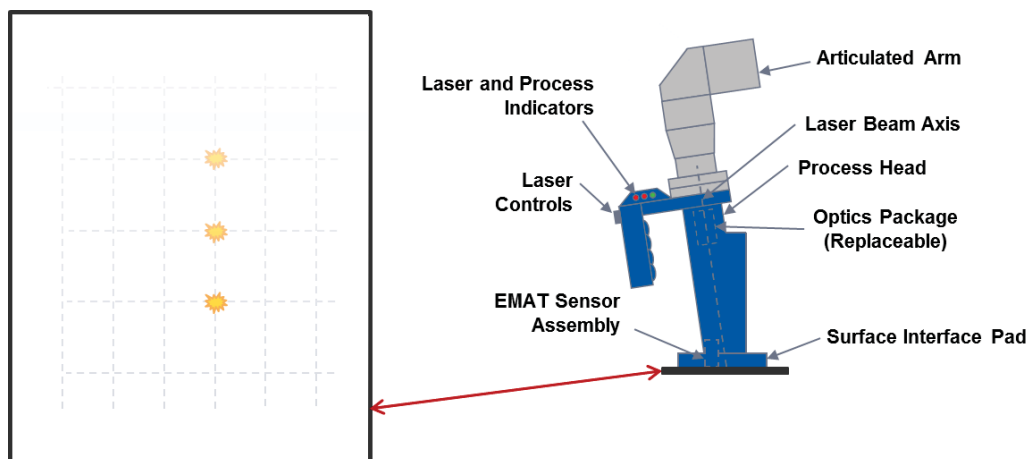
The previous tests A, B and this last one, test C, involve specific series of measurements for which the time-resolved diagnosis tools are avoided. A last test, test D, aims at evaluating this last feature of each laser proof test setup.

### 3.4 Test D - Use of integrated time-resolved diagnosis from laser proof test methods

Test D is designed close to test A in order to evaluate the signals that can be expected from all time-resolved diagnosis tool, the EMAT and the VISAR, for the direct evaluation of a laser shock as represented in Figure D.9. A reference specimen (without contamination) is tested by the mobile laser prototype with the EMAT probe head in the case of the 200 ns laser. In the case of the 25 ns laser, the VISAR laser is used on the back face of the composite to measure the back face velocity.

The selected intensities cover a range below and above the threshold in order to ensure a damage generation in the CFRP specimen. The diagnosis tool should hence distinguish the shot by lower and higher intensities above thresholds based on the effect on the waves propagation in the damaged structure. Test D shall thus check the capability and reliability of tests with the existing prototype as it has been developed up to date.

No particular grid pattern or consign for this test is provided for this test. Only a phased-array ultrasonic inspection is conducted before and after the laser shocks to verify the damage generation in the CFRP specimen. The relevant results are the EMAT and the VISAR signals.



**Figure D.9: Setup of laser test D for the evaluation of the capabilities of time-resolved diagnosis tools proposed by each laser proof test technique**

All tests performed with the two laser setups are summarized in Table D.2. The effort demanded is concentrated in Test A on the determination of the intensities threshold for all specimens families and contamination states (five states for each of the three families – refer to chapter C).

The additional laser tests B, C and D are performed only on standard specimen, cured and without any contamination, in order to evaluate the effects of the laser tests on a specimen representative of what an adhesive bond should be like in manufacturing. The experimental approach is oriented on a comparison of both laser systems, requiring thus a similar specimen for tests.

**Table D.2: Summary of laser tests organization with relevant composite specimens families and contamination states investigated as defined in Chapter 3**

	<b>Laser 25 ns</b>	<b>Laser 200 ns</b>
<b>Test A</b>	- Cured C - States 1 to 5 - Partially Cured PC - States 1 to 5	- Cured C - States 1 to 5 - Partially Cured PC - States 1 to 5
	- Moisture contaminated MOC - States 1 to 5	
<b>Test B</b>	- Cured C - State 1	- Cured C - State 1
<b>Test C</b>	- Cured C - State 1	- Cured C - State 1
<b>Test D</b>	- Cured C - State 1	- Cured C - State 1

### 3.5 Characterization methods and type of damages post-shocks

The composite specimens tested by laser proof test are inspected with phased-array ultrasonic method to reveal the presence and, when requested, analyze the debonding and other collateral damages. After this first non-destructive analysis, the most relevant damages are selected for microscopy preparation and investigation of the fractures with magnifications. This step allow a finer determination of the damages size, numbers and repartition in the specimens. Both analysis of damages post laser shocks are introduced hereafter.

#### 3.5.1 Evaluation of phased-array ultrasonic scans for damage size determination

The phased-array ultrasonic (PAUT) scans are done before and after laser shocks. The experimental steps for the acquisition are not presented again here – for more information, refer to Chapter C – section 4.2. The inspection is performed to avoid misinterpretation of potential damages with any inhomogeneity from specimen production. The ultrasonic scans made on the front side (the side impacted by the laser shock) are used for the damage characterization. This choice is encouraged by two reasons: first, the detection of damages with ultrasonic testing (UT) is more precise when the damages are far from the surface, in the ‘far field’ due to the absence of sound waves interferences. Secondly, an industrial consideration with the usual accessibility to the structure in a manufacturing and repair environment, where complex airplane composite structures might prevent any sensor from accessing to the back face. Based on Figure D.5, the tension shall be concentrated in the rear laminate and also close to the rear free surface, so that the UT inspection from the front face would lead to better results.

The main objective of the UT analysis post-shock is to detect and evaluate the damages in the composite specimens resulting from a laser shock. Any damage shall induce an acoustic impedance change and hence an increase of signal in the adhesive bondline echo. By consequence, damages are detectable in certain segments of the ultrasonic signal also called gates. In this case, the detection is optimal behind the adhesive layer, in the backwall echo.

The PAUT C-scans are therefore analyzed via the NDT Kit software in order to evaluate where and how severely the composites are damaged [5]. Signal gates are set manually by comparing a sound and a damaged location in the specimen as represented in Figure D.10.

The gates are set in a way that the damage signals are accounted, but no changes are reported in a sound area. In this study, five gates are defined: the entry echo at the front face, the laminate A, the bondline, the laminate B and the backwall echo. The gates measurement parameters are set on 'max' and 'amplitude' in order to record the maximum amplitude and visualize the size of the defect with at the gates' positions.

To evaluate systematically the damage size, the signal amplitude loss by half (-6 dB criteria) is chosen. This criteria relies on the principle that when the ultrasound beam hits the edge of a damage, only half of the signal is reflected. Therefore the amplitude of the signal is divided by two compared to the signal from the maximal reflection when the damage is completely exposed to the beam. A necessary condition is that the defects are smaller than the sound beam, otherwise beam interferences may occur below the defect. The 6 dB attenuation is made visible by adjusting the color palette from the interesting cartography – here the backwall echo (see Figure D.10 bottom). The damage detection can then be launched manually without minimal damage size. Damages are detected in circular and rectangular shapes. The rectangular shape is only attributed when a damage detected has a length  $L$  superior to two widths  $W$ . In case of multiple uncontinuous damages (due to parts with attenuation inferior to 6 dB), the option 'damage grouping' is chosen. The criteria for grouping two damages implies that the distance between those two damages is less than half the smallest damage radius, or mathematically if damage  $D1 < D2$ , then  $D_{d1-d2} < r_{D1}/2$ .

Regarding the depth of indications in the composite: if the laminate A or B gates reveal an event, an indication of damage in the composite substrate itself is yielded. In this case, an additional C-scan cartography is plotted in Times of Flight to evaluate the depth of the damages with their size. This information is useful to understand at which depth the composite substrate was delaminated and so, correlate the depth with the maximal tensile strength depth from the crossing waves. In most cases, the damage surface (size) is measured in the backwall echo. It is later correlated to the laser intensity from the corresponding laser shock and correlated to the crack measured via optical microscopy.



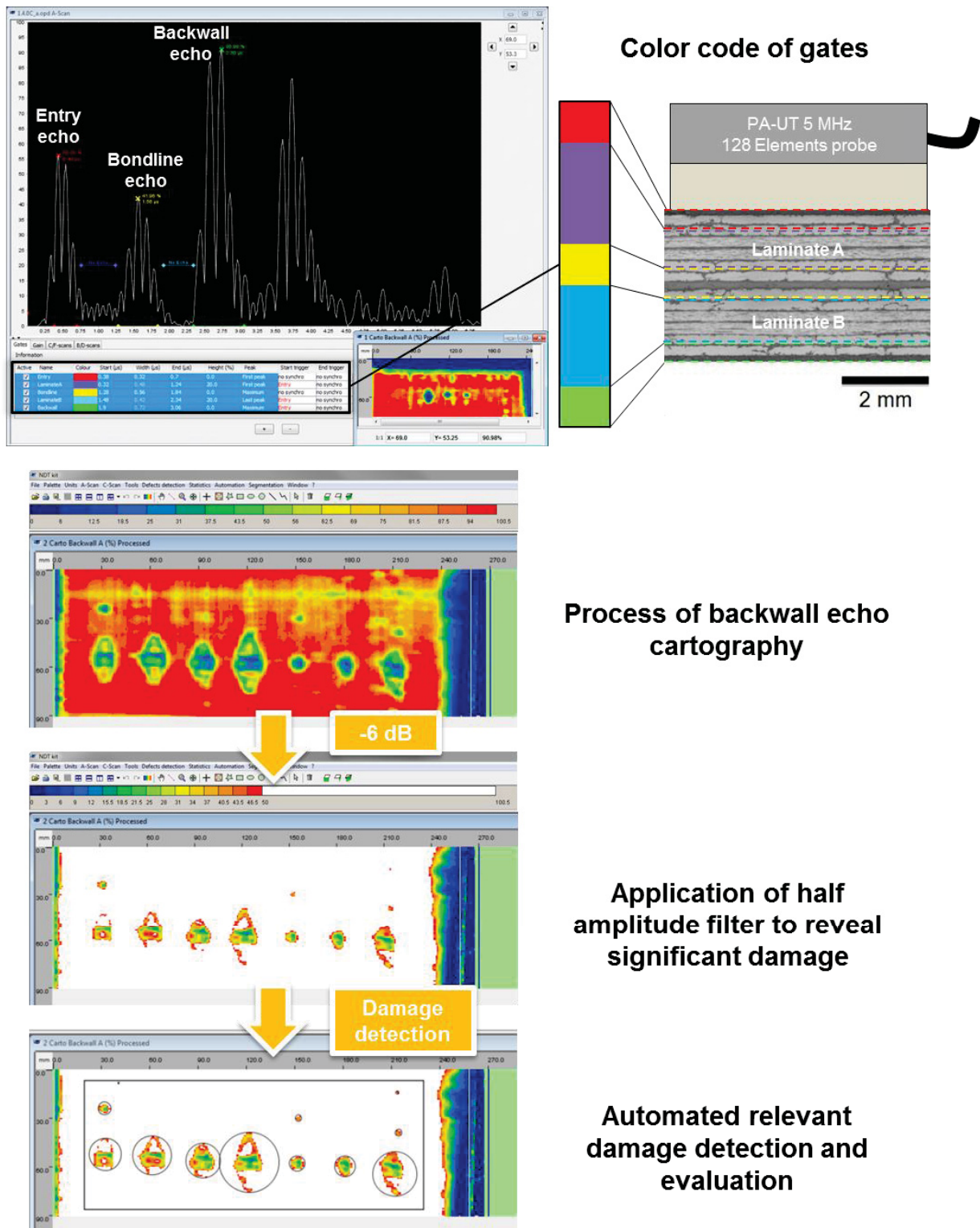


Figure D.10: Analysis of UT phased-array results with the position of gates for signal processing, cartography of backwall echo, application of -6dB criteria and signal evaluation

### 3.5.2 Observations of damages with optical microscopy

After non-destructive investigations, the specimens are cut and prepared for optical microscopy. The preparation protocol was described previously in Chapter C – section. 4.6. Observations with optical microscopy enable a precise visualization of the damages below the laser impact location.

Different magnifications can be used and a full view of the cross section is captured with 2.5x magnification for each relevant location on one CFRP specimen. This full capture represented in Figure D.11a consists in a high resolution picture displaying all layers, the matrix and fibers and the adhesive bondline. Due to the high resolution, the identification of damages in the thickness can be done manually as represented in Figure D.11b. This process is long and subjective but also more precise than the automatic recognition function of the software. An automated damage recognition is indeed possible but did not provide satisfying results due to the low contrast and the similar aspects of recording artefacts and actual cracks. All cross-sections are hence observed and marked digitally with the multiple line tool from the Stream software [6]. The marking accounts both the number of cracks per sample and the size of each crack. Both pieces of information are used for correlations with the other laser test results.

Different types of damage can be observed. The nature of these damage is depending on the laminate very local quality and mostly on the laser parameters that condition the shock waves generation and by extension, the area submitted to tensions in the specimen depth. Observations thanks to optical microscopy can reveal several types of damages:

- **undamaged areas** where no cracks are visible despite a laser shock impact.
- **Debond** at the conditioned interface. Debond is the expected type of damage where the adhesive bondline has been broken by the shock wave at the interface adhesive-substrate. The failure is adhesive and this kind of damage is detectable via ultrasonic inspection. This is the 'adhesion test' which is expected via laser proof test.
- **delamination** between plies. Delamination may occur between the fiber layers of the laminate, independently of the fibers orientation ( $0^\circ$  or  $90^\circ$ ). This damage type illustrates a 'wrong' placed concentration of tensile stress loading, responsible for an opening at a different depth than at the adhesive bondline layer. In certain cases, delamination also shows poor quality of the laminate itself, depending on the laser shot intensity and the specimens properties.
- **intralaminar cracks** which are caused by bending effects in z-direction induced by the shock waves travel through the thickness. This type of crack can be present regularly and be frequent in a single location.

In the majority of the investigated samples, more than two types of cracks are present together at a single location. The effects are then mixed as visible in Figure D.11.

The analysis of damages with UT is now compared to the number and size of cracks and altogether are correlated to the laser parameters to assess the potential of laser proof techniques. The results are presented in part 4 Results .

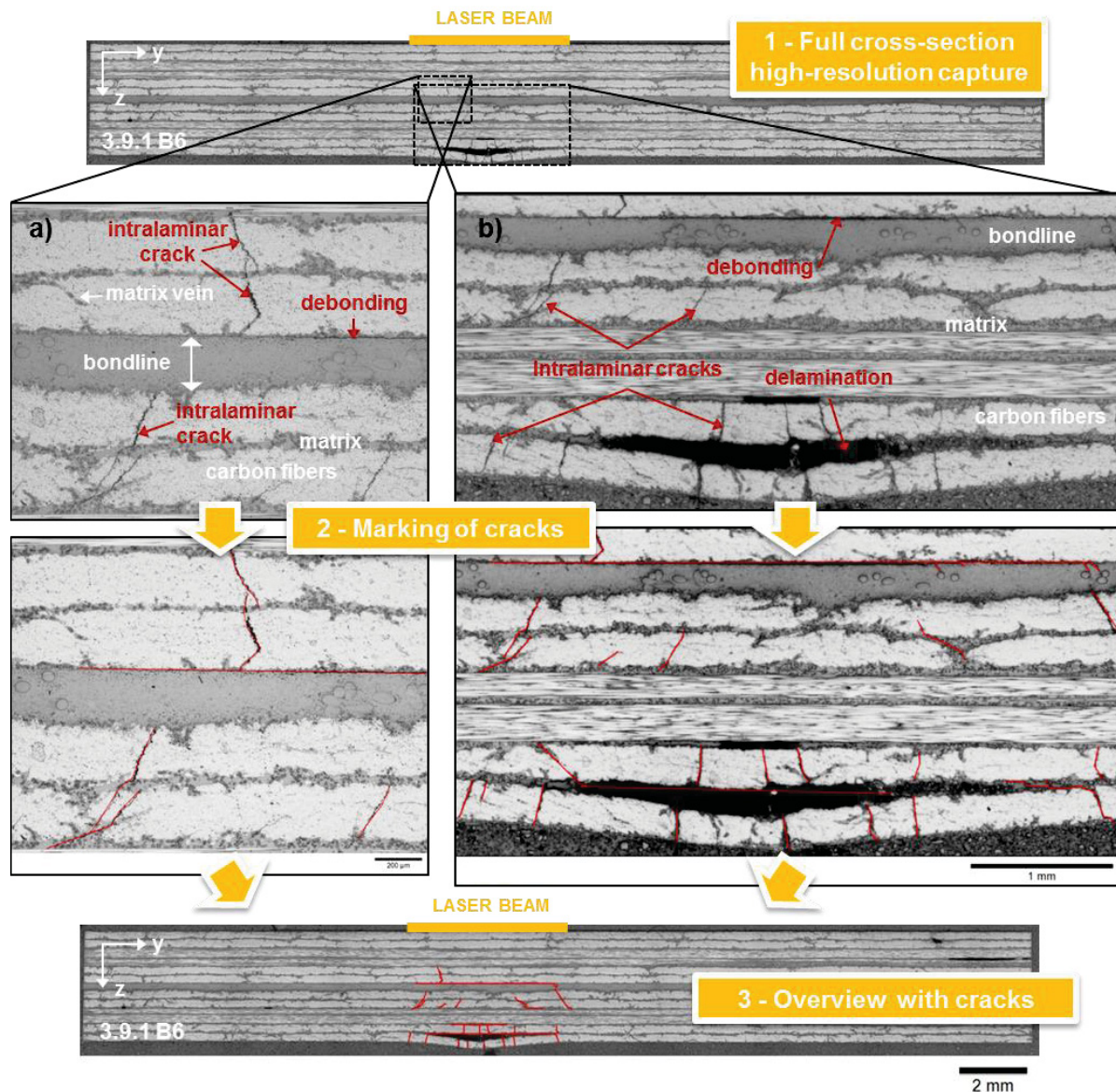


Figure D.11: Types of damages observed and marked with optical microscope. Representation of debond corresponding to aimed damage, delamination between plies and intralaminar cracks through plies in z-direction

## 4. RESULTS

The present part introduces the results of the laser tests A, B, C and D introduced in part 3. The results are a compilation of parameters which are correlated to each other. Several results are also illustrated by specific micro-sections to enhance the interpretations. The discussion of the results is integrated in each section directly.

### 4.1 Evaluation of intensity thresholds

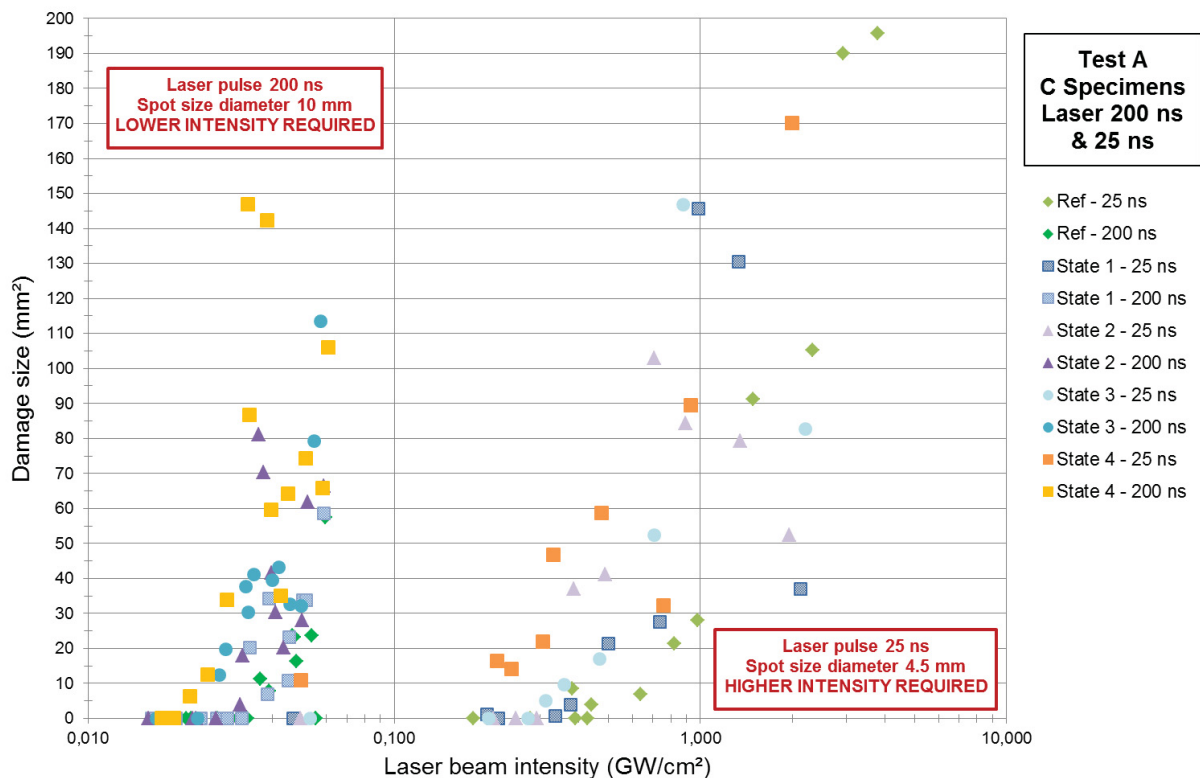
The first test is conducted on fully cured (C) specimens in order to evaluate the threshold of specimens with solely different adhesive bond conditions. Further configurations of adhesive bonded specimens, namely the partially cured (PC) and moisture contaminated (MOC)

families, are inspected in a further step. The threshold is established for a standard and cured C specimens.

#### 4.1.1 Intensity thresholds of cured specimens

Both laser setups are investigated with their default configuration, without any time-resolved diagnosis tool as described in part 2.

The results presented in Figure D.12 are a compilation of all the relevant shock data from laser 25 ns and laser 200 ns. Figure D.12 represents the damage size in mm<sup>2</sup> as evaluated with PAUT and the methodology described in Figure D.10 as function of the intensity applied for each laser shock in GW/cm<sup>2</sup>. The cracks generated are not represented more precisely in this figure, the results from measurements with the microscope are represented later in another illustration. In Figure D.12, a dedicated symbol and color tone is selected for each contamination state. This codification shall ease the comparison of the two ranges of laser beam intensities and similar contamination states.



**Figure D.12: Damage size vs. Laser beam intensity for laser shocks on the five adhesive bond configurations. Comparison of laser 25 ns and 200 ns on C specimens**

As a first observation, the range of intensities for both laser areas can be distinguished. A factor ten exists between the intensities of laser 25 ns and laser 200 ns. This factor ten is directly linked to the pulse duration itself and the spot size diameter, respectively 4.5 mm and 10 mm. It can be noticed that to generate a damage of ~20 mm<sup>2</sup> in a reference state specimen, the laser 25 ns requires an intensity of ~0.9 GW/cm<sup>2</sup> whereas the laser 200 ns only requires an intensity of ~0.05 GW/cm<sup>2</sup>.

The data scatter is large for both setup but significantly higher for the laser 25 ns. For each specimen state, no clear linear relation between the damage size and the laser intensity can be derived from the data.

The threshold intensity has been identified based on the different laser shock conditions at the different shot locations. Figure D.13 represents the threshold intensity value (in white in the bars) for each contamination state in the case of laser 25 ns. The fracture toughness energy is represented to illustrate the mechanical tests performance decrease in comparison.

For each laser configuration a threshold value can be specified. This threshold value is given when two conditions are satisfied: i) a damage must have been detected by PAUT and ii) the micro-observation of the detected damage must reveal a debond. This threshold is defined independently of any size in mm<sup>2</sup> of damage detected. The threshold intensity is thus an intensity limit level for which debonding would systematically occur. This type of damage is the one targeted since laser proof test is meant to assess the adhesive bond quality. The ultrasonic detection ability is also mandatory to be able to detect such a debond in a non-destructive way [5].

Few indications via PAUT without debonds were noticed. They correspond to the detection of other types of cracks in the laminate thickness, especially delamination which are also perpendicular to the UT waves propagation. The opposite case (debond but no PAUT indication) also occurred and can be due to the limit of 6 dB criteria, which may not be reached by all size of debonds. In any case, such results are very rare and almost all PAUT damage indications match a debond.

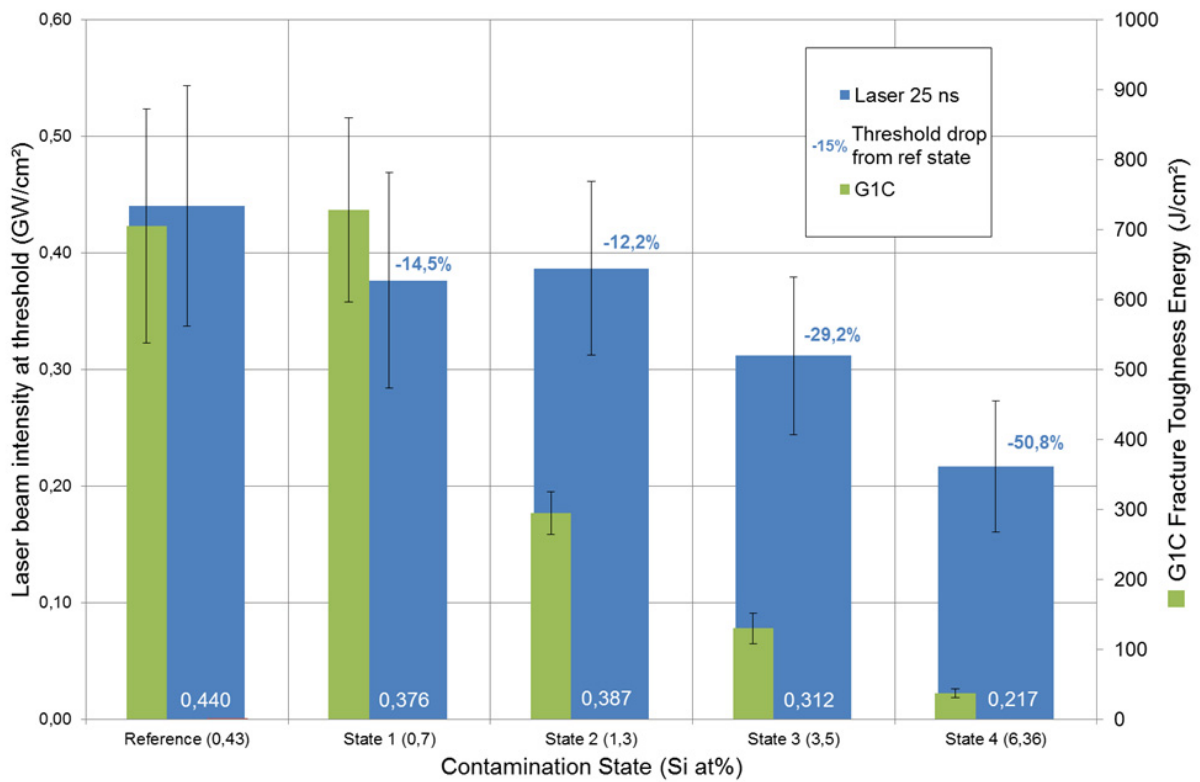
The uncertainty of the intensity  $\Phi$  is determined by the addition of all relative uncertainties from the definition terms: the energy  $E$  in (J), the pulse duration  $\tau$  in (ns) and the laser beam spot size  $S = \pi(d/2)^2$  in (mm<sup>2</sup>) (see Eq. 1). For laser 25 ns,  $\Delta E = 0.2$  J,  $\Delta \tau = 0.1$  ns and  $\Delta d = 0.1$  mm. The uncertainties rise up from ~8 % to ~16 % for the contamination state 4 where very low energy levels were applied.

$$\Phi = \frac{E}{\tau \cdot S} \rightarrow \frac{\Delta \Phi}{\Phi} = \frac{\Delta E}{E} + \frac{\Delta \tau}{\tau} + 2 \frac{\Delta d}{d} \quad \text{Eq. 1}$$

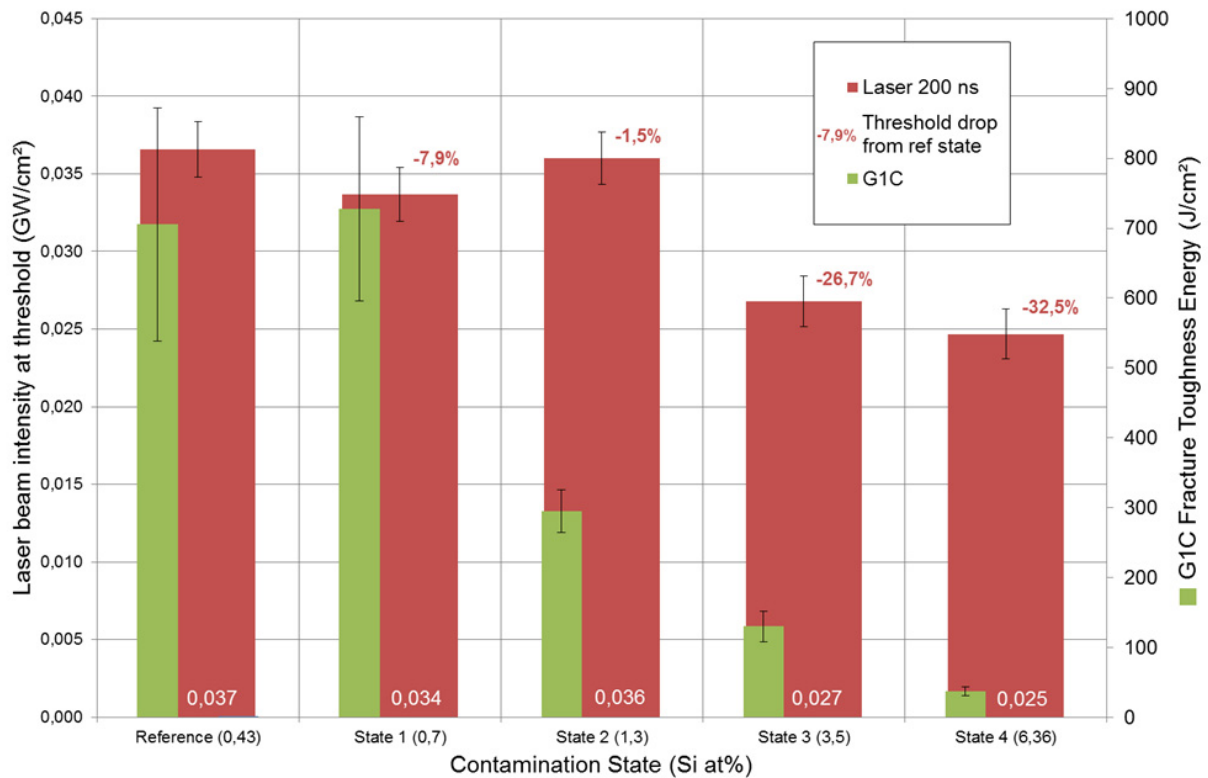
Figure D.13 illustrates the drop of threshold intensities along with the increase of Si at.% contamination on the adherent surface. Due to the uncertainty of about 10%, the reference state (0.43 at.%) and the states 1 (0.7 at.%) and 2 (1.3 at.%) are hardly distinguishable from another. Only states 4 (3.5 at.%) and 5 (6.37 at.%) can be clearly distinguished. For comparison purposes, the  $G_{1C}$  values seen in chapter C are plotted for each contamination states. The  $G_{1C}$  values are noticeable on the right y-axis of the diagrams. They allow one to gauge the evolution of the laser intensities with the evolution of the former reference mechanical characterization, on specimens without laser shocks.

The laser threshold intensities for laser 200 ns can be represented alike. In this case,  $\Delta E = 0.1$  J,  $\Delta \tau = 1$  ns and  $\Delta d = 0.1$  mm. The uncertainties are calculated in the same way and are around 4 % for all contamination states. This low uncertainty is directly to be related to the long pulse duration (200 ns vs. 25 ns) and the diameter of the laser spot size (10 mm vs. 4.5 mm).

Figure D.14 shows the same tendency for laser 200 ns as for 25 ns: the threshold intensities for debonding decrease along with increasing contamination. An exception is the case of state 2 (1.3 at.%) where the threshold is higher than for state 1 and only 1.5 % lower than the reference state threshold.



**Figure D.13: Threshold intensities requested for debonding vs. contamination state. Case of laser 25 ns on cured C specimens. The  $G_{1C}$  values evolution is indicated for comparison purposes.**



**Figure D.14: Threshold intensities requested for debonding vs. contamination state. Case of laser 200 ns on cured C specimens. The  $G_{1C}$  values evolution is indicated for comparison purposes.**

The representation of the threshold intensities is however only referring to one single laser shot for which debonding starts appearing systematically. This can be completed by another representation for a higher statistic relevance. The ratio of the sum of laser intensities for all shocks divided by the sum of damage size corresponding to all the laser shots is represented in Figure D.15 and Figure D.16. The ratio itself has no direct meaning but is an average indicator of the complete results. The error bars represent the sum of the mean standard deviations of both the laser intensities and the defect size as given by NDT Kit.

Based on Figure D.15, the laser 25 ns appears as not adapted to the geometry of the tested specimens. The damages are similar and the different adhesive bond states are not clearly distinguishable from each other. Only a significant higher threshold value can be observed for the reference state. In comparison, Figure D.16 represents the more regular decrease of this ratio for laser 200 ns. For laser 200 ns, only the state 2 (1.3 at.%) and 3 (3.5 at.%) are showing almost similar results in term of ratio with respectively 49.3 % and 45.7 % of the reference ratio value. Both values show a similar uncertainty range and are hardly distinguishable from another.

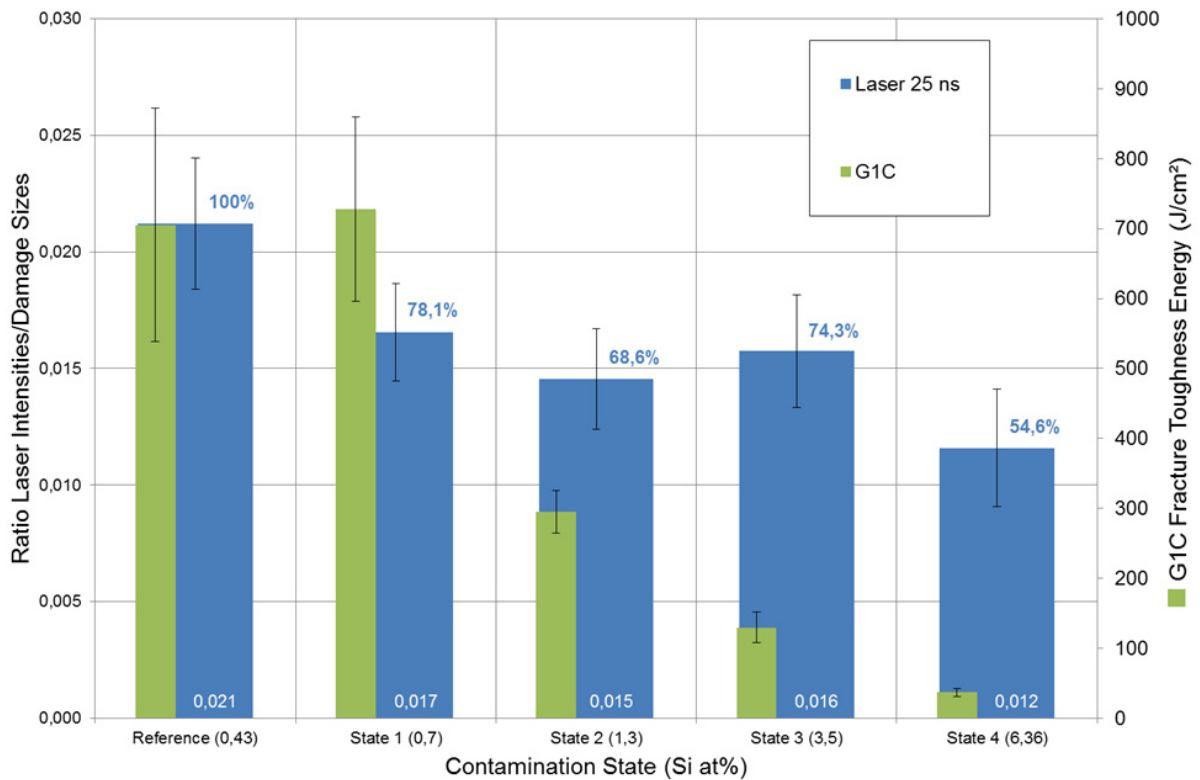


Figure D.15: Ratio total laser intensity/total damage size vs. contamination state. Case of laser 25 ns on cured C specimens. The  $G_{1C}$  values evolution is indicated for comparison purposes.

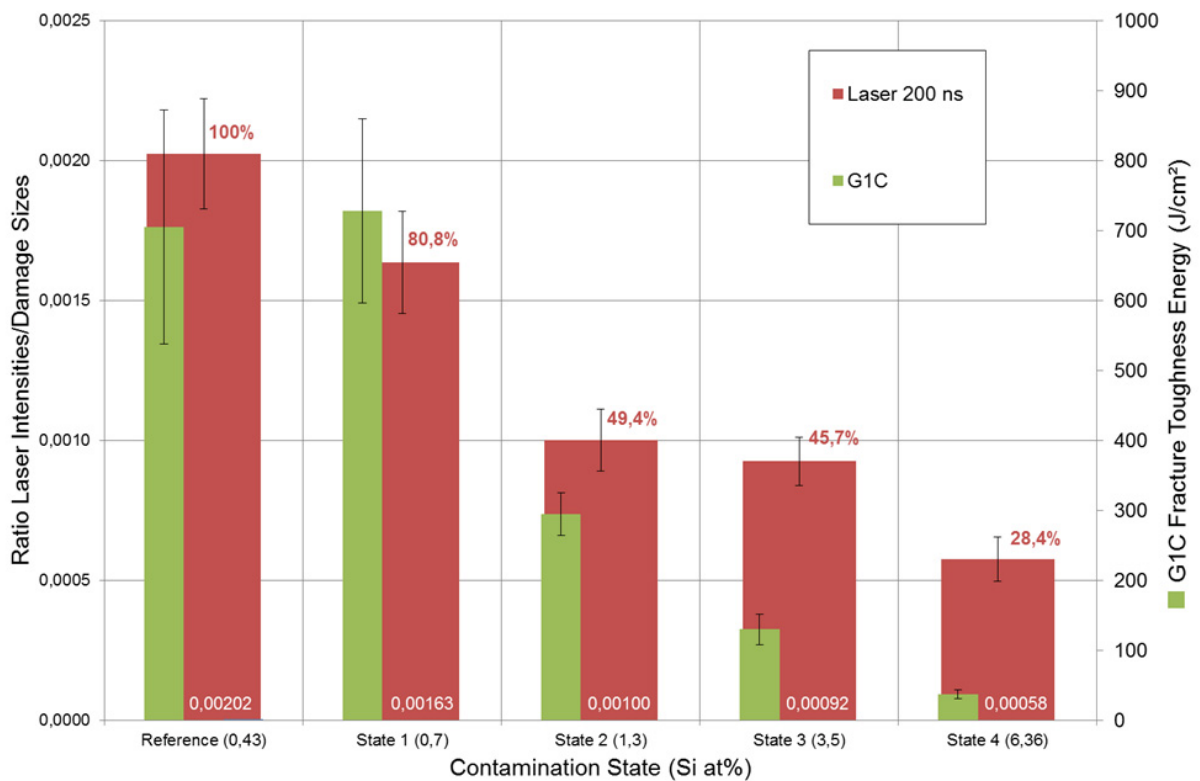


Figure D.16: Ratio total laser intensity/total damage size vs. contamination state. Case of laser 200 ns on cured C specimens. The  $G_{1C}$  values evolution is indicated for comparison purposes



The first tests on cured specimens have revealed the feasibility in distinguishing the different contamination states between one another. The errors and uncertainties have been determined with a simple conservative approach and reveal a higher uncertainty for laser 25 ns (about 8 to 16 %) than for the laser 200 ns (4 to 5 %) due to the laser pulse duration and the laser beam spot size.

Both laser setups, 25 ns and 200 ns, led to damages and for a certain intensity, to a debond. For a standard cured reference state, the threshold value i.e. the 100 % of intensity for which debonding starts occurring, is of 0,44 GW/cm<sup>2</sup> for laser 25 ns and 0,037 GW/cm<sup>2</sup> for laser 200 ns. Again, a magnitude 10 is present between the two threshold values, principally due to the difference in pulse duration and the laser beam spot size.

These observations are in line with the simulation in Figure D.5, representing the 5 % max. of tensile stress occurring in the material thickness for both laser setup.

The irregularities observed in the ratio intensities/damage size plotted for laser 25 ns can be attributed to the fact that the max. stress concentration is close to the rear free surface instead of the adhesive bondline. This feature is better represented by the laser 200 ns. A confirmation is given by the cut views in Figure D.17. Delamination occurs in the rear laminate and last plies for laser 25 ns whereas not any can be observed for laser 200 ns. Instead of delamination, the number of intralaminar cracks reveal important bending effects happening during a laser shock. The formation of these cracks seems to be favored with a wider laser beam spot size, possibly due to a 'pinch' effect (in the case of laser 200 ns).

In conclusion, the laser 200 ns has proven its better adaptation to the specimens thickness and geometry. The tensile stress generated by the crossing of the shock waves causes spallation at the adhesive/adherent surface interface. The adhesion quality is hence tested. This encourage tests on intensity threshold determination on partially cured specimens and moisture aged specimens with the most adapted laser, laser 200 ns.

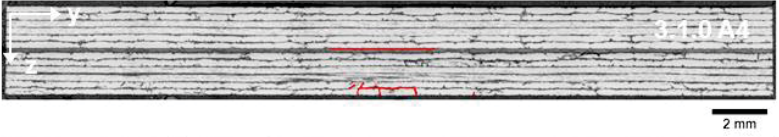
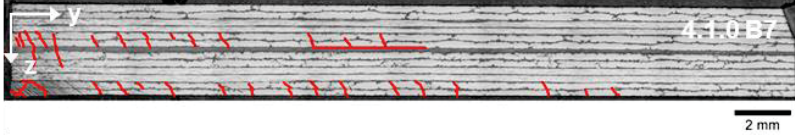
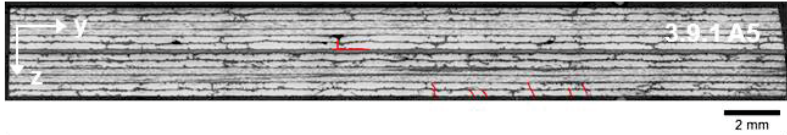
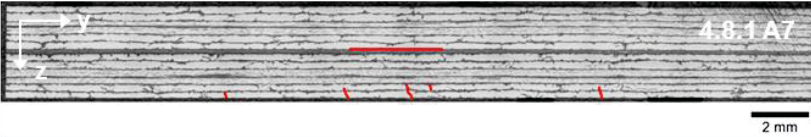
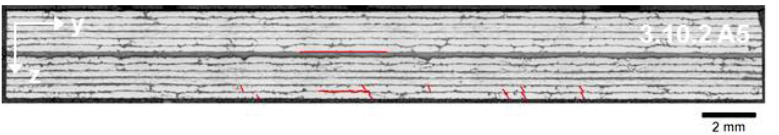
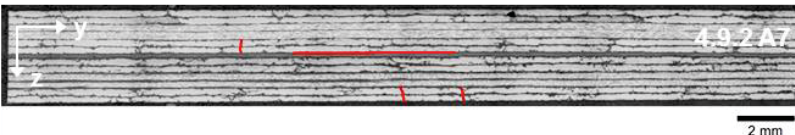
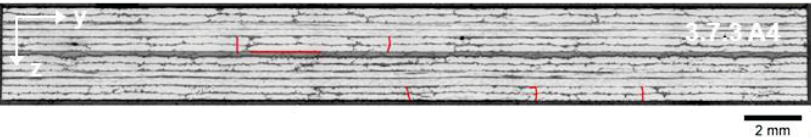
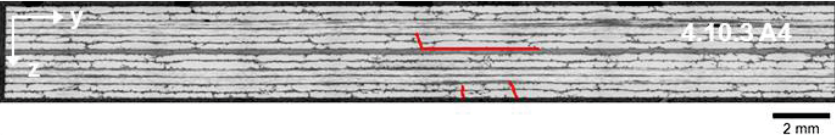
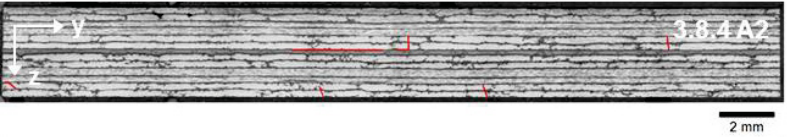
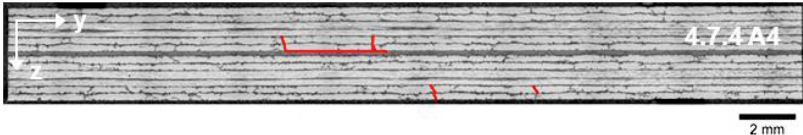
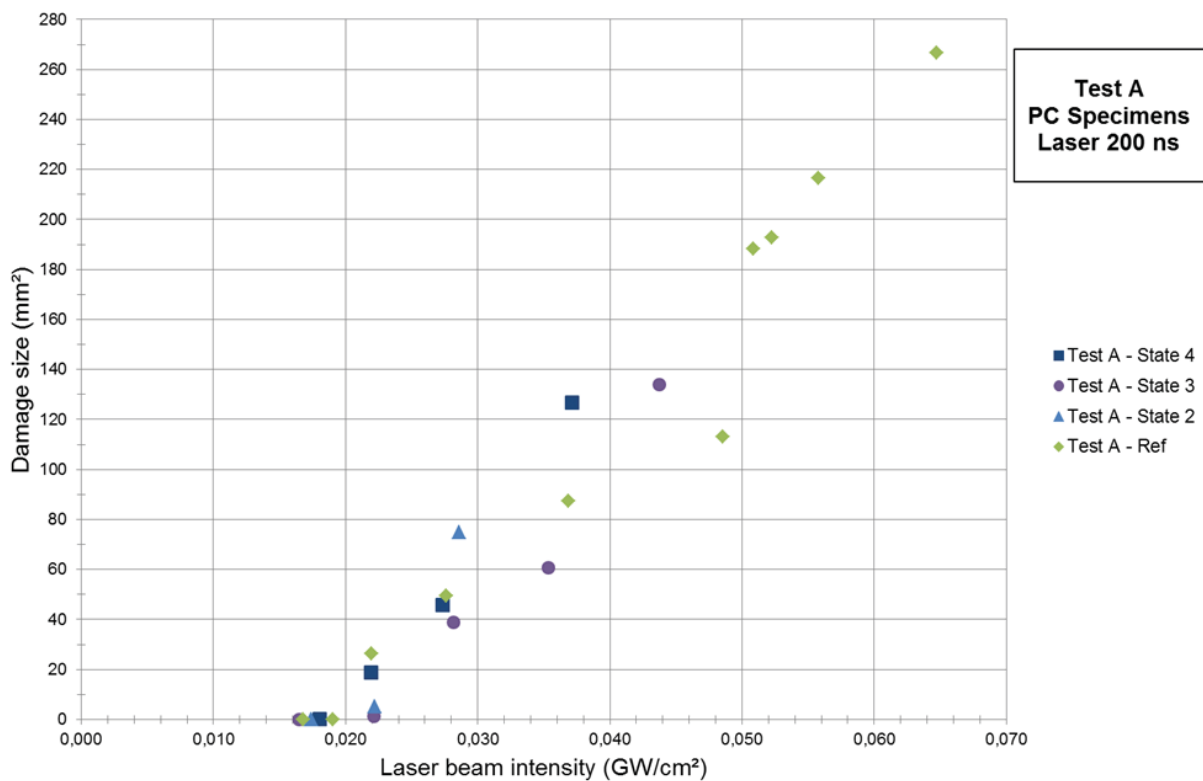
State	Laser	Micro-sections of C specimens at threshold
0 (ref)	25 ns	
	200 ns	
1	25 ns	
	200 ns	
2	25 ns	
	200 ns	
3	25 ns	
	200 ns	
4	25 ns	
	200 ns	

Figure D.17: Comparison of micro-sections of C specimens impacted at threshold intensity in each contamination state with laser 25 ns and laser 200 ns, observed with optical microscope

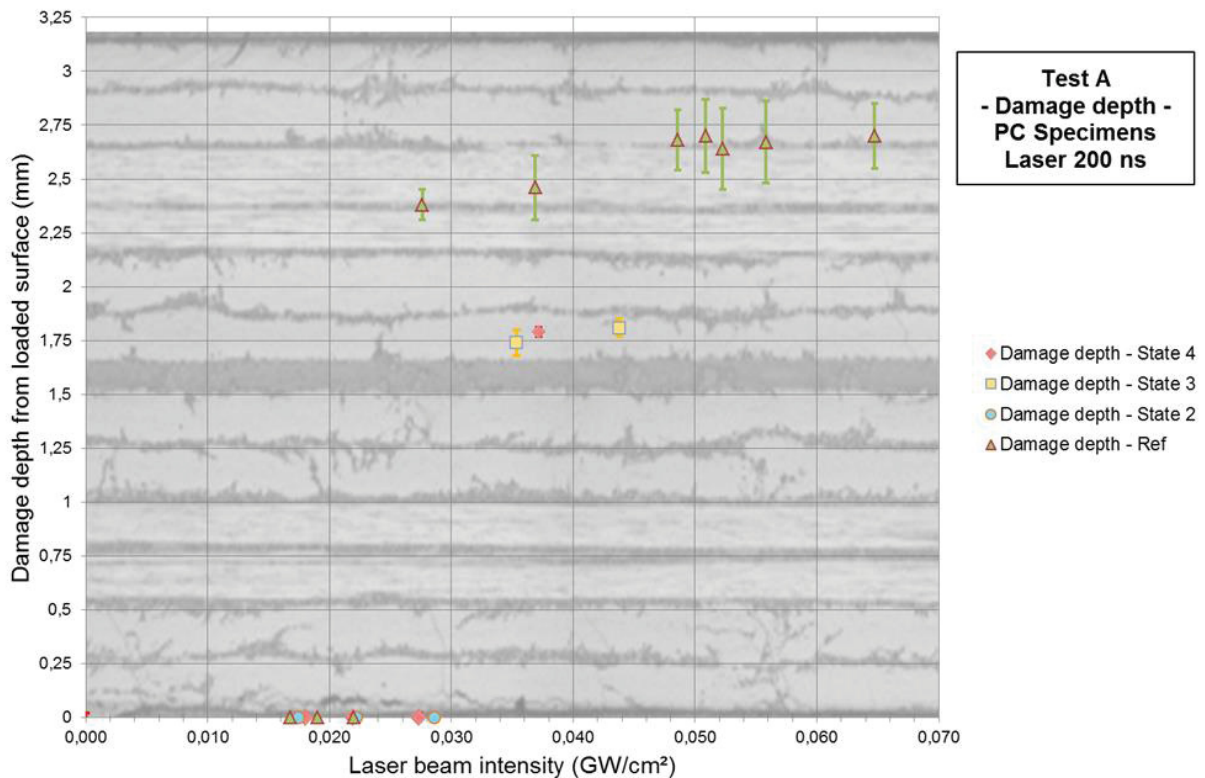
### 4.1.2 Intensity thresholds of partially cured specimens

In the case of partially cured specimens, the laser threshold intensities are assumed to be affected by the lowest cure degree of the laminate. The medium with acoustic impedance  $Z$  where the shock wave travels is directly affected by the cure degree. This effect is investigated in the frame of Test A of PC samples, in order to compare them to C specimens performances.

The damage size represented in Figure D.18 show the results of laser 200 ns on PC specimens. Due to unnoticed overwritten ultrasonic data from the specimen from state 1, no results can be presented for this specimen. In general, a common tendency for all specimens is noticeable. Independently of the contamination states, the damage size increases regularly with the laser beam intensity. The depth of the damages is represented in Figure D.19, which also includes the ultrasonic signal scatter based on the software indications. The defect depth is representative of the poor quality of the rear laminate which was co-bonded. The damages have mainly the same depth of 2.7 mm in the case of the reference specimen. Only states 3 and 4 reveal damages close the adhesive bondline with 1.75 mm depth. This may be attributed to the higher contamination levels, which could lead to another type of interaction and propagation of the shock and release waves for these states.



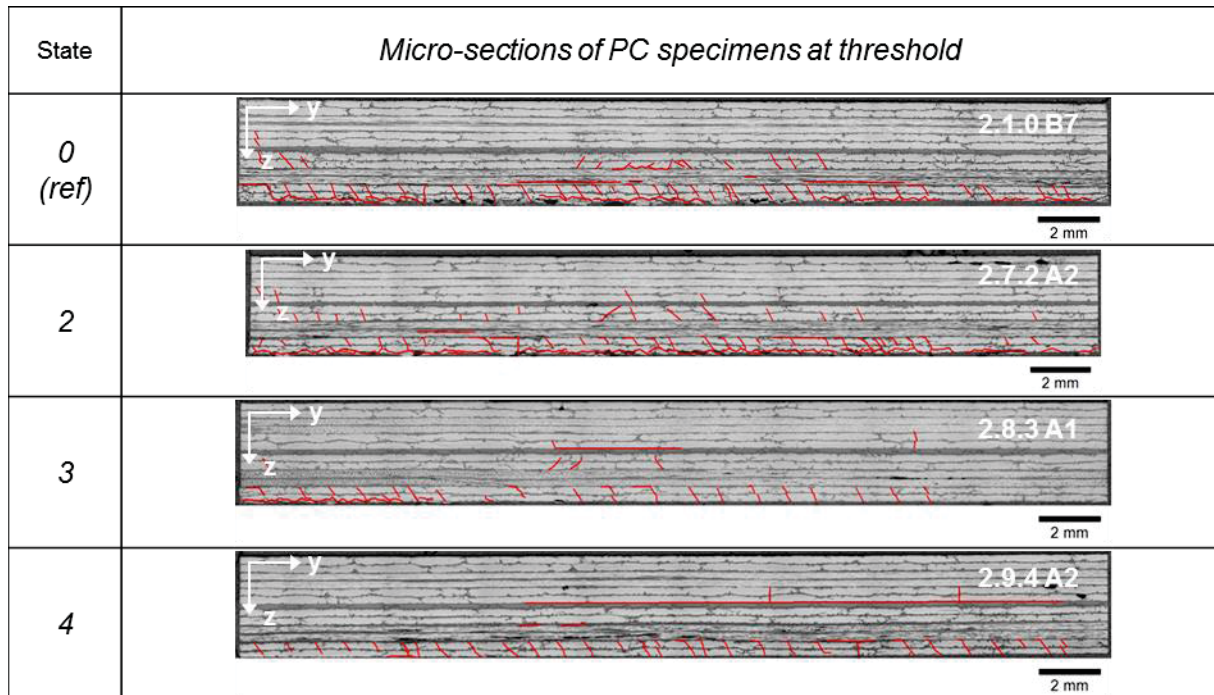
**Figure D.18: Damage size in the laminate vs. Laser beam intensity for laser shocks on the five adhesive bond configurations - laser 200 ns on PC specimens**



**Figure D.19: Damage depth in the laminate vs. Laser beam intensity for laser shocks on the five adhesive bond configurations - laser 200 ns on PC specimens**

An observation of the cross sections from the impacted specimens reveals a large number of intralaminar cracks and delaminations in the rear laminate (Figure D.20). It can be noticed that no debond is present in the case of state 0 to state 2. For all intensities tested in those states, no debonding could be achieved, confirming that the intralaminar cohesive strength of the partially cured laminate did not withstand the tensile stress and was less resistant than the adhesive bondline up to the contamination of 1.3 at.% for state 2. Above state 2, debonding starts appearing. This is obviously to be attributed to the higher contamination of the adherent surface, that decrease the adhesion quality and break due the tensile stress.

Due to the absence of debond for the states 0 and 2, the threshold and micro-sections represented are set at the first damage detected by PAUT. It is interesting to notice that all four micro-sections represented in Figure D.20 are resulting from shots with 0,022 GW/cm<sup>2</sup>. This common threshold illustrates that the common cure state of all PC specimens is responsible for the damage significance to PAUT. The cure grade of the composite matrix is responsible for the optimal material intralaminar cohesive strength, which was not reached in the case of the PC specimens. This result was partly expected but the effect of contamination to induce a weak adhesive bondline was awaited. This contamination is responsible for the decrease of the number of intralaminar cracks and delaminations while debonding appears and increases with the increase of at.% Si.



**Figure D.20: Micro-sections of PC specimens impacted at threshold intensity in each contamination state with laser 200 ns, observed with optical microscope**

The rear laminate was cracked and severely damaged due to the lack of cohesion induced by the partial cure. The adhesive bond was not opened for contamination up to state 2 (1.3 at.% Si). The contamination was however high enough in state 3 and 4 (above 3.5 at.% Si) to lead to debonding in addition to the damage in the partially cured CFRP substrate.

In conclusion, the systematic important damages with 0,022 GW/cm<sup>2</sup> allow one to use laser proof test to verify the optimal cure grade of the composite substrates reveal the partial cure of the rear laminate.

#### 4.1.3 Intensity thresholds of moisture contaminated specimens

The last investigation of laser threshold intensity was performed on cured specimens saturated with moisture. All five adhesive bond conditions were tested with help of the laser 200 ns.

Due to the effort needed for the specimens preparation, 12 laser shots were performed on moisture saturated specimens. The results of the PAUT analysis of these 12 locations can be observed in Figure D.21. The highest contamination is the first showing with a noticeable damage and the reference state, the last one. The damage size increases rapidly.

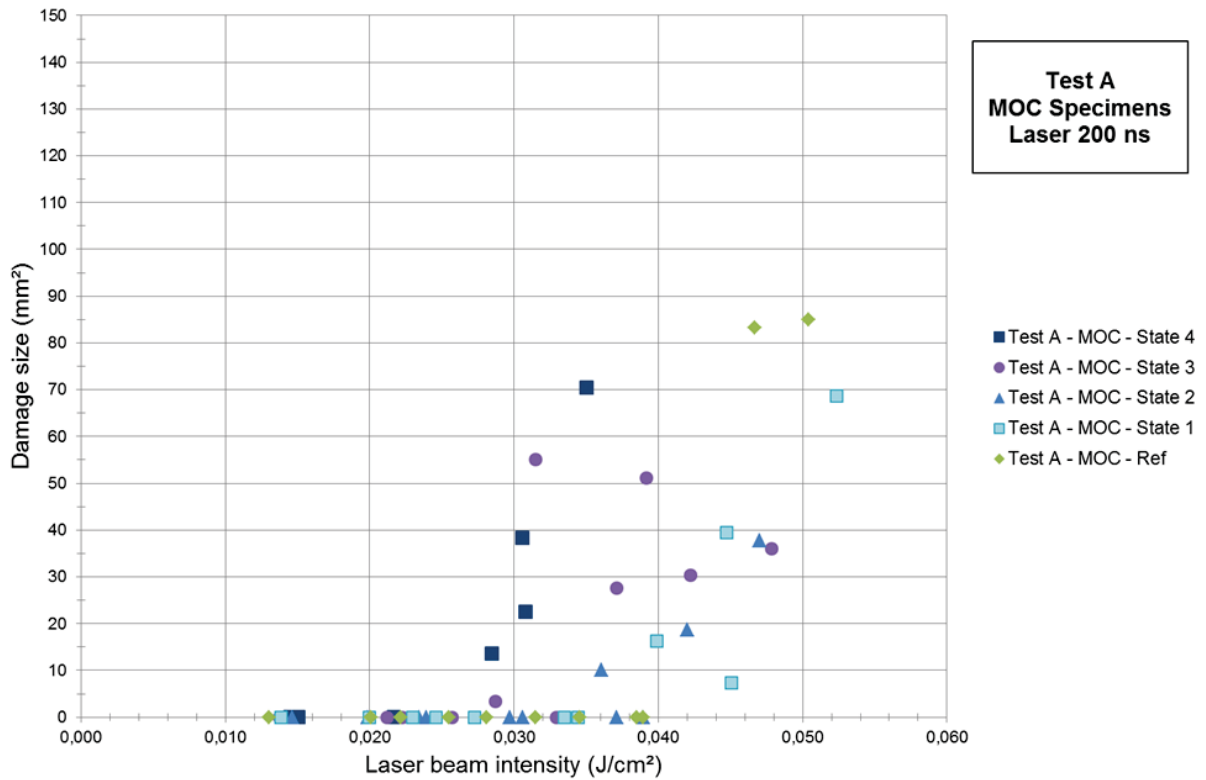


Figure D.21: Damage size in the laminate vs. Laser beam intensity for laser shocks on the five adhesive bond configurations - laser 200 ns on MOC specimens

State	Micro-sections of MOC specimens at threshold
0 (ref)	
1	
2	
3	
4	

Figure D.22: Micro-sections of MOC specimens impacted at threshold intensity in each contamination state with laser 200 ns, observed with optical microscope

In comparison to the previous specimens C and PC, the number of damages is low and the proper debonding as well as few intralaminar cracks are visible and the micro-sections in Figure D.22.

Two assumptions can be made to justify these results: first, the saturation of moisture may have induced a plasticization of the composite matrix and so, a reduction of the glass transition temperature  $T_g$ . This would enable a better tolerance toward the bending effect in case of laser shock and so, justify the low number of intralaminar cracks [7].

Secondly, the adhesion at the contaminated surface may also have been reduced by the moisture ingress. De-wetting effects occur at the fibers/matrix interface and a similar effect could affect the substrate/adhesive bond interface [8]. Chemical ageing at molecular level can be responsible of larger adhesive failure and large debondings. In her work, Parker revealed the complex combination of moisture and additional loadings on the reduction of mechanical performance of bonded CFRP specimens [9]. Here, moisture loading in the extreme case of saturation combined with adherent surface contamination obviously lead to mixed effects regarding tolerance to shock waves and damages induced.

The comparison of all threshold intensities for laser 200 ns and all specimens states C, PC and MOC is summarized and discussed in the next part.

#### 4.1.4 Overview for all tests

Threshold intensities corresponding to the intensity required for debonding have been researched for all contamination states and all specimens: fully cured C, partially cured PC and moisture contaminated MOC.

The results of the laser 25 ns did show that the intensity requested was much higher due to the laser properties. It also appeared to be inadequate with the generation of delamination in the last plies, close to the rear face, mainly due to the short pulse duration of the laser. The laser 200 ns provide better results with the tested specimen geometry with less cases of delaminations in the rear substrate.

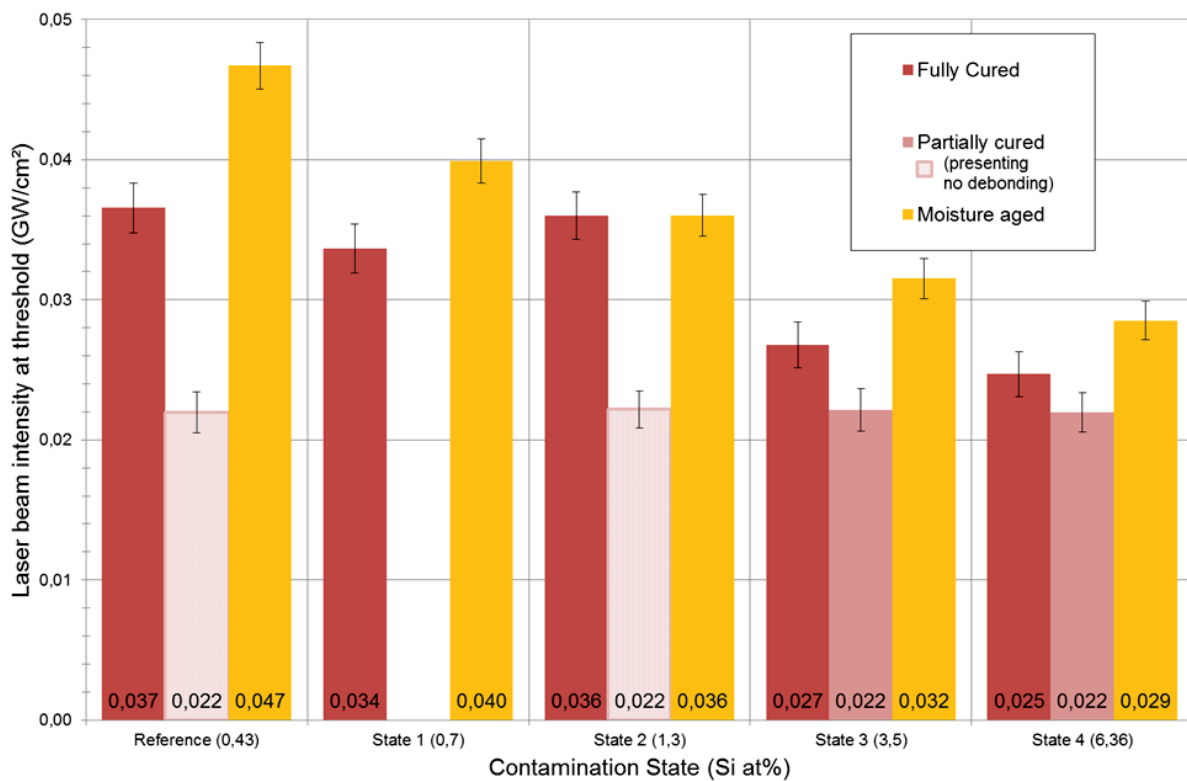
The threshold intensities for all states are represented in Figure D.23. A direct comparison between the specimens states is possible:

- For fully cured C specimens: the threshold decrease slowly with increasing contamination. The error on the intensity of about  $\pm 5\%$  attenuates the differences. The effects follow a predictable trend. The results are to be considered as the standards for the material and adhesive bond geometry.
- For partially cured PC specimens: the threshold is common to all contaminations states.  $0,022 \text{ GW/cm}^2$  were necessary to damage the rear laminate up to state 2 but the adhesive bondline could not be opened (no debonding), even with higher intensities. For  $0,022 \text{ GW/cm}^2$ , state 3 and 4 presented both damages in the rear laminate and debonds, due to the important contamination in the adhesive bondline.
- For moisture contaminated MOC specimen: the thresholds are higher than for the C specimens without moisture ingress. They however continuously decrease with increasing contamination in the adhesive bondline. The same trend, even clearer, is observable

Figure D.24 provides a statistically representative overview of the results with the ratio of the sum of intensities (in  $\text{GW/cm}^2$ ) divided by the sum of generated damage surface (in  $\text{mm}^2$ ).

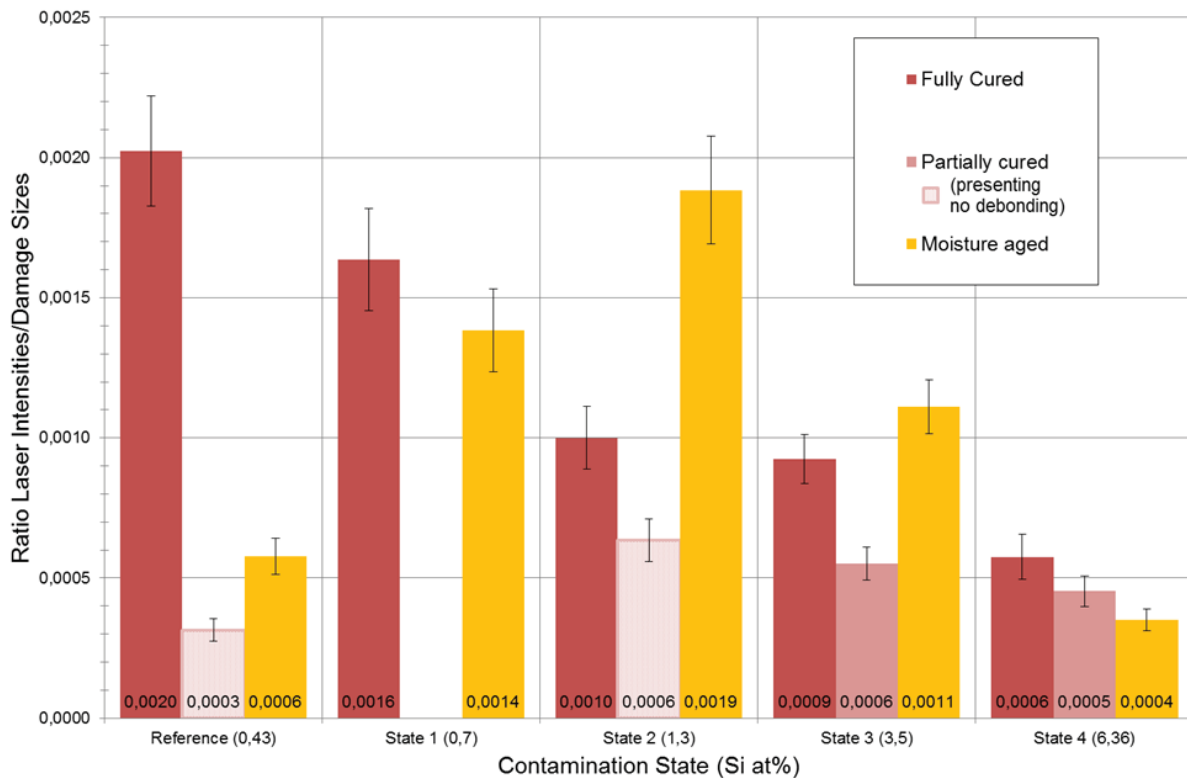
This ratio has no physical meaning but in opposition to the Figure D.23 is not relying on a single shot location since all the impacts are considered for each contamination state. With the ratio representation, the result comparison has more signification. A low ratio value indicates that either low intensities were required for debonding, or that debond were of important size.

- For fully cured C specimens: the previous statements are enhanced with use of the ratio. When the contamination increases, damages size increase and threshold values decrease.
- For partially cured PC specimens: the ratio are almost constant and significantly low, as were the threshold intensities.
- For moisture contaminated MOC specimen: the tendency shown by the single values in Figure D.23 is not confirmed immediately by the ratios. A similar tendency as the one of the cured specimens would have been expected. Instead, the ratio increases from 0,0006 for reference state 0 to 0,0019 for state 2. After state 2, a decrease of the ratio down to 0,0004 for state 4 is noticeable. The particular evolutions of the ratios in the MOC case is attributed to the lower amount of impacts available for tests (12 locations) and the presence of large debonds for specific intensity, which lowers the ratio considerably in comparison to several smaller debonds or intralaminar cracks



**Figure D.23: Threshold intensities for C, PC and MOC specimens obtained with laser 200 ns :lmshocks on the five adhesive bond configurations**





**Figure D.24: Ratio total laser intensity/total damage size vs. contamination state for C, PC and MOC specimens obtained with laser 200 ns shocks on the five adhesive bond configurations**

#### 4.1.5 Summary of intensity thresholds

In the first test series, it has been demonstrated that laser proof test can distinguish different quality levels of specimen. Within the specimens cured C, partially cured PC and moisture saturated MOC families, different contamination grades in the adhesive bond were debonded with different laser intensity thresholds.

The cured specimens have shown a decrease of the intensity threshold with increasing contamination levels, as expected. The higher the contamination, the larger are the debonds for a precise intensity.

Regarding the partially cured specimens, the threshold intensity was identical for all contamination levels. The damages were all located in the rear laminate instead of the adhesive bondline. This consistency confirms the low resistance of the rear laminate in general, which does not benefit from its optimal cohesion strength due to the partial cure state. Finally, in the case of the moisture contaminated specimens, the results are following the same trend as for the cured specimens. However, a plasticization of the composite matrix and the presence of moisture in the specimens during the test may be responsible for higher intensity threshold general. The breakage of bonds between the epoxy resin and the carbon fibers due to the moisture could have strengthened the composite resistance to bending. The shock wave propagation and the tensile stress generation in the thickness may have been affected.

## 4.2 Evaluation of damage effects due to repeated shots

The second test relies on the conclusions from test A. The threshold value for the fully cured specimen with reference state is now considered the reference threshold for this particular material and geometry. The threshold is also depending on the laser used.

In the present part, the question of damages appearing below the threshold is raised. It is evaluated if the laser proof test approach can truly be considered a non-destructive technique when a laser shot is done with lower intensity than threshold value. At the same time, the test aims at assessing the damage generation in case of repeated laser shock at the same location.

### 4.2.1 Effect of repeated laser shock on reference cured specimens

Test B focuses on a standard specimen, corresponding to a bonded composite fully cured and in the reference surface state (without contamination). The threshold intensities were determined with test A for this specimens for both laser setups. For test B, both laser setup are tested in order to evaluate the type of damages when the laser properties are not optimized. Only the laser energy is adjusted. The tensile stress is thus generated at a depth which is proper to each laser setup.

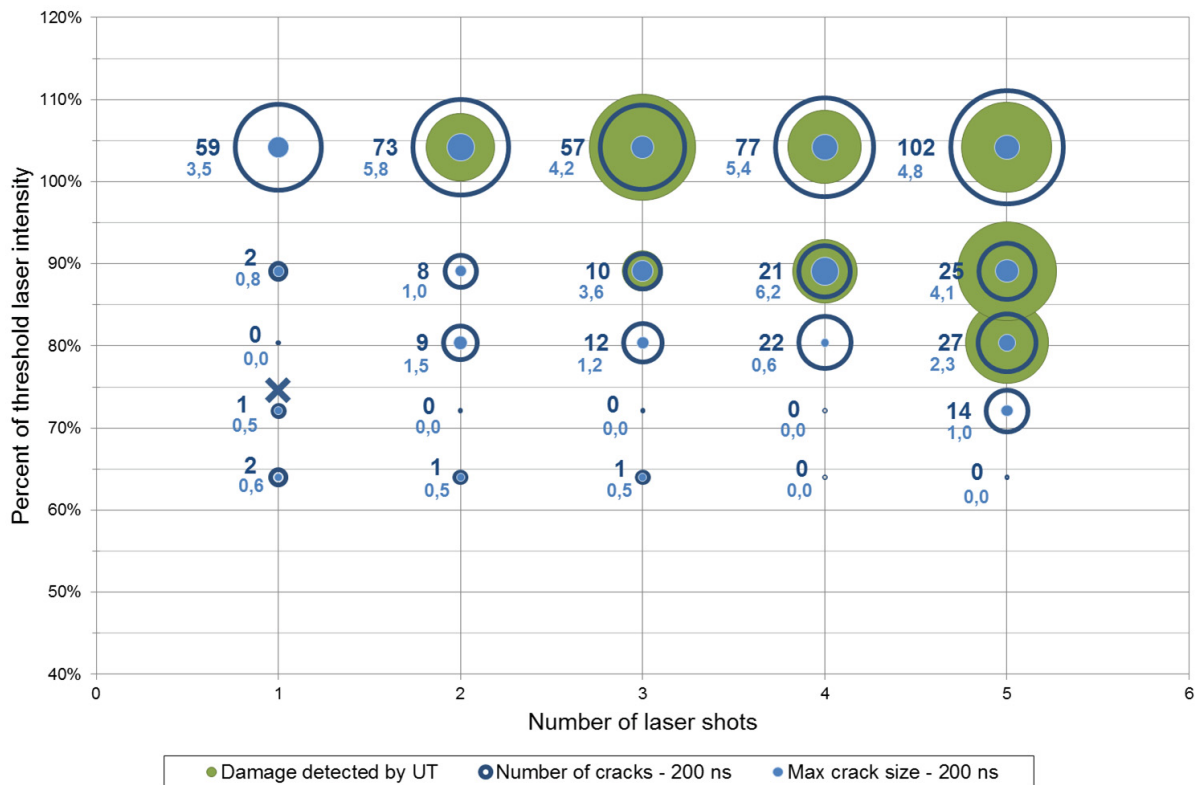
The results from laser 200 ns are introduced in Figure D.25. The representation of the damage generation is complex due to the amount of relevant information. The figure represents each impacted location on the composite specimen panel. Each location has been shot from 1 to 5 times (x-axis), at a precise level of intensity (y-axis) around and inferior to the threshold value for a C reference panel: 0.037 GW/cm<sup>2</sup>. For each location, the number of cracks counted at this location is reported in dark blue as a circle. The size of the circle is a subjective indication for the amount which is reported left to it. The light blue dots indicate the size of the largest crack observed at the location. The blue cross at ~75% is an information related to Test C, detailed later in section 4.3.

It must be noted that when the maximum size of crack is inferior to 1 mm, the location does only feature intralaminar cracks but no delamination or debonding. The green discs represent (subjectively) the location where the PAUT inspection revealed a damage, again based on the 6dB criteria. Based on all these information, several comments regarding test B with laser 200ns can be done. They can be divided in three main points:

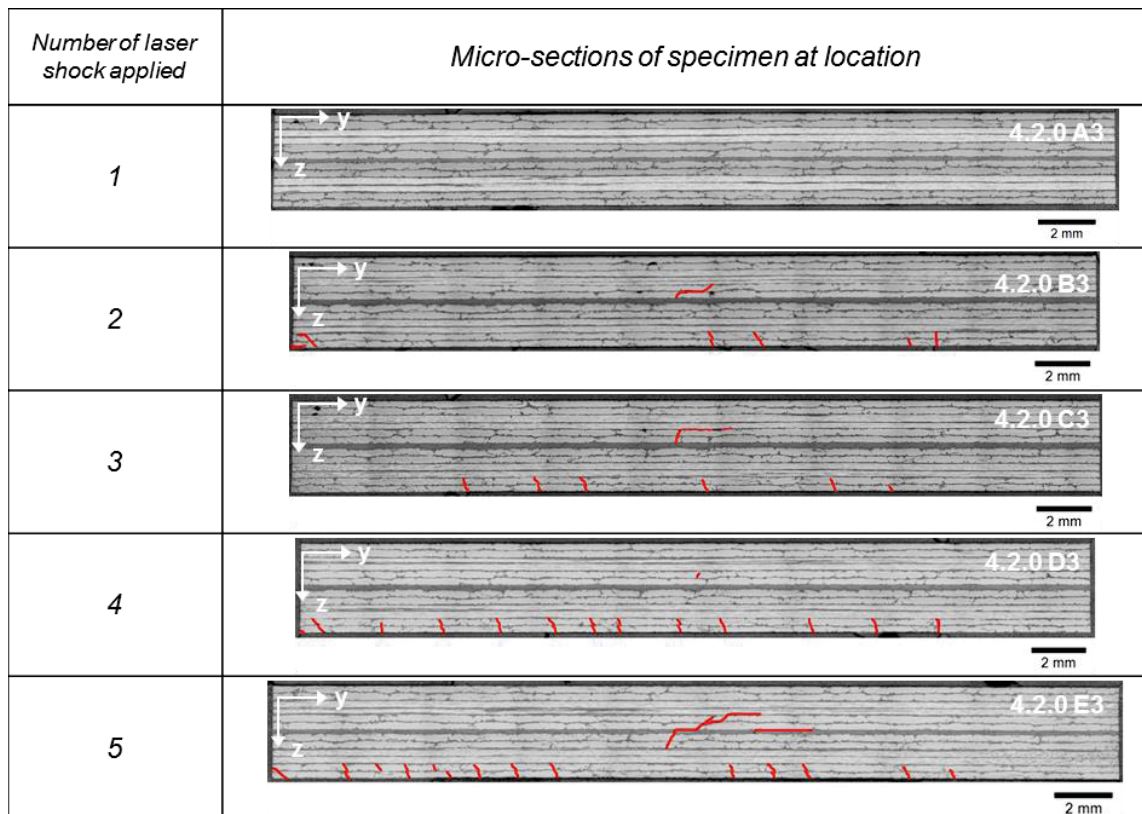
- The top line was shot with an intensity slightly above the threshold but within the uncertainty established in test A – laser 200 ns (104 %). The results confirm that all locations were damaged and most of them were confirmed with PAUT previous observations. With the repetition of laser shots, the size of the largest damage (few mm) does not significantly grow in opposition to the number of cracks. This characteristic seem to be valid only for shots whose intensity is above the threshold.
- For the laser shots with 89 % and 80 % (illustrated in Figure D.25) of threshold, an inconstant damage growth is observed with repeated shocks. Few repetitions can cause larger damages with debonds than more repetitions. As an example: for 89 %, with four repetitions, the largest crack is 6.2 mm long whereas with five repetitions, the longest crack is 4.1 mm long. Also for 80 %, two and three repetitions have induced respectively 1.5 and 1.2 mm, more than for three repetitions with 0.6 mm. The total number of cracks present is however increasing regularly and illustrate how repeated laser shocks lead to more cracks in the composite laminate.

- For the lowest two levels of intensities (72 % and 64 % of threshold), the results are not constant and do not show a clear trend. Several locations do not present any damage, even after five repeated laser shocks. However, the fact that few intralaminar cracks appear even at 64 % show that the bending effect may lead to little sporadic damages, probably linked to the material local quality. Their effect on the structure may be questioned, even though their detection with NDT technique would be challenging.

In general for laser 200 ns, below the threshold intensity, the more laser shocks are applied on the same location, the larger the damages. The same rule applies to the number of damages, especially the intralaminar cracks which are resulting from the laminate flexure. Below 72 % of the threshold, the damages observed are not following any particular trend. Few intralaminar cracks are likely to occur depending on the local material intralaminar cohesive strength what randomize the occurrence of little intralaminar cracks.



**Figure D.25: Evaluation of damage from repeated laser shocks with various intensities at same shot location. Experiments performed on a C reference state adhesive bond with laser 200 ns**



**Figure D.26: Micro-sections of specimens with repeated laser impacts at 80 % threshold intensity. Tests with laser 200 ns, observed with optical microscope.**

The same test B has been conducted with the laser 25 ns and are represented in Figure D.27 as in Figure D.25. Another reference C composite panel was used and impacted. The percentage of threshold value for the different series of repetition is lower in this case than for laser 200 ns. This is due to the fact that the threshold value intensity was corrected to a higher intensity after the UT and optical microscope observations.

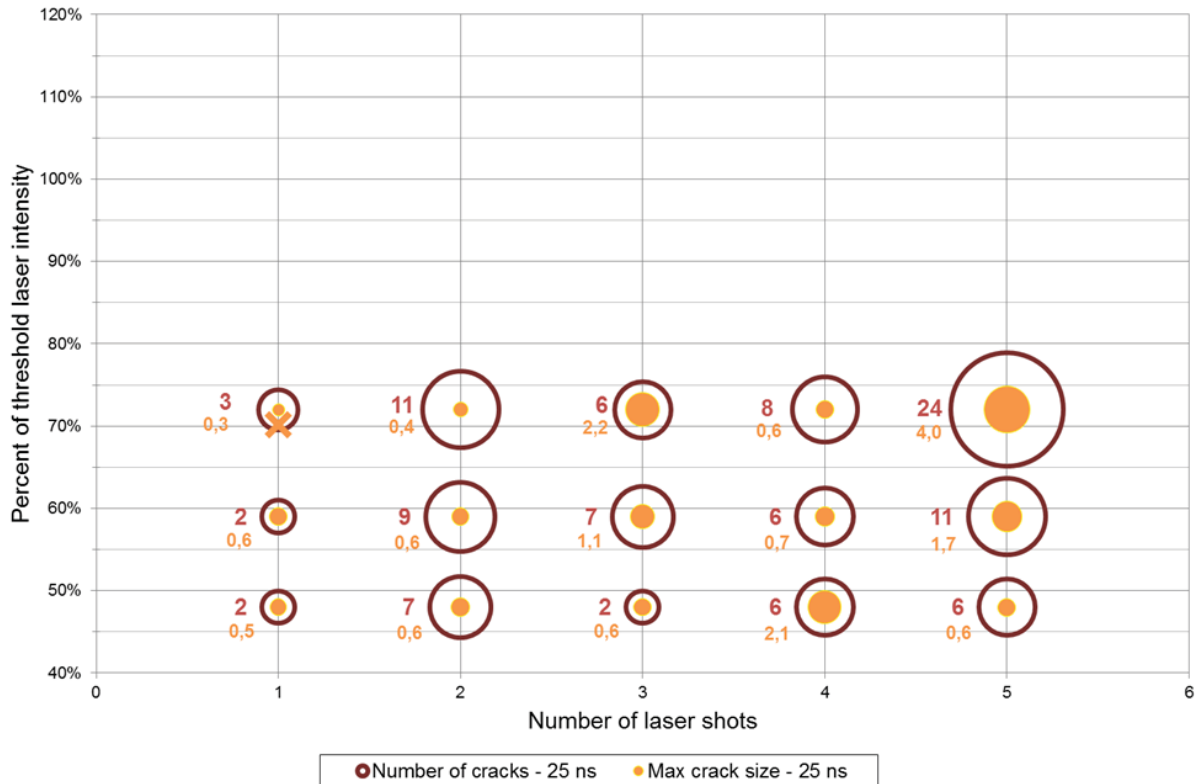
It can be noticed that no damage could be detected by PAUT inspection for laser 25 ns.

For all laser shots performed around 72 %, 59 % and 47 % of threshold intensity, the damages size and the damage number tend to increase with the amount of laser shot repetition and the intensity of the laser. All damages are relatively small with size around 2 mm max. except for the five impacts at 72 %. Despite the tendency, the maximum size of damages is not totally consistent with the amount of shot repetition and the material quality locally may play a role in the damage maximum size. It must be highlighted that the damages are still numerous even below 50 % of the reference threshold value.

The difference of laser beam intensity levels for each laser configuration is important. In comparison with the laser 200 ns where almost no damages were appearing below 72 %, the effect of laser 25 ns are noticeable. All the tests performed below the 72 % reveal an important number of damages in the structure.

The conclusion of this test is that the pulse duration is responsible for the inadequate tensile stress formation close to the back surface. This correspond to the theory of the shock wave propagation developed in Chapter 2. Additionally, it can be assumed that the smaller laser beam spot size and hence a higher intensity of the shock could increase the bending effects, provoking more intralaminar cracks. These observations illustrate again the parameter

optimization possible between both laser setups. In the present state, the laser 25 ns is not adapted to the geometry of specimen investigated.



**Figure D.27: Evaluation of damage from repeated laser shocks with various intensities at same shot location. Experience performed on a C reference state adhesive bond with laser 25 ns. No damage could be detected by PAUT inspection for laser 25 ns.**

#### 4.2.2 Effect of repeated laser shock on the microstructure

It is assumed that the CFRP material could have its microstructure changed by laser shocks. This assumption is justified by the high energy used and the resulting high strain generated in the material. Possible damages in the molecular network would increase the molecular mobility and result in the decrease of the glass transition temperature. Another possible effect could be a post-curing effect due to the local and very short temperature increase. This effect would lead then to increase of the glass temperature.

To verify those assumptions, the literature reports DSC tests conducted on the front faces and back faces of epoxy CFRP samples before (as reference) and after laser shocks. For both the front and the back face, no significant changes in the glass transition temperature could be measured on very high pressures and short pulse durations (few ns) [1]. The same test was performed for two different laser configurations to make sure that this effect was not depending on a particular laser parameter. A slight increase of  $T_g$  of about 5% was then stated for lower pressure levels and longer pulse durations (30 ns). This effect was however only visible on the back face and when spallation of the epoxy composite had occurred. An alternative test could have focused on DMA measurements for the determination of Young modulus, but this would have required the DMA to be performed at the exact location of a

laser shocks whereas these specimens have been investigated destructively for microscope observations. This test constitutes an option for further studies.

The level of compression being low in the shot regime applied, the origins of this  $T_g$  increase are not clear but may be attributed to an additional cure due to very short temperature increase locally as a consequence from the laser shots. Non-exhaustive parameters such as the pulse duration, strain regime and damage initiation should be considered playing a role in the  $T_g$  increase [1]. Additional tests should be performed to better understand this phenomenon. In general, the slight  $T_g$  increase has two effects: first, the laser shock leads to a local post-curing effect which increase the  $T_g$  of the epoxy CFRP and so, lead to better global cure of the substrate. Secondly, this effect should not be observed in the case where no spallation occur, which should never be the case in the frame of a bonded structure inspection and optimal laser shot setup. Indeed, the spallation occurs only when the tension loading is set in the composite thickness instead of the adhesive-substrate interface.

#### 4.2.3 Summary on damage generation after repeated shocks

Test B involved repeated laser shocks at different locations and with laser intensities lower than the threshold value. It has been performed to evaluate any potential damage generation due to the successive laser shots. Several minutes occur between two laser shocks at the same location, so that this test aims more at assessing the consequences of laser shocks over the same location over the adhesive bond lifetime, or also in the case where two laser shots should be applied close to each other is one decide to have a high density of shots to map the adhesive bond quality on the whole structure. At the same time, it allowed the investigation of the low intensity laser shots on the structure.

Both laser 25 ns and 200 ns were used for this test. The laser 25 ns was used with proportionally lower laser intensities compared to the laser 200 ns. The damages observed for laser 25 ns confirmed the systematic presence of intralaminar cracks and even delamination whereas almost no damage could be seen for intensities below 72 % for laser 200 ns. Ultrasonic inspection did however not detect the cracks present in the laser 25 ns, probably due to their low number conjugated with their small size and mainly their intralaminar orientation, parallel to the ultrasonic waves which are hence not reflected.

The general trend for all laser is the increasing damage size and damage number with laser shock intensity and repetition. Lower intensity than the debonding threshold generate damages as well and the technique of laser proof test cannot be considered a non-destructive technique above a certain laser intensity level and also, when the laser shocks are repeated on the same location.

The microstructure investigation reported in the literature indicates that for the “worst” case of the laser 25-30 ns (about 10 time higher intensities than laser 200 ns), glass transition measurements via DSC did only reveal slight increase (5 %) when the intensity was large enough to provoke spallation. In case without spallation, no changes in the glass transition was reported. The next test aims at evaluating if regular laser shots below the intensity threshold, as would happen in the case of an adhesive bond quality control, affect the mechanical performances of the adhesive bond.

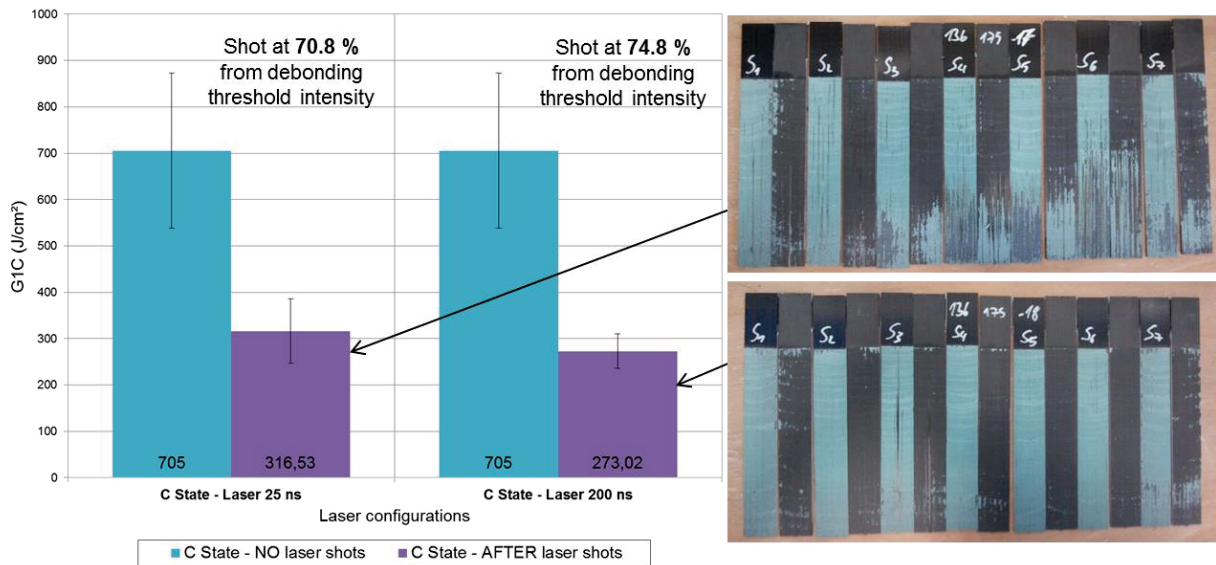
### 4.3 Effect of low intensity laser shots on adhesive bond mechanical performances

Test C is performed with fully cured C and reference adhesive bonds panels, with laser 25 ns and laser 200 ns. The panels are shot at all locations possible with the same laser intensity corresponding to 70.8 % of the threshold value for laser 25 ns and 74.8 % for laser 200 ns. These values are represented by the cross on Figure D.25 and Figure D.27.

The specimens were inspected in non-destructive way via PAUT before and after the laser shocks and did not reveal any damage at any shock location. No observation with optical microscope could be performed since the impacted locations were part of the mechanical test coupons. The specimens were hence cut out of the composite plate in their final form of  $G_{1C}$  test coupon with water jet. They were then tested mechanically in the same manner as the standard sets of  $G_{1C}$  coupons for the reference destructive test characterization. The outcome of the mechanical test is compared with the reference values obtained and are presented in Figure D.28.

The  $G_{1C}$  results from the impacted specimens are consistent for both laser setups. The error is of respectively 21.9 % and 13.4 % for laser 25 ns and 200 ns. The  $G_{1C}$  values obtained after impact are however much lower than for the specimen before impact. The  $G_{1C}$  values are reduced by more than half and the effect is similar for both laser setup, if we consider the error on the  $G_{1C}$  data. The uncertainty on the intensity generated by each laser source must also be considered: based on Eq. 1, the uncertainties reach 4.79 % for laser 200 ns and 13.26 % for laser 25 ns. The precision on the intensity levels from test C is thus significantly reduced. The observations must be made in consequence.

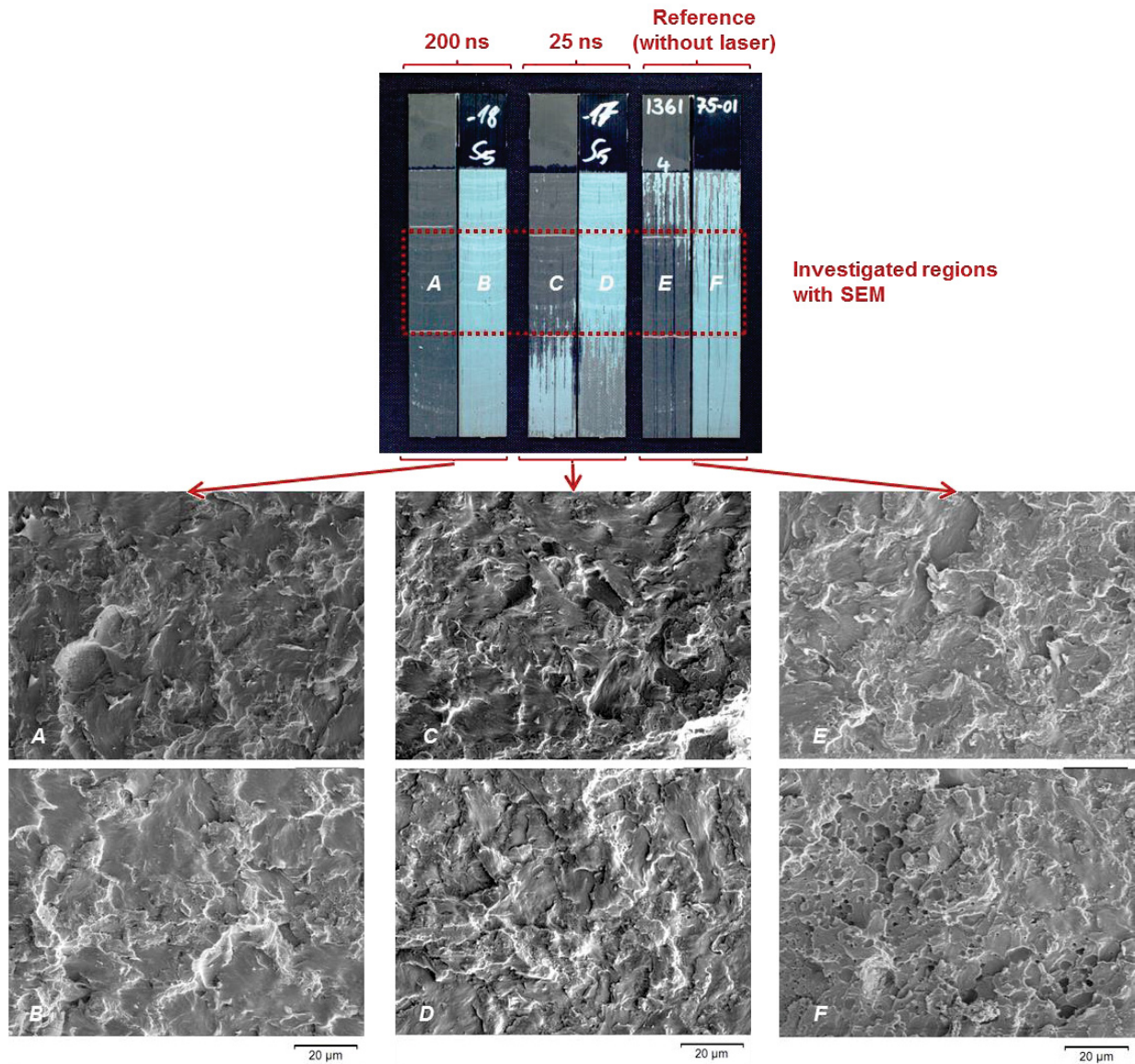
The observation of the failure profiles from the coupon reveal adhesive ruptures. This is particularly visible for the 200 ns, where the tensile stress is focused in the adhesive layer. Parts of the coupons 4, 5, 6 and 7 from laser 25 ns show small delamination and mix-modes, which can be responsible for the larger error on the  $G_{1C}$  data. It must be noted that no particular crack propagation or even sign of laser shot is noticeable on the failure profiles, neither on the adhesive side, nor on the adherent surface side. Figure D.25 and Figure D.27 however indicate that intralaminar cracks are susceptible to occur in the laminates in the domain of the chosen intensities (~70 %). The bending of the specimen under laser shot could be responsible for a diminution of the fracture toughness resistance. Despite the absence of detectable damage, the loss of fracture toughness resistance  $G_{1C}$  reveals that the specimen bending, intralaminar cracks previously observed in test B, or another effect at microstructural level could have been induced by the shock waves.



**Figure D.28: effect of simulated 'control' with laser shock around 70% of threshold intensity on the  $G_{1C}$  mechanical test performance. Test performed on C and PC families for laser 200 ns and laser 25 ns**

The surface of opened  $G_{1C}$  coupons have been investigated with scanning electronic microscope (SEM) to evaluate if the shock waves had any visible effect on the interphase adherent surface/adhesive bond. Regions from the failure profiles of the different specimens from each laser (represented by A to D) and the reference specimen (E and F) are displayed in Figure D.29. The reference specimen (right side) has not been impacted by laser shocks. The SEM images (magnification x1000) show the same patterns which are characteristic from an adhesive rupture as thought from the simple macroscopic observation. This observation also means that the potential effects from laser shocks on the  $G_{1C}$  performances is not explainable at this microscopic level. The responsibility of laser shocks on the  $G_{1C}$  performances can thus not be confirmed with the observations of the failure profiles. It may be assumed that the loss of  $G_{1C}$  strength is related to a presence of intralaminar micro-cracks, as highlighted previously.





**Figure D.29: SEM Observations of G<sub>1C</sub> failure profiles from reference unshocked coupon, laser 200 ns and laser 25 ns shocked coupons**

#### 4.3.1 Summary on low intensity shock effect on mechanical performances

Test C included laser shot of reference specimens, with a lower intensity (70 to 75%) than threshold. The specimens were impacted along the length of future G<sub>1C</sub> test coupons, four times every 30 mm. The inspection with PAUT did not reveal any difference before and after laser shocks.

The G<sub>1C</sub> performances are however severely affected by both laser setups (25 ns and 200 ns). The performances are reduced by more than half compared to a similar specimen without laser shock.

The intensities chosen are close to domain where intralaminar cracks can appear. Another effect of the shock waves on the adhesive bondline may have happened to reduce the  $G_{1C}$  data so significantly. Investigations were conducted on the coupons failure profiles to assess any microscopic effect but could not evidence a direct effect from laser shock on the microstructure of the adherent surfaces and their rupture profiles.

#### 4.4 Integrated time-resolved diagnostic tool for calibration of system

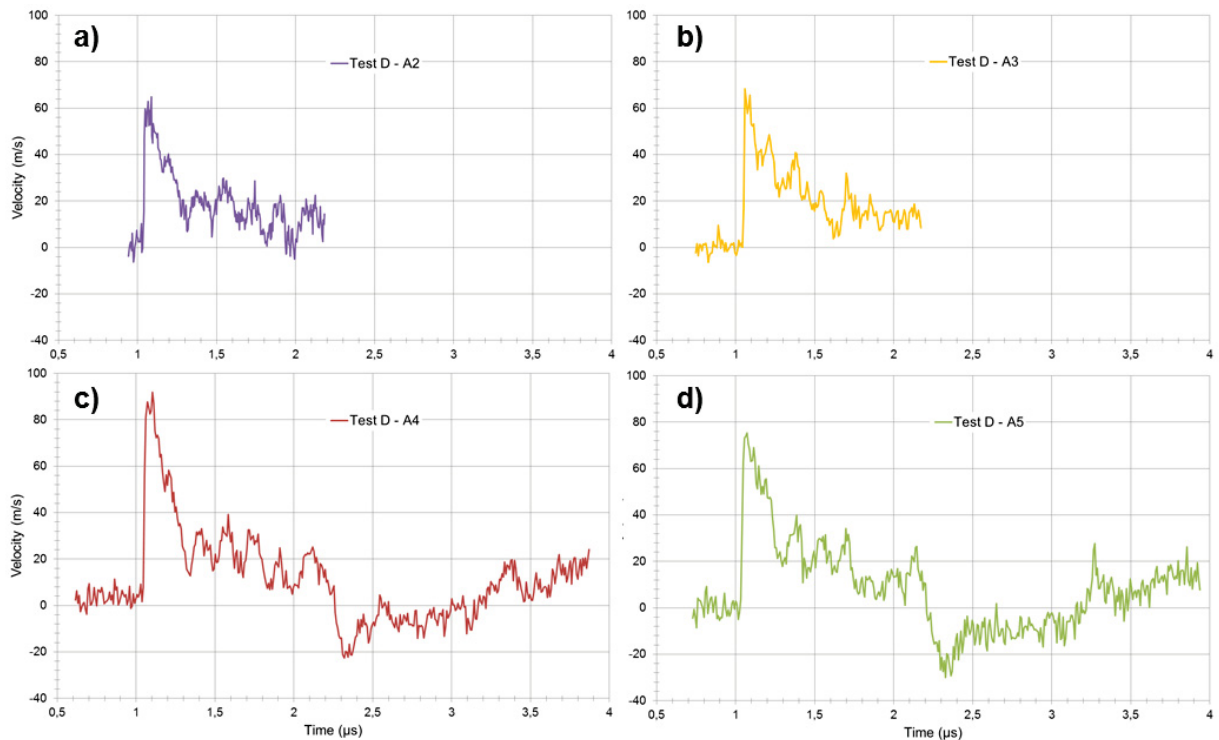
The final test corresponds to the evaluation of the integrated diagnosis tools for laser 200 ns and laser 25 ns. These are respectively the EMAT and the VISAR, previously presented in Chapter B part 3.3. Their use can yield information concerning the occurrence of a spallation in the structure. The quality of this information and its relevance for an industrial use is investigated in this test.

##### 4.4.1 Investigation of VISAR capabilities with laser 25 ns

The VISAR technique is applied in combination with the laser 25 ns. It measures the rear free surface velocity via the interferences in a second continuous laser beam signal. The surface velocity can directly be correlated to the shock wave induced events in the composite material.

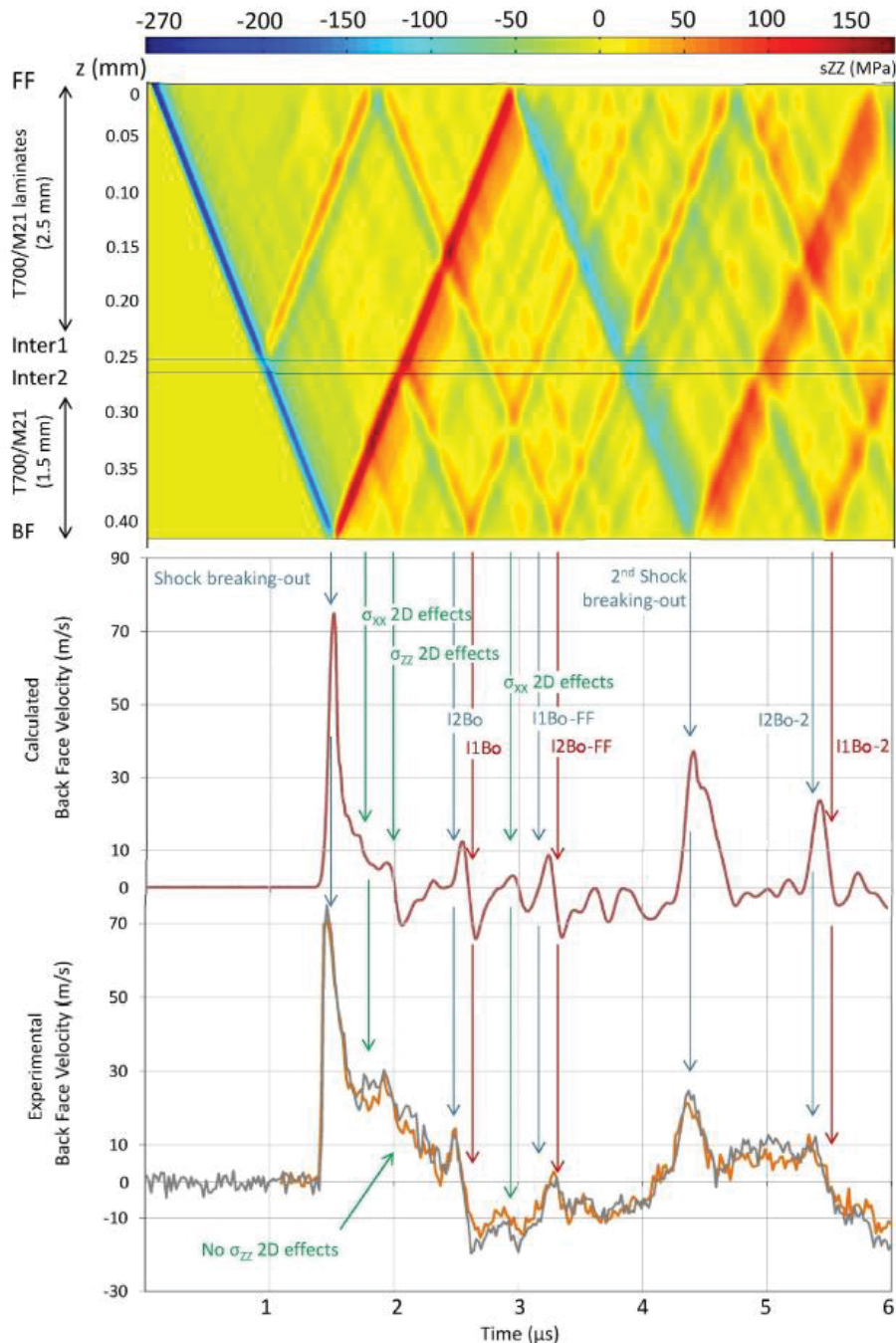
Attempts to capture the rear free surface velocity were performed on reference C specimen. The quality of the VISAR signals recorded on CFRP surfaces is however relatively low because of the poor reflectivity of carbon fibers composite. The effect can be reduced thanks to a metallic spray paint, in order to improve the reflectivity. Paint was thus applied to mottle the surface in a random way. The velocity signals from four shot at locations A2, A3, A4 and A5 can be observed in Figure D.30 respectively a), b), c) and d). The analysis of the signals induced in the VISAR by each laser reveal patterns common to all four locations presented in the graphs a, b, c and d. One can be introduced at first with the main first peak illustrating the arrival of the shock wave at the rear free surface. Further smaller peaks follow and are linked to physical effects of the shock waves reflection and propagation in the material thickness. The time (in  $\mu\text{s}$ ) allow a calculation to determine where the shock wave front is progressing. The differences in length of signal are however due to the poor quality of the recordings. They show how difficult the implementation of VISAR on the composite surface can be.

It must be noted that no location represented here featured any damage after PAUT inspection.



**Figure D.30: Rear free surface velocities measured experimentally with VISAR, on a reference C specimen, at different intensities and location (a, b, c, d) without spallation**

The recent work with VISAR and numerical modeling present in the literature has led to successful correlations between the surface velocity and the mechanical stresses [1], [10]. A fine presentation of the relation between the stresses and the VISAR measurements is reported in Figure D.31. In this case, a non-symmetrical (4 mm thick) composite system with resin M21 and T700 fibers is shocked with the laser 25 ns with a low intensity for which no spallation occur. The time/position diagram is generated by numerical model, validated experimentally by Ecault, and is compared to the simulated and experimental shock wave velocities. The arrows represent very well the origins of each peak in the surface velocity. A detailed description of the correlation is given.



**Figure D.31:** time/position diagram of a non-symmetrical reference specimen correlated with the experimental VISAR and numerical rear free surface velocity curves. Case without spallation [1].

At first, after the laser shot, the shock wave starts propagating in the composite bonded structure. It rapidly reaches a first front interface substrate/adhesive where a part of the shock wave is reflected due to the acoustic impedance mismatch of the composite and the adhesive layer at the interfaces 1 and 2 (resp. I1Bo-FF and I2Bo-FF). These first reflections are not visible on the back face velocity yet. The phenomenon starts when the shock wave breaks out with the large increase of the back face velocity. This phenomenon is followed by 2D anisotropic effects (see Chapter B part 2.3.4)  $\sigma_{xx}$  and later  $\sigma_{zz}$  and at the same time, the main shock wave is reflected back in the specimen [1].

On its way back to the front face, the shock wave encounters impedance mismatches at the interfaces 2 and 1 (resp. I2Bo and I1Bo) between the composite substrate and the adhesive

bond, which are high enough to generate the small bounce in the rear face velocity [1]. This little bounce is important enough to induces 2D anisotropic effects  $\sigma_{xx}$  again. The propagation of the shock wave continues and again, the shock wave is reflected at the front face. The first interface effect is then visible on the rear free surface velocity with peaks corresponding to I1Bo-FF and I2Bo-FF. The phenomena of reflection due to interfaces or free surfaces are repeated until the hydrodynamic and elasto-plastic attenuation (see chapter B part 2.3.4) reduce the stress levels to a too low level for detection. The optimal match of the peaks from the rear free surface velocity with the identified stresses accounted in the model is a confirmation of the model validity.

The representation of the shock wave propagation mechanism is done in the same way in the case of the location A5 (Figure D.30d). The same numerical model is used to evaluate the laser shot effects in the symmetrical case and correlate the rear face velocity. Figure D.32 represents hence the case of a symmetrical specimen with 3,2 mm thickness, with the result of the simulated back face velocity and the velocity measured with the VISAR. After the laser shot, the shock wave propagates in the composite bonded structure. A part of the shock wave is reflected at the first front interface substrate/adhesive due to the acoustic impedance mismatch at the interfaces 1 and 2. These reflections correspond to the reflections named I1Bo-FF and I2Bo-FF in the previous Figure D.31. They travel back to the front face of the specimen, where they will be again sent back, while the initial shock wave breaks out at the rear face of the specimen. This one is also reflected back in a release wave, which generates the tension (in red) in the composite. Little 2D assymetrical effects  $\sigma_{xx}$  and later  $\sigma_{zz}$  can be noticed in a region where several peaks appear in the measured rear face velocity.

The next large peak named “Inter Bo” is the effect of the symmetry of the specimen: the wave from the multiple reflections from the Ibo-FF and the reflection from the main release wave at the rear interface composite substrate/adhesive layer get mixed and travel back toward the rear free surface again. The phenomenon go on until the hydrodynamic and elasto-plastic attenuation totally annihilate the shock wave propagation.

The particular effect of the symmetrical specimen is that the main shock wave and its reflections due to the acoustic impedances changes in the bondline (at middle thickness) cross each other in opposite directions, in the adhesive bondline, and so, annihilates each others rapidly. An indication of this is the diffuse and low pressure and tension levels observed for the 2<sup>nd</sup> shock wave break-out and later peaks.

A final remark concerning the case of spallation: based on the phenomenon measured by VISAR and the numerical model, if a spallation occur, a new interface is created in the material. This spall disturbs the shock wave propagation and by extent, the rear face velocity. No measurements in such a case could however be performed in this study.

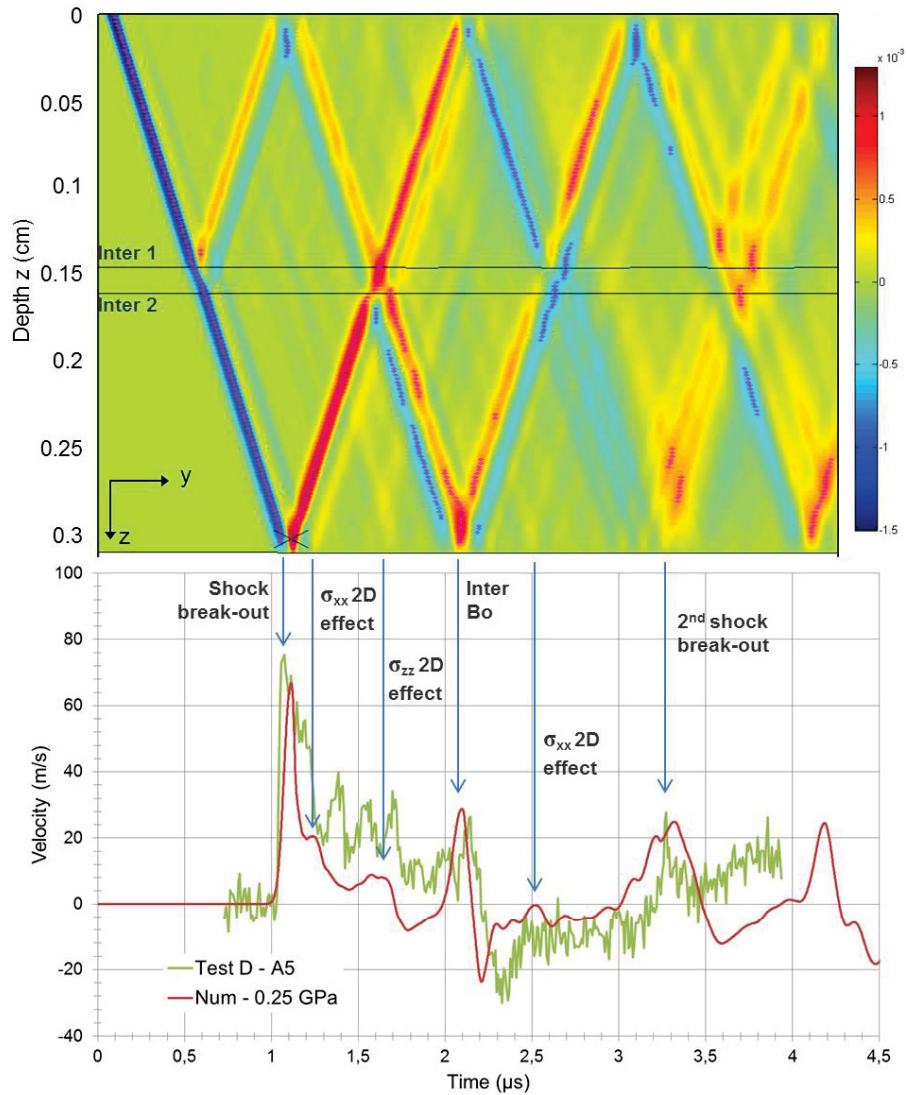


Figure D.32: time/position diagram of C reference symmetrical specimen correlated with the experimental VISAR and numerical rear free surface velocity curves. Case without spallation.

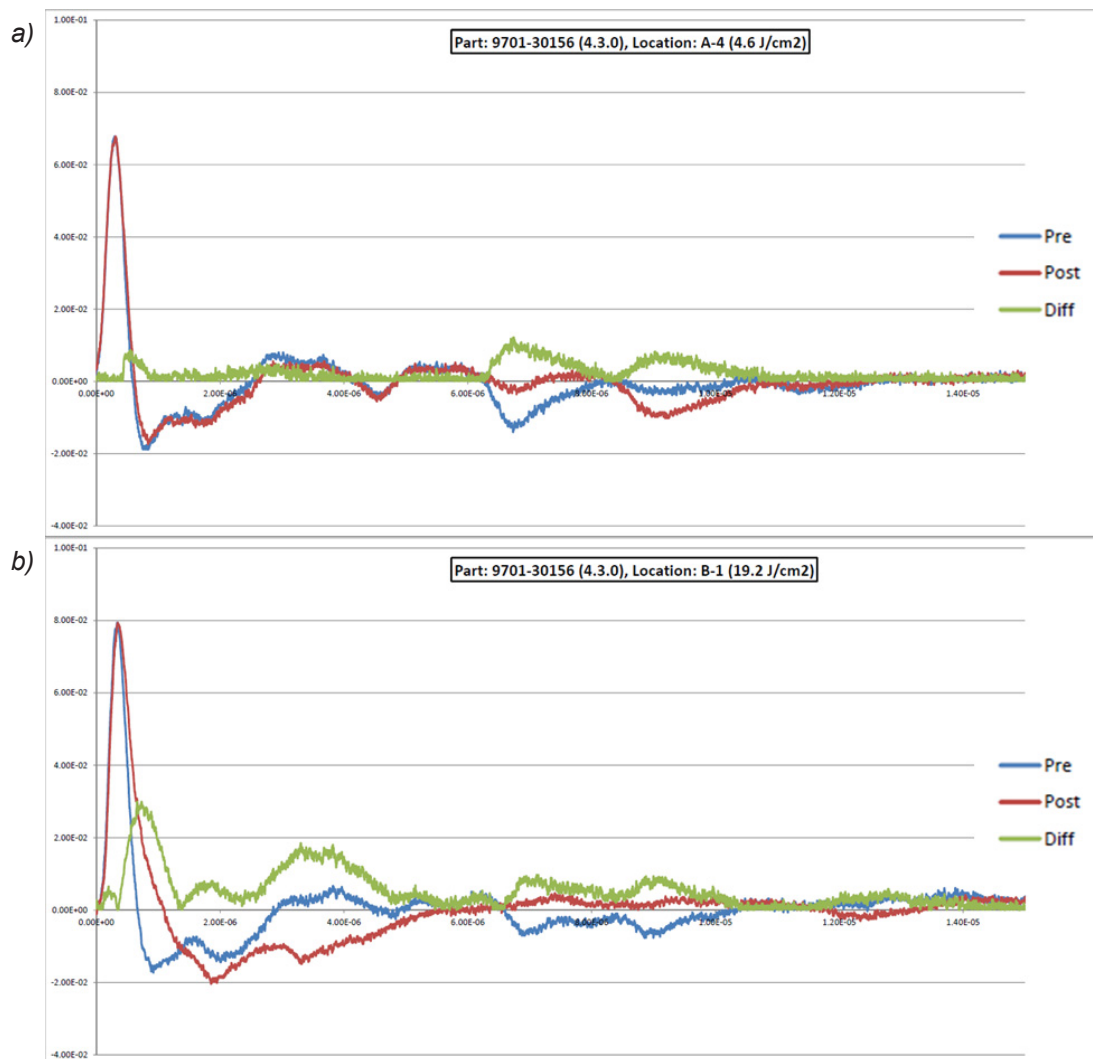
#### 4.4.2 Investigation of EMAT capabilities with laser 200 ns

The EMAT sensor is the diagnosis tool from the LBI, here named laser 200 ns. The approach for the evaluation of the shock effects with use of the EMAT is different from the one of the VISAR, though it is also based on rear or front face velocity. The mobile laser prototype with same properties as the laboratory setup was used since the EMAT is built in the probe head of the laser arm (Figure D.4). Measurements are hence done on the front face of the specimen, this is a first difference with the VISAR. To proceed, several laser shots have been applied on a reference cured C panel with use of the EMAT sensor.

The measurements are performed based on the so-called “Low-High-Low” method and is reported by Bossi et al. [11]. Instead of a direct measurement during the laser shock, a first low intensity probe pulse is emitted onto the surface. A shot with higher intensity (intensity of test) is then performed, and then again a second low one. The comparison of the surface velocities between the two low intensity pulses give an indication of a spallation in the target

thickness as illustrated in Figure D.33. The evaluation of a failed adhesive bond is only based on the difference of EMAT signals. No further information is or can be derived from the EMAT signals. This is mainly due to the absence of characterization from the adhesive tape sacrificial layer at the surface which is measured.

The position of this spallation in the bonded part is not given and this approach relies on a strong assumption that the adhesive bond interfaces with the substrates have the lowest fracture toughness limit load. In the case of composite assemblies, this means that the bondline would be debonded before any delamination in the plies occur.



**Figure D.33: EMAT signals representing the Low-High-Low shots method to diagnostic a failure generation in the tested material**

**a) No significant difference (green) = No failure occurred (0,022 GW/cm<sup>2</sup>)**

**b) Significant difference (green) = failure occurred due to higher intensity (0,096 GW/cm<sup>2</sup>)**

## 5. SUMMARY

In this chapter, the experimental setups, methods of investigation and final results of laser tests are presented. Two laser setups offering different conditions, laser 25 ns “LASAT” and laser 200 ns “LBI”, have been investigated with the same composite bonded specimens to enable a comparison of the results. All specimens have been characterized by ultrasonic inspection before and after laser proof test. This has enabled a damage detection and their objective size determination. The most relevant shot locations were further cut-out from the composite plates and micro-sections in the middle of a laser shock were observed with optical microscope. This final observations allowed the precise count of the damage, as well as the measure of their size.

Four tests have been designed to assess the effect on both lasers on the bonded composite:

- The first test aims at the determination of intensity thresholds for each adhesive bond state (one reference state and four contamination grades) and for three states of specimens: fully cured C as standard, partially cured PC and, moisture saturated MOC. Fully Cured specimens revealed different threshold levels decreasing with decreasing adhesion quality. A magnitude ten between the intensities required by both laser is due to the laser pulse duration and laser beam spot size. For laser 25 ns, the occurrence of delamination in the rear laminate together with debonding highlighted the importance of the long pulse duration. Further tests were hence only performed with laser 200 ns. They revealed that the partially cured PC specimens were damaged in the rear laminate for a relative low intensity value. Debonds were only observed when the contamination effects dominate the intralaminar cohesive strength of the rear face laminate.

The moisture contaminated MOC specimens requested higher threshold values than for specimens without moisture, but showed at the same time larger damages in low contaminated states. An effect of swelling and plasticization could be responsible for the higher shock wave tolerance and simultaneously an adhesive bond weakening.

- The second test aims at evaluating if repeated laser shots below the threshold intensity could damage the composite structure. The laser shot were applied from 1 to 5 times on the same location, with several intensities from 105 % to about 50 % of the threshold values.

In the case of the laser 200 ns, a general tendency of damage size and number increase with the threshold and with the repetition rate is visible. Above threshold the damage size stay the same, illustrating that the shock wave cannot travel further in the material and extend the size of the damage once created. Little intralaminar cracks occurred even with the lowest intensity levels on one single laser shot.

For laser 25 ns, lower intensity levels than for laser 200 ns were tested. The same general remarks stay valid, however with the observation of even larger damage size in the structure, probably to be related to the inadapted tensile stress concentration in the specimen thickness.

Focusing on the modification of the microstructure of the composite matrix, the literature reports that the glass transition temperature after laser impact is not significantly modified. This test was however performed with even lower intensity levels that the ones investigated.



- A third test aims at evaluating whether laser shots applied below threshold would affect the mechanical performance, here represented by double cantilever beam test  $G_{1C}$ . No damage could be detected after the laser shocks, what was expected for the intensity level chosen (approx. 70 % of threshold). The  $G_{1C}$  values for laser 25 ns and 200 ns were reduced by half compared to an impact-free specimen. This result indicates that the laser proof test methods may have weakened the adhesive bond at a microstructural level, which is not detectable by current means of NDT inspection. SEM investigations did not reveal any additional information regarding the failure profile patterns. No differences are visible between a shocked specimen and a reference (without shock) specimen in our case.
- Finally, the fourth and last test focuses on the integrated time-resolved diagnosis tools, the EMAT probe and the VISAR system, in order to assess any damage in the composite structure. For laser 25 ns, the VISAR system was investigated. Its setup was complex due to the low reflectivity of the black CFRP surface but enough signal could be detected for analysis. The signals reveal the detection of shock waves arriving at the rear free surface and even other waves phenomenon, such as 2D effects and plies interferences. The quality of the signals could however not deliver precise information about the tested structure after impact. The locations impacted did not present any damage after PAUT inspection, what highlighted the challenge in the data acquisition on row CFRP surfaces and its interpretation. An extract of the signal correlation to the model from Ecault illustrates however the potential of VISAR for fine phenomenon at the rear free surface.  
In the case of laser 200 ns, the prototype of laser used includes the EMAT sensor. The approach relies on a low-high-low method, which only compares two 'signature' free surface velocity signals before and after the effective laser shock. The signal difference is used as an indicator of damage in the structure, however without any further precise indication of type or depth of damage. This technique is only qualitative and not properly time-resolved. Both use of EMAT and VISAR are discussed further in the following chapter.

These four major tests have brought relevant answers in the assessment of the non-destructive character of the laser proof test methods. The challenges and the potential for their use as a quality inspection technique for adhesive bonded structure must be discussed. The next and final chapter reviews these and introduces ways of improvement for an industrial use.

## REFERENCES – CHAPTER D

- [1] R. Ecault, „Experimental and numerical investigations on the dynamic behaviour of aeronautic composites under laser shock - Optimization of a shock wave adhesion test for bonded composites“, E.N.S.M.A. - Sciences et Ingénierie en Matériaux, Mécanique, Energétique et Aéronautique, Poitiers, PhD, 2013.
- [2] R. Bossi, K. Housen, W. Shepherd, und M. Voss, „Bond Strength Measurement System Using Shock Loads“, US 2003/0079552 A1, 01-Mai-2003.
- [3] D. W. Sokol, C. T. Walters, J. L. Dulaney, und S. M. Toller, „Laser System and Method for Non-destructive Bond Detection and Evaluation“, US 2005/0120803 A1, 09-Juni-2005.
- [4] LSP Technologies Inc., „Laser Bond Inspection.“ LSP Technologies, Inc., 2011.
- [5] S. Barut, V. Bissauge, G. Ithurralde, und W. Claasens, „Computer-aided analysis of ultrasound data to speed-up the release of aerospace CFRP components“, gehalten auf der 18th World Conference on Nondestructive Testing, Durban, South Africa, 2012.
- [6] Olympus, *Stream Image Analysis Software*. Olympus.
- [7] W. W. Wright, „The effect of diffusion of water into epoxy resins and their carbon-fibre reinforced composites“, *Composites*, Bd. 12, Nr. 3, S. 201–205, Juli 1981.
- [8] W. M. Banks, F. Dumolin, S. T. Halliday, D. Hayward, Z.-C. Li, und R. A. Pethrick, „Dielectric and mechanical assessment of water ingress into carbon fibre composite materials“, *Computers & Structures*, Bd. 76, Nr. 1–3, S. 43–55, Juin 2000.
- [9] B. M. Parker, „Some effects of moisture on adhesive-bonded CFRP-CFRP joints“, *Composite Structures*, Bd. 6, Nr. 1–3, S. 123–139, 1986.
- [10] R. Ecault, M. Boustie, L. Berthe, F. Touchard, H. Voillaume, B. Campagne, und D. Loison, „Development of a laser shock wave adhesion test for the detection of weak composite bonds“, gehalten auf der NDT in Aerospace, Singapore, 2013.
- [11] R. Bossi, K. Housen, C. Walters, und D. Sokol, „Laser bond testing“, *Materials Evaluation*, Bd. Vol. 67, Nr. 7, S. 819–827, 2009.

# CHAPTER E: REVIEW OF ACHIEVEMENTS AND LEADS TO A NON-DESTRUCTIVE ADHESION QUALITY TEST

## TABLE OF CONTENTS

1. INTRODUCTION .....	158
2. LESSONS LEARNED .....	158
2.1 Manufacturing of weak adhesive bond .....	158
2.2 Intensity threshold for debonding in different bonded composite specimens .....	159
2.3 Effects from repeated occurrences of laser shot at same location .....	160
2.4 Effects of laser shock on the mechanical performances in mode I.....	161
2.5 Evaluation of the associated time-resolved diagnosis techniques capabilities .....	162
3. POTENTIAL FOR LASER PROOF TEST IMPROVEMENTS .....	163
3.1 Leads to laser sources improvements .....	164
3.1.1 Tunable laser shock parameters .....	164
3.1.2 Repeated laser shock.....	165
3.1.3 Symmetrical laser shock .....	166
3.2 Leads to an advanced diagnosis tool .....	167
4. REQUIREMENTS AND APPROACH FOR IMPLEMENTATION OF LASER PROOF TESTS .....	170
4.1 Requirements for the laser proof test implementation in production .....	170
4.2 Approach for the use of Laser Proof Test.....	171
5. SUMMARY .....	174
REFERENCES – CHAPTER E.....	176

## 1. INTRODUCTION

Chapter E reviews the state-of-the-technology of the laser proof test based on the different configuration investigated within this study. It discusses the results obtained in term of damages in the material in the previous chapter D. The present chapter also discusses in what extent the scientific objectives specified at the beginning of the study have been reached. These objectives can be summarized as follow:

- manufacture a proper weak adhesive bond with a precise adhesion performance by influencing some precise parameters.
- measure the adhesion performance in a non-destructive way or evaluate the potential damages induced in the structure if the adhesive bond has an optimal quality.
- evaluate which parameters are essential and should be optimized to match the bondline quality inspection method.
- investigate the effect of the high energy and the pressure released by the laser proof technique in a sound adhesive bond or in the substrate.
- investigate the effect of an inadequate setup of the laser proof technique.
- evaluate the diagnosis tool possibilities for the assessment of a safe adhesive bond after or during the laser proof test.

The requirements for an implementation as a non-destructive testing method within a quality assessment process chain for adhesive bonding processes are specified. This final chapter concludes with a discussion on the potential of improvement in term of laser configurations.

## 2. LESSONS LEARNED

The tests performed in this study have highlighted several characteristics of the laser proof test approach. This study relies on the investigation of two very different laser setups despite their common physical principle for the adhesion quality assessment. The preparation of specimens with weak adhesive bond was the first mandatory step. Afterwards, four major tests aiming at reaching the scientific objectives have been conducted.

This section does not recall the tests principles or the results developed in the previous chapter. Instead, it focuses on the key information learned through these results.

### 2.1 Manufacturing of weak adhesive bond

The first objective in this work consisted in the production of weak adhesive bonds. A range of adhesive bond levels are a pre-requisite in order to assess a technology aiming at verifying the level of adhesion mechanical performance. In this study, the process involved the production of CFRP monolithic plates, pre-treatment by sanding, cleaning, contamination of surface substrate and co-bonding operations.

The adhesion quality of the specimens was conditioned by the substrate surface contamination before co-bonding. A reference state was produced according to normal manufacturing standards and without use of any contaminant. Four different grades were prepared with silicon based release agent applied at the substrate surface. The application of release agent was conducted by dip-coating. X-Ray photon spectroscopy enabled the local control of the surface chemical composition after contamination to verify the homogeneity, which was satisfying despite a large scatter (standard deviation of 30 % in average)

All these steps led to the so called “fully cured (C)” also meaning here ‘standard’ set of 5 specimens, each with another level of adhesion. After bonding, the specimens passed the control via X-Ray and ultrasonic inspection to verify the absence of any physical defects and the compliance to manufacturing standards. A destructive mechanical test, the double cantilever beam test, enabled the determination of the adhesion performances generated:  $G_{1C}$  values start around  $700 \text{ J/cm}^2$  for contamination below 1 Si at.% (in mixed mode) and decrease rapidly down to the worst case of  $50 \text{ J/cm}^2$  with adhesive failure profiles when the silicon content overcomes 3.5 Si at.%. Such results correspond to the weak adhesive bond ranges required for investigations with laser proof test techniques.

Additionally to the standard set, another set of specimens was prepared by partial cure (PC) during the co-bonding process. This complementary set aimed at reaching poor intralaminar cohesion strength properties of the composite substrate in comparison to the adhesive bond properties. The double cracks generation in both the adhesive and the substrate co-bonded during DCB tests confirmed the low cohesive strength performances of the assembly but prevented the determination of  $G_{1C}$  values due to the record of two crack propagations simultaneously.

A third and last set of specimens was based on a fully cured set exposed later to moisture until complete saturation (MOC). This set of specimens represents an aged composite material in the case of an adhesive bonded repair on a structure already in service. Moisture saturation on a set of specimen led to low  $G_{1C}$  values and more adhesive failures.

In all cases, the criteria for weak adhesive bonds (absence of defect detected via NDT, 20% or more reduction of nominal mechanical performances, adhesive failure) could be verified for the three highest levels of contamination. This validates the process used for the preparation of weak adhesive bonds.

## 2.2 Intensity threshold for debonding in different bonded composite specimens

The determination of intensity thresholds depending on the quality of the adhesive bond focuses on the second scientific objective: to measure the adhesion strength and evaluate the potential damages. The three sets of specimens were tested: fully cured C, partially cured PC and moisture saturated MOC.

Starting with general remarks: for the two laser setups tested, a factor of 10 was observed between the two intensities to generate the same effects in the composite structure. This can be explained by the differences in the pulse duration (25 ns vs. 200 ns) but also by the laser beam spot size on the surface with respectively 4 mm vs. 10 mm diameter. This factor of 10 is linked to the time of application (pulse duration) at the material surface and the energy concentration on the surface (beam spot size). Both are key parameters towards the assessment of adhesive bond quality. This observations validates the theory and roles of these parameters developed in chapter B. Also, the ratio laser beam spot size/thickness of the adhesive bonded structure is as important as the laser pulse duration: phenomena like the 2D effects of the shock waves or waves crossing at inadequate depth in the laminate (see chapter B) influence the proper inspection of the adhesive bond interface with the substrate.

Concerning the “fully cured” C specimens and potential damages in the laminates: the delaminations in the rear plies observed for example in the case of the 4 mm spot size and 25 ns are a confirmation that the laser parameters are not optimal for this structure. This effect is discussed further on in the next section 2.3. On the whole, the results of the standard state were according to the expectations, the intensity for debonding was decreasing with the decreasing adhesive bond strength due to surface contamination. Above state 2 (1.3 at.% Si), the failure profiles of mechanic tests showed an adhesive failure profile due to the important contamination. This feature could also be observed in the low  $G_{1C}$  values.

Among the other sets, the moisture contaminated MOC specimens requested higher threshold values than for specimens without moisture, but showed at the same time larger damages in low contaminated states. An effect of swelling and plasticization of the substrate epoxy composite could be responsible for the higher shock wave tenacity and simultaneously an adhesive bond weakening.

The partially cured PC specimens were damaged in the rear laminate for a relative low intensity value. The threshold was stable at 0,022 GW/cm<sup>2</sup> while delaminations occurred in the partially cured layer for all laser impacts above this threshold. This observation confirms that the intralaminar cohesive strength is weaker than the adhesive strength in the case of the low contamination levels. Debonds only occurred at the contaminated interface when the contamination effects reduces the adhesive bond strength below the intralaminar cohesive strength. More precisely, with a cure rate of  $55 \pm 8 \%$ , the debond occurs for specimens of level 3 and 4. The intralaminar cohesive strength can be assumed equal or higher than the adhesive strength at the contaminated interface for level 2 and levels below for which the contamination has not been so relevant.

In the present experimental case for which the lasers are not optimized for the inspected structure, these results confirm that the ratio adhesive bond strength over substrate intralaminar cohesive strength is determining. It also highlight the capability of assessment of cure degree of a laminate through laser shock tests. This application was not the aim of this study but the results have shown that the intralaminar cohesive strength can be investigated.

In conclusion, laser thresholds intensities could be determined for debonding of all level of contaminations in the three families of specimens C, PC and MOC. The adhesion strength is not directly measurable but can be correlated if destructive mechanical data,  $G_{1C}$  for example, are available. The setup of both laser proof test techniques are however not optimized and generated damages in the substrates. Delaminations and other cracks must be avoided to make the laser proof test a non-destructive testing method.

Also, the application of laser proof test to other materials or geometries has not been conducted yet. Results shall hence be considered with care for the specific cases presented.

### 2.3 Effects from repeated occurrences of laser shot at same location

Both laser 200 ns and 25 ns were used for repeated laser shocks at the same location on a reference uncontaminated fully cured specimen. This test aims at evaluating the effects of energy release and local repeated pressure application in the composite substrate. The sacrificial layer and confinement layer were applied between two laser shocks. The frequency of the laser shocks was not relevant since the specimen surface had to be prepared again and

again for each laser shock. The intensity of the laser beam was set to different levels from the reference threshold intensity down to about 50 % of the threshold value.

Observations of impacts revealed a general trend of increasing damage (delaminations and intralaminar transversal cracks) size and number with increasing laser shock intensity and repetitions. Beyond this outcome, it is the level of intensity for which these damages still occur that must be noticed: for respectively the laser 200 ns and 25 ns, down to 64 % and 47 % of the reference debonding threshold intensity level. At these intensity levels, no delamination between plies is observed and very few transversal cracks occur in the substrate layer. The number of transversal cracks generated is not depending on the repetition of laser shock anymore. It can be assumed that the transversal cracks may be also linked to local structural weaknesses.

This difference of intensity levels between both lasers can be linked to the intrinsic laser own characteristics. Indeed, the pulse duration and laser beam spot size play a decisive role in the shock wave propagation as seen in section 2.2. However, due to the same characteristics, the uncertainty for all compared data raise to 13.2 % for laser 25 ns and 4.8 % for laser 200 ns. A precise range of intensity level can hardly be derived from the results due to this large uncertainty. The presence of the random number of transversal cracks, even at half the intensity level from the reference debonding threshold intensity may be considered a major obstacle. However, the optimization of the laser parameters shall improve the efficiency of the shock wave and prevent from a too large stress in the substrate layers. The effect of transversal cracks on the mechanical performances is discussed further in the next section.

## 2.4 Effects of laser shock on the mechanical performances in mode I

This test aimed at assessing the adhesive bond mechanical performances after laser shock. For this purpose, the level of intensity chosen for both lasers 25 ns and 200 ns was set below the debonding threshold intensity to simulate a potential inspection in a manufacturing quality control process. For each laser setup, a standard C panel was impacted with one laser shock at 28 locations regularly placed over the panel. The panel was kept as a single piece to better approach a large structure behavior during laser shot. After verification by UT inspection that no defect had been induced, 7 coupons for double cantilever beam tests ( $G_{1C}$ ) were cut with water jet to avoid micro-stresses of any other mechanical saw. The intensity selected turned to be around 70.8 % from the debonding threshold for laser 25 ns vs. 74.8% from debonding threshold for laser 200 ns. A value of 70 % was approximatively targeted and the real values could only be determined precisely after all characterizations yielding the debonding threshold intensity itself. This explains the little difference between both levels.

In general, the results obtained from the DCB test on impacted coupons indicate more than 50 % loss of mechanical fracture toughness in mode I. The investigation of microstructures in the frame of repeated shots at the same location however revealed that at 70 % from the threshold intensity, transversal micro-cracks may occur in the external plies. Micro-cracks in the coupons cannot be totally excluded even if no defect could be detected after the laser shocks. Due to their size below the mm range, the micro-cracks cannot be detected by UT inspections. Table E.1 gives the uncertainties and errors to appraise the  $G_{1C}$  results relevance.

**Table E.1: Summary of intensity levels and their uncertainty for repeated laser shock test**

	<b>Laser 25 ns</b>	<b>Laser 200 ns</b>
<b>Intensity level (% of reference debonding threshold)</b>	70.8	74.8
<b>Error in repeatability of the laser shock (%)</b>	6	6
<b>Uncertainty in intensity determination (%)</b>	13.2	4.8
<b>Intensity level approx. (%)</b>	<b>70.8 ± 19.2</b>	<b>74.8 ± 10.8</b>

It appears that the errors and uncertainties from the intensity determination are too high to be negligible. With respectively 20 % or 11 % added to the 70.8 % or 74 %, the assumed intensity applied may be too close to debonding threshold intensity. It cannot be ensured that the  $G_{1C}$  performances obtained are not related to any laser shot with much higher intensity. As a confirmation, the repeated impacts at the same location (section 2.3) had revealed important damages for intensity levels higher than 80 %. In the present case, the  $G_{1C}$  coupons were also investigated by SEM but did not reveal any remarkable feature at the substrate/adhesive interface that failed.

In conclusion, it was possible to observe a significant decrease of mechanical strength from the adhesive bond after laser shock. The level of about 70 % of the debonding threshold intensity is not satisfying for any adhesion quality assessment with the actual laser configurations because the uncertainties remain too high. In the future, this test must be conducted again with adapted laser systems and probably lower levels of intensity (if reachable). The optimized laser setup shall lead to more precise intensities and hence, to  $G_{1C}$  performances close to the ones from specimens without laser shocks.

## 2.5 Evaluation of the associated time-resolved diagnosis techniques capabilities

To complete the experimental assessment of the laser systems, two methods of time-resolved diagnosis were investigated within this study. Both of them were each propriety of the associated scientific partner owning its laser source:

- An EMAT for front/rear face velocity measurement with laser 200 ns, and
- A VISAR for rear face velocity with laser 25 ns.

Laser shock were applied on a reference uncontaminated panel around the threshold intensity level. This allowed similar tests than described in section 2.2 with use of the time-resolved diagnostics, knowing what intensity shall generate a debonding and by consequence, provoke a change in the diagnosis technique signal.

The setup of both techniques was not easy and requested care and time. The composite substrate is mainly responsible: the black surface of non-painted composite is neither reflecting in the case of the VISAR nor is the composite conductive enough for the EMAT requirements. Specific preparation such as aluminum painting for the rear face of specimen (VISAR) or metallic adhesive tapes for electromagnetic signals were required (EMAT). These obstacles are hurdles against a generalized use of these time resolved techniques.



The successful measurements could be used for correlation of results. In particular for the VISAR signal which is more precise, the correlation to simulated shock wave positions in over time and space can be used for learning processes. The data, when its acquisition is successful, can be used to understand what occurs in the material thickness during the adhesive bond quality assessment. The efforts demanded to setup and analyze such signals is however too consequent to encourage its use in a serial quality control process. The level of information is, in such a case, not required.

On the other side, the EMAT technique was only used with a “low-high-low” approach requiring three laser shots for one measurement and the metallic adhesive tape to ensure an electromagnetic signal. The first “low” laser shock represents a shockwave “signature” travel in the structure, the “high” represents the real structural test and the last “low” is compared to the first one. The information obtained is only a qualitative indication of an event in the material thickness. No precise information regarding the depth, size or nature of the damage can be extracted from any difference of the two low intensity laser shock. The EMAT “low-high-low” method becomes interesting when the adhesive bond is weaker than the composite substrate.

It must also be noticed that both the VISAR and EMAT needed to be activated during the laser shot but could not (at the present stage of development) deliver any diagnostic right after the laser shock due to necessary post-processing of signals (VISAR). The low-high-low approach itself (EMAT) does not allow a diagnostic during the proofing laser shock (“high”) due to the very aim of this comparison test.

As a conclusion, both VISAR and EMAT could be used to assess the shock wave effects in the structures. Their implementation is costly in time and efforts. The level of information from both methods is not equal and none of them is adapted for a serial use in the case of an industrial quality assessment process. The VISAR however particularly showed its potential as a precise tool to calibrate the laser parameters. It can be helpful for an optimal shock wave generation. Investigation of other diagnosis tool methods could be of advantage.

### **3. POTENTIAL FOR LASER PROOF TEST IMPROVEMENTS**

The scientific objectives of this study have been reached but have also shown a way forward. Laser proof test techniques were evaluated successfully and have the potential to become an adhesive bond performance quality control method. Yet, both installations tested do not allow reaching a proper control of the adhesion bond quality without damaging the bonded substrates. The potential for improvement toward a technique able to focus on the adhesive layer-substrate interface is large. The diagnosis tool necessary to control the status of the adhesive bonded structure after laser shock must also progress. This section introduces concepts for improvements of the techniques.

### 3.1 Leads to laser sources improvements

In the current state of development shown by this study, the laser sources are not optimized for the application on materials of 3.2 mm thickness with an adhesive bondline at mid-thickness. The results in chapter D have shown that the composite substrate is damaged even when the adhesive bond interface stays intact.

Few concepts may be developed regarding alternatives in the principle of laser proof test. The approach are i. the tunable laser parameters with the current laser shock configurations, ii. the repeated laser shock and iii. the symmetrical laser shock. If the first approach seems natural, the other concepts are more sophisticated. The validity of the concepts has been verified via simulation in the frame of Ecault's PhD thesis [1].

#### 3.1.1 Tunable laser shock parameters

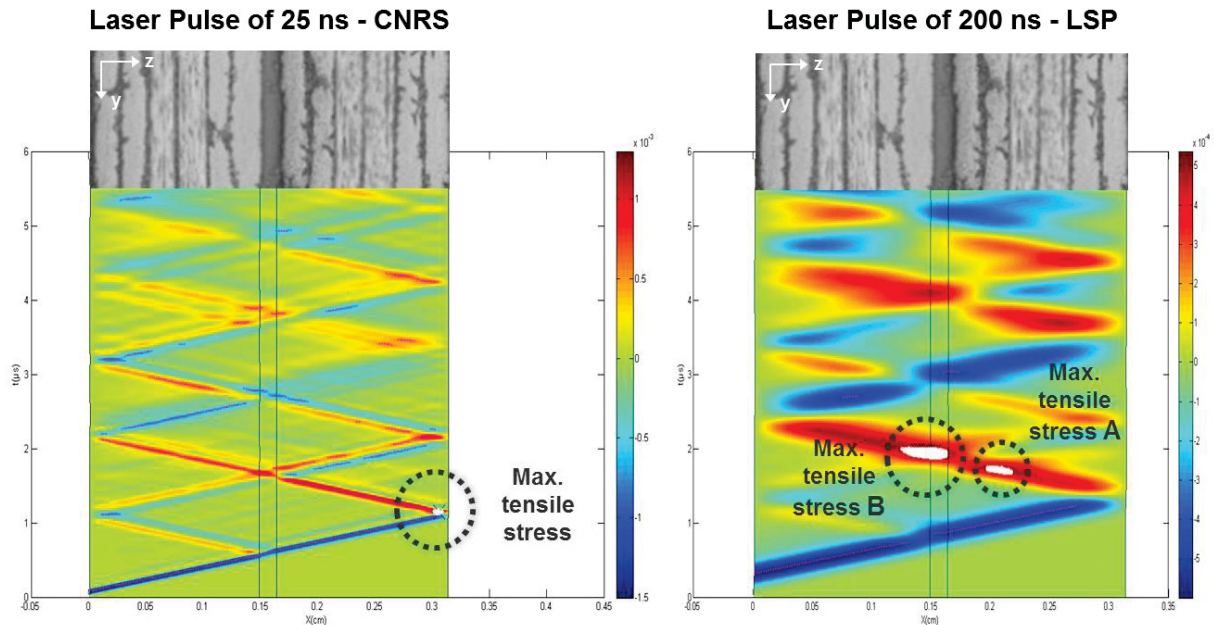
Among the parameters of the lasers, the only one used in this study was the laser beam intensity. The other parameters are intrinsic properties of the laser construction and can hardly be changed. According to the theory developed in chapter B, an adjustment of the laser pulse duration and/or the laser beam spot size (by extent, the focus of the laser beam) could however be an ideal solution.

On one hand, the laser beam spot size: investigations on unidirectional composite M21/T800 and bonded M21/T700 highlight the influence of 2D effects [1]. Below 2 mm in diameter, the 2D effects are so high that they significantly reduce the tensile stresses  $\sigma_{zz}$ . Above 3 mm diameter, the tensile stresses  $\sigma_{zz}$  have reached their maximum. The 2D effects are however influenced by the impedance mismatch occurring at the adhesive layer-substrate interface, and by extension, influenced by the structure geometry. In specific case, a late stress concentration may be induced inside the substrate [1]. This phenomenon must be prevented to avoid damaging the substrate.

On the other hand, the laser pulse duration offer more possibilities. Depending on its length, the maximal tensile stress can be focused more or less deeper into the impacted structure. With the laser 25 ns in its actual configuration (4.5 mm laser beam spot diameter, confinement with water and metallic paint sacrificial layer), a simulation determined the adhesive bond strength required for a proper adhesive bond quality assessment [1]. It was shown that for an adhesive bond strength assumed to be at 40 % of the substrate intralaminar strength, the weak adhesive bond interface could be debonded [1]. This means that without any optimization of this laser, only adhesive bonds whose adhesion strength is equal or inferior to 40 % of the intralaminar cohesive strength can be tested. This result is illustrated in chapter D within the section 2 "Laser Proof Test Set-up". The illustration is recalled in Figure E.1 in this chapter to highlight the influence of the pulse duration on the maximal tensile stress  $\sigma_{zz}$  zones. The 25 ns pulse localizes the maximal tensile stress region (the highest 5% are represented in white) closer to the back face than the 200 ns pulse duration.

The 200 ns pulse configuration is better adapted to the tested geometry. The impedance mismatch at the first change substrate-adhesive layer reflects a part of the shock wave. This reflection is optimal as its next crossing with the main release wave creates the 5 % of maximal  $\sigma_{zz}$  tensile stresses (maximal stress area B). Area B is located at the right depth to

test the adhesive bond interface. It can also be observed that another smaller area of maximal  $\sigma_{zz}$  tensile stresses region is located distributed in the rear substrate (maximal stress area A). This last remark highlights another challenge: the tensile stresses are distributed within the substrate. They are likely to cause cracks as observed in this study. The pressure loading (directly linked to the beam intensity and interaction) must be precisely adapted to the structure to avoid any damage.

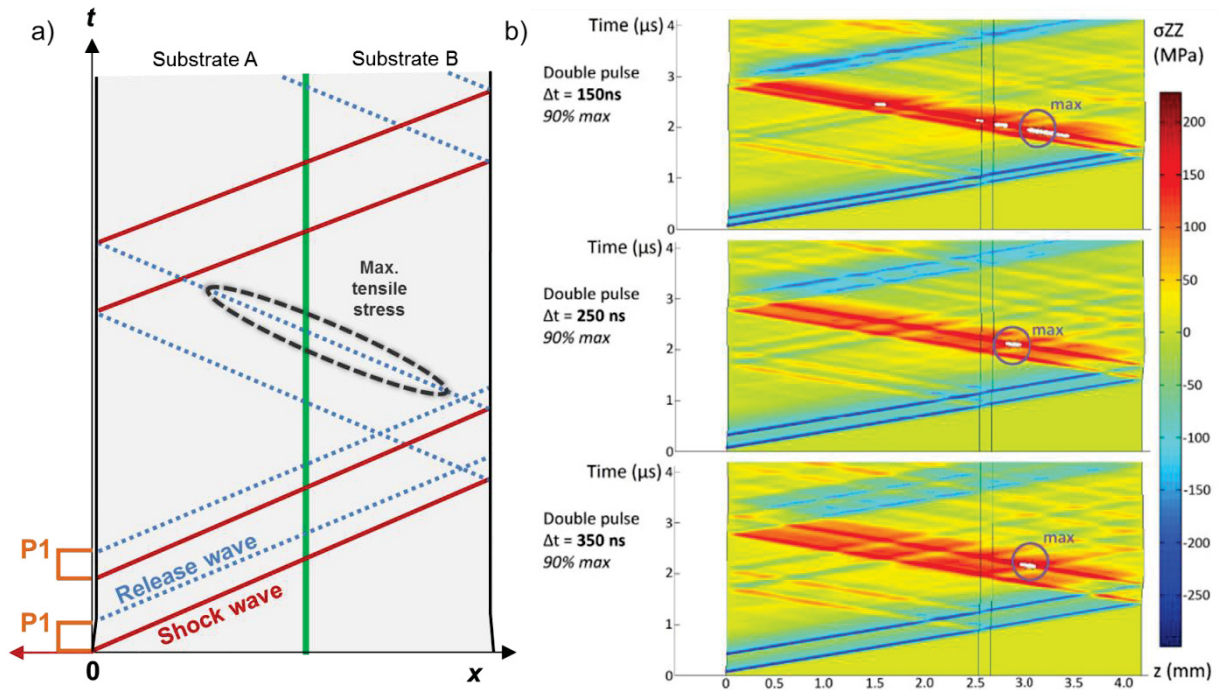


**Figure E.1: Numerical time/position diagrams showing the 5% max. tensile stress loadings in z-direction (white areas) in a 3.2 mm thick symmetrical adhesive bonded CFRP laminate for laser 25 ns (left) and laser 200 ns (right)**

Experimentation with other parameters such as the laser pulse confinement or the sacrificial layer are required to prevent any damage in the substrate.

### 3.1.2 Repeated laser shock

An alternative approach to the single laser pulse relies in the use of repeated short laser pulses on the front face of the structure. In principle, the use of the crossing of the first release wave and the second shock wave create the tensile stress at the depth required. This depth is conditioned by the delay between the two laser pulse. In practice, the double pulse would be based on a laser shooting twice on the same location after short delay (few ns). Figure E.2 introduces the role of this delay in the depth of the maximal stress generation.



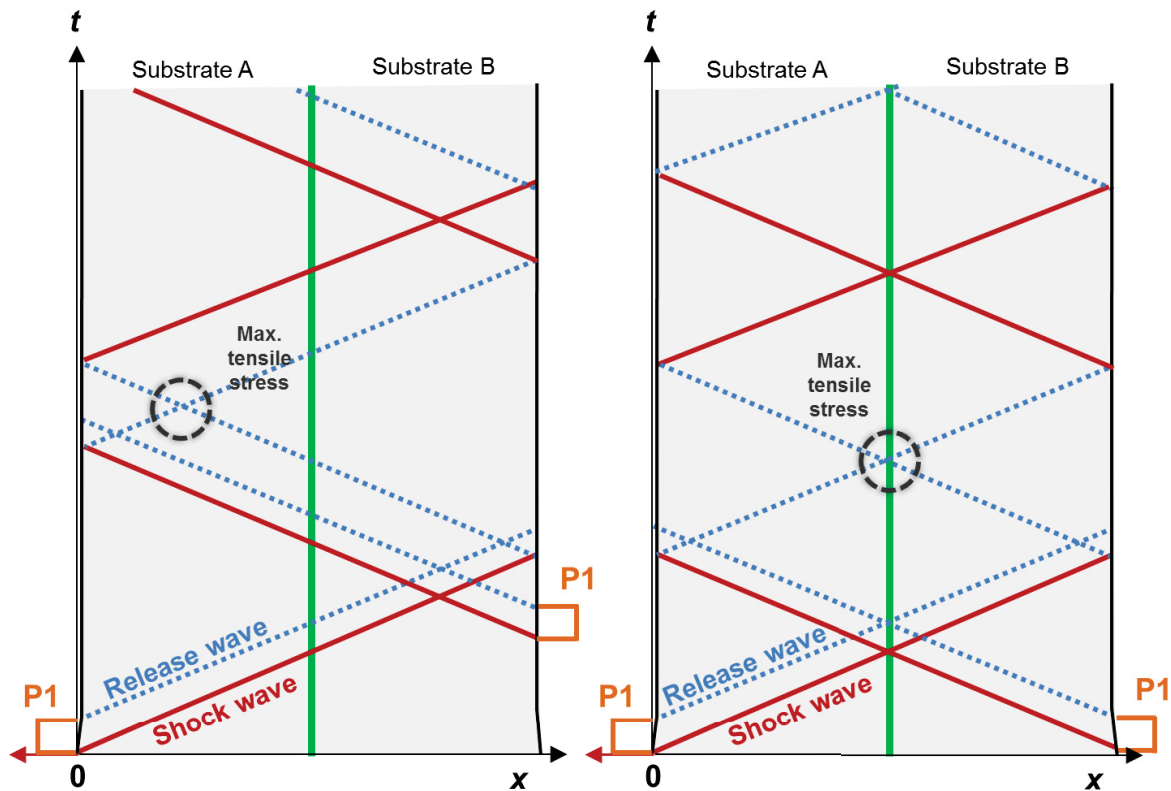
**Figure E.2: Time-position diagrams (x,t) representing a) the functioning principle and b) the importance of the delay between laser pulses for the tensile stress generation in different simulations [1]**

This approach is potentially better than the single pulse approach because each laser pulse requires less energy than a single long laser pulses for an equivalent interface strength tested [1].

The main challenges with repeated laser shocks would be the need for sacrificial layers sustaining two laser shocks and the need for a confinement layer staying over the surface in between the laser pulses. No actual laser shock configurations, neither the 25 ns nor the 200 ns, are not offering these two capabilities. The repetition rate of the lasers becomes an important characteristic due to the fine tuning in the short delay required between two laser shocks. The best rate is currently of 10 Hz for the ND:Glass laser present at the CNRS PIMM institute (see chapter B – Table 1), corresponding to 0.1 second between two shocks. The lasers are still far from a repetition rate in nanoseconds.

### 3.1.3 Symmetrical laser shock

The last alternative approach is based on the use of two laser pulses applied on each face of the structure. In principle, the tensile stress loading occurs at the location where both release waves issued from the first shock waves reflection cross each other paths. The adaptation of the depth position is realized by adapting the delay between both laser shock pulses. Figure E.3 represents the application of two laser pulses on each face of a bonded structure. The role of the delay in the positioning of the tensile stress is illustrated: the latest the second pulse is applied, the closer to the opposite face the tensile loading will be generated. In case of simultaneous laser pulse, the tensile loading will occur in the middle of the structure thickness.



**Figure E.3: Time-position diagrams (x,t) representing the symmetrical approach leading to precise high level of pressure. The delay between both laser shock is responsible for the depth of the maximal tensile stress zone.**

First experimentation with this recent approach have been conducted and are further ongoing. The tests done have led to interesting results showing that in the case of weak bonds, the adhesive bondline could be delaminated without causing more than few intralaminar cracks in the substrate loaded [1]. The interface strength which can be tested can reach the composite almost the interlaminar strength. This approach is also a patented solution filed from CNRS in 2013.

Despite the interesting results, the symmetrical approach is an hardly practicable solution for the industrial environment. The need for an access of the adhesive bonded structure from both sides would be an obstacle to the technology deployment. If it is assumed that adhesive bonding is used to enable the design of always more complex geometries and large composite parts, the accessibility would also decrease. The margin in operating the symmetrical laser shock approach would decrease with it. The other parameters are however speaking for the use of this approach: the sacrificial layer can be used, as well as a plasma confinement layer system (water flow, transparent adhesive tape, etc.).

### 3.2 Leads to an advanced diagnosis tool

The laser proof test is itself only a method applying a local stress to a structure in order to verify that the structure can withstand this precise stress. The laser source can only generate the shock wave necessary for this test and does not play any other role. Another technology is

requested for the inspection of the impacted location. This method is a diagnosis tool that can be either time-resolved for a measure during the laser shock or simply, post laser shock. With regard to the industrial application, a technical tool may satisfy certain requirements. The methods shall be simple to handle, enable a fast data evaluation, universal application, inspect a large area, deliver clear diagnostics, have specific detection capability, be robust and all of these at the lowest cost possible.

The two time resolved diagnosis methods assessed within this study were the EMAT for laser 200 ns and the VISAR for laser 25 ns. They have demonstrated their potential and limits in the type and amount of information that they can yield to the end user. Their implementation as diagnosis tools for a use in an industrial quality assessment process is limited.

To summarize, in the actual configuration, the **VISAR** has the following characteristics:

- *Pros*: precise, correlate signal with mechanical stress in structure, contactless method.
- *Cons*: hard to set-up due to reflective surface required, complex signal processing, very sensitive, access from rear free surface preferred, laser used may degrade composite (high continuous energy).

On the other side, the **EMAT** has following characteristics:

- *Pros*: simple in set-up, only front face access is required
- *Cons*: purely qualitative judgment without information about damages generated in the CFRP structure, requires electromagnetic material (or metallic tape on composite).

The literature also mentions positive experience with an alternative time resolved method: the Photonic Doppler Velocimetry (PDV) [1]. The PDV has a similar principle than the VISAR but uses two lasers. The interferences resulting from the reflected beam from one laser with the frequency of the reference laser is analyzed. This characteristic from the PDV requires that the temporal resolution is adjusted for the velocity calculation. The **PDV** is said to be easier to set up because of a lower number of parameters to adjust than for the VISAR, especially regarding the interferences research. The **PDV** characteristics can be summarized as follow:

- *Pros*: simple in set-up, contactless, less energy required than VISAR lead to less degradation of composite surface.
- *Cons*: temporal resolution limited for small phenomenon.

In opposition to the time-resolved techniques, other methods of conventional characterization may be applied after laser shock. Among them, the NDT techniques such as ultrasonic testing techniques UT or the thermography IRT are standardized in the current manufacturing processes and can easily be deployed for the detection of debonds. Indeed, **UT inspections** after shock have been used in this study as a reference method to check the presence of damages and characterize the damages induced by laser shock in the composite assemblies.

- *Pros*: standardized solution already used in manufacturing, fast inspection of large surface, existing criteria for defect detection, quantitative results for debonds and any spallation.
- *Cons*: inspection requests time after laser shock.

To conclude on the diagnosis method required for the assessment, Table E.2 summarizes the characteristics of the two investigated time-resolved techniques (EMAT and VISAR), another time-resolved technique identified in the literature (PDV) and post-shock techniques such as ultrasonic testing (UT). The deployed techniques such as UT have a significant advantage but involve that the inspection is done after the laser shock. The ideal technique shall be a

compromise between the level of information required and the time frame given for the evaluation.

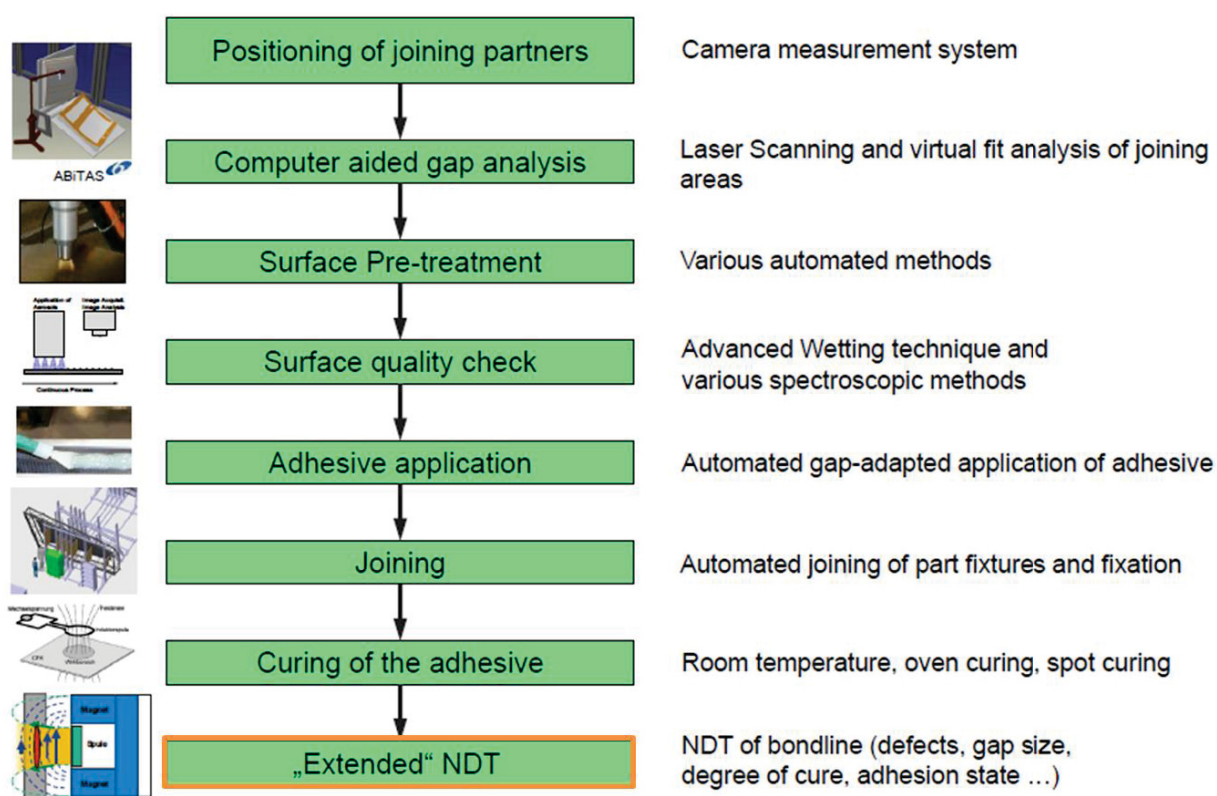
**Table E.2: Comparative table of diagnosis tool methods for characterization of the laser proof test effects in the composite structure.**

Requirements	Diagnosis technique <sup>*as tested in this study</sup>				
	EMAT*	VISAR*	PDV	Ultrasonic	Ideal method
<b>Handling</b>	- Small integrated probe applied on front surface	- Laser system requiring manual adjustments	- laser system requiring manual adjustments	- scanning probe head driven manually or automatically	- simple system with easy setup
<b>Fastness for data processing</b>	- medium (low-high-low approach)	- slow due to experimental data processing	- slow due to experimental data processing	- fast possible real-time data evaluation	- real-time data acquisition and processing
<b>Universal application</b>	- not on complex geometries, requires magnetic material, contact required	- requires access to rear face and laser reflective surface, contactless	- requires access to rear face and laser reflective surface, contactless	- probe head adapted to any type of material and structure, contact preferred	- no limitation of material/geometry, absence of contact
<b>Large area inspection capacity</b>	- Limited to local inspection (laser spot size)	- Limited to local inspection (laser spot size)	- Limited to local inspection (laser spot size)	- small to large area possible depending on probe head	- large area covering the whole adhesive layer
<b>Clear diagnostics</b>	- simple with “low-high-low” approach	- complex processing and interpretation of signal	- complex processing and interpretation of signal	- quantitative information with depth, size and geometry of damage	- information on adhesion strength or correlation damage-strength
<b>Detection capability</b>	- only qualitative results without assurance of debonding	- precise indication of mechanical events in the material thickness, no size of damage	- precise indication of mechanical events in the material thickness, no size of damage	- depth, size and geometry of damage, limited to NDT standards in use	- quantitative information with depth, size and geometry of damage incl. adhesion strength info
<b>Robustness</b>	- Sensitive to environment	- Very sensitive to environment	- Sensitive to environment	- Robust	- Robust

## 4. REQUIREMENTS AND APPROACH FOR IMPLEMENTATION OF LASER PROOF TESTS

### 4.1 Requirements for the laser proof test implementation in production

The interest of end-users for a technology allowing adhesive bonding for high loaded primary structures is large. Figure E.4 illustrates the manufacturing process concept. The innovative process involves several technologies to position and pre-treat the adherent substrate, check their surface cleanliness, apply the adhesive layer, join the substrate, cure the adhesive and finally and evaluate the bondline quality for example via laser proof test.



**Figure E.4: manufacturing process chain for adhesive bonding including the quality assessment of surface cleanliness and adhesive bond performances [2]**

To optimize the laser proof tests results, several ways have been introduced in section 3.1 and 3.2. In particular the double pulse approaches (repeated pulse, symmetrical pulse) are limited. They deserve attention for research purposes but involve either new sacrificial and confinement layer, or access to both faces of the structure to inspect.

More generally, the technology needs to reach a higher level of maturity in order to get compatible with the requirements of the manufacturing process chain. For manufacturing processes, a new technology must show a compliance to the existing standards and avoid perturbing the rest of the process. Few characteristics of the laser proof test technology as they stand today would therefore discourage any potential end user. The following characteristics, even if they are identified as entire parts of the techniques must be thought over to develop more practicable solutions:



- **The sacrificial layer:** required to avoid damaging the composite matrix and to ensure the interaction laser-matter (chapter B – section 3.2). Its use is however hardly realizable since it would involve an additional step of coating application before performing the laser test.
- **The confinement layer:** required to increase the pressure generated in the material by the laser pulse and so, use lower laser intensities. It represents an inconvenient if it means that the structure inspected must be wet or have a tape layer applied on it.
- **Any additional surface preparation regarding diagnosis tool:** the use of VISAR required painting the rear face of the substrate to get a sufficient reflectivity whereas the EMAT included a magnetic tape layer at the top surface to get a proper signal from the composite top surface. Other techniques may include other preparations. These preparations are costly in time and equipment and would slow down the manufacturing process.

As an alternative, it can be proposed to extend the existing implementation of NDT methods well established in manufacturing processes. Ultrasonic inspection UT (or PA-UT used in chapter D) is a standardized automated method. UT enable a precise characterization of the defects present in the adhesive bonds. It can be used for the characterization of the adhesive bonded structure after laser shock to evaluate the presence of debonds and delamination.

Additionally to the mentioned parameters, the uncertainties on i. the material local intralaminar strength (may slightly vary depending on manufacturing process parameters), ii. the laser robustness and stability to provide the precise energy level required, iii. The laser pulse-matter interaction due to the sacrificial and confinement layers, must all be accounted. This list is not exhaustive since several parameters may have an effect of the interaction of the shock waves generation or propagation. The current capabilities of the lasers show a potential of improvement, which will be required to move to an higher level of maturity for adhesive bond quality assessment.

## 4.2 Approach for the use of Laser Proof Test

Provided that technological improvements are completed, a practical approach for the use of laser proof test as performed in this study has been specified [1]. It gathers all necessary steps for the use of the laser proof test as a quality assessment method of any adhesive bonded assembly whose adhesive and/or materials has never been tested by laser. This process involves the realization of numerical model and therefore, first tests to determine the intrinsic parameters of the elementary materials present in the final adhesive bonded assembly.

In Figure E.5, a five-steps process including two main tasks is represented:

- The first step consists in the characterization of the laser-matter interaction with all materials, the adhesive and the substrate, in presence in the future assembly. Laser tests are performed with measures involving a time-resolved diagnosis tool such as the VISAR. Several levels of energy are tested to get key information regarding the response of the materials towards dynamic loadings up to damage generation (step 1).

Based on the characteristics determined, the models can be created to match the response of the elementary materials (step 2). This data enables also the creation of a model of the final adhesive bonded assembly. It is helpful for the choice of the laser parameters for the test on the adhesive bonded structure.

It must be noticed that this first task is only required if the dynamic response of the elementary materials is unknown. It is indeed impossible to create a model without these intrinsic parameters.

- The second step consists in reproducing the laser tests on the adhesive bonded structure. These laser tests are done in the same manner than the tests with the elementary components, including the time-resolved diagnosis tool (ex. VISAR) and the analysis of the structure post-laser shock (step 3). The data collected from several laser shots at different intensities defines the performances of the adhesive bonded structure. The results are hence used to validate the model previously created in task one (step 4).
- Finally, the step 5 is a refinement of the model to determine what are the optimal settings for the adhesive bonding assessment. The laser proof test can be adjusted for the adhesive bonded structure inspection.

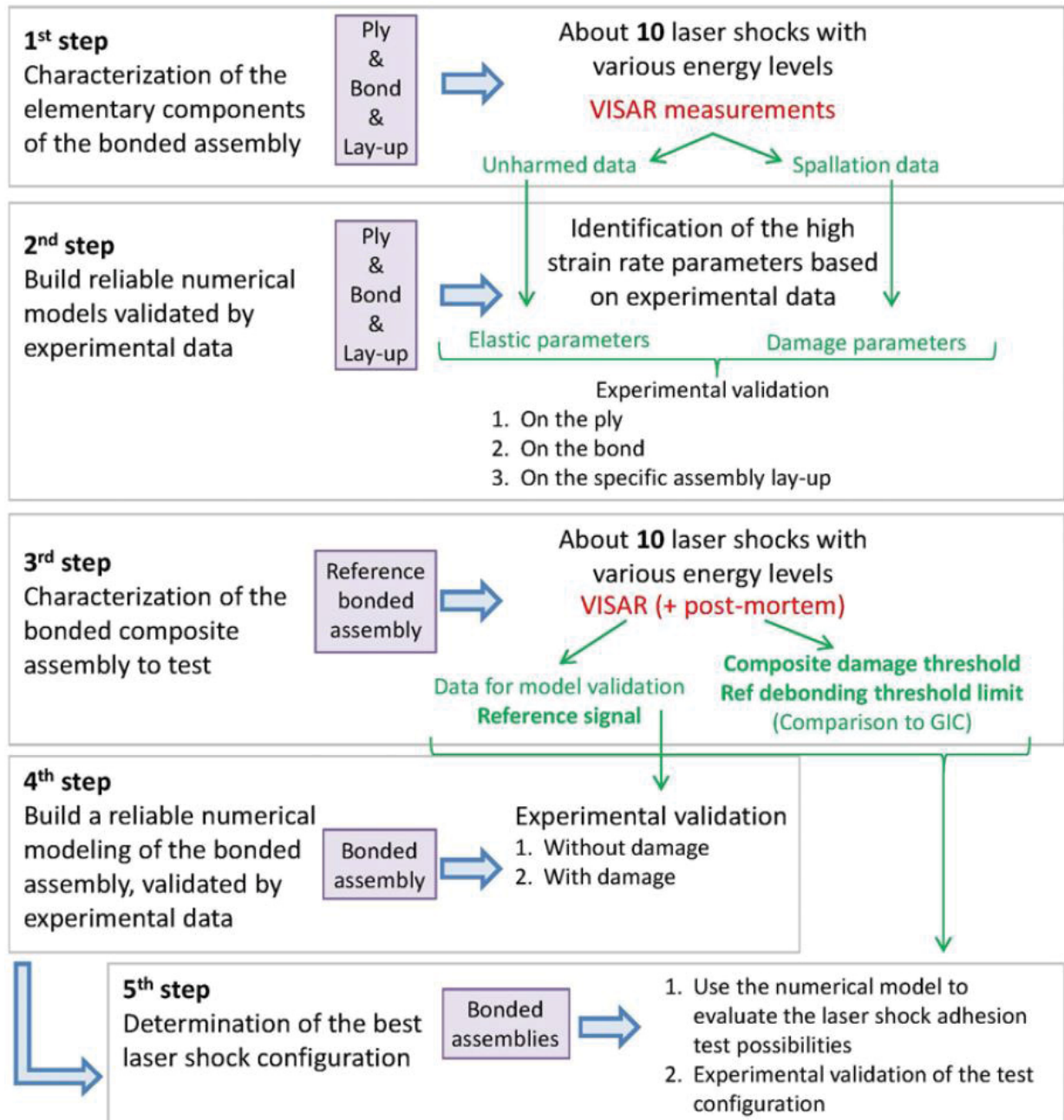


Figure E.5: suggested protocol for implementation of laser proof test for any adhesive bonded assembly according to [1]

## 5. SUMMARY

The laser proof test approach for adhesive bond inspection has been investigated experimentally in two configurations of pulse length : 25 ns and 200 ns. The laser tests led to the determination of debonding thresholds intensities for all level of contaminations in the three families of specimens: cured C, partially PC and moisture contaminated MOC.

The main scientific objective is achieved: laser proof test could successfully debond weak adhesive bonds. The investigation of specimens however revealed that the laser also induced damages in the composite substrates. Tests including repeated laser shocks at the same locations indicated that the number of damages increases with the laser intensity and laser shots. The damage occurrence is such that for the laser 25 ns even 47 % of the threshold intensity causes intralaminar cracks. The mechanical test performed on specimens which were previously impacted at around 70 % of the debonding threshold intensity revealed a loss of  $G_{1c}$  performances. In general, the investigations of specimens after laser shocks revealed that both laser systems are inducing stresses in the material substrates and are not yet optimized enough for a precise adhesive bond assessment. The intensity level required for debonding cannot be given precisely because both configurations involve large uncertainties on the intensities (13.2 % for laser 25 ns, 4.8 % for laser 200 ns).

Three ways of optimization are specified in order to increase the efficiency of the method:

- the adaptation of the laser pulse duration which is an improvement of the approach evaluated within this study with the comparison 25 ns to 200 ns. It is the most practicable solution on the industrial point of view since it only implies changes in the laser technology.
- the repeated laser shots (high frequency), would concentrate the tensile stress in a specific depth thanks to a short delay between two laser shocks. This solution requires a better approach for the laser beam coupling at the material surface.
- the symmetrical laser shock, potentially the most effective alternative as the tensile stress can be generated precisely at any depth in the material thanks to shock waves coming from both sides. A delay between the laser shocks would be the parameter to adjust in order to specify the depth where the tensile stress occur. This solution however represent an industrial challenge since both side of a structure must be shocked by a laser (accessibility, geometry, etc.).

In any case, the optimization of technology shall go through laser improvements in term of energy stability, tunable pulse duration and frequency of laser shocks.

The adhesive bondline status after shock is not directly revealed by the laser shock technique itself. Diagnosis tool methods must be used to check the presence of a debond or not. Both VISAR and EMAT methods were tested to assess the shock wave effects in the structures. The precision of the VISAR enable the calibration of the laser shock proof method to the structure. Its implementation is however complex and costly. Tests with both methods revealed that the level of information is not comparable and none of them is adapted in the case of an industrial quality assessment process. Investigation of alternative diagnosis tools were not done in this work but appear in the literature (case of PDV). The requirements for an industrial method have been discussed in this chapter and a diagnosis method may be similar to the NDT methods in place which can even quantify the potential damages (eg. ultrasonic

inspection). Moreover, the implementation of laser proof test would be facilitated by a smooth integration in the existing control processes.

Finally, in its current principle of functioning, no direct adhesion performance is given by the laser proof test. The debonding threshold intensity is correlated to a destructive mechanical test such as the  $G_{1C}$  test in this study. The use of calibration on raw materials and simulation of the final assembly shall enable a direct application of the laser proof test. This objective shall remain the ultimate goal of any adhesive bond quality method. If its implementation may be demanding in term of efforts, it is believed that the laser proof test approach is a valid candidate for this challenge.

## REFERENCES – CHAPTER E

- [1] R. Ecault, „Experimental and numerical investigations on the dynamic behaviour of aeronautic composites under laser shock - Optimization of a shock wave adhesion test for bonded composites“, E.N.S.M.A. - Sciences et Ingénierie en Matériaux, Mécanique, Energétique et Aéronautique, Poitiers, PhD, 2013.
- [2] T. Stöven, „Rivetless Aircraft Assembly - a dream or feasible concept“, gehalten auf der Eucomas 2010, Berlin, Mai-2010.

---

## CONCLUSION

The deployment of the adhesive bonding technology for high-loaded structural elements in aeronautic require that the adhesion quality can be controlled on the assembled part. A non-destructive method is therefore needed to control the final bonded parts instead of testing destructively process control specimens. In this study, the focus is set on lightweight epoxy composite with carbon fibers materials, which correspond to the need of lighter structures and assemblies.

The literature in the first chapter underlines that adhesion quality is a critical parameter that cannot be assessed by appropriate NDT techniques yet. Deviations in manufacturing processes or surface contamination may lead to weak adhesive bonds. Up to now, only structural parameters are determined by mechanical testing to assess a global quality of the assembly but without focusing on the adhesion parameter. NDT methods have been further developed to target the measure of the adhesive bond strength. Among the promising methods, the laser proof test approach is the technique deserving the most interest. Indeed, previous studies report developments conducted with success towards an inspection method for the adhesion of coatings, metal assemblies and even adhesive bonded composite over the last decade.

The approach of laser proof test is based on high pressure loadings travelling back and forth through the target tested. The crossing of incident shock waves and their release waves after reflection generates the tensile stress in the target thickness. It is this tensile stress which acts as a local mechanical test in the adhesive bonded structure. The scientific objectives from this study aim at verifying their non-destructive character for the adhesive bonded assemblies. Their effects are investigated experimentally on a range of different quality of adhesive bonds. The laser proof test setup, the physical parameters and the mechanisms of laser proof tests are evaluated. The potential for further development is finally derived from the experimental results with correlation to the literature.

First, to enable a better understanding of the key characteristics, the 2<sup>nd</sup> chapter introduces the laser proof test functioning principles. It is highlighted that the lasers generate a shock wave propagating inside the material and being reflected at all interfaces. The phenomenon takes place at high level of pressures and high strain. The shock wave theory is therefore presented with the particular case of composite materials. Due to the complexity of the anisotropic composite, shock waves interaction and propagation models are however still poorly described in the literature. It is agreed that the level of pressure reached in the material (<10 GPa) allow one to approach the behavior with the classical sound wave propagation principles. The literature also uniformly tends to elastic-orthotropic models for all modelling purposes. More complex models are only at development stages as this conclusion is being written.

Among the parameters responsible for the a shock wave induction in the bonded structure, three main properties may be mentioned: the laser wavelength, the pulse duration and the energy. These parameters can be adjusted to obtain the most optimal shockwave/specimen interaction. They constitute the variable parameters investigated in the frame of this work.

The presentation of the two experimental laser setup LASAT and LBI introduced their approach for the shock wave induction: both involve water confinement to maximize the pressure generated by the plasma's expansion (respectively by thin layers or by thin flowing film) and sacrificial layer to regulate the plasma/matter interaction at the surface (respectively with aluminum paint or black polyvinyl tape). The differences between the two experimental setup remain the laser pulse profile, laser beam spot size (density) and over all, the laser pulse duration range.

In order to assess the laser proof test methods, a specific range of 5 weak adhesive bond were manufactured. This step was a first challenge in this study, due to the inexistence of a specific operational mode. A process involving surface contamination by silicon based release agent gave the expected range of weak adhesive bonds. The 3 specified criteria for weak adhesive bonds (absence of defect detected via NDT, 20% or more reduction of nominal mechanical performances, adhesive failure) were verified for the three highest levels of contamination. Additional states with moisture ageing of the bonded structure and poor curing of the adhesive were also prepared.

All specimens were characterized by reference methods before and after laser testing: The degree of cure of the composite and the adhesive were verified by DSC, XPS revealed the atomic composition of the contaminated surfaces, contact angle measurements validated the difference between levels of contamination with release agent. Conventional NDT method with X-ray provided information about the absence of porosity in the composite and in the bondline while UT & PAUT could reveal any defect in the composite and weak adhesive bond layers. Finally, mechanical testing method with the double cantilever beam test showed the decreasing G1C values with increasing contamination amount. Later, the impacts of laser shock on the bondline were also evaluated by DCB. Micro-cuts of laser impacted structure were also prepared to witness the damage and verify the other diagnosis indications.

After the characterization of the specimens, the experimental phase of this work opposed the two laser LASAT with 25 ns and LBI with 200 ns pulse duration by adapting their energy for each shock. Laser shock were applied in the frame of 4 major tests.

The first test was applied on the three families of specimens (fully cured C as standard, partially cured PC and moisture saturated MOC) to determine the debonding threshold intensity. This parameter defines the laser beam intensity for which each adhesive bond state show damages in the adhesive bondline. In general, fully cured specimens revealed threshold levels decreasing with weaker adhesive bonds. The laser with 25 ns pulse duration showed however that damages in the rear substrates where occurring simultaneously to debonding. It was not investigated any further because of the unsuitable pulse duration. The laser with 200 ns did not induce as many cracks in the composite substrate. Regarding partially cured PC specimens, damages could be observed in the poorly cured substrate layer. The adhesive bond layer only got affected in the when the adhesive bond strength was lower than the substrate cohesive strength. This result highlights a novel possible application of the laser proof test for the evaluation of the cure degree of a composite. Indeed, if the material has not reached 100% cure, its mechanical properties are affected and the cohesive strength is slightly reduced. This parameter can be targeted by laser proof test.



For moisture contaminated MOC specimens, higher threshold values together with larger damages in low contaminated states were observed. This effect was attributed to swelling and plasticization of the bonded structures.

In general, the intensity levels shall not be considered with precaution due to the large uncertainties: 13.2 % for laser 25 ns versus 4.8 % for laser 200 ns.

Assuming that a control of an adhesive bond layer would involve laser shock with intensity level below a specific threshold value, the second test assessed the effects of this kind of shock. Laser shocks were applied repeatedly from 1 to 5 times at the same location, with several intensities from 105 % to about 50 % of the threshold values.

Observations post-impact, both by ultrasonic inspection and micro-cuts revealed damages in the form of delaminations and transversal cracks (with length <200 $\mu$ m) one-ply in the composite substrate. Their number increased with the laser intensity and the repetition rate, which confirms that the present configurations are not properly non-destructive. This remark is emphasized by the occurrence of single transversal intralaminar cracks after shock of very low intensity, around 47 % for laser 25 ns and 70 % for laser 200 ns.

The third test aimed at evaluating whether laser shots applied below threshold would affect the mechanical properties of the assembly. This test was performed based on fully cured DCB coupons, which were impacted by laser shock at approximately 70% of the threshold values. Despite no damage detectable by UT inspection, the mechanical performances were decreased by around 50 %. The origins of this decrease may be related to the previous observation in the second test. Occasional micro-transversal cracks may appear at this level of shock intensity. However, no observation of the failure profiles or impact locations did reveal differences compared to any standard coupon (without shock), so that the origins of this decrease are not established yet.

The last test involved standard laser shock test on C specimens with the two diagnosis tool from both laser setup tested. Because both were based in separated lab or company, no switch between diagnosis and laser type could be done. This test allowed only an overview of the capability and limitations of the diagnosis systems. On one side, an Electromagnetic transducer (EMAT) probe was used for the laser 200 ns, providing a so called low-high-low approach to compare the state before/after laser shock. This diagnosis enables a simple qualitative statement on any change in the tested material. On the other side, the velocimeter for any reflector (VISAR) was tested with the laser 25 ns. After a difficult setup and complex data treatment, it provided valuable information thanks to time-resolved measurements on the rear face of the tested panel. The signals revealed the detection of shock waves and other interferences, which highlight the need of the VISAR or similar tool for modeling of the laser shock process in a new material.

Alternative diagnosis tools were not investigated in this study. The literature however mentions additional leads for monitoring of laser proof tests.

The final chapter proposes three optimizations in order to improve the laser proof test approach and bring it to the next level of maturity:

1. the adaptation of the laser pulse duration, the most practicable solution on the industrial point of view because directly linked to laser technology. This solution does

not solve all the challenges related to the tensile stress concentration but is the easiest to develop for short terms improvements.

2. the use of repeated laser shots at high frequency to focus the tensile stress in a specific depth. This solution requires a better approach for the laser beam coupling at the material surface.
3. the symmetrical laser shock with delay in order to generate the crossing of the shock waves at precise depth in the material. This solution is potentially hard to deploy in the industry since both side of a structure must be shocked by laser (accessibility, geometry, etc.).

In any case, the optimization of technology shall go through laser improvements in term of energy stability, tunable pulse duration and frequency of laser shocks.

To conclude, this study shows that laser proof test methods could successfully debond weak adhesive bonds. All tests completed lead to the conclusion that in the present state of development, collateral damages in the composite substrate are however not negligible. Furthermore, this study has demonstrated that with their current functioning principle, the laser proof test do not provide a direct information about the adhesion level. This would only be possible after precise calibration of the laser proof system on the desired material assembly. The calibration on row materials and simulation of the final assembly shall enable a direct application of the laser proof test. The outlook highlights a way forward to the ideal laser proof test technique.

## OUTLOOK

This study has revealed limitations of the current laser proof test approaches. The lasers tested (25 ns and 200 ns pulse duration) with their respective confinement and sacrificial layers are not optimal for adhesion test on the specimens tested. The main focus was set on the comparison of the laser beam intensity for both laser systems and their effect on the composite materials. Results have shown that even a laser shock intensity at approximately 70 % of the debonding threshold intensity damaged the CFRP substrate. Also, no other geometry than symmetrical bonded CFRP specimens of 3 mm thickness were tested. Therefore, no comments can be made on other geometries or other materials.

Provided the fact that the laser systems allow improvements in repeatability, stability and precision with the laser beam intensity, it is advised to investigate lower levels of intensity to assess the presence of damages in the substrates and visualize for which proportion of the threshold intensity the laser proof test can be assimilated to an NDE technique. Future works shall also address the simulation of the laser shock propagation and interaction with each type of material.

Upcoming studies shall also analyze the feasibility of the three concepts for improvements (i. the adaptation of laser parameters, ii. the repeated laser shocks and iii. the symmetrical laser shock). These improvements will have to deal implicitly with the question of laser pulse confinement (here with water or tape) and sacrificial layer (metallic paint or tape) because they represent the first technological obstacles. First studies on alternatives may be necessary at first to improve the understanding and dependency to these parameters.

Finally, the implementation of a new technique as a diagnosis-tool or use the existing NDT ones (UT) shall be developed in the next studies.

It is believed that with the further research and dynamic around this topic, that the technology could reach an industrial maturity in 3 to 5 years.